

**Coating of Wellbore Grain Surfaces to Prevent Scale
Deposition/Adhesion**

Nasim Kazemi

Submitted in accordance with the requirements for the degree of
Doctor of Philosophy

The University of Leeds
School of Mechanical Engineering

June, 2014

The candidate confirms that the work submitted is her own, except where work which has formed part of jointly-authored publications has been included. The candidate confirms that appropriate credit has been given within the thesis where reference has been made to the work of others.

This copy has been supplied on the understanding that it is copyright material and that no quotation from the thesis may be published without proper acknowledgement.

Assertion of moral rights:

The right of Nasim Kazemi to be identified as Author of this work has been asserted by her in accordance with the Copyright, Designs and Patents Act 1988.

Acknowledgements

First of all, I would like to express my sincere gratitude to my great supervisors Prof. A. Neville, Dr. M. Wilson, and Prof. N. Kapur for their help, guidance and also being supportive and encouraging through my PhD. This PhD would not have been possible without your support. I would also show my appreciation to Statoil funding this project and my sponsor advisors: Dr. N. Fleming and T. Tjomsland for their support.

I am also thankful to the members of iETSI research group, especially to Eleftheria, Thibaut, Laura, Wendy, Violette, Abinash, Ali, Ashley, Louise, Nick, Joe, Young, Benissa, Louise, Mike, John, Simon, Rocky, Diego, Juan, and Liu for the discussion and friendships. Many thanks to the iETSI staff Ron Cellier, Graham Jakeman (R.I.P), Brian Leach, Jane Tillotson, Adrian Eagles, Jackie Kidd, Fiona Slade, Dr. Chun Wang, Dr. Tomasz Liskiewicz and Dr. Ardian Morina. I would also like to thank my friends, especially Akhtar, Marmar, Simin, Bahareh, Reza, Pariya, Wahid, Helia, Pouya, Ali, Mahan. I also would like to thank Graham, the officer who authorised my driving license which helped me to drive when I was recovering from an incident. I will forever be thankful to my beloved friend, Shahrzad. Without her help, it would not be possible for me to recover quickly from the incident that happened to me two years ago.

I especially thank my mom (Sara Sasanpour), dad (Latif Kazemi), brother (Navid) and sisters (Nazanin, Neda). My hard working parents have sacrificed their lives for their children with unconditional care and love. I could not be at this stage without their constant support. Mommy, Daddy, Navid, Nazanin, and Neda, I love you so much and thank you for everything. Also I would like to thank my cutie baby, Lucy for the happy time that we spend together.

At the end, I would like to thank the special person of my life. The glamorous moment in these past four years was the moment that I married to my soul-mate, and lovely husband. I married the best person out there for me. There are no words to convey how much I love him. Nasser has been a true and great support and has unconditionally loved me during my good and bad times. He has also been instrumental in helping me and instilling confidence. He has faith in me even when I felt digging a hole and crawling in to one because I did not feel confident. These past several years would not have been an easy ride, both academically and personally, without him. I truly thank Nasser for sticking by my side, even when I was irritable and depressed. His constant support, love, motivation, encouragement

and patience during my PhD made me realise how lucky I am to have him in my life forever.

*I dedicate this thesis to
my mom, Sara, dad, Latif, and my beloved husband, Nasser,
For their constant support, unconditional love and care.*

Abstract

Mineral scale deposition/adhesion is one of the major challenges in the oil and gas industry. Besides, the new regulations in the oil and gas industry suggest substituting conventional inhibitors by more environmentally-friendly strategies which may include anti-scaling surfaces as a potential methodology. The objective of this work was to study a new potential application for surface modification near the wellbore to reduce mineral scale deposition in the rock. To achieve this purpose, it was required to form a thin layer of a chemical, which has a strong bond with quartz and does not block the oil path; and has a potential to reduce the scale deposition/adhesion on the rock. 3-aminopropyl-triethoxysilane (APTES) and p-aminophenyltrimethoxysilane (APhS) with various concentrations were chosen to create self assembled monolayer to alter the physical and chemical properties of the surface. The kinetics of the APTES (2-8%) film formation on the surface was studied by QCM. Langmuir isotherm was used to interpret the QCM results and to calculate the surface coverage of APTES film on the surface. Also the performance of quartz surfaces which were treated by different concentrations of APTES and APhS in terms of reduction of scale deposition was studied in low=4.77 and high=54.8 saturation ratios. The best film performances (up to 95%) were obtained by 0.06% APhS and 6% APTES, respectively. It was assumed that the reduction of scale deposition could be related to the reduction of nucleation sites on the treated surfaces due to changing the surface charge of quartz surface from negative to neutral (slightly positive) surface. Surface composition, wettability and the roughness of APTES and APhS films were characterised by XPS, Contact angle Goniometry and surface profiler, respectively. Based on the film characterisation results, the most effective parameters in reduction of scale deposition were the surface composition and film conformation.

Table of Contents

Acknowledgements	iii
<i>I dedicate this thesis to</i>	<i>v</i>
<i>my mom, Sara, dad, Latif, and my beloved husband, Nasser,.....</i>	<i>v</i>
<i>For their constant support, unconditional love and care.....</i>	<i>v</i>
Abstract.....	vii
Chapter 1	1
Introduction.....	1
1.1 Objective	3
1.2 Thesis outline	4
Chapter 2 Literature Review.....	7
2.1 Introduction.....	7
2.2 Scale formation literature.....	7
2.2.1 Scale formation location.....	9
2.2.2 Calcium carbonate scale formation	9
2.2.2.1 Supersaturation, a driving force of calcium carbonate scale formation	11
2.2.2.2 Basic principals of scale formation: induction, nucleation and growth	13
2.2.3 Adhesion.....	21
2.2.3.1 Adhesion forces and surface energy.....	22
2.3 Factors influencing calcium carbonate formation	22
2.3.1 Effect of pH.....	23
2.3.2 Effect of saturation ratio	24
2.3.3 Effect of temperature	24
2.3.4 Effect of calcium and carbonate ions concentration	26
2.3.5 Effect of impurities	26
2.4 Prediction of scale formation by using software	27
2.5 Scale removal and inhibition methods	27
2.5.1 Mechanical removal mechanism	28
2.5.2 Chemical removal mechanism	28
2.5.3 Inhibition of scaling by scale inhibitors	28
2.5.3.1 Green chemistry and inhibitors	30
2.5.4 Squeeze Treatment	31
2.5.4.1 Temperature.....	33
2.5.4.2 pH solution	33

2.5.4.3	Divalent cations.....	33
2.5.4.4	Mineralogy	34
2.6	Controlling mineral scale and fouling by applying new substrates on surface	35
2.6.1	Effects of different substrates on inorganic scale deposition.....	36
2.6.1.1	Surface composition.....	36
2.6.1.2	Surface energy.....	40
2.6.2	Effect of roughness	42
2.7	Surface modification applying a self assembled mono-layer technique	44
2.7.1	Silanes	44
2.7.1.1	Amine-terminated films	46
2.8	Liquid-phase silanization of aminosilanes to create a SAM film on surface.....	48
2.8.1	Confirmations of aminosilane	49
2.8.2	Parameters affecting SAM process	49
2.8.2.1	Water content.....	50
2.8.2.2	Reaction time.....	50
2.8.2.3	Concentration of aminosilanes	52
2.8.2.4	Solvent.....	53
2.8.2.5	Curing	53
2.8.3	Comparison between APTES and APhS	55
Chapter 3	Methodology and Experimental Techniques.....	57
3.1	Introduction.....	57
3.2	Organosilanes	58
3.3	Experimental methodology and materials	60
3.3.1	Materials	61
3.3.2	Experiment methods	62
3.3.2.1	APTES film formation study by QCM	62
3.3.2.2	Silanization of quartz coupons by APTES and APhS.....	62
3.3.2.3	Calcium carbonate scale deposition test.....	63
3.4	Characterisation techniques.....	64
3.4.1	Quartz Crystal Microbalance (QCM).....	64
3.4.1.1	Sauerbrey model	65
3.4.2	X-ray Photoelectron Spectroscopy (XPS).....	67
3.4.2.1	Qualitative analysis.....	68

3.4.2.2 Quantitative analysis	69
3.4.3 Contact angle.....	69
3.4.3.1 Surface Profiler-NPFLEX- (roughness measurement)	71
3.4.3.2 Scanning Electron Microscopy (SEM)	71
3.5 Film kinetics	73
Chapter 4 Film Formation of APTES on Quartz Crystal	75
4.1 Introduction	75
4.2 Using QCM crystals as surrogate rock surface	77
4.3 Film formation kinetics.....	78
4.4 Monolayer or multilayers?	84
4.5 Summary.....	88
Chapter 5 Scale Prevention Performance	90
5.1 Introduction	90
5.2 The effects of APTES coating on scale deposition	91
5.2.1 APTES coating behaviour in low SR= 4.77	92
5.2.1.1 Visualization of calcium carbonate deposited on untreated and APTES-treated quartz surfaces in low SR=4.77	94
5.2.1.2 Morphology of calcium carbonate deposited on untreated and APTES-treated quartz surfaces in low SR=4.77	97
5.2.2 APTES coating behaviour in high SR= 54.8.....	99
5.2.2.1 Visualization of calcium carbonate deposited on untreated and APTES-treated quartz surfaces in high SR=54.8.....	102
5.2.2.2 Morphology of calcium carbonate deposited on untreated and APTES-treated quartz surfaces in high SR=54.8.....	104
5.3 The effects of APhS coating on scale deposition	107
5.3.1 APhS coating behaviour in low SR= 4.77	107
5.3.1.1 Visualization of calcium carbonate deposited on untreated and APhS-treated quartz surfaces in low SR=4.77	109
5.3.1.2 Morphology of calcium carbonate deposited on untreated and APhS-treated quartz surfaces in low SR=4.77	110
5.3.2 APhS coating behaviour in high SR = 54.8	111
5.3.2.1 Visualization of calcium carbonate deposited on untreated and APhS-treated quartz surfaces in high SR=54.8.....	112

5.3.2.2 Morphology of calcium carbonate deposited on untreated and APhS-treated quartz surfaces in high SR=54.8	113
5.4 Comparison of APTES and APhS coated surface performances in CaCO ₃ deposition reduction	114
5.5 Summary	121
Chapter 6 Film Characterisation and Surface Properties of APTES and APhS Coating.....	122
6.1 Introduction.....	122
6.2 X-ray Photoelectron Spectroscopy results of APTES- and APhS-treated surfaces	123
6.2.1 Chemicals states and binding energy shifts of APTES-treated surface	126
6.2.2 Chemicals states and binding energy shifts of APhS-treated surface	131
6.2.3 Comparison of film characterization of APTES- and APhS-treated surfaces by XPS.....	133
6.3 Wettability and surface energy results of APTES- and APhS-treated surfaces	137
6.3.1 Surface energy of treated surfaces by APTES	138
6.3.2 Surface energy of treated surfaces by APhS	140
6.4 Topography of surfaces treated by APTES and APhS	141
6.4.1 Roughness of APTES-treated surfaces	142
6.4.2 Roughness of APhS-treated surfaces.....	144
6.4.3 Comparison results of roughness of APTES- and APhS-treated surfaces.....	145
6.5 Structure of APTES and APhS film formation on quartz surface	146
6.5.1 Possible APTES film structures on quartz surface.....	147
6.5.1.1 APTES film structure on quartz surface at low concentrations (0.05-0.2%).....	148
6.5.1.2 APTES film structure on quartz surface at high concentrations (2-8%).....	149
6.5.2 Possible APhS film structures on quartz surface	150
6.6 Summary	152
Chapter 7 Discussion.....	154
7.1 Introduction.....	154
7.2 The performance of the quartz surface treated by APTES in reduction of calcium carbonate scale deposition	155
7.3 The performance of the quartz surface treated by APhS in reduction of calcium carbonate scale deposition.....	163

7.4 Comparison of APTES and APhS film performances in reduction of calcium carbonate scale deposition	167
7.5 Immunizing near wellbore area from CaCO ₃ deposition/adhesion by SAM formation.....	174
7.5.1 Kinetics of APTES film formation on quartz surface	176
7.5.2 Treatments performance in reduction of scale deposition	177
7.5.3 Characterisations APTES and APhS films on the quartz surfaces	179
Chapter 8 Conclusion and Future Work.....	184
8.1 Summary of the results.....	184
8.1.1 Chapter 4: kinetics of film formation on quartz surface.....	184
8.1.2 Chapter 5: performance of APTES- and APhS-treated surfaces	185
8.1.3 Chapter 6: Characterisation of APTES and APhS treatments ...	185
8.1.4 Chapter 7: Discussion.....	186
8.2 Suggestions for future work	186
8.2.1 The formation of anti-scale films on the surface	187
8.2.2 The tendency of mineral scale to the treated surface	187
Chapter 9 Reference	188
Appendix A.....	210

List of Figures

Figure 1-1. Image of mineral scale which has been formed inside the pipe (1).....	1
Figure 1-2. SEM image of calcium carbonate with the surface pattern	2
Figure 2-1. Calcium carbonate morphology: a) calcite, b) aragonite and c) vaterite (21)	10
Figure 2-2. Temperature-pressure diagram of phase dependency of carbon dioxide (4)	11
Figure 2-3. Two-dimensional crystallization procedure with and without adding seed crystal (27)	13
Figure 2-4. Schematic of scale formation a) ion pairing, b) prenucleation aggregate growth, c) homogeneous nucleation and d) heterogeneous nucleation (47, 48)	16
Figure 2-5. Free energy diagram of nucleation as a function of nuclei radius (32) .	17
Figure 2-6. Kinetics of scale formation and precipitation (54, 55).....	18
Figure 2-7. Different processes of crystal growth: a) Frank-Van der Merwe method b) Volmer-Weber method c) Stranski-Krastanov	19
Figure 2-8. Growth of crystal by screw dislocation process at low SR: a) one screw dislocation b) two screw dislocations	20
Figure 2-9. Schematic of scale deposition process after nucleation: a) particle adsorption, b) agglomeration and c) phase transitions (47)	20
Figure 2-10. Schematic of crystal deposition/adsorption on a surface (60)	21
Figure 2-11. Carbon total fraction versus pH (4).....	23
Figure 2-12. Effects of temperature on the saturation of scaling species in the solution (94)	25
Figure 2-13. Polyphosphate inhibitor structure, n=4-20	29
Figure 2-14. Chemical structure of DETPMP scale inhibitor	29
Figure 2-15. PPCA structure	29
Figure 2-16. PAA chemical formula	30
Figure 2-17. Schematic of an oil well using squeeze treatment (132)	31
Figure 2-18. Schematic of the squeeze treatment process (144).....	32
Figure 2-19. Impact of Ca on adsorption of SI on sandstone at 25°C (134)	34
Figure 2-20. Schematic of biofouling procedures on a surface (177)	36
Figure 2-21. Calcium and bicarbonate ions attraction on a) stainless steel surface and b) PPCA-treated surface (4, 181)	37
Figure 2-22. Calcium carbonate deposition on different surfaces for two different brines (4).....	39
Figure 2-23. Tendency of various substrates to calcium carbonate scale formation (189).....	40

Figure 2-24. Mass gain of various substrates as function of contact angle measurements (3).....	41
Figure 2-25. Roughness of the various types of surfaces as function of mass gain (189).....	43
Figure 2-26. Mechanism of silanization on a surface.....	45
Figure 2-27. Molecular structure of a) APTES and b) APhS.....	46
Figure 2-28. High resolution nitrogen spectra for the silicon surface treated by APTES a) in liquid phase b) in vapour phase.....	47
Figure 2-29. AFM images (topography) of a) treated silicon dioxide surface by APTES in gas phase and b) treated silicon dioxide surface by APTES in liquid phase.....	48
Figure 2-30. Possible APTES conformations on silicon surface (269).....	49
Figure 2-31. Film topography of APTES for different water contents, A) 0%, B)0.1% and C)1% (v/v) (244).....	50
Figure 2-32. Water contact angle measurements for APTES treated surfaces in different time period (247).....	51
Figure 2-33. Thickness of APTES film in different time period (247).....	52
Figure 2-34. Film topography of APTES for different APTES concentrations, A) 3mM, B) 5 mM and C) 10 mM (244).....	52
Figure 2-35. AFM images for a) before post treatment b) after post treatment by aqueous phosphate buffer (284).....	55
Figure 2-36. High resolution of N_{1s} spectra of quartz treated by A) APhS and B) APTES (244).....	56
Figure 2-37. Topography of A) APTES and B) APhS film presenting smoother film for APhS (244).....	56
Figure 3-1. DW adsorption on quartz crystal surface as function of time by QCM at ambient temperature.....	60
Figure 3-2. Compositions of calcium carbonate brines in scale deposition tests ...	63
Figure 3-3. The picture of the scale experiment set up.....	64
Figure 3-4. QCM200 set up (QCM200 Digital Controller, QCM25 Crystal Oscillator, crystal Holder and Quartz sensors).....	65
Figure 3-5. Front and back sides of QCM crystal.....	65
Figure 3-6. A model of QCM's graph showing the rate of deposition as a function of time.....	66
Figure 3-7. Schematic of photoionisation process and the relaxation mechanisms	68
Figure 3-8. Contact angle measurement instrument.....	70

Figure 3-9. Schematic of liquid droplet on a solid surface presenting the Young's equation	71
Figure 3-10. Different parts of a SEM device involved in creating a picture	72
Figure 3-11. SEM image of calcium carbonate crystals	73
Figure 4-1. Summary of Film Formation, Chapter 4.....	76
Figure 4-2. Survey spectrums scan of gold section of QCM crystal after 2 h experiment in APTES solution.....	77
Figure 4-3. Non peak area around binding energy of silicon at 99.5 eV on gold part of crystal.....	78
Figure 4-4. A gold spectrum of the survey scans of the QCM electrode	78
Figure 4-5. Mass growth of APTES on quartz crystals as a function of time by QCM	79
Figure 4-6. Maximum adsorption of APTES on QCM crystal for various concentrations after 2 h experiment on ambient temperature	80
Figure 4-7. Experimental data fitted by Matlab code for a) 2% and b) 4% APTES concentration.....	81
Figure 4-8. Experimental data fitted by Matlab code for a) 6% and b) 8% APTES concentration.....	82
Figure 4-9. Plot of K_{obs} versus APTES concentration at ambient temperature	83
Figure 4-10. Surface coverage of APTES at different concentrations after 2 h experiment at ambient temperature.....	84
Figure 4-11. Image of relaxation mode of APTES a) 3D and b) 2D – drawn by ChemDraw software.....	84
Figure 4-12. An ideal schematic of APTES reaction with a quartz surface.....	85
Figure 4-13. Top view of APTES on a quartz surface showing the possible surface area covered by one APTES	85
Figure 4-14. Schematic reaction of polymerised APTES	88
Figure 5-1. Workflow of scale prevention study in this chapter	91
Figure 5-2. Calcium carbonate mass deposition versus concentration at 4.77 SR and 80°C after 24 h experiment.....	92
Figure 5-3. The reduction of scale deposition as function of APTES concentration at 4.77SR and 80°C after 24 h experiment	93
Figure 5-4. The scale deposition reduction as function of APTES concentration at 4.77SR and 80°C with eliminating the value at 8%	94
Figure 5-5. Low magnification SEM images of calcium carbonate deposited on a) non-treated quartz surface, b) 0.05%, c) 0.1%, d) 0.15% and e) 0.2% APTES coated quartz surfaces in low SR= 4.77 at 80°C.....	95

Figure 5-6. Low magnification SEM images of calcium carbonate deposited on a) non-treated quartz surface, b) 2%, c) 4%, d) 6% and e) 8% APTES coated quartz surfaces in low SR= 4.77 at 80°C.....	96
Figure 5-7. Systematic ranking of APTES coating performance in terms of amount of scale deposited on the quartz surface in low SR=4.77	97
Figure 5-8. High magnification SEM images of calcium carbonate deposited on a) non-treated quartz surface, b) 0.05%, c) 0.1%, d) 0.15% and e) 0.2% APTES coated quartz surfaces in high SR= 4.77 at 80°C.....	98
Figure 5-9. High magnification SEM images of calcium carbonate deposited on a) non-treated quartz surface, b) 2%, c) 4%, d) 6% and e) 8% APTES coated quartz surfaces in high SR=4.77 at 80°C	99
Figure 5-10. The mass of calcium carbonate deposited on the APTES treated surface as a function of concentration at high SR=54.8	100
Figure 5-11. The amount of scale deposition reduction as function of APTES concentration at 54.8SR and 80°C.....	101
Figure 5-12. The scale deposition reduction as function of APTES concentration at 54.8 SR and 80°C with eliminating the value at 8%.....	102
Figure 5-13. Systematic ranking of surface performance coated by APTES in terms of amount of scale reduction on surface in high SR=54.8 at pseudo-dynamic condition at 80°C.....	102
Figure 5-14. Low magnification SEM images of calcium carbonate deposited on a) non-treated quartz surface, b) 0.05%, c) 0.1%, d) 0.15% and e) 0.2% APTES coated quartz surfaces in low SR= 54.8 at 80°C	103
Figure 5-15. Low magnification SEM images of calcium carbonate deposited on a) non-treated quartz surface, b) 2%, c) 4%, d) 6% and e) 8% APTES coated quartz surfaces in low SR= 54.8 at 80°C.....	104
Figure 5-16. High magnification SEM images of calcium carbonate deposited on a) non-treated quartz surface, b) 0.05%, c) 0.1%, d) 0.15% and e) 0.2% APTES coated quartz surfaces in high SR= 54.8 at 80°C.....	105
Figure 5-17. High magnification SEM images of calcium carbonate deposited on a) non-treated quartz surface, b) 2%, c) 4%, d) 6% and e) 8% APTES coated quartz surfaces in high SR=54.8 at 80°C	106
Figure 5-18. The mass of calcium carbonate deposited on the APhS treated surface as a function of concentration at low SR=4.77 (error bars are too small and hidden in the markers).....	107
Figure 5-19. The scale deposition reduction as function of APhS concentration at 4.77SR and 80°C.....	108

Figure 5-20. Systematic ranking of surface performance in terms of amount of scale reduction on APhS-coated surface in high SR=4.77 at pseudo-dynamic condition at 80°C	108
Figure 5-21. Low magnification SEM images of calcium carbonate deposited on a) non-treated quartz surface, b) 0.03%, c) 0.06%, d) 0.12%, e) 0.18% and f) 0.24% APhS coated quartz surfaces in low SR= 4.77 at 80°C.....	109
Figure 5-22. High magnification SEM images of calcium carbonate deposited on a) non-treated quartz surface, b) 0.03%, c) 0.06%, d) 0.12%, e) 0.18% and f) 0.24% APhS coated quartz surfaces in low SR= 4.77 at 80°C.....	110
Figure 5-23. The mass of calcium carbonate deposited on the APhS treated surface as a function of concentration at high SR=54.8 (error bars are too small and hidden in the markers)	111
Figure 5-24. Scale deposition reduction as function of APhS concentration at 54.8 SR and 80°C	112
Figure 5-25. Systematic ranking of surface performance in terms of amount of scale reduction on APhS-SAM surface in high SR=54.8 at pseudo-dynamic condition at 80°C	112
Figure 5-26. Low magnification SEM images of calcium carbonate deposited on a) non-treated quartz surface, b) 0.03%, c) 0.06%, d) 0.12%, e) 0.18% and f) 0.24% APhS coated quartz surfaces in low SR= 54.8 at 80°C.....	113
Figure 5-27. High magnification SEM images of calcium carbonate deposited on a) non-treated quartz surface, b) 0.03%, c) 0.06%, d) 0.12%, e) 0.18% and f) 0.24% APhS coated quartz surfaces in low SR= 54.8 at 80°C.....	114
Figure 5-28. Comparison results of the amount of mass deposited on the surface versus coating material concentration in low and high saturation ratio solutions at 80°C after 24 h experiment.....	115
Figure 5-29. Comparison results of the surface performance versus coating material concentration in low and high saturation ratio solutions at 80°C after 24 h experiment	116
Figure 5-30. Surface charge distribution of a) untreated and b) aminosilane-treated behaviours in aqueous solution	117
Figure 5-31. The ability of water to stabilize the corresponding ammonium ion is diminished in presence of alkyl group which results in formation of stronger basis and reduction of APTES acidity	118
Figure 5-32. The theoretical basis for the diminished basicity of APhS.....	118
Figure 5-33. Phenyl group of APhS causes creating a molecule with higher pK_b , introducing weaker basis and stronger in acidity	119

Figure 5-34. Possible schematic of film formation structures of a) APTES and b) APhS on quartz surface	120
Figure 6-1. APTES and APhS molecular structures	122
Figure 6-2. Summary of Film Characterisation analyses in Chapter 6	123
Figure 6-3. A survey scan of the blank quartz surface showing main composition of the surface	124
Figure 6-4. A survey scan of the treated quartz surface by 0.06% with the main compositions.....	125
Figure 6-5. C1s high resolution spectra of the a) bare quartz and b) treated quartz by 0.6% APhS.....	125
Figure 6-6. High resolutions N1s spectra of the quartz surfaces coated with a) 0.05%, b) 0.1%, c) 0.15% and d) 0.2% APTES.....	127
Figure 6-7. Percentage of free amine and H-bonded/protonated amines of the quartz surfaces treated by different concentrations of APTES	128
Figure 6-8. High resolutions N1s spectra of the quartz surfaces coated with a) 2%, b) 4%, c) 6% and d) 8% APTES	129
Figure 6-9. Percentage of free amine and hydrogen bonded/protonated amine of the quartz surfaces coated with different concentrations of APTES	130
Figure 6-10. High resolutions N1s spectra of the quartz surfaces coated with a) 0.03%, b) 0.06%, c) 0.12%, d) 0.18% and e) 0.24% APTES.....	132
Figure 6-11. Percentage of free amine and hydrogen bonded/protonated amines of the quartz surfaces coated with different concentrations of APhS	133
Figure 6-12. Percentage of primary amines, hydrogen bonded/protonated amines and total percentage of nitrogen for the quartz crystals treated by APTES and APhS	135
Figure 6-13. Contact angle measurements for a) blank quartz surface and b-e) treated surfaces by APTES.....	138
Figure 6-14. Static water contact angles for the quartz surfaces treated by different concentrations of APTES.....	140
Figure 6-15. Static water contact angles for the quartz surfaces treated by different concentrations of APhS	141
Figure 6-16. Topography images of a) untreated quartz and b) surface treated by 0.2% APTES c) surface treated by 6% APTES and d) surface treated by 0.06% APhS	142
Figure 6-17. Roughness (rms) of blank and the treated surfaces treated by APTES in 30 min at ambient temperature.....	142

Figure 6-18. Skewness of APTES-treated surfaces after 30 min silanization in ambient temperature 143

Figure 6-19. Roughness (rms) of blank and APhS-treated surfaces after 2 h silanization in ambient temperature 144

Figure 6-20. Skewness of APhS-treated surfaces after 2 h silanization in ambient temperature 145

Figure 6-21. Roughness (rms) of blank, APTES- and APhS-treated surfaces 146

Figure 6-22. Skewness of blank, APTES-treated APhS-treated surfaces 146

Figure 6-23. Various APTES conformations on quartz surface: a) upright and b) tilted conformations, and c) hydrogen bonding 147

Figure 6-24. Schematic structures of deposited aminosilanes on quartz surface at low range of APTES (0.05-0.2%)..... 148

Figure 6-25. Schematic structures of 2-6% APTES film formed on quartz surface 149

Figure 6-26. Schematic structures of 8% APTES film possibly formed on quartz surface 150

Figure 6-27. Schematics of possible APhS conformation on quartz surface at a) 0.06%, b) 0.03% and c) 0.12-0.24% concentrations 151

Figure 7-1. Behaviour of surfaces treated by different APTES concentrations in reduction of calcium carbonate scale deposition at 80°C and after 24 h experiment at SR=4.77 as a function of primary amine contents 156

Figure 7-2. Behaviour of surfaces treated by different APTES concentrations in reduction of calcium carbonate scale deposition at 80°C and after 24 h experiment at SR=54.8 as a function of primary amine contents 157

Figure 7-3. Behaviour of surfaces treated by different APTES concentrations in reduction of calcium carbonate scale deposition at 80°C and after 24 h experiment as a function of contact angles 158

Figure 7-4. Behaviour of surfaces treated by different APTES concentrations in reduction of calcium carbonate scale deposition at 80°C and after 24 h experiment as a function of surface roughness..... 158

Figure 7-5. Experimental and estimated data versus experimental data for the surfaces treated by different APTES concentrations at 80°C and after 24 h experiment in SR=4.77 solution..... 161

Figure 7-6. Experimental and estimated data versus experimental data for the surfaces treated by different APTES concentrations at 80°C and after 24 h experiment in SR=54.8 solution..... 162

Figure 7-7. Behaviour of surfaces treated by different APhS concentrations in reduction of calcium carbonate scale deposition at 80°C and after 24 h experiment at SR=4.77 as a function of primary amine contents	163
Figure 7-8. Behaviour of surfaces treated by different APhS concentrations in reduction of calcium carbonate scale deposition at 80°C and after 24 h experiment at SR=54.8 as a function of primary amine contents	164
Figure 7-9. Behaviour of surfaces treated by different APhS concentrations in reduction of calcium carbonate scale deposition at 80°C and after 24 h experiment as a function of contact angles.....	165
Figure 7-10. Behaviour of surfaces treated by different APhS concentrations in reduction of calcium carbonate scale deposition at 80°C and after 24 h experiment as a function of surface roughness	165
Figure 7-11. Experimental and estimated data versus experimental data for the surfaces treated by different APhS concentrations at 80°C and after 24 h experiment in SR=4.77 solution	166
Figure 7-12. Experimental and estimated data versus experimental data for the surfaces treated by different APhS concentrations at 80°C and after 24 h experiment in SR=54.8 solution	167
Figure 7-13. Behaviour of surfaces treated by different APTES and APhS concentrations in reduction of calcium carbonate scale deposition at 80°C and after 24 h experiment as a function of contact angles	168
Figure 7-14. Behaviour of surfaces treated by different APTES and APhS concentrations in reduction of calcium carbonate scale deposition at 80°C and after 24 h experiment as a function of film roughness (R_{rms}).....	169
Figure 7-15. Behaviour of surfaces treated by all APTES and APhS concentrations in reduction of calcium carbonate scale deposition at 80°C and after 24 h experiment at SR=4.77 as a function of primary amine contents.....	170
Figure 7-16. Behaviour of surfaces treated by all APTES and APhS concentrations in reduction of calcium carbonate scale deposition at 80°C and after 24 h experiment at SR=54.8 as a function of primary amine contents.....	170
Figure 7-17. Experimental and estimated data versus experimental data for the surfaces treated by different APTES and APhS concentrations at 80°C and after 24 h experiment in SR=4.77 solution	171
Figure 7-18. Experimental and estimated data versus experimental data for the surfaces treated by different APTES and APhS concentrations at 80°C and after 24 h experiment in SR=54.8 solution	172
Figure 7-19. SI injection Schematic in an oil well using squeeze treatment.....	175

Figure 7-20. Schematic structure of APTES film..... 177

Figure 7-21. Schematic structures of ideal silanization of a) APTES and b) APhS
..... 180

Figure 7-22. Schematic structure of 6% APTES film formed on quartz surface ... 181

Figure 7-23. Schematic of possible APhS conformation on quartz surface at 0.06%
..... 182

List of Tables

Table 2-1. Most common mineral scale and influencing factors of formation in the oil and gas industry (10-12)	8
Table 2-2. Calcium carbonate crystallographic and favourite forming conditions descriptions (7, 22-26)	10
Table 2-3. Composition of Brine A (4)	38
Table 2-4. Composition of Brine B (4)	38
Table 2-5. Effect of deposition solvent on APTES film adhesion (271).....	53
Table 2-6. Effect of different curing methodologies on thickness of APTES films (271).....	54
Table 3-1. Different types of organosilanes with the structures, formulas and physical properties.....	59
Table 3-2. Some of the influencing factors in roughness studies (quoted from (325-327))	71
Table 4-1. K_{obs} at various concentrations of APTES.....	82
Table 4-2. Mean surface coverage of APTES at each concentration	83
Table 6-1. Ratio of primary amines to hydrogen/protonated amines on the treated surfaces by APTES (0.05%-0.2%)	128
Table 6-2. Ratio of primary amines to hydrogen/protonated amines on the treated surfaces by APTES (2%-8%)	130
Table 6-3. Ratio of primary amines to hydrogen/protonated amines on the treated surfaces by APhS (0.06%-0.24%).....	133
Table 7-1. Calculated constants in Equation 7-2	160

Nomenclature

TDS	Total Dissolved Solid
Θ	contact angle
$(1 - \Theta)$	remaining free available sites
A	effective area of the electrode (m^2)
Å	Angstrom
A	surface area of crystals
BE	binding energy of the emitted electron
C	concentration of the reactant ($mol.l^{-1}$)
C	empirical constant
Ca	molar concentration of Ca^{2+}
CP	coating performance
D	constant
$D(E_{kin})$	detection efficiency of transmitted each electron transmitted
d_q	quartz density ($2.648 g/cm^3$)
EK	kinetic energy of the photoelectron
$f(\theta)$	correction factor depends on nucleation type
f_o	resonance frequency (Hz)
h ν	photon energy
I	intensity of a photoelectron
J	X-ray flux in photons/ $cm^2.s$
K	the solubility product. Depending on temperature and pressure
k_a	adsorption constant
K_c	crystal growth constant
k_d	desorption constant
K_{eq}	equilibrium constant
L	angular asymmetry of the intensity of the photoemission from each atom
N	number of crystals
n	number of atoms of the element per volume
N	number of crystals
N_A	Avodadro's number
Θ	measured angle of emission of electron from surface
Θ	Fraction of surface occupied by adsorbate
$^{\circ}C$	Centigrade celsius
R	gas constant (J/mol.K)
R_{rms}	Roughness (m)
SI	superstation index
S_{ku}	kurtosis
S_q	Root mean square height
S_q	computes the standard deviation for the amplitudes of the surface (RMS)
SR	Saturation Ratio
S_{sk}	Skewness

T	analyser transmission
T	absolute temperature (Kelvin)
T	temperature
t_{ind}	induction time
V_m	molecular volume
α	ion activity of calcium and bicarbonate in the solution (mol.l^{-1})
α_{0-3}	constants
β	geometric factor for the spherical nucleus
γ	ionic activity coefficient
γ	surface energy (J/m^2)
γ_l	liquid surface tension
γ_s	surface energy of solid
γ_{sl}	surface energy of solid/liquid interphases
Δf	measured frequency shift (Hz)
ΔG	Gibbs free energy
Δm	the mass change (g)
η_l	Viscosity of the liquid in contact with the electrode
$\lambda (E_{\text{kin}})$	inelastic mean free path of photoelectrons
μ_q	shear modulus of the quartz ($2.947 \times 10^{11} \text{ g}\cdot\text{cm}^{-1}\cdot\text{s}^{-2}$)
ρ_l	density of liquid in contact with the electrode
$\sigma(E_{\text{kin}})$	photoelectric ionization (cm^2)
ϕ_s	photometer work function

Publication

N. Kazemi, M. Wilson, N. Kapur, N. Fleming, A. Neville, "Preventing Adhesion of Scale on Rock by Nanoscale Modification of the Surface". Paper 156955, Society of Petroleum Engineers (SPE). SPE International Oilfield Nanotechnology Conference and Exhibition, Noordwijk, Netherlands, 12-14 June 2012.

Chapter 1

Introduction

Mineral scale deposition is one of the major problems in the oil and gas industry causing production loss by blocking pipelines (Figure 0-1) and pores of formation rock (1). Scale is defined as the deposition of sparingly soluble inorganic minerals (mainly carbonate and sulphate scales), such as CaCO_3 , BaSO_4 , CaSO_4 , etc. (2) when production water becomes supersaturated. Scaling occurs in two different mechanisms, mixture of two incompatible fluids and pressure loss and temperature change in the system:

1. Seawater containing sulphate ions is injected to support the pressure of reservoir for enhanced oil recovery. Due to incompatibility of seawater with formation water – which contains barium, strontium, etc. – sulphate scales may precipitate where these two fluids meet.
2. Due to depletion of reservoir, the pressure of production fluids decreases resulting in evaporation of carbon dioxide from fluid phase to gas phase; this may lead to risk of carbonate scale precipitation. In addition, variation of production temperature may facilitate or worsen the probability of carbonate precipitation.



Figure 0-1. Image of mineral scale which has been formed inside the pipe (1)

The consequence of scaling can be major and costly leading to lose a well in some cases. Hence, chemical treatments are normally used in the oil and gas industry to prevent and control scaling in the production system. Scale inhibitors are used in squeeze treatments or in chemical injection lines to slow down nucleation and growth of scaling in the solution and on the surface. Inhibition of production system from scaling is an expensive treatment; hence many works have been carried out to improve the current methodologies.

Attention in the oil and gas industry had been paid to study the precipitation of mineral scale in bulk solution rather than surface deposition. Recently, surface engineering was studied (3-6) to better understand scale deposition phenomena on the surface. Various types of substrates such as copper, different types of coating on stainless steel, Diamond-Like Carbon (DLC), polytetrafluoroethylene (PTFE), polymers, etc. were studied to comprehend the mechanisms of crystallisation on surfaces. Although it well known in biofouling research that surface energy is the dominant factor to reduce amounts of biofouling on the substrate, the effects of different properties of surface on mineral scale deposition are not yet fully understood in the oil and gas industry. Thus, chemical and physical characteristics of substrates such as surface composition, wettability and roughness were investigated. It was shown (3-9) that surface characteristics can influence amounts of mineral scale deposition and morphology of scales; present a scanning electron microscope (SEM) image of calcium carbonate on a surface which shows that the scale followed the pattern of the surface.

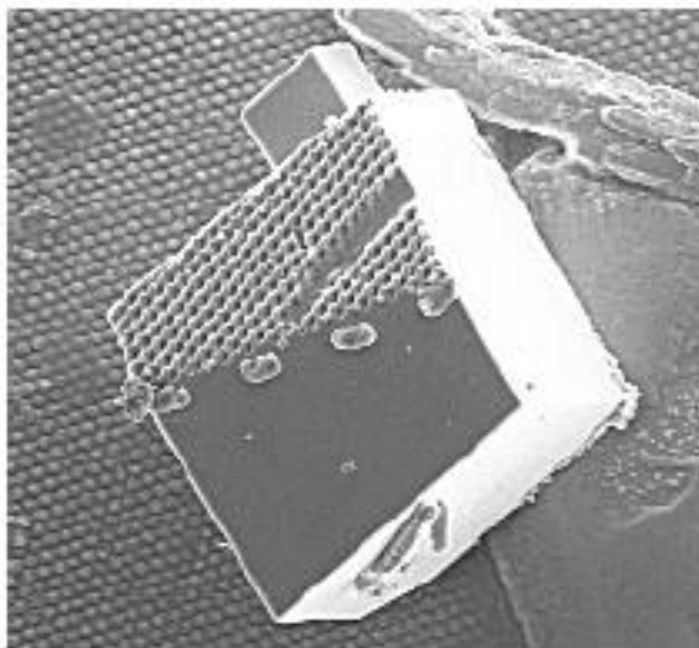


Figure 1-2. SEM image of calcium carbonate with the surface pattern

As mentioned, scaling can occur inside formation rock which causes blocking the oil path from reservoir through near wellbore area. This thesis focuses on possible treatments on formation rock in order to reduce the risk of inorganic scale depositions.

1.1 Objective

The aim of this project is to study the possible chemicals to treat internal surfaces of formation rock being able to reduce or prevent mineral scale deposition. This could be used in addition to current squeeze treatments or an independent methodology for inhibition mineral scale deposition near wellbore. However, the main focus is to demonstrate feasibility of such techniques to be applied to the oil and gas industry.

As mentioned, using surface engineering to reduce the potential of mineral scale deposition was recently started, which is applicable to critical surfaces like downhole chemical valves and choke at subsea templates. The major differentiation between the coating studies on metal surfaces (for topside purposes) and this research is that treatment has to be performed remotely and offshore, which makes this work more complicated. Effects of surface alteration due to the chemical treatments on hydrocarbon production need to be considered in this research. This means that the treatment needs to be thin enough not to block the hydrocarbon path. This was the one of the main challenges in this work. However, the main challenge of the work was to identify chemicals that have potential to reduce the amount of mineral scale deposition and simultaneously to have covalent bonds on formation rock. The second consideration was to find a methodology to be applicable to in the oil and gas industry and could be performed remotely offshore. It could be very beneficial if the methodology for applying these chemicals in the near wellbore area introduced in this work could use one of the current methods in scale managements like squeeze treatment in order to treat the formation rock near the wellbore by some minor modifications. Therefore, the main objectives of this work were:

- ❖ To identify possible chemicals to treat formation rock that have specific features such as:
 - Having strong affinity to the formation rock
 - Reducing mineral scale deposition on rock surface
 - Being remotely applied to the near wellbore area

- Not blocking internal pores of formation rock
- Having correct wettability for hydrocarbon production

- ❖ Understanding film conformations formed on the surfaces by these chemicals

- ❖ Understanding effects of different properties of the treated-surface on scale deposition

1.2 Thesis outline

In this thesis, eight chapters are presented consists of Introduction, Literature Review, Methodology and Experiments, Theory and Techniques, Film Formation, Scale Prevention Performance, Film Characterization, Discussion, and finally Conclusion and Future work.

In Chapter 2, the inorganic scale formation problems, the factors affecting scale formation, coating materials on metal surfaces and their effects on scaling, self assembled monolayer (SAM) technique, aminosilanes and their film structures on surfaces, and influence of different parameters on aminosilane film formation will be reviewed.

Chapter 3 presents methodology and experimental techniques of this PhD. It first reviews different types of organosilanes followed by describing the experimental methodology of this work. In addition, the characterisation methods to study the chemical and physical properties of the surfaces are included in this chapter. At the end, the aminosilanes film kinetics are discussed.

In Chapter 4, formation and the kinetics of 3-aminopropyltriethoxysilane (APTES) films at different concentrations on quartz crystals are studied by QCM. In this chapter the coverage of films obtained by various APTES concentrations are calculated. Matlab software is also used for curve fitting. Besides, the maximum mass APTES approximately required for creating SAM on quartz crystal is calculated and compared with the results of QCM.

In Chapter 5, performances of APTES and p-aminophenyltrimethoxy silane (APhS) on reduction of calcium carbonate scale on treated-surfaces are

investigated. Reduction of scale deposition on treated-surfaces by various concentrations of APTES and APhS molecules are measured. Scanning Electron Microscopy (SEM) and weighing scale are used to study the morphology and amount of mass on the quartz surfaces, respectively.

In Chapter 6, chemical and physical properties of APTES and APhS films treated by various concentrations are studied by different characterisation techniques such as X-ray Photoelectron Spectroscopy (XPS), contact angle and roughness measurements. The results are compared with literature to better understand film formation mechanisms. These results are also to suggest possible conformations obtained on the surface by using different APTES and APhS concentrations, which are later related to performance of the treated surfaces on reduction of calcium carbonate deposition (this is presented in Chapter 8).

In Chapter 7, the performance APTES and APhS films on reduction of scale deposition are interpreted by the film properties created on the surface. The effects of surface composition, wettability and roughness on reduction of scale deposition are individually studied. Contribution of each property on total calcium carbonate mass reduction is evaluated. The main contribution of this work is presented in this chapter.

In Chapter 8, the main conclusion of this research and the possible future work in order to develop this methodology to be employed in the oil and gas industry are presented.

Chapter 2

Literature Review

2.1 Introduction

This chapter reviews the scale formation process mainly calcium carbonate, Self-Assembly Monolayer (SAM) and coating applications to inhibit mineral scale deposition. In the first part of this chapter the mechanism of calcium carbonate scale formation and precipitation is reviewed followed by scaling phenomenon in bulk and surface. Scale inhibition by scale inhibitors and squeeze treatment are also discussed briefly in this chapter. The second part of this chapter presents the literature related to effects of various substrates on scale deposition.

SAM technique is reviewed to modify substrates for changing the surface characteristics. SAM of organosilane followed by behaviours of different aminosilanes during film formation and conformations of aminosilane films on the substrate are also studied in this chapter. Different surface characteristics techniques are presented to analyse the aminosilane film formed on the surface.

2.2 Scale formation literature

One of the major issues in the oil and gas industry is formation and precipitation of mineral scales. The challenge is that mineral scales are sparingly soluble depending on conditions in the system. There are two phenomena that cause scale formation: i) reservoir conditions such as temperature and pressure are changed resulting in precipitation of carbonate and halite scale and ii) where seawater meets formation water in reservoir which results in sulphate scales. In fact scale forms to equilibrate the system by reactions between ions in the system. Carbonate scale normally is due to producing formation water from the reservoir along with hydrocarbon. On the other hand, sulphate scales are formed due to enhance oil recovery (EOR), as produced water and/or seawater are used to maintain the pressure in reservoir. Most common mineral scales in the oil and gas industry are presented in Table 2-1.

Table 2-1. Most common mineral scale and influencing factors of formation in the oil and gas industry (10-12)

Scale mineral	Chemical formula	Influencing factors	Relative solubility (mg/l)
Calcium carbonate	CaCO ₃	p _{CO2} , total pressure, temperature, TDS	196
Iron carbonate	FeCO ₃	p _{CO2} , TDS, temperature, total pressure, corrosion, pH	100
Barium sulphate	BaSO ₄	Pressure, temperature, TDS	44
Strontium sulphate	SrSO ₄	Pressure, temperature, TDS	520
Calcium sulphate	CaSO ₄	Pressure, temperature, TDS	3270

Production loss and damage to equipment (mainly to safety valves) are the main issues with scale formation which requires a costly remedy. Scale formation is a chemical phenomenon being affected by several chemical and physical factors. Reservoir reached equilibrium conditions (pressure, temperature and ions saturation) with formation rock after millions of years. Any changes in these conditions which can be during drilling, production or injection of fluid for enhanced recovery can disturb the equilibrium. For example, CO₂ - which plays an important role in calcium carbonate scale formation – is at equilibrium with hydrocarbon phases and formation water in the reservoir. The moment that any changes happen in the reservoir conditions such as pressure depletion and evaporation of CO₂ from liquid phase to gas phase - these increase pH of liquid phase - resulting in precipitation of calcium carbonate. Mechanical methods are normally employed to remove scale in production pipes and perforations. However chemical methods are used to remove and also to prevent scale formation in near wellbore, pipelines, safety valves and separators. Removal of scale by acid treatments is not always efficient specifically for barium sulphate (BaSO₄) due to strong affinity of barium sulphate nature to surface and very low solubility. Hence, preventing is more favourable amongst operators than other methods. Scale inhibitors (SIs) are squeezed into reservoir from production line into near wellbore area to adsorb or precipitate onto the rock surface. The well is shut for 12-24 hrs in order to give

formation rock sufficient time to adsorb scale inhibitor (SI). The scale inhibitor desorbs from rock surface during production in order to prevent scale formation in near the wellbore and production system. In order to monitor performance of squeeze job, the concentration of SI desorbed to production fluid is measured. Normally a low concentration of SI is required to prevent scale formation, which is called minimum inhibitor concentration (MIC). Wells are re-squeezed when the concentration of SI in production line reaches below MIC. In addition, SI is sometimes injected continuously into production well or wellhead to inhibit scale formation in production facilities if the risk of scale formation is not high. The squeeze treatment procedure will be discussed later in this chapter.

2.2.1 Scale formation location

Scale phenomenon occurs in different places during drilling, water pumping and production systems which due to cost of remedy (squeeze treatment, downhole chemical injection line, acid treatments, etc.) and environmental issues, some areas become more important. One of the places that scaling takes place is near the wellbore in porous of rocks resulting in a thick and stiff layer which blocks the oil path. Scaling can happen on topside and downhole and ions in the water can react in different conditions and form different types of inorganic scaling such as calcium carbonate and barium sulphate. Calcium carbonate formation normally occurs where the pressure drops in the system. Scaling phenomenon precipitates in bulk or deposits on the surface which the amount of precipitation can be studied by change of calcium concentration in solution (13) and turbidity measurements (14). Scale precipitation in the bulk is not a problem if the scale does not deposit on the surface or adhere on the surface (15, 16).

2.2.2 Calcium carbonate scale formation

The most common type of mineral scale is calcium carbonate occurring due to the mixture of calcium cations with carbonate ions in the solution, and reduction of pressure in system. Calcium carbonate (CaCO_3) precipitations are found in three different crystal structures: i) calcite, ii) aragonite and iii) vaterite; morphologies are presented in Figure 2-1. Calcite and aragonite are found in nature and are the most stable forms of calcium carbonate crystals; in contrast, vaterite is not stable (17). The tendency of calcite to stick to surface is higher than others specially vaterite which is easier to be removed from surface (18, 19). In order to characterise the

morphology of calcium carbonate, various techniques such as Raman Spectroscopy (20) and X-ray diffraction (17) are used.

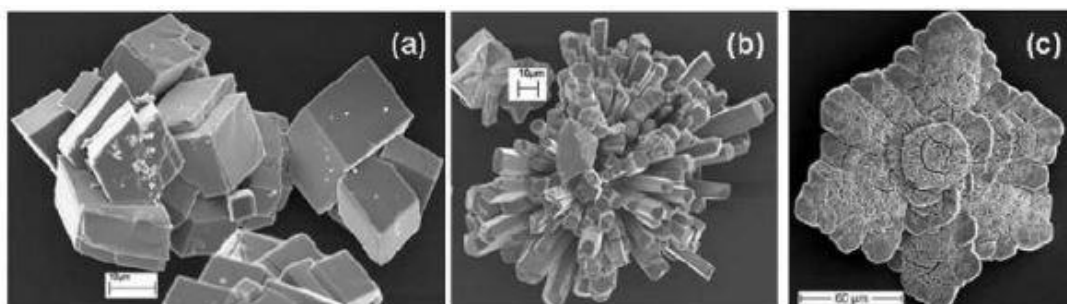


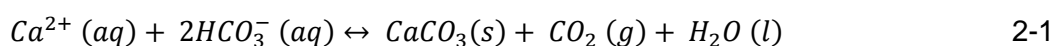
Figure 2-1. Calcium carbonate morphology: a) calcite, b) aragonite and c) vaterite (21)

The physical and chemical factors determining calcium carbonate crystallisation include temperature, the concentration of the reactant, pH value of the solution and presence of impurities in the system. The crystallography of calcium carbonate is presented in Table 2-2.

Table 2-2. Calcium carbonate crystallographic and favourite forming conditions descriptions (7, 22-26)

	Calcite	Aragonite	Vaterite
Crystal Sytem	Hexagonal-rhombohedral	Hexagonal	Hexagonal
Morphology	Cubic to rhombohedral	Needlelike	Spherical or dislike
Favourite condition	<ul style="list-style-type: none"> ❖ Instantaneous nucleation ❖ Room temperature 	<ul style="list-style-type: none"> ❖ Temperature above 50°C ❖ High pH 	<ul style="list-style-type: none"> ❖ High supersaturation ❖ Strong affinity to spread laterally
State	<ul style="list-style-type: none"> ❖ Most stable ❖ Single crystal 	<ul style="list-style-type: none"> ❖ Stable ❖ Single crystal but more porous 	<ul style="list-style-type: none"> ❖ Metastable ❖ Microcrystalline ❖ porous
Density (g/m³)	2.71	2.93	2.66

The main effective parameter in formation of calcium carbonate is evaporation of CO₂ where the partial pressure of carbon dioxide decreases to below bubble point which results in an increase in calcium carbonate precipitation.



In a related manner, concentration of carbonic acid reduces due to evaporation of CO₂ from the system, which causes increasing pH of the solution. Calcium carbonate solubility is related to the pH solution and reduces by increasing the pH.

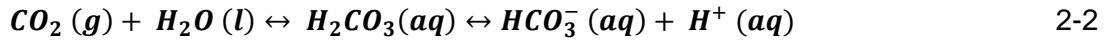


Figure 2-2 presents the temperature-pressure dependency of carbon dioxide.

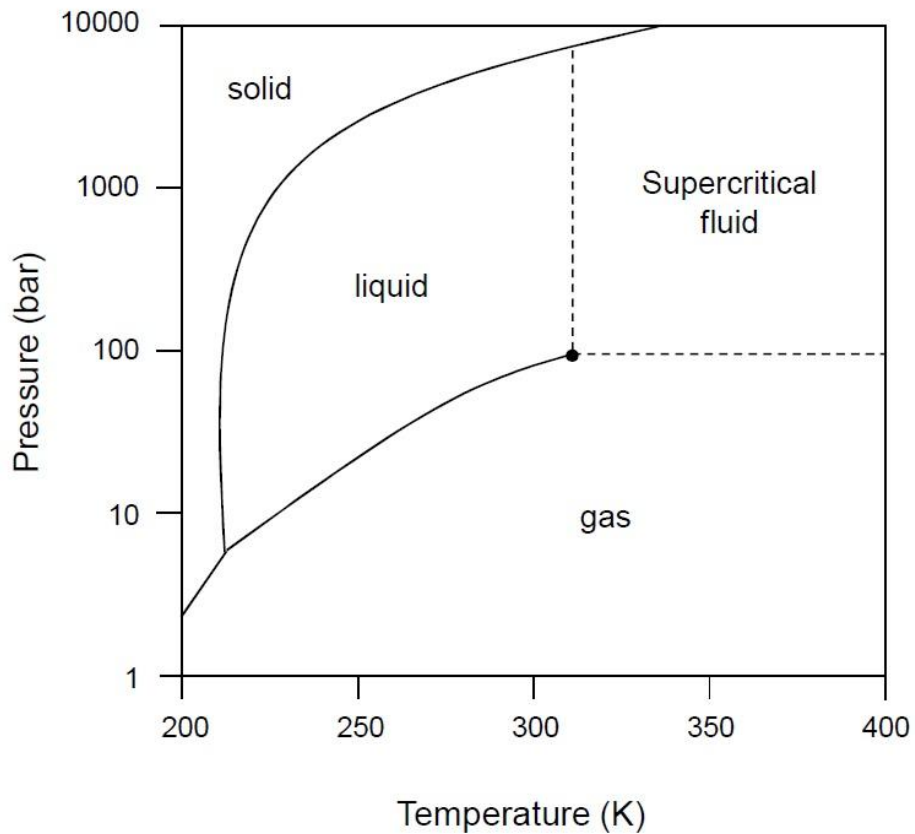


Figure 2-2. Temperature-pressure diagram of phase dependency of carbon dioxide (4)

2.2.2.1 Supersaturation, a driving force of calcium carbonate scale formation

The reaction of calcium carbonate formation is shown below:



Saturation of the solution system is the foremost determining factor of crystal formation in the solution or precipitation on the surface (27). The saturation ratio of calcium carbonate is presented below.

$$SR = (\alpha_{Ca^{2+}} \times \alpha_{HCO_3^-})/K$$

Equation 2-4

Where α (mol.l^{-1}) is the ion activity of calcium and bicarbonate in the solution and K is the solubility product. Depending on temperature and pressure, the value of K changes, which was found 4.55×10^9 at 25°C and 1.06×10^9 at 80°C by Larson and Buswell (28). Also, $\alpha = \gamma \times C$ where γ is ionic activity coefficient and C (mol.l^{-1}) is concentration of the reactant. Thermodynamically, formation of scale happens when SR is above 1. SR is categorized into three ranges presented below:

- $SR < 1$ shows that the solution is under saturated and mineral scale cannot form in the solution.
- $SR = 1$ determines that the solution is saturated, which means that formation and dissolution of scale are in equilibrium and precipitation cannot be formed. This means that nucleation is not created and the existed crystal does not grow.
- $SR > 1$ indicates that the solution is in the crucial condition and is supersaturated. Scale can form.

$SR > 40$: spontaneous calcium carbonate precipitation occurs.

Saturation ratio (SR) is the determining element in a solution to control precipitation of mineral scales. In case of SR above 1, some mineral salts need to precipitate from the solution in order to make solution equilibrium. Several parameters such as temperature, pH and pressure of the solution affect the SR value the solution; these parameters may continuously alter during hydrocarbon production. Hence, SR may be known as the thermodynamic “driving force” for precipitation. However, SR is not the absolute factor of precipitation of scale where adequate energy to start the nucleation of crystal is required in a solution (27, 29). As mentioned earlier, evaporation of carbon dioxide from production is the main factor of scaling. SR is easy information can be obtained as an indication of possibility of scaling. Although it may be convenient to predict bulk scale formation from SR ; one solution with high value of SR can be without scale precipitation. This means that until providing necessary energy to initiate nucleation of scale, the solution can stay supersaturated. The thermodynamic driving force of scale precipitation is governed by Gibbs free energy ($\Delta G = G_2 - G_1$), which is the difference in free energy of crystallization in a supersaturation solution (phase 1) and in the crystals (phase 2). When $\Delta G < 0$ scale formation spontaneously occurs.

2.2.2.2 Basic principles of scale formation: induction, nucleation and growth

The key factor of crystallization is saturation of the solution, which indicates the possibility of crystallization. This is schematically presented in Figure 2-3, which is divided into three major zones: undersaturated, saturated and supersaturated zone. Undersaturated zone is under the solubility line; no homogeneous nucleation starts and a crystal added to the solution may dissolve depends on the solution SR value. Saturation value – which is shown by solubility curve - is measured experimentally. In this stage, homogeneous spontaneous nucleation cannot thermodynamically happen and the size of crystals placed in the solution stay constant and will not dissolve. The next zone - supersaturation area - includes metastable, labile supersaturation and precipitation area. In the metastable area, homogeneous nucleation does not occur; in contrast, the size of the crystal placed in the solution can increase in this stage. Contrary to metastable zone, both the size of the crystal grows and homogeneous nucleation can occur in labile zone. Seeds placed in the solution at labile stage can disturb the solution condition and create undue nucleation. In the last zone - precipitated area - crystals grow and aggregate on the surface.

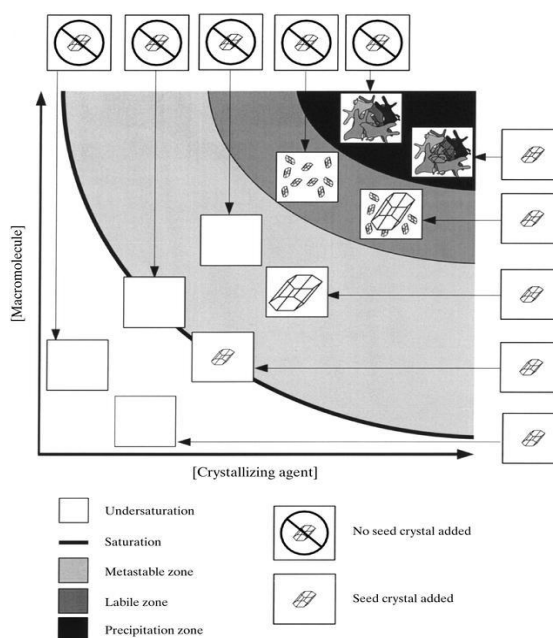


Figure 2-3. Two-dimensional crystallization procedure with and without adding seed crystal (27)

Crystallisation of calcium carbonate includes three stages: induction, nucleation and growth.

2.2.2.2.1 Induction

Spontaneous nucleation does not occur in the metastable zone. In order to allow nucleation to happen, the solution needs to be in an unstable zone, which may take some time. This period is called induction time, t_{ind} , which is the time that the system remains in metastable zone. The first nuclei in the solution cannot be spotted, hence it is not possible to accurately measure induction time (30). Several theoretical approaches have been suggested to predict induction time of calcium carbonate. One assumption is based on that formation of huge amount of nuclei and their growth are related to distribution of metastable equilibrium (31) i.e. polynuclei mechanism in the solution transfer the metastability of the solution to next stage. Another presumption is that the occurrence of first nuclei is the sign of metastable equilibrium in the solution (32). Based on simple nucleation assumption to model the induction process, the induction time (t_{ind}) can be just correlated to saturation of the solution which is given in Equation 2-5:

$$\log(t_{ind}) = C + \frac{B}{(\log S)^2 T^3} \quad \text{Equation 2-5}$$

Where C is an empirical constant and dimensionless, T is the absolute temperature (Kelvin) and B is:

$$B = \frac{\beta \gamma^3 V_m^2 N_A f(\theta)}{(1.3R)^3}$$

Where β is a geometric factor for the spherical nucleus, γ is the surface energy (J/m^2), V_m is the molecular volume, N_A is Avogadro's number $f(\theta)$ is a correction factor depends on nucleation type and R is the gas constant ($J/mol.K$).

Equation 2-5 gives a linear correlation between t_{ind} and $1/(\log S)^2$, which assumes homogeneous nucleation in the solution (33, 34). However, heterogeneous nucleation in flowing system may occur (34). Prediction of induction time in flowing system was developed based on a semi-empirical correlation (34):

$$\log(t_{ind}) = \alpha_0 - (\alpha_1/SI) - (\alpha_2/T) + (\alpha_3/SI.T) \quad \text{Equation 2-6}$$

Where α_{0-3} are constants depend on flow rate and calculated experimentally, SI is supersatation index and T is temperature.

In order to experimentally measure the induction time, the period between supersaturation and the first visible change in the physical properties such as turbidity, solution conductivity or composition is measured as the induction time. Hence, experimentally measurement of induction time is affected to a degree by measurement instrument and the method of detection. Induction time can be

determined by several methods such as visual, turbidimetric and conductimetric (35-37). The elapsed time after mixing the solutions and observation of first crystals or turbidity by naked eyes is measured as the induction time. If this period is measured by photocolourimeter, this is called turbidimetric method. Measuring the conductivity of the solution can give useful information; this is used in conductometric methods. The time - after mixing the solution - when the solution becomes steady in terms of conductivity is considered as the induction time.

2.2.2.2.2 Nucleation

Changes in the solution after induction period is due to crystal nucleation and growth of crystals, which is called nucleation time, i.e. the period when a large amount of crystals form quickly after induction period in the metastable zone. The scaling process occurs in several sequences: (i) transporting scale lattice ions up to the crystal surface or an external substrate with suitable nucleation sites; (ii) on the substrate, ions in the solution may adsorb on the surface; (iii) the paired ions experience diffusion to the practically active sites; and (iv) completing crystal lattice by attaching paired ions to the growth sites, simultaneously with dehydration (38).

The number of small particles formed in the nucleation stage dramatically increases along with the growth of particles take place during this period. It is assumed that the number of the crystals precipitated in the solution increases very quickly at the beginning of the nucleation and growth mechanism happens at the later step of nucleation process (39, 40). On the other hand, there is another assumption that considers these two mechanisms (nucleation and growth) taking place at the same time (41, 42). It seems that detecting whether these mechanisms happen sequentially or simultaneously is difficult for interpreting the experimental results purposes, hence it is presumed that both the size and distribution of crystals happen at the same time (43, 44).

Nucleation process can also be categorised in primary and secondary nucleation, which the earlier includes homogeneous and heterogeneous nucleation; this is schematically illustrated in Figure 2-4. Homogeneous nucleation mechanism takes place in the absence of external stimuli and in the bulk (45, 46), in contrast, heterogeneous nucleation grows on an active site.

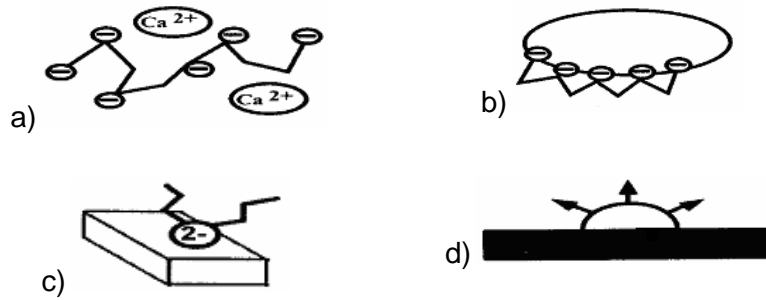


Figure 2-4. Schematic of scale formation a) ion pairing, b) prenucleation aggregate growth, c) homogeneous nucleation and d) heterogeneous nucleation (47, 48)

The kinetics of scaling is the electrostatic interactions between ions dissolved in the solution that leading to ion pairing stage; this is shown in Figure 2-4a). At higher supersaturation the number of ion-paired increases resulting in aggregation of these ion pairs; this builds larger particles. These particles are in dynamic equilibrium in the solution (see Figure 2-4b). Nucleation of solid-state particles starts once the aggregate particles in the solution grow to a critical size (49). This phenomenon requires sufficient energy which is provided by supersaturation in the system. Since particles are not in equilibrium phase in the solution, the precipitation commences (49); this is illustrated in Figure 2-4c and Figure 2-4d as a schematic of homogeneous and heterogeneous nucleation, respectively. Two enthalpy terms control the initial homogeneous nucleation in a system which are related to the nuclei radius: (i) the favourable free energy referring to release of supersaturation (ΔG_v) and (ii) unfavourable free energy relating to the interfacial energy i.e. creation of a surface (ΔG_s). The latter is corresponded to the variation of free energy between growing crystalline surface and the solution. This is presented in Figure 2-5. The overall free energy increases up to critical size of crystal. The overall free energy decreases when the crystal size increases larger than critical size. This phenomenon leads to create stable nuclei which grow to build macroscopic crystals. Critical nuclei - which refers to maximum free energy - is conversely corresponded to logarithm of the solution saturation (32). The determining factor for formation of new nuclei is the rate of overcoming the maximum overall free energy by aggregation of crystals. At low supersaturation, the nucleation rate can surmount a few amount of critical size of nuclei, but when the saturation ratio goes beyond critical value, nucleation rate rapidly increases and nucleation is extensively occurs (42).

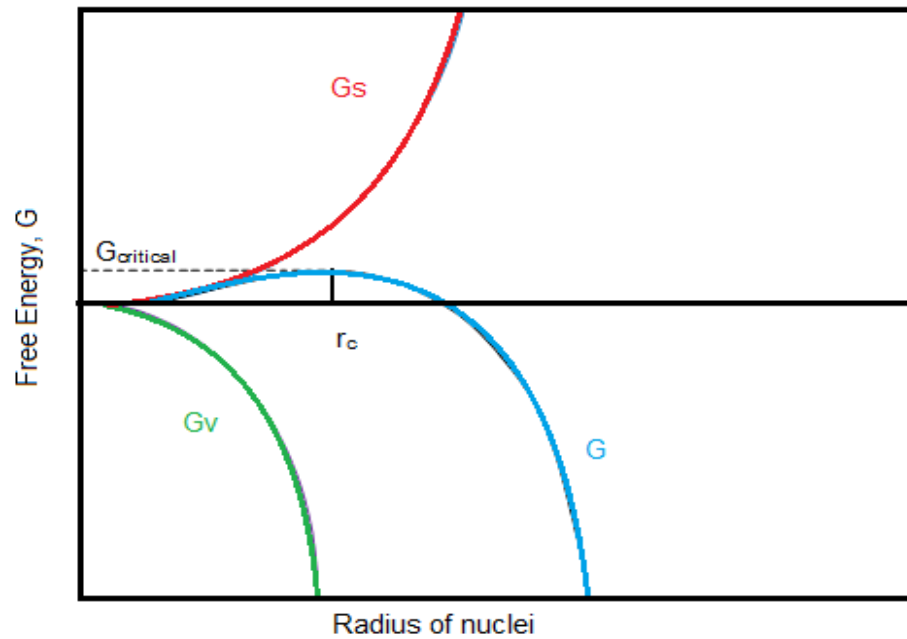


Figure 2-5. Free energy diagram of nucleation as a function of nuclei radius (32)

The number of crystals created in saturated solution is given by Equation 2-7 (31):

$$\log N = D - a_N / (\log Sa)^2 \quad \text{Equation 2-7}$$

Where N presents the number of crystals, D is constant, the slope of log N versus $(\log S_a)^{-2}$ and saturation ratio index are shown by a_N and S_a , respectively.

It can be assumed that both heterogeneous and homogeneous nucleation happen at a heterogeneous interface since disregarding the presence of dust, impurity, etc. in the bulk solution is difficult (29). Generally, it is assumed in the oil and gas industry that the scale precipitates on surfaces existing in the production system could be surfaces of the pipelines, existing scale deposits or formation rock. Since the presence of such surfaces in the production system decreases the free energy barrier, the scaling in production fluid favours heterogeneous nucleation on the surfaces than homogeneous nucleation (50). These nucleation mechanisms (either homogeneous or heterogeneous) are categorized as primary nucleation (32), which become highlighted in very high supersaturated solutions. However, such mechanisms cannot contribute in low saturation ratio and other nucleation processes describe nucleation in low saturation solution, which is classified as secondary nucleation. This type of nucleation only happens in the presence of existing crystals in the solution (51). The secondary nucleation occurs for several

reasons (51, 52), for instance, if first dry crystals are introduced in the solution, primary breeding takes place. The small crystal bit can be washed by the solution to create a new nuclei in the system (29). Microscopic observations of a growing crystal on a solid rod illustrated that the crystal surface can assist to a rapid secondary nucleation process (53). Appearance of a crystal solid in the system consists of several stages such as primary and secondary nucleation, crystal growth and secondary changes (recrystallization, aggregation, etc.) (54). The process of scale formation and precipitation is shown in Figure 2-6.

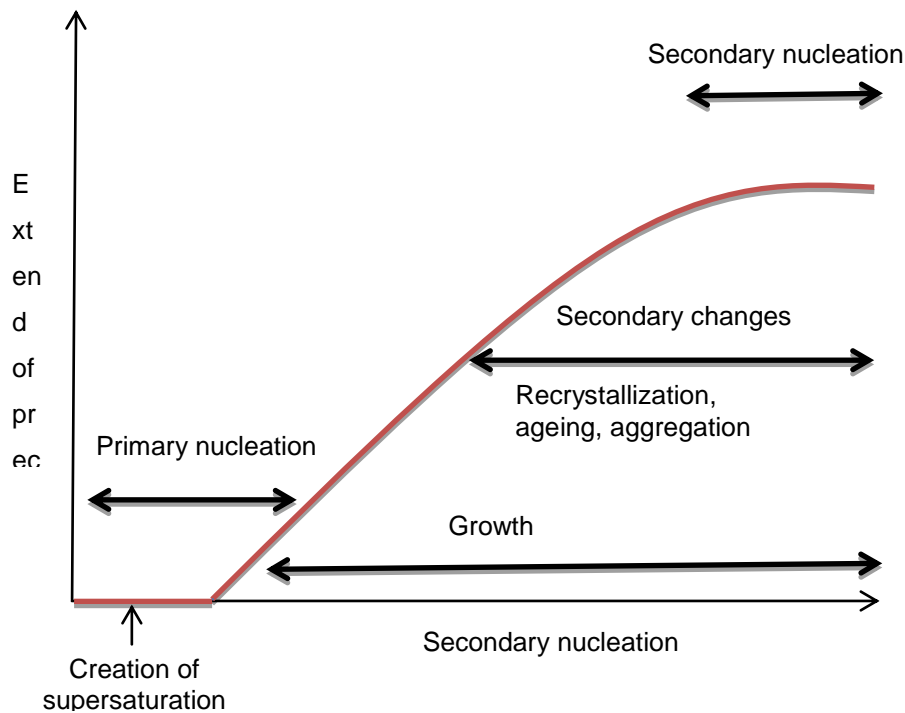


Figure 2-6. Kinetics of scale formation and precipitation (54, 55)

2.2.2.2.3 Growth

After occurrence of nucleation (homogeneous and heterogeneous), crystal growth continues in order to reduce the saturation of the system. There are many theories (surface energy, adsorption layer and dislocation theories) which improved the crystal growth mechanism. The first hypothesis was suggested by Noyes and Whitney describing the crystal growth as diffusion process (45), later this theory was developed by Berthoud and Valetton and two-step process was defined for growth of crystals: i) diffusion and ii) integration process, which means that the soluble ions diffuse from the solution to the crystal surface followed by aggregation into crystal lattice (45).

The surface energy theories inspired by Gibbs energy by assuming a perfect crystal growth in a certain volume to have a minimum total surface free energy (45). This indicates that the shape of crystal remains constant and the size of a crystal increases proportionally to its surface energy. This theory was challenged by Volmer who suggested that the presence of a self-adsorbed layer of crystals in growth process (56). Volmer's theory assumes a mobile adsorption process on the surface allowing the growth mechanisms happen without nucleation (56). Following Volmer's work, other proposals for growth of crystal based on adsorption layer theory were developed such as Frank-Van der Merwe method (two-dimensional growth), Volmer-Weber (three-dimensional growth) and Stranski-Krastanov mode. Figure 2-7 presents the different modes of crystal growth based on adsorption layer theory. In Frank-Van der Merwe mode, a new layer can adsorb when the underneath layer is complete; on the other hand, in Volmer-Weber mode, different layer can form simultaneously. Strabski-Krastanov mode, the crystal growth commence with a two-dimensional mode followed by a three-dimensional mode which is a combination of both Frank-Van der Merwe and Volmer-Weber modes (57). These theories are able to explain the crystal growth in a locally high supersaturation.

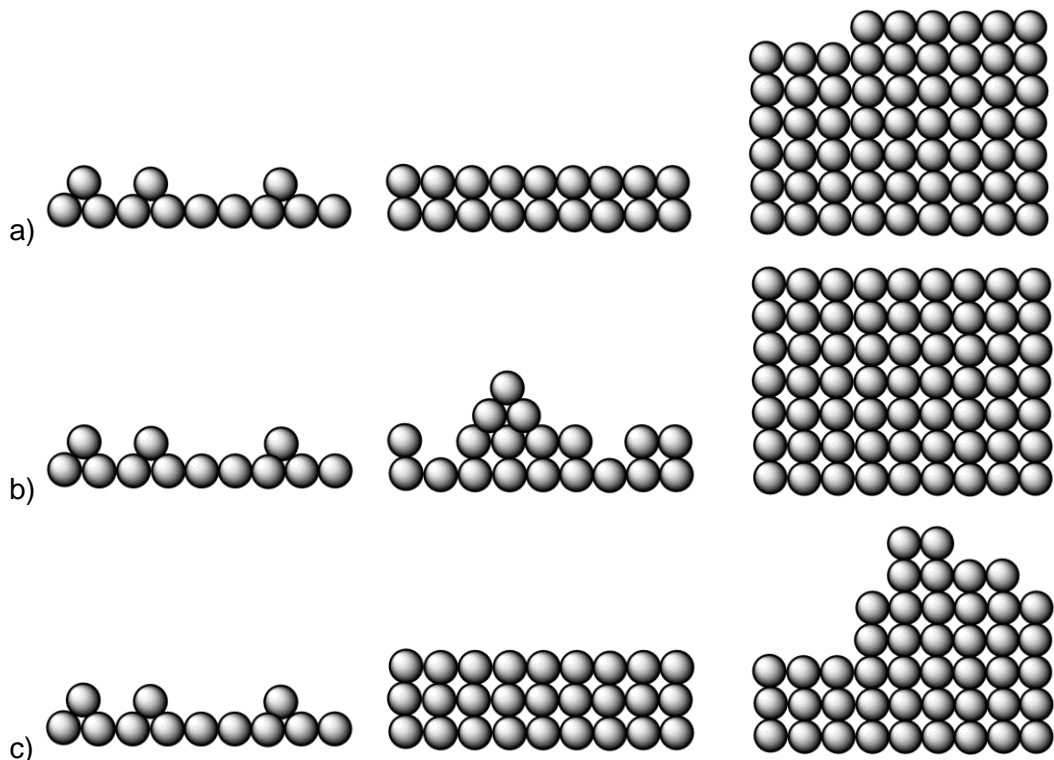


Figure 2-7. Different processes of crystal growth: a) Frank-Van der Merwe method b) Volmer-Weber method c) Stranski-Krastanov

Crystal growth in low supersaturation was first explained by Frank based on dislocation theory present in the crystal indicating spiral crystal growth where the edge of crystal is dislocated and twisted (58); this is shown in Figure 2-8.

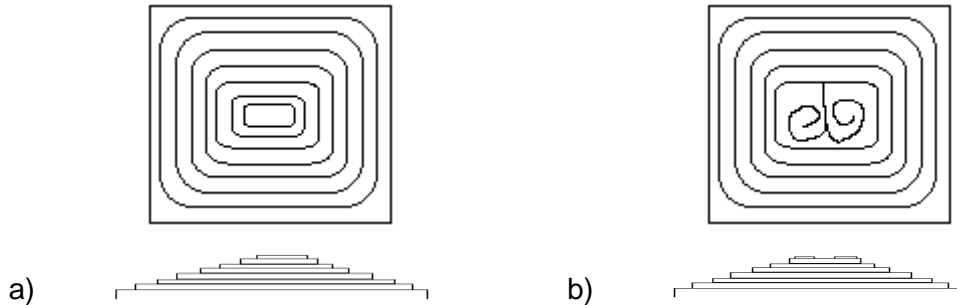


Figure 2-8. Growth of crystal by screw dislocation process at low SR: a) one screw dislocation b) two screw dislocations

Based on this theory, the available molecules expose to the surface of crystals in order to integrate and form into crystal lattice (45). In addition, the crystallisation growth was defined as a fact which is depended to other factors such as surface energy (45) i.e. the lower the surface free energy is, the crystal become more stable.

When the nucleation either homogeneous or heterogeneous occurs, the saturation ratio of the solution decreases owing to increase of the crystals size. Crystal growth consists of an increase in the size of crystal together with aggregation of particles. The mechanism of scale formation is complex and depends on several factors (47), which is depicted in Figure 2-9. Although nucleation process is expected to start after nucleation, these phenomena are assumed to happen at the same time (59).

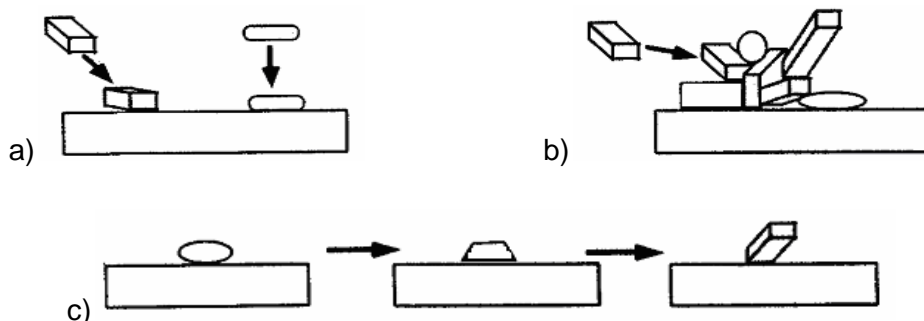


Figure 2-9. Schematic of scale deposition process after nucleation: a) particle adsorption, b) agglomeration and c) phase transitions (47)

Scale deposition takes place on the active sites of surface which can return back into the solution after adsorbing on the substrate due to weak bounds with the surface. Finally, they are adsorbed at the active sites by several bindings (19). Figure 2-10 illustrates the deposition of crystals on the available sites of surface.

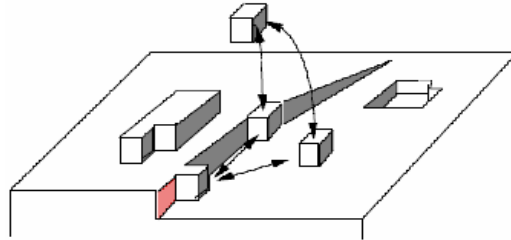


Figure 2-10. Schematic of crystal deposition/adsorption on a surface (60)

The kinetics of scale growth depends on the saturation ratio of the solution, ionic strength of the solution and the type of electrolyte present (29).

The reduction of calcium concentration during precipitation is gained by Equation 2-8 (61).

$$d[Ca]/dt = K_c A(t) ([Ca] - [Ca]_{eq})^g \quad \text{Equation 2-8}$$

Where $[Ca]$ presents molar concentration of Ca^{2+} , K_c is crystal growth constant and A is surface area of crystals. Since the total surface area of crystals increases over time, this should be involved in Equation 2-8 by considering the number of crystals (N). This was developed by Sohnle and Mullin (37) by considering a constant number of crystals with the similar shape, $A(t)$ was estimated over time in order to develop the growth rate equation.

2.2.3 Adhesion

The last parameter for better understanding the formation of mineral scale on surfaces is the adhesion phenomenon, where two solids stick together by interfacial forces like valence and interlocking forces (62, 63) which may happen on the surface of rock and/or pipes. Scale adhesion on the surface is a complicated process and requires involving different fields of science such as surface engineering, chemistry, physics and material science.

2.2.3.1 Adhesion forces and surface energy

DLVO (Derjaguin, Landau, Verwey, Overbeek) theory is used to describe the adhesion of particles and colloid on surfaces in fouling applications (64), which was principally used by others to explain the adhesion of particles (65) and colloids (66). The description of DLVO hypothesis is based on attractive Van der Waals forces and the repulsion forces from adsorbed layers (64). Van der Waals forces is a weak interactions between atoms, molecules and crystals, and repulsion forces is owing to creation of an electrical Double-Layer near to the surface (64). Other parameters such as hydrophobic interactions, short-range repulsive forces or bridging are described by Oliveria (64) to have effects on the adhesion of foulant on a surface, which are not included in DLVO theory.

Roughness and surface energy are also shown to affect the adhesion of mineral scales. Effects of these parameters on scale deposition will widely be studied in section 2.6, which illustrates that the characteristics of the surface and of the interface needs to be considered in order to be able to explain the adhesion of scale on a surface.

Contact angle of water droplet on the surface is measure to study adhesion of foulant on the surface. The contact angles of liquid on a surface are in relation with the strength of bonds between liquid and the surface indicating the lower contact angle is, the stronger bonds between liquid and the surface (67). More detail regarding contact angle measurement is provided in Chapter 3. Besides, the roughness and topography of a surface can influence the contact angles and finally the adhesion of the surface (68-75). The impact of roughness on contact angle value was first described by Wenzel who introduced a roughness factor in order to explain the value of contact angle measured on the surface (68, 69). Cassie also introduced another model since the Wenzel's model was not capable of interpreting the effect of roughness on contact angle value for all types of surface by involving air existence between liquid and the solid (70). Although wettability of a surface can be characterised by topography of the surface (72, 73, 76), its consequence on adhesion and surface free energy stays as an open discussion (74, 75).

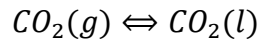
2.3 Factors influencing calcium carbonate formation

In water treatment, it has been attempted to assess the rate of scale formation by studying thermodynamics factors such as pH, temperature or concentration of solution. However, these are not the only factors that influence the calcium carbonate formation; the kinetics factors such as hydrodynamic condition,

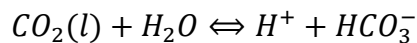
water quality, partial pressure of CO_2 play important roles in CaCO_3 formation to predict the possibility of scaling (77). Three types of crystals are defined for calcium carbonate; vaterite, aragonite and calcite depend on different conditions. Different morphologies of calcium carbonate can be obtained by different crystals of CaCO_3 which may influence the adhesion of calcium carbonate on the substrate as well as the porosity of surface.

2.3.1 Effect of pH

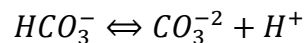
One of the important parameters in the carbonate scale formation system is the equilibrium among CO_3^{2-} , HCO_3^- and H_2CO_3 . The equilibrium of CaCO_3 is presented in Equation 2-9, Equation 2-10 and Equation 2-11 (78).



Equation 2-9



Equation 2-10



Equation 2-11

Figure 2-11 illustrates the total percentage of carbon as function of pH, which shows different carbon species concentrations under various pH conditions. It is seen that the pH of solution has an important role on the ratio of bicarbonate and carbonate ions in the system.

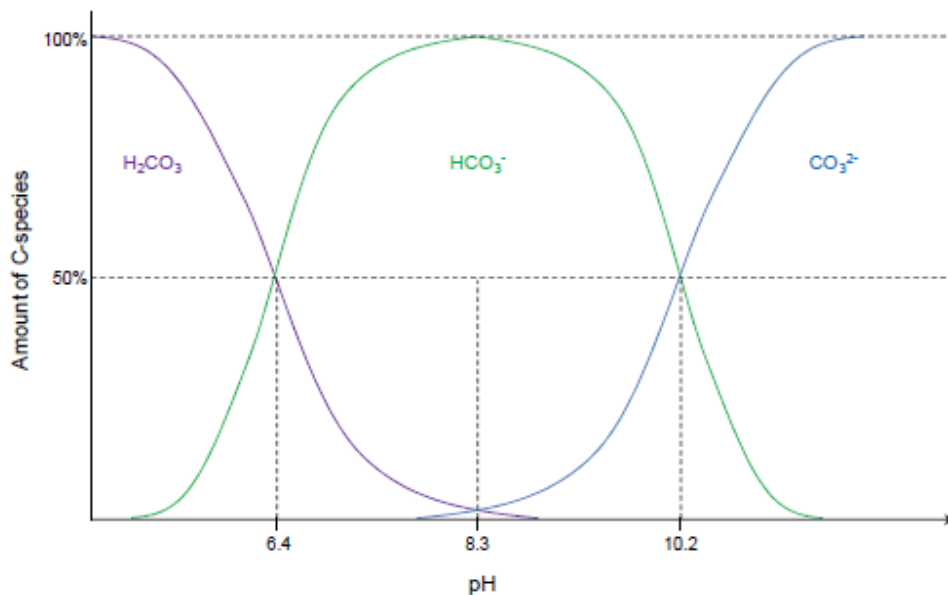


Figure 2-11. Carbon total fraction versus pH (4)

It is observed that precipitation of calcium carbonate decreases with pH since lower carbonate ions are available in lower pH. The effects of pH changes in the solution on precipitation of calcium carbonate were investigated (79, 80). Saturation ratio of the solution increased with pH where the effects of pH on calcium carbonate in the presence of PAA (additive) at 80°C for 24 h were studied (80). It was also shown that the particle size decreases with pH (80). In addition, the nucleation rate was also affected by pH (80). They showed that the crystal morphology was influenced by pH even under controlled conditions. Effects of pH solution on morphology of scale were also studied by others (81). The effect of pH on scale particle size was also studied by Feng et al. (82) who illustrated that the size of crystals decreased with higher pH values due to the influence of pH on nucleation rate.

2.3.2 Effect of saturation ratio

Inorganic scale formation is strongly depended on the saturation ratio of the solution influencing different stages of scale formation like induction, growth, morphology and rate (83-85).

The study on effect of water hardness on the calcium carbonate formation showed only heterogeneous precipitation occurred at low supersaturation whereas homogeneous precipitation was observed at high supersaturation (86). Also on heat transfer surfaces studies, the SR of the solution is monitored and it was observed that in high saturation ratio the aragonite crystals formed whereas calcite crystals were dominant in lower SR (87). On heat transfer surfaces studies, it was also shown that the rate of crystal nucleation is relatively proportional to the value of the supersaturation at the surface (85).

The relation between saturation ratio of the solution on induction time of scale formation showed that the induction time increases in low saturation ratio whereas in high saturation ratio the induction time is very short (88, 89).

2.3.3 Effect of temperature

Temperature is well known to be one of the main parameters for calcium carbonate scale crystallisation. It was shown that when the solubility of the most salts decreases with temperature leading to tendency of crystallisation on the warm surfaces (90, 91). Moreover an increase in heterogeneous crystals in low temperature was observed whereas the homogeneous crystals deposition increased in high temperature (86). Low solution temperature results in slow

kinetics of calcium carbonate scale formation, but in high temperature the kinetics accelerates causing precipitation take place at earlier stage (92), which shows that process and kinetics of crystallisation depends on temperature (82, 93). By using ScaleSoftPitzer TM Version 4.0, it was shown that saturation ratio of scale in the solution changed at different temperature (94), which was shown in Figure 2-12. The impact of temperature on saturation degree was also studied by a simulation and an experimental works Dyer and Graham (93).

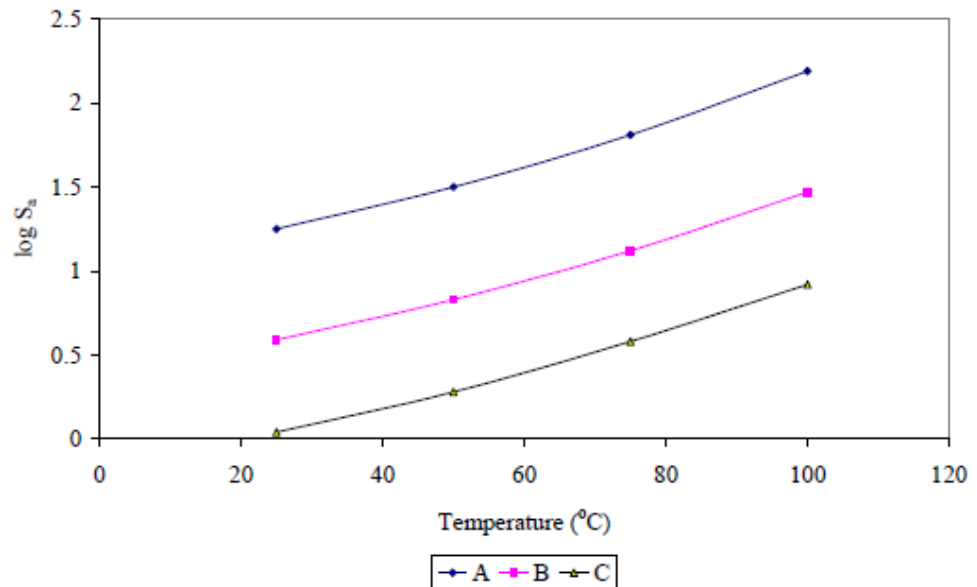


Figure 2-12. Effects of temperature on the saturation of scaling species in the solution (94)

The effects of temperature on the size of the crystal was also demonstrated (91). Yu et al. (91) monitored the crystallisation in two different temperature (25 and 80°C) and observed that the size of crystals decreased from 6-12 μm to 4-10 μm when the temperature increased. Feng et al. (82) also observed the change of crystal size at various temperature, but the size of particles reported in their work was different from others (91). They noticed that using various additives in the solution could be the factor that giving different size of crystals in their report than others (91) reported in the literature.

The impact of temperature on morphology of calcium carbonate showed that different types of crystals form in low and high temperature (95-97). It is observed when temperature decreases it favours calcite and vaterite crystals in the solution whereas in high temperature, aragonite is the predominant crystal form. It was also shown that the affinity of scale to deposit on the substrate increased with the temperature (93).

2.3.4 Effect of calcium and carbonate ions concentration

Calcium and carbonate ions are the factors that influence the saturation ratio of solution. The concentration of these ions can affect the morphology on calcium carbonate scale (29). Calcium carbonate crystal polymorph is predominantly affected by the precipitation rate (98); this results in different types of morphology at different precipitation rates. Although calcite crystal is the thermodynamically stable phase of calcium carbonate, metastable aragonite may be obtained where the rate of supply of CO_3^{2-} ions is high in the solution (99). Concentration of calcium ion was also shown to influence CaCO_3 crystals morphology (100); high Ca^{2+} ion concentration favoured calcite which is known as stable crystal whereas at low Ca^{2+} ion concentration unstable vaterite is the predominant crystal.

2.3.5 Effect of impurities

The rate of scale precipitation and the morphology of crystals are influenced by existing particles in a supersaturated solution. The presence of impurities such as Mg^{+2} , Zn^{+2} , Fe^{+3} , Ni^{+2} promotes formation of aragonite crystals; on the other hand, Mn^{+2} , Pb^{+2} and Ba^{+2} induce calcite crystals (29). Amongst these ions, magnesium has been paid more attention since it has a bigger effect on calcium carbonate morphology and the induction time of CaCO_3 scaling (101). Although inhibiting aspect of Mg^{2+} in bulk precipitation was reported, a lower inhibition effect on scale deposition on surface was observed (102). It has been reported that in the presence of Mg^{2+} , the growth of calcite reduced whereas aragonite crystals were still growing (37, 41, 102-106); increase in Mg^{2+} concentration results in increase of aragonite (107).

The effects of seven divalent cations on calcium carbonate morphology and kinetics of scaling were investigated by Wada et al. (108), who showed that impurities such as Fe^{2+} , Mg^{2+} , Ni^{2+} , Co^{2+} , Zn^{2+} and Cu^{2+} favoured formation of aragonite and Cd^{2+} showed no impact. The explanations from the author (108) were that the presence of impurities either permitted the metastable aragonite to be more stable than the calcite or impurities adsorbed onto aragonite which inhibited its growth.

Effects of Ag^+ , Al^{+3} and Cr^{3+} on crystal growth rate and morphology of scaling were also studied (109) It was shown that these ions also promoted the precipitation of aragonite and decreased the rate of crystal growth.

It was also demonstrated that the formation of calcium carbonate can be decreased by adding sufficient amounts of copper and zinc and shown that the copper was most effective than zinc (110).

2.4 Prediction of scale formation by using software

As shown, formation of mineral scale is a complicated phenomenon influenced by a wide range of parameters such as pH, temperature, degree of saturation ratio, etc.. Hence, calculation of saturation degree of solution in the oil and gas industry is important to predict and control the different factors influencing scale formation. The saturation ratio (SR) of solution is one of the most important parameters in order to understand the best effective strategy for scale management in terms of reducing the risk of scaling in the production system. Different software such as ScaleSoftPitzerTM (94) and MultiScaleTM (111) were established to calculate SR or other effective factors in scale formation in different conditions. Different studies like Langelier Saturation Index (LSI), Ryznar Stability Index (RSI), Puckorius Scaling Index (PSI) Stiff-Davis Index (SDI) and Odd and Tomas Index (OTI) were carried out to understand the effect of saturation indices on scale formation (112, 113).

In order to predicting scale formation, two different softwares based on Pitzer theory (114-116) have been developed which are able to calculate the equilibrium composition for the whole system and each phase, separately. Although saturation ratio of the whole system can be calculated by providing pH, pressure, total alkalinity, concentration and temperature; these thermodynamic factors cannot explain the scale phenomenon, alone. None of these softwares are able to predict the amount of scale on a specific area, since these are not able to predict the kinetics scaling.

2.5 Scale removal and inhibition methods

Formation of mineral scale in different places causes production loss and blockage of flow of oil path. In order to remove scale different methods: chemical, mechanical or combination of both (117) are used without inducing any damage to wells and the wellbore, pipes and in total the oil path.

2.5.1 Mechanical removal mechanism

If the scale layers are too thick to be removed by chemical removals, mechanical equipment and techniques are employed in order to drill rocks (a thick layer of scale). Explosives such as string shots are known as the first methodology that cleans and removes scale in pipelines (118). One of the methods is water jetting which with a help of chemical washes removes soft scale such as halite (119). However this technique is not effective for hard scales such as calcium carbonate (calcite) or barium sulphate. Mechanical tools cannot be used to all the locations that scales formed and also the correct technique should be applied for a specific type of scale and well.

2.5.2 Chemical removal mechanism

Limited ranges of mechanical techniques are applicable in the well leading to uses of chemical removals. These removals are cost effective compare to the mechanical methods and are able to dissolve mineral scales remotely (120). Calcium carbonate can be removed by exposing to hydrochloric acid while sulphate scales needs to be dissolved by a chelating agent. However, chemicals like Ethylene Diamene Tetra Acetic acid (EDTA) are able to remove nanocarbonate scale, to dissolve and chelate CaCO_3 (121). EDTA and its variations are more costly and have slower effective reactions with calcium carbonate compared with hydrochloric acid. The inhibitors which are commonly applied in oilfields are presented below.

2.5.3 Inhibition of scaling by scale inhibitors

One of the most effective methods to control scaling in the oil and gas industry is the scale inhibitors. Based on composition and mechanisms, scale inhibitors are classified in different categories: polyphosphates, phosphonates, polyelectrolytes and polycarboxylic.

Polyphosphate are used for both corrosion and scale inhibition. The use of these scale inhibitors in the oil and gas industry declined due to poor thermal stability (break down temperature at 90°C) (29). According to the new regulation, the sue of these materials are mainly forbidden in the North sea (122). The chemical structure of polyphosphate is shown in Figure 2-13.

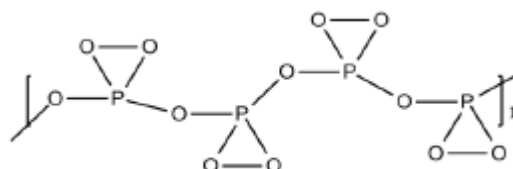


Figure 2-13. Polyphosphate inhibitor structure, n=4-20

Phosphonates are also applied when corrosion and scale needs to be inhibited. These chemicals are differentiated by their PO_3H groups. It is well known that phosphonate scale inhibitors are mostly efficient during crystal growth not in nucleation process (29). Diethylenetriaminepenta(methylenephosphonic acid) (DETPMP) is one of the inhibitors in phosphonate category and commonly used in the oil and gas industry, the schematic of DETPMP is shown in Figure 2-14. Phosphonate inhibitors are also well-known for being resistant in high temperature (61).

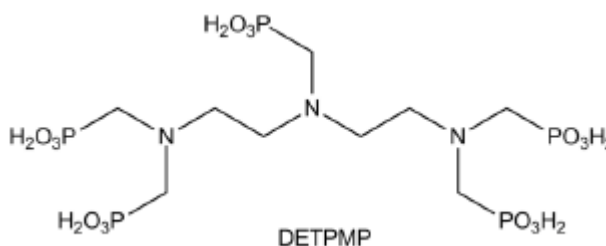


Figure 2-14. Chemical structure of DETPMP scale inhibitor

Polyelectrolytes include a larger variety of monomers like carboxyl, hydroxyl, sulphonate, phosphate and phosphonate. Polyelectrolyte inhibitors are effective during nucleation process and can delay the crystal growth for the most mineral scale formation (29). Polyphosphinocarboxylic (PPCA) is one of the most common inhibitors in this group of which the schematic is illustrated in Figure 2-15.

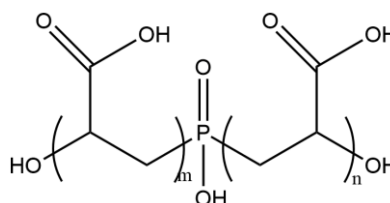


Figure 2-15. PPCA structure

Polycarboxylic acids are distinguished by COOH groups, which are one widely used in squeezed treatments. Polyacrylates (PAA) is one the well-known inhibitors in this group of which the chemical formula is illustrated in Figure 2-16. A negative impact on calcium carbonated inhibition was seen where higher molecular weight of PAA was used (123). PAA influences the morphology, size and shape of calcium carbonate and inhibits CaCO₃ growth (91, 124).

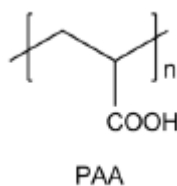


Figure 2-16. PAA chemical formula

2.5.3.1 Green chemistry and inhibitors

Recently, more environmentally accepted inhibitors have being demanded by the oil and gas industry due to more strict regulations by the authorities. The focus is to apply green and environmental friendly chemicals to reduce pollution (125). Some molecules are introduced below as more environmentally-accepted chemical inhibitors.

❖ **Polyaspartate (PASP)**

Polyaspartate is known as a molecule from aspartic acid group with good biodegradability properties. To synthesize PASP, a thermal technique is used which does not require non-desirable reagents. Three different mechanisms are together involved in the inhibition of mineral scale by PASP: adsorption, complexation and dispersion processes. When the molecular weight of Polyaspartate increases the adsorption of this chemical decreases. This molecule inhibits CaCO₃ scale during nucleation and crystal growth processes (126, 127).

❖ **Polymaleic acid (PMA)**

Polymaleic acid is a carboxylic acid enabling to inhibit the rate of calcite growth at low supersaturation solution of which the mechanism of inhibition is thought to be by adsorption of carboxyl ions on nulcei (128, 129).

❖ Carboxymethyl Inulin (CMI)

Carboxymethyl Inulin is synthesised from inulin (a polysaccharide). CMI influences morphology of the calcium carbonate crystals and the rate of growth. It is believed that anionic carboxylate groups adsorb on the calcium carbonate crystals and stop the crystal growth (130).

2.5.4 Squeeze Treatment

In the oil and gas industry, squeeze treatment (131) is known as a methodology which prevents scale formation near the wellbore reservoir by pumping a massive amounts of scale inhibitors downhole to retain in near the wellbore areas. In general, passing a high concentration of scale inhibitor through the rock, which is slowly released later into the production fluid to prevent scaling, is called squeeze treatment. Figure 2-17 shows the schematic of squeeze treatment from a platform.

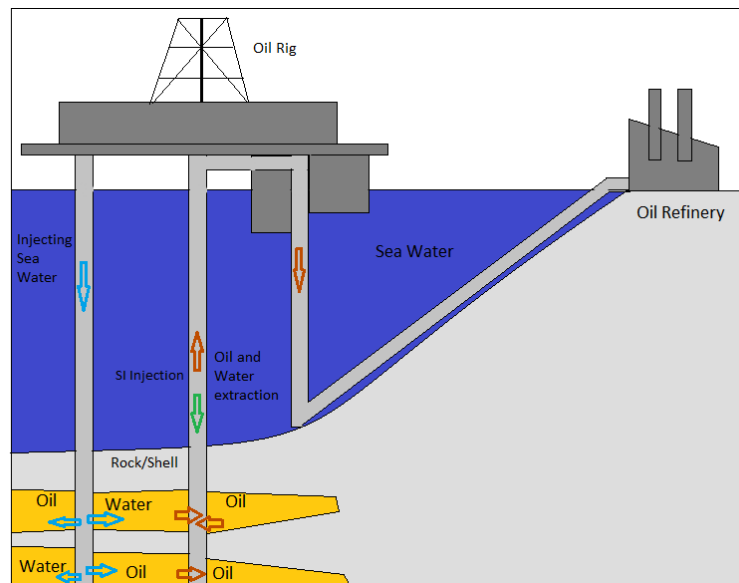


Figure 2-17. Schematic of an oil well using squeeze treatment (132)

Squeeze treatment can be applied in two different ways: i). precipitation/dissolution (133) and ii). adsorption/desorption (131). Between these two methods, adsorption/desorption is the common used method in the oil and gas industry. Van der Waals and electrostatic forces between the reservoir rock and scale inhibitors are the main mechanisms in adsorption squeeze treatment (134-136) of which the efficiency is defined by adsorption isotherm (136-138). In precipitation method, the mechanism consists of the reaction between inhibitor and divalent cations forming

scale inhibitor-metal complexes which precipitate on formation rock near the wellbore and release later to inhibit the solution from scaling (133, 135). In the precipitation/dissolution mechanism, nucleation kinetics plays an important role to diffuse SI further into reservoir (139); this increases the squeeze lifetime. The period that a well needs to be squeezed again is called squeeze lifetime. Acidic solution of SI is normally injected to promote precipitation mechanism (140).

In desorption squeeze treatments, SI is gradually released into the solution. The problem with this mechanism is the irreversibility of SI adsorption; i.e. the same amount of SI injected to the rock does not return to the production system (141). Since squeeze treatment implementation is a very expensive process resulting in production loss, the squeeze lifetime plays an important role to have a cost-effective strategy (142).

The process of squeeze treatment takes place in six stages (143): 1) employing surfactants to wet the rock, 2) pumping a low concentration of SI to help the surfactants move further into reservoirs, 3) injecting a high SI concentration (2.5-20%) as the major treatment, 4) pumping brine to diffuse SI further into the reservoir 5) shutting the well for 8-24 h to have a maximum adsorption of SI on the formation rock 6) eventually, extracting production. The squeeze treatment procedure is depicted in Figure 2-18.

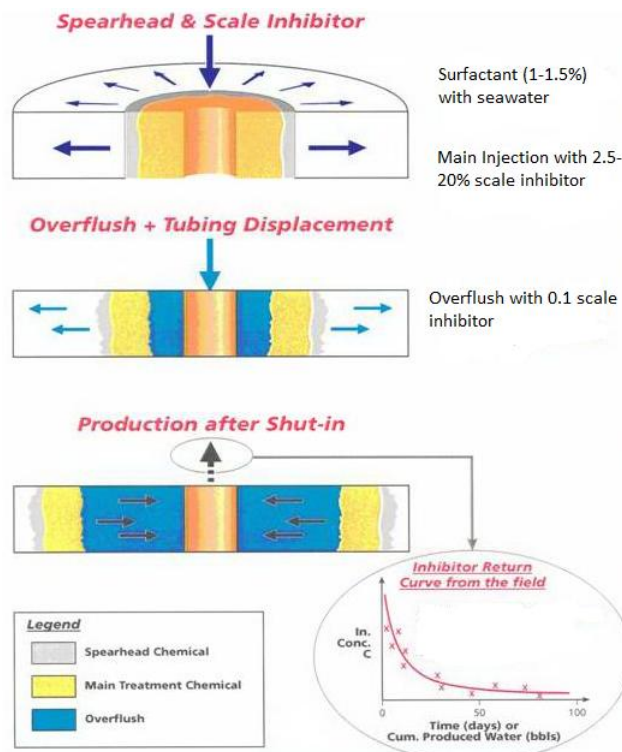


Figure 2-18. Schematic of the squeeze treatment process (144)

In squeeze treatment, it is expected that SI retains in the well for a longer time and slowly releases to the solution in order to have an optimum squeeze lifetime. However, in the reality a high concentration of SI returns after a few days (145). A wide range of discussions about enhancing squeeze treatment to reduce the cost of the procedure is available in the literature (134, 137, 143, 146-156).

There are many parameters such as temperature, mineralogy, pH, divalent cations that can affect the squeeze lifetime. These factors will be briefly discussed below.

2.5.4.1 Temperature

The change of temperature can result in precipitation squeeze treatment leading to an increase in the squeeze life time (134, 141, 157). It was demonstrated that the adsorption of both inhibitors (PPCA and phosphonate) increases when the temperature of the system goes up (157).

2.5.4.2 pH solution

Adsorption of different inhibitors was studied when the pH of the solution changed (134, 157, 158). The adsorption of SI (low concentration) in the system at $pH > 4$ and $pH = 2$ became equilibrium after 1 h and 10 h, respectively (134). PPCA and Phosphonate inhibitors showed different behaviour in terms of pH solution changes (158). It was observed that the adsorption of PPCA at high temperature (95°C) increases when the pH of the solution increases; however, PPCA adsorption decreases at low temperature (25°C) when the pH solution increases from 4 to 6. The adsorption of phosphonate in both low and high temperatures (25°C and 95°C) reduced from 2 to 4 and increased from 4 to 6. Besides, the adsorption of SI for $pH < 4$ did not change and reached zero when $pH > 7$. A clear reduction in adsorption was observed when the $5 < pH < 6$ (158). Adsorption of SI on the rock were observed to be negligible for $pH < 4$, for pH 5 to 6 adsorption intensely dropped and for pH above 7 reaches zero (158).

2.5.4.3 Divalent cations

Divalent cations such as calcium can influence adsorption of inhibitor on the formation rock (134, 135, 145, 146, 152, 159-162). Adsorption of DETPMP decreased with increasing the pH solution at 25°C where no calcium existed in the solution (134). It was observed that in $pH = 6$, the presence of calcium caused

increasing the adsorption of DETPMP. Figure 2-19 presents the effect of calcium on SI adsorption on sandstone in various pH. However, the impact of Ca^{2+} is different for each inhibitor (146); the adsorption of PPCA on the crushed core in the presence of calcium was not significant as DETPMP.

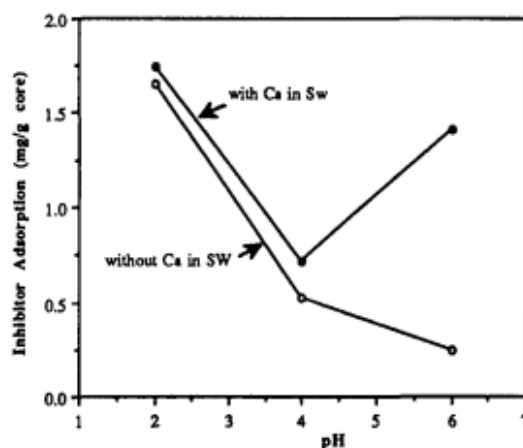


Figure 2-19. Impact of Ca on adsorption of SI on sandstone at 25°C (134)

2.5.4.4 Mineralogy

Mineralogy plays an important role in squeeze lifetime; the interaction between inhibitor and the formation rock can govern the achievements of a squeeze treatment (143). Rock consists of different minerals, mainly quartz, carbonate, clays etc.. Apart from quartz, other minerals affects the interaction between inhibitor and the formation (153). The effects of mineralogy on squeeze lifetime were investigated by Jordan et al. (143). Adsorption of PPCA and DETPMP on sandstone were tested and it was illustrated that the presence of clay mineral has an important affect on adsorption process (143).

The surface of alumina is positively charged when pH of formation water increases the tendency of SI to alumina surface (153). The silica-type formation rock contains kaolinite, quartz and feldspars which causes the formation becomes negatively charged at the pH of formation water (153). This results in a repulsive force between scale inhibitors and the surface of silica reducing the tendency of scale inhibitors to adsorb on the formation rock (153). Kaolinite has a larger surface area compared with silica and feldspars which eliminates the effects of silica and feldspars in adsorption process; however, kaolinite is naturally negatively charged in the pH of formation water. Thus, concentration of kaolinite can play an important role to adsorb scale inhibitor (153).

2.6 Controlling mineral scale and fouling by applying new substrates on surface

Scale deposition on surfaces is not an issue only in the oil and gas industry but also in wastewater treatment, water purification, condensers, heat exchangers and chemical plants industries (163-167). For instance, scaling and fouling occurring near metal surfaces in cooling crystallisation processes due to the high saturation ratio happening mostly near the heat exchangers reduce heat transfer coefficients resulting decreasing production rates (168).

In biomedical science, the hydrophobicity of surfaces, which are coated by proteins, lipids etc., increased and affected bacterial accumulation (169). The surface treated by Ni-P is another example of creating new substrate which is capable of preventing fouling deposition on the surface (170). Compared with the untreated stainless steel and copper, the adhesion of crystals decreased on the Ni-P surface owing to the lower surface energy. Recently, the attention towards the influence of substrate as the nature of the surface on scale deposition was paid, which will widely be discussed in this section. Effects of different types of substrates with various modifications using coating, ion implementation, or ion sputtering on scale deposition were studied and will be discussed in this section. Biofouling deposition is well understood in literature as a wider range of work has been performed on this part.

Biofouling studies the aggregation of living species on a surface or within water treatment membranes (4). The biofouling process is primarily an adhesion of particles on a surface, which varies from crystallisation of mineral scales on a substrate. A schematic of biofouling process on a substrate is presented in Figure 2-20. Generally, the main parameter affects biofouling on a surface is surface energy; the lower surface energy, the lower adhesion of particles (171, 172). Hydrophobic surfaces which present low surface energy have been correlated to reduction of biofouling materials on the surfaces. However, recent studies (173-175) showed contradict of the work mentioned above. It was shown that some organisms intended to adhere on the hydrophobic surface (174). Surface chemistry was shown to also have effects on diary fouling by Permathilaka et al. (176).

As a conclusion, it can be stated that the adhesion of organisms were mainly focused on the anti-biofouling studies and it was shown that the lower surface energy generally gives better surfaces. Since it was previously assumed that the scaling process on the surfaces follows biofouling mechanism from bulk precipitation to the surface deposition, most researches have been focused on

investigating effects of low surface energy substrates in order to decrease scale adhesion.

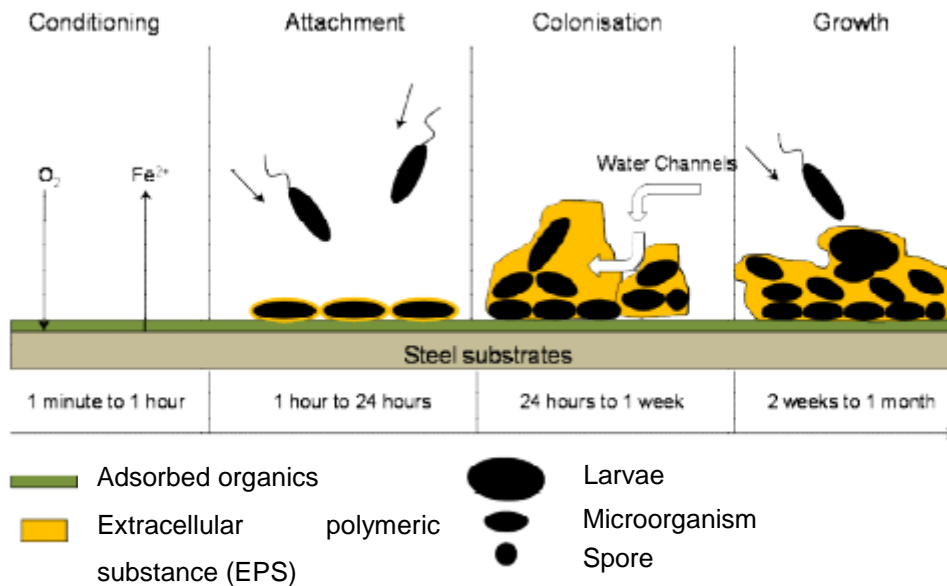


Figure 2-20. Schematic of biofouling procedures on a surface (177)

2.6.1 Effects of different substrates on inorganic scale deposition

Finding an anti-scale surface for different applications induced researchers to investigate the behaviour of these surfaces on crystallisation process. The parameters which are believed to have most impact are surface energy, surface composition and roughness.

2.6.1.1 Surface composition

One of the factors that can influence scale deposition on the surface is surface composition including surface structure and existing charges on the surface.

Available ions in surface composition could affect the crystallisation on calcium carbonate formation. Ledion et al (178) examined four different substrates under the same saturation ratio degrees ($SR=1.16$ and 1.32). Different types of copper were compared with stainless steel, polyethylene and tin plated surfaces in terms of reduction in scale formation, which was shown that under the same condition copper had the least scale deposition among all surfaces. The reason for lower scale deposition of the copper was claimed to be migration of copper ions into water which prevents scaling; dissolved copper ions in the solution act like scale

inhibition. On the other hand, another study (179) showed that higher scale deposition on copper surface compared with aluminium and stainless steel surfaces under different conditions, which conflicted from the previous work.

The crystallisation of CaCO_3 was also studied on bronze, stainless and gold by Jahouari et al. (7) by using an electrochemical technique. Deposition kinetics which affected morphology of the crystals was dissimilar for different surfaces owing to the surface structure and composition. The mineral scale crystals deposited quicker on gold surface and then bronze followed by stainless steel, since the presence of oxides on the surfaces blocked precipitation of calcium carbonate by using oxygen reduction methodology for the measurement. Since tendency of gold for oxidation is lower than other surfaces, the polymorphs can form on the gold surface.

Deposition of carbonate sulphate on stainless steel surface showed packed crystals on the bare surface whereas stainless steel surface coated by Ni-Cu-P-PTFE presented loose and cubic shape of CaSO_4 (8). PTFE is known as a coating with non-stick property; however, due to poor thermal conductivity and poor adhesion to metal surfaces this coating are not currently interested for commercial usages (180).

The stainless steel surface treated by PPCA showed reduction of calcium carbonate deposition on the surface (181). It appeared that the uncharged part of coated-PPCA on the surface is exposed to the solution which creates a neutral surface, thus the available ions in the solution have lower tendency to react with the surface (181). The schematic of inhibition process by PPCA-treated stainless steel surface was presented in Figure 2-21.

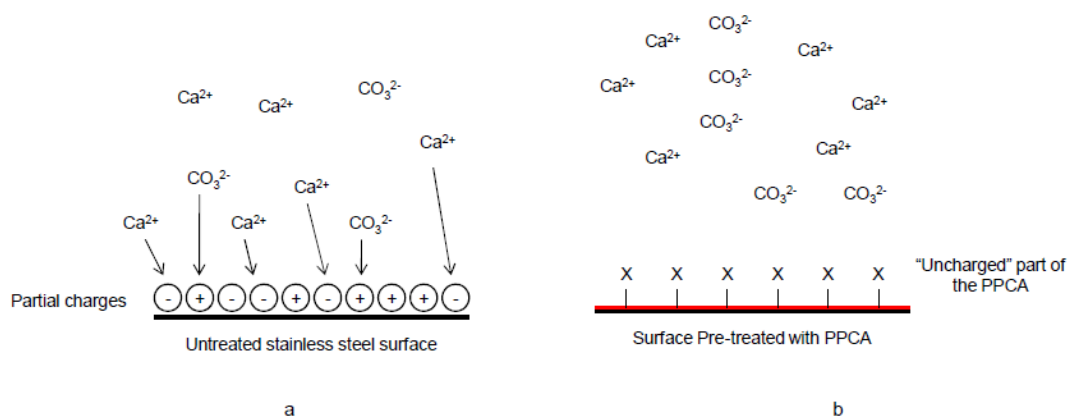


Figure 2-21. Calcium and bicarbonate ions attraction on a) stainless steel surface and b) PPCA-treated surface (4, 181)

Previously, it was demonstrated (62) that PPCA molecules adsorb on the surface and reduce the nucleation sites on the surface leading to inhibition of calcium carbonate formation. The mechanism of PPCA-treated surface was believed to be due to the presence of carboxyl group of PPCA on the top layer of surface exposing to the solution. However, Martinod et al. (5) believed that PPCA could not directly interact with metal surface due to repulsion forces between negative charge of PPCA and stainless surface. In the solution the carboxyl group of PPCA becomes negatively charged and the surface is also negatively charged, thus they cannot interact with each other directly. It was hypothesised that PPCA first interacts with the magnesium presence during treatment and then PPCA-Mg⁺ reacts with the negative-charged metal surface. Therefore, exposed surface to the scaling solution remains uncharged showing lower propensity to scaling ions; this results in poor formation of calcium carbonate on the surface treated by PPCA.

Eroini, V. (4) studied the effect of surface composition of various surfaces in reduction of calcium carbonate scale deposition. Two different brines were used in Eroini's work of which the compositions are presented in Table 2-3 and Table 2-4. The saturation ratio values for brine A and brine B were 34 and 11, respectively.

Table 2-3. Composition of Brine A (4)

	Brine 1A (mg/l)	Brine 2A (mg/l)
NaCl	17119	17119
CaCl ₂ .6H ₂ O	7871	
NaHCO ₃		2560

Table 2-4. Composition of Brine B (4)

	Brine 1B (mg/l)	Brine 2B (mg/l)
NaCl	17498	17498
CaCl ₂ .6H ₂ O	3826	
NaHCO ₃		1469

The results of Eroini's work is presented in Figure 2-22, which shows that in comparison with stainless steel (the reference surface) the scale deposition decreased on ISF (isotropic super finished stainless steel surface) and PPCA-treated surfaces. The reduction of calcium carbonate on ISF and PPCA-treated surfaces was claimed to be due to surface properties creating neutral surface. Also DLC (Diamond Like Carbon) and PTFE (polytetrafluoroethylene) surfaces showed almost the same calcium carbonate coverage as stainless steel on the surface. Polymer and ceramic surfaces had the most mineral scale deposition on the surface; this behaviour was also seen by others (182, 183). In the matter of scale

deposition, ceramic composition coating preformed poorly due to the surface charge and electrostatic forces (182, 183). However, surface charge can have positive or negative effects on scale deposition (183). Since the amount of calcium carbonate deposition on DLC and PTFE surfaces did not change before and after erosion, this indicates that roughness does not influence the mineral scale deposition on these two surfaces (4). It was stated that the surface composition and surface energy of DLC and PTFE substrates were the dominant factors in reduction of inorganic scale deposition. In pervious works (62, 184-188), it was also reported that the efficiency of DLC and PTFE in terms of reduction of fouling materials is related to their non-sticky properties and low surface energies.

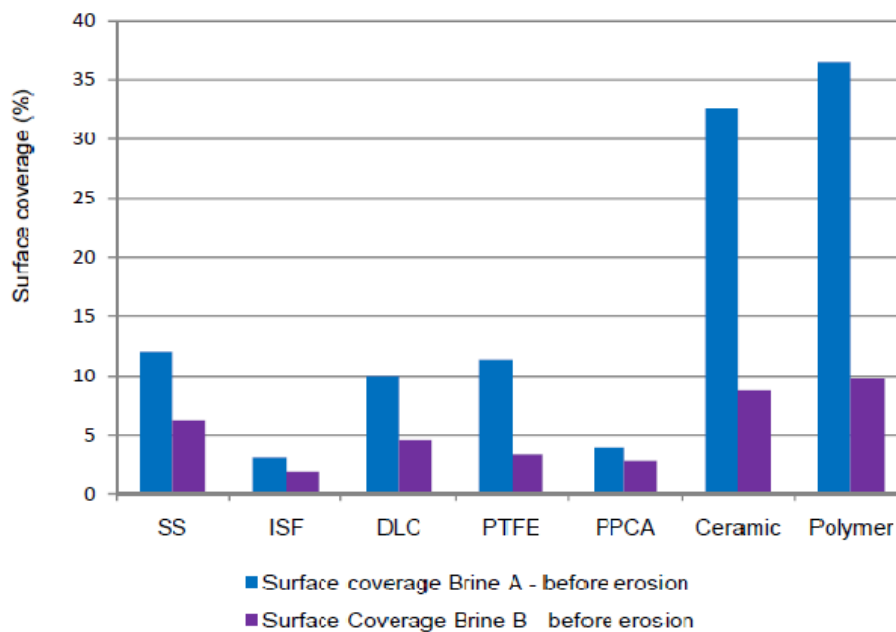


Figure 2-22. Calcium carbonate deposition on different surfaces for two different brines (4)

Cheong et al. (189) investigated scale deposition on DLC, Tech 23, Tech 100, stainless steel and six types of different polymers of which results are presented in Figure 2-23. DLC, Tech 23 and Tech 100 showed the least tendency for formation of inorganic scale. The calcium carbonate formation on polymers showed frequent results; however, the most scale deposition was observed on stainless steel (189). Zhao et al. (8) reported that the top layer of calcium carbonate formed on the substrate is affected by the first layer deposited on the surface, which may introduce various types of layers such as densely packed, loose or porous layer. The hardship of removal of these layers by hydrodynamic shear forces is influenced by morphology of these layers.

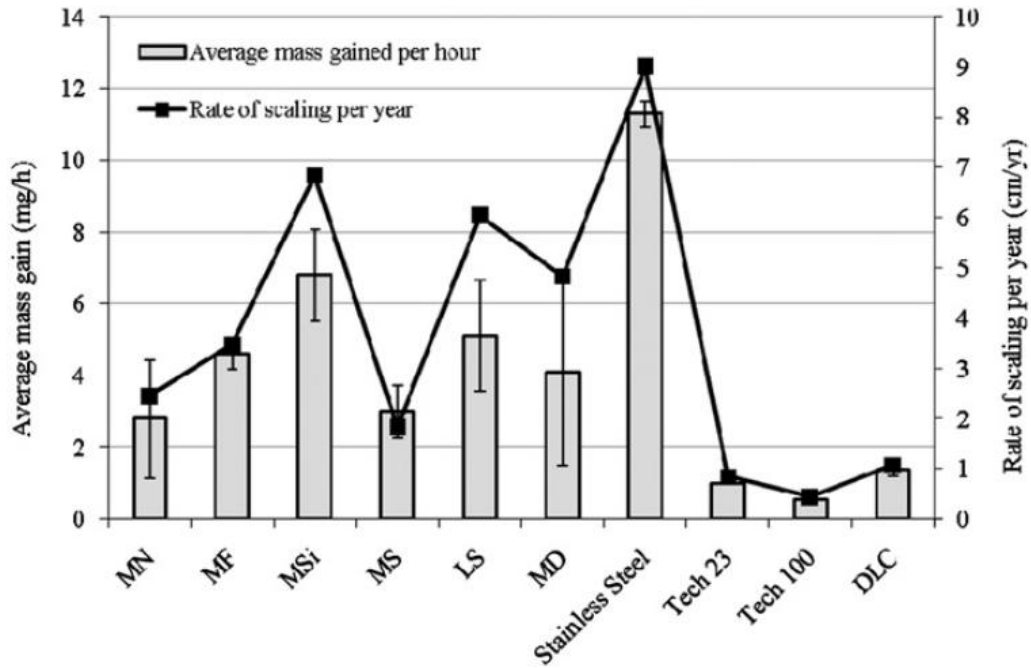


Figure 2-23. Tendency of various substrates to calcium carbonate scale formation (189)

The morphology of calcium carbonate on different substrates was also studied (4). It was shown that the stainless steel and PPCA-treated surfaces promoted cubic crystals which are in agreement with the other studies that demonstrated the change of crystals in the presence of additives (190, 191). Although ISF surface has a similar composition with stainless steel, both calcite and amorphous calcium carbonate were observed on ISF surface whereas only calcite crystals were seen on the stainless steel surface. It was shown (4) that on PPCA-treated surface the morphology of calcium carbonate crystal did not change compared with stainless steel. It was shown that morphology of calcium carbonate on DLC surfaces was similar to morphology on stainless steel (4). In contrast, PTFE showed that the surface composition is the dominant factor to change morphology of the crystals.

2.6.1.2 Surface energy

Surface energy is another parameter that can influence the tendency of the surface to deposition of mineral scale. There is a conflict in the literature (3, 4, 9, 187, 192-196) regarding the influence of surface energy on inorganic scale deposition. Some studies showed that a surface with lower surface energy has lower tendency for scale adhesion (195) whereas some investigations reported that surface energy of substrates is not the dominant factor in the scale reduction (192, 194).

Cheong et al. (189) studied surface energy of different substrates and showed that the scale formation tendency did not decrease for the substrates with lower surface energy. It is observed in Figure 2-24 that the mass on the polymer substrates increased when the surface energy decreased (3, 189). Also the lowest mass gain was illustrated for TECH 100 and TECH 23 where the reported contact angle measurements show the lowest surface energy for the substrates. Ultimately, Cheong et al. (189) suggested both the surface energy and roughness of different substrates are in correlation with mass reduction.

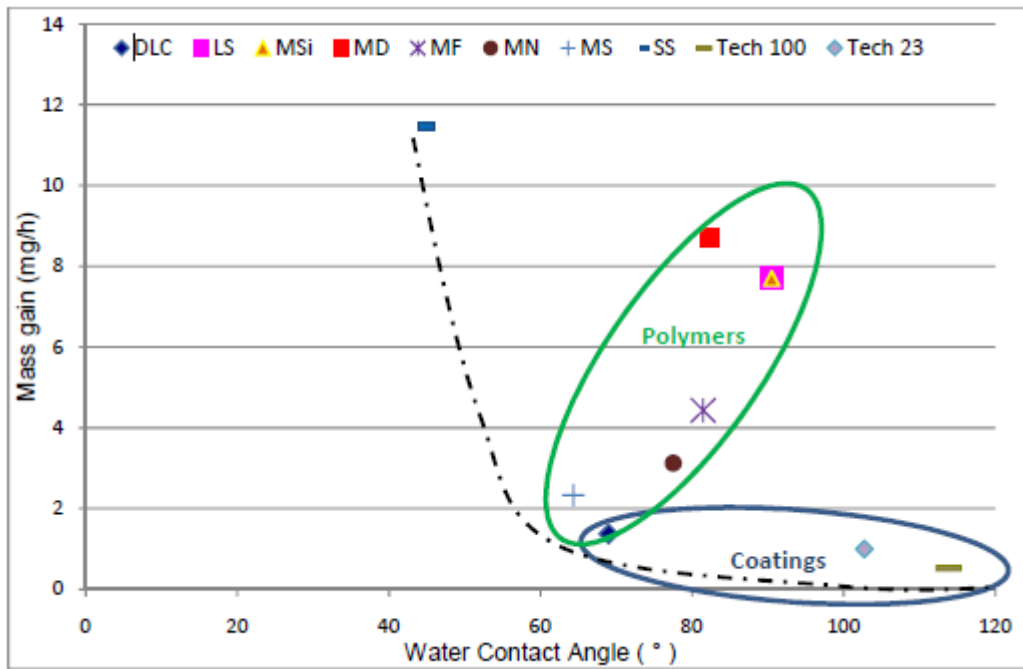


Figure 2-24. Mass gain of various substrates as function of contact angle measurements (3)

Yang et al. (9) modified copper surfaces with two different coatings (Docosanoic Acid (Cu-DSA) and Poly Tetra Fluoro Ethylene (PTFE) co-deposited in electroless nickel solution (Ni-P-PTFE)). It was noticed (9) that compared with the bare surface of Cu, the nucleation rate slowed down and smaller crystals formed on the treated surfaces owing to the lower surface energy; moreover, the mineral scale bonded weakly to the modified surface.

Diamond Like Carbon (DLC) surfaces were also compared with stainless steel and the studies showed that the surface energy of the substrate influenced scale deposition (187). Calcium sulphate deposited on DLC and stainless steel which resulted in formation of very thick layer of scale on stainless steel whereas a thin layer on DLC (196). Moreover, when DLC surface was fluorinated (to have lower surface energy compared with DLC surface), the result after scale test

(CaSO₄ deposition) presented even thinner layer of scale on the surface than DLC surfaces (196).

Eroini, V. reported that higher contact angles of the surfaces generally showed lower reduction of calcium carbonate scale deposition on the surfaces (higher surface coverage of calcium carbonate). These results are in contrast with the biofouling research, which mostly assumes that the surface with lower surface energy is more efficient in terms of reduction of biofouling materials deposition on the surface (197). It is assumed that in biofouling process, the particles form in the bulk and then adhere to the surface. Eroini, V. suggested that in the crystallisation process of mineral scale, the surface energy cannot be the predominant factor reducing scale deposition on the surface and other parameters such as surface composition and roughness influence the scale deposition.

2.6.2 Effect of roughness

As shown earlier, scale deposition is not always associated to lower surface energy. Roughness could be evaluated as another factor that could sometimes be dominant in scale deposition. In general, it is expected more mineral scale deposition on surface with higher roughness values owing to higher surface contact between the substrate and mineral scale surfaces (198-201).

Although PTFE coating has lower surface energy compare to DLC and stainless steel but maximum calcium sulphate formed on the PTFE surface (202). It appears that roughness of polymer coating was the dominant factor resulted in stable nuclei formation on PTFE surfaces (202).

Adhesion strength and nucleation rate of scale were compared for metal and organic surfaces (203). Ranking and Adamson noticed that the surface with higher energy became more adhesive and increased the adsorption of scale on the substrate. Although the surface energy of composition of top layer of surface is affected by impurities, roughness may determine the surface energy of the surface (203). They showed that the greater is the roughness the higher is the surface energy leading to more adhesive surface in terms of scale deposition (203).

Higher amounts of mineral scale was also observed on smoother surface than rougher surface by Keysar et al. (198). In addition to affecting the adhesion strength by roughness, the porosity of the scale deposited on a surface is also influenced by roughness (198).

Herz et al. (199) also examined stainless steel surfaces (rough and smooth) and observed more scale formed on the rough surface. Besides, it was noted that the induction time for rougher surfaces become shorter.

In contrast with these works mentioned above, Cheong et al. (189) reported that the mass on the most of surfaces decreased when the roughness of the surfaces increased due to other factors such as surface energy. Figure 2-25 illustrates the relation between different substrates and roughness in terms of weight gain.

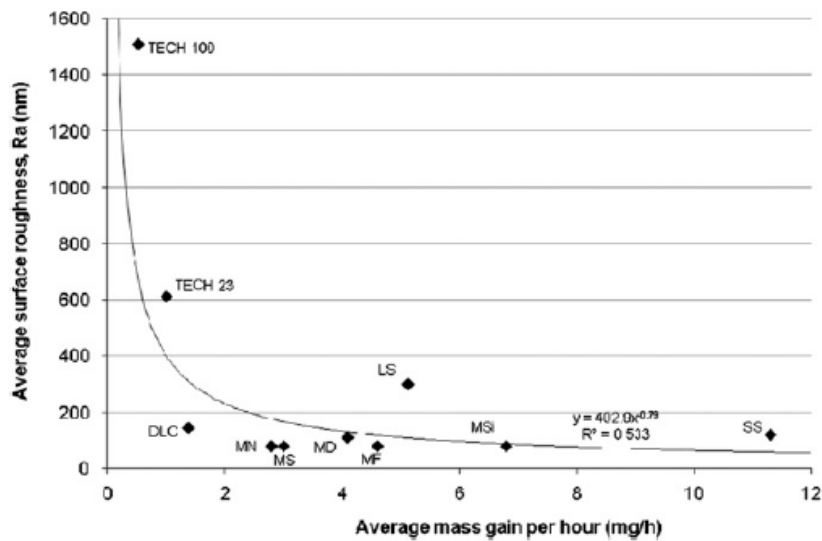


Figure 2-25. Roughness of the various types of surfaces as function of mass gain (189)

It was also illustrated that the roughness of stainless steel affected morphology of calcium carbonate (198). Undefined shape crystals were observed on the ISF surface owing to surface effect on induction time (4). Few nucleation sites were assumed on ISF surfaces as a consequence of surface topography; this may act on the kinetics of calcium carbonate crystallisation. Hence, it was concluded (4) that different morphology observed on ISF could be owing to slow kinetics which may indicate the calcium carbonate crystals were at the beginning of the crystallisation stage (4). Delaying induction time by surface properties was also showed by others (204).

In general, it was shown there is no relation between roughness and scale deposition (4). It was noticed that on the stainless steel surface the scale deposition increased when the roughness of surface increased (193, 199). However, small effects of the roughness on PPCA treated surface, DLC and PTFE was observed before and after erosion. Regarding PTFE and DLC coating, the surface composition plays a major role. The roughness of polymer and ceramic surfaces was shown to be an important factor as well as surface composition in calcium

carbonate deposition. Despite having similar elemental composition (fluorine) and roughness values in PTFE and polymer surfaces, both showed very different behaviour in terms of scale reduction. Roughness is a dominant factor for polymer surfaces whereas roughness has a small effect on PTFE. The difference between polymer and PTFE is believed to be related to the chemical bonds and molecular structure (199, 205).

2.7 Surface modification applying a self assembled monolayer technique

As mentioned, the objective of this work is to study the potential treatments of formation rock in order to reduce the risk of inorganic scale deposition near the wellbore area. Hence, it is crucial to apply a very thin film (nanometre thickness) being capable of altering the surface characteristics in order to reduce the tendency of formation rock to mineral scaling as well as not blocking the oil path through pores. A self assembled monolayer (SAM) is defined as a single layer of organic molecules on a solid surface which is capable of changing surface properties (206-208). Organic molecules create a densely packed layer on a solid surface by hydrogen, covalent bonds or electrostatic interactions. SAM technique was first applied in 1946 by Bigelow et al. (209) who studied adsorption of n-alkyl amine-based surfactant to a metallic surface.

Since nanotechnology accelerated in the past decades, SAM technique was known as one of the interesting areas due to creating nanostructure film on a surface (208). SAM was employed for different applications such as electrode modification (210), corrosion (211), biomedical (212, 213). SAM formation on a substrate is a complex process which requires extremely controlled conditions.

2.7.1 Silanes

Prior to employing SAM technique in this research, it was essential to find potential materials which could be able to reduce mineral scale deposition and simultaneously being capable of binding covalently with formation rock. Most formation rocks in hydrocarbon reservoirs consist of different mineral components such as clay, friable, quartz, etc. (214) of which quartz is the highest percentage. In order to have a covalent bond on formation rock the chosen chemicals must have a strong affinity to quartz materials (SiO_2). Therefore, organosilane group can be the best option since these materials have been shown to easily react with many

different types of surfaces (215-227) such as aluminium, nickel, copper, silica and quartz. This group is also capable of creating a strong bond between organic molecules and inorganic materials. In addition, various tails can be used with one similar head, which is beneficial as potential of different tails can be tested. These coupling agents are applied in different fields of sciences such as adhesion (228) and immobilise polymers such as proteins, DNA, etc. (229-233).

Silanes are known with the general structure of $R-(CH_2)_n-Si-X_3$ where R is an organofunctional group, $(CH_2)_n$ is the linker, and X_3 is hydrolysable groups (234). Different chemical and physical surface properties can be achieved by using a variety of organosilane group (211, 235-241). The silanization process of surface occurs in four steps, which is shown in Figure 2-26. Hydrolyzation of alkoxy groups of organosilanes first happens to create silanol-containing species. After that, these labile groups are hydrolysed followed by condensation to oligomers. Then, these oligomers undergo hydrogen bindings with OH groups on the substrates. Finally, covalent bonds between the surface and organosilanes form during drying or curing stage (242, 243). It is worth to mention that the presence of water during silanization is a critical parameter to create a uniform SAM layer on the substrate (244-247).

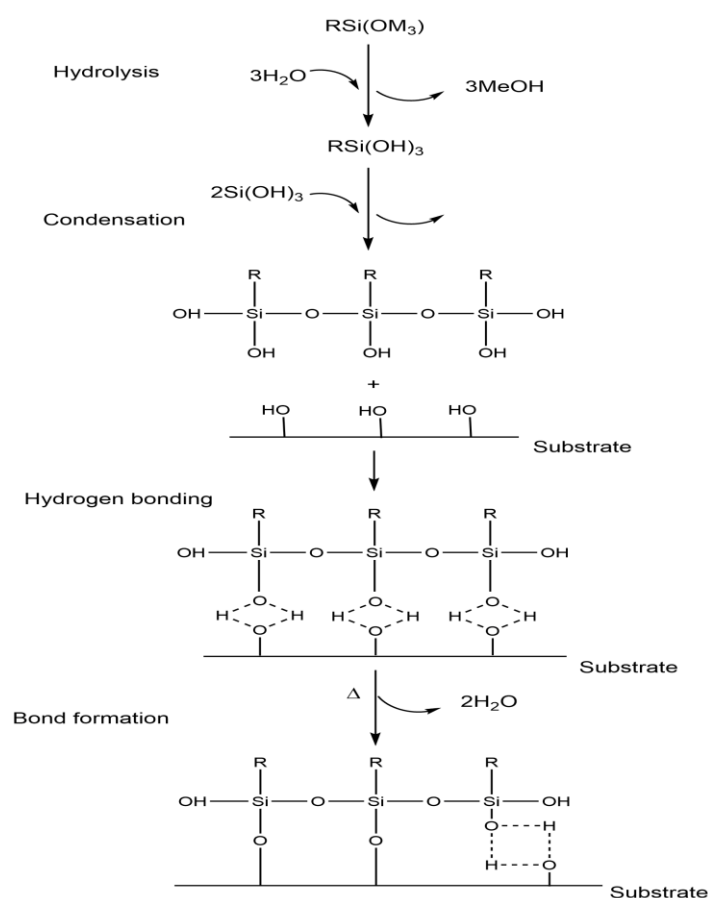


Figure 2-26. Mechanism of silanization on a surface

2.7.1.1 Amine-terminated films

Aminated surfaces are formed from organic molecules with amino group on the tail that anchor on solid surface while the amine group is upward. The amine-terminated films are utilised in numerous applications such as immobilising biomolecules and cell growth, covalent bonding of bioactive, metal corrosion protection and SAM foundation for ionic polymers (211, 235-241). Also amine moieties available on the film can improve adhesion between fibres and polymer matrix which is employed in light composition(240). Two aminosilanes (3-aminopropyltriethoxysilane (APTES) and p-aminophenyltrimethoxysilane (APhS)) were selected to treat the quartz surfaces in order to investigate the behaviour of new substrate coatings on scale deposition; Figure 2-27 shows the structure of APTES and APhS. APTES and APhS are known as alkoxy-based silane molecules which are able to adsorb on silicon based surfaces and form a densely packed layer via covalent bonds (248-253).

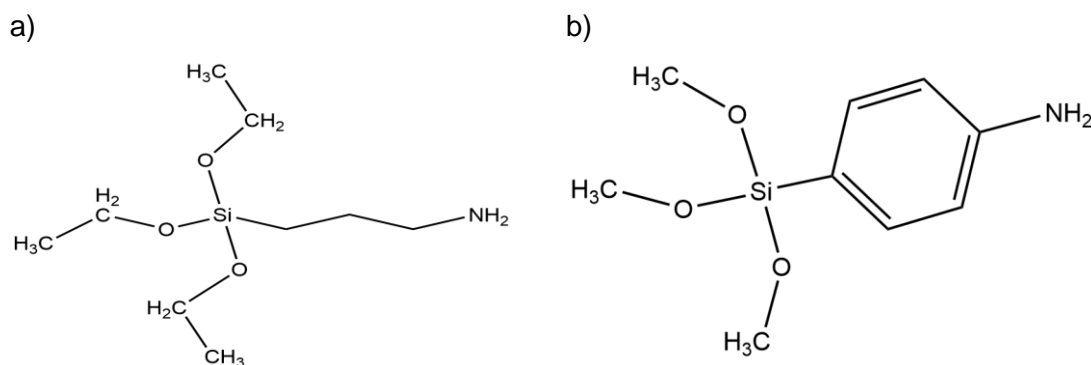


Figure 2-27. Molecular structure of a) APTES and b) APhS

There is a wide range of discussion available in literature for SAM formation of aminosilanes on the silicon based surfaces, which individually introduce a specific methodology that creates a homogenous surface. There are two different methods (liquid and vapour phases) to create aminosilane SAM on a substrate. In vapour phase, the studies showed that aminosilane SAM is reproducible; however, achieving a repeatable aminosilane SAM on surface is much difficult in liquid phase experiments (254-256). Wieringa and Schouten (257) used 5 wt% solution of APTES in toluene at 120°C for 16 h by a vapour phase method to create a SAM film on a silica surface; however, Siqueira Perti et al. (258) found this methodology cumbersome. Song et al. (259) also introduced another methodology to create SAM film on the substrate which was shown to be reproducible; they used vapour phase in 100°C with 0.1 APTMS with 0.7 ml toluene solution of silane in toluene for 1 h

(259). As mentioned earlier, it can be seen that creating a reproducible SAM film of an aminosilane on surface is a complex process.

Fiorilli et al. (255) formed SAM under liquid and vapour phases. In vapour phase, silicon dioxide substrate was exposed to APTES in plasma chamber at 80°C for 10 min. Also water steam delivered to the chamber for 10 min to hydrolyse ethoxy group of APTES. In solution phase, the silicon dioxide surface was treated by 1% (v/v) APTES in toluene at 60°C. Then the coated surface was rinsed with toluene several times followed by drying under nitrogen stream. The treated surfaces in both phases were characterised by XPS and AFM. XPS results for the surface coated under vapour phase showed a peak at 400 eV presenting free amine whereas in solution phase, a small shoulder was observed next to the peak of primary amine at 401.6eV indicating protonated amines. Figure 2-28 presents nitrogen (N) spectra for APTES treated surfaces under liquid and gas phases by Fiorilli et al. (255).

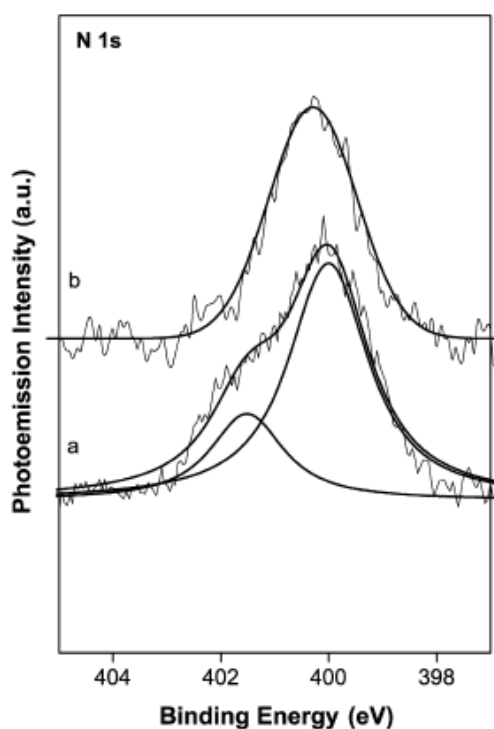


Figure 2-28. High resolution nitrogen spectra for the silicon surface treated by APTES a) in liquid phase b) in vapour phase

Based on the results of topography (Figure 2-29) for the treated surfaces in liquid and gas phase, Fiorilli et al. (255) observed smoother surface with smaller clumps for the substrate coated in vapour phase. Also the water contact angle measurements showed higher contact angles for the wet-based surface than vapour-based surface, which could be due to the presence of polymerised APTES

clusters on the wet-based surface where the methyl group of alkoxy chains were oriented upward leading to create a more hydrophobic surface (255). The same behaviour was also observed by Song et al. (259).

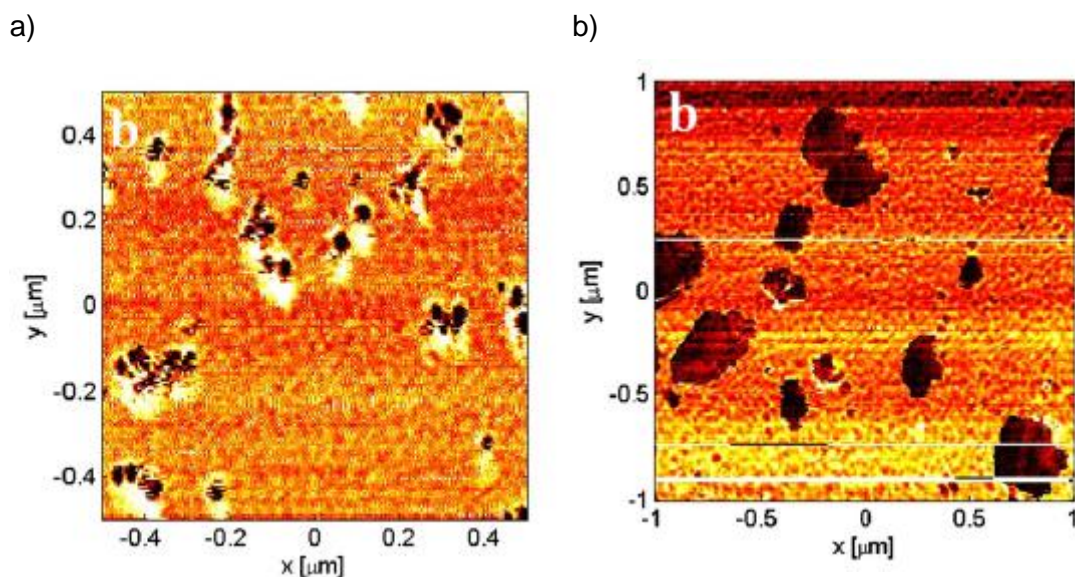


Figure 2-29. AFM images (topography) of a) treated silicon dioxide surface by APTES in gas phase and b) treated silicon dioxide surface by APTES in liquid phase

The formation of aminosilane monolayers in liquid phase is a very complex process and even under extremely controlled experimental conditions the polymerisation still happens in the solution; however, it is possible to form aminosilane SAM on silicon based surfaces (222, 260, 261). Thus, liquid-phase silanization of aminosilanes along with the mechanisms related conformations are extensively reviewed since liquid-phase method is used in this research.

2.8 Liquid-phase silanization of aminosilanes to create a SAM film on surface

Silanization of a surface occurs in two steps on the surface with OH bond on top layer; first the alkoxy group of aminosilane is substituted by hydroxyl group of the surface. Then the water molecule condenses and forms siloxane bonds which covalently attached on the surface. Silanization process was presented earlier in Figure 2-26. In order to comprehend the important parameters affecting silanization process, understanding the possible conformation of aminosilanes on surface is required.

2.8.1 Confirmations of aminosilane

Interaction between aminosilane and silicon dioxide surface can form siloxane bonds which are covalently attached to the surface. Ideally, aminosilane molecules attach to the surface via siloxane bonds with the amine moiety upward. However, the amine group can tilt towards surface due to the attraction between positive charge of amine and hydroxyl group of surface. Conformations of aminosilanes are determined by the type of reaction and density of molecules (262-267). Aminosilanes have the ability to cross-link horizontally or vertically to each other leading to polymerisation (268). Hence, different conformation can be obtained during silanization process depends on many factors. Figure 2-30 illustrates the possible APTES conformations that could form on a silicon-based surface.

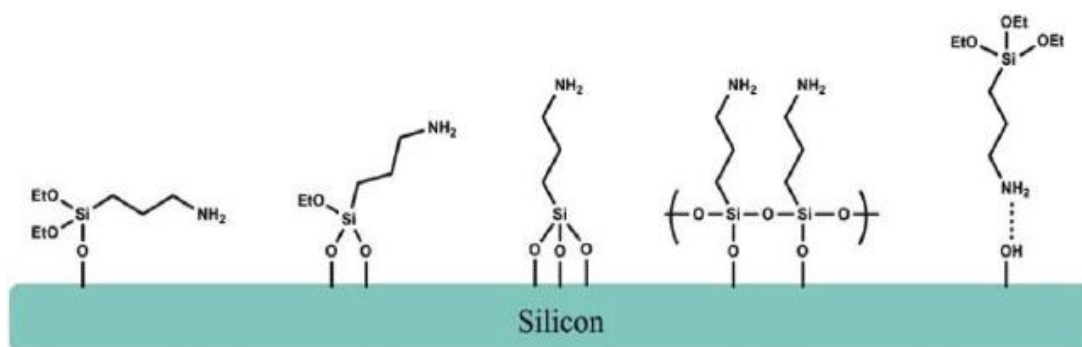


Figure 2-30. Possible APTES conformations on silicon surface (269)

As mentioned, formation of aminosilane SAM in aqueous solution is a very complex process and depends on several parameters such as pre-treatment process, experimental conditions (temperature, water content, aminosilane concentration, time of experiments, impurity of aminosilanes, solvent, etc.) and post-curing of aminosilane film. In addition, different cleaning methodologies of the surface before silanization experiment could result in different results. Effects of some of these parameters in liquid-phase are discussed below.

2.8.2 Parameters affecting SAM process

In this section, water content, concentration of aminosilanes, reaction time, solvent and curing on SAM film are discussed.

2.8.2.1 Water content

Silane adsorption strongly depends on the amount of water presented in the experiment. Silanization does not happen without water; however, the excess of water results in polymerisation (244, 245). Comparison between different percentages of water, either in liquid or gas phase showed that the lack of water prevents hydrolysis of ethoxyl or methoxyl moieties and condensation of hydroxyl groups on the surface, which leads to catalysing amino group. This resulted in more disordered and oriented aminosilane molecules in film structure (244, 245). On the other hand, an increase in water concentration resulted in polymerisation and agglomeration of molecules (237, 244, 270). Therefore, in order to create a uniform film of APTES or APhS, the optimum quantity of water is needed. Figure 2-31 presents AFM images of APTES film for different water concentrations, which shows the most uniform film in image B. The surface in image B was treated by 0.1% (v/v) APTES in solution of toluene.

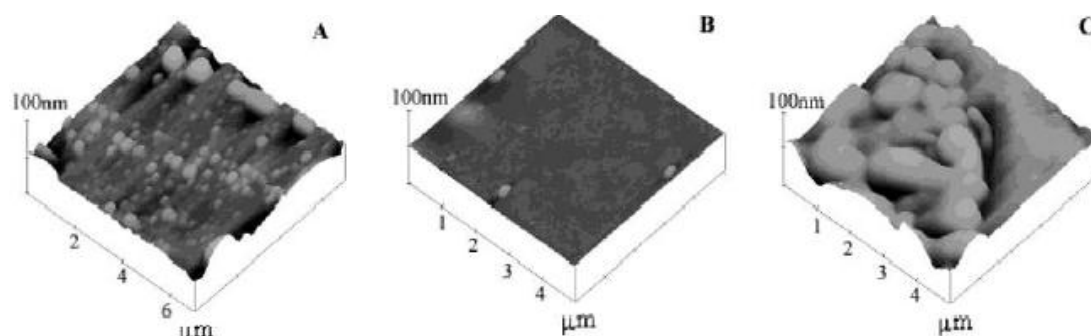


Figure 2-31. Film topography of APTES for different water contents, A) 0%, B) 0.1% and C) 1% (v/v) (244)

2.8.2.2 Reaction time

Time of deposition can also affect the film structure on the surface. It was shown (271, 272) that in a certain temperature and an aminosilane concentration but different reaction time, the types of bonding alter. Vandenberg et al. (271) and Simon A. et al. (272) found that the APTES coverage increased with the reaction time. However, Moiseev et al. (273) stated that a sufficient time is required for silanization on the surface and longer time results in APTES polymerisation and non-uniform coverage. Zhang et al. (244) demonstrated that in the early stages of silanization most aminosilanes attach to the surface via hydrogen bonding. They also showed that as the experimental time increased the H-bonded molecules broke and condensed, which resulted in attaching covalent siloxane bonds. Moreover, it was noticed (244) that overtime experiment led to aggregation of

aminosilanes and formation of multilayers. Song et al. (259) carried out silanization of APTMS on silicon surfaces for two reaction times (1 and 3 h) in order to optimising the film formation condition (259). After 1 h a smooth surface without clumps was observed while after 3 h aggregations of aminosilane were seen; AFM was used to display the topography of the treated surfaces. The roughness of surfaces was reported 0.45 nm and 0.78 nm for 1 and 3 h experiments, respectively. Moreover, the wettability of the silanized surfaces decreased due to aggregation and polymerisation of aminosilane.

Heiney et al. (247) dipped silicon wafers in the solution of 1% APTES, 5% deionised water, 94% methanol and 1 mM solution of acetic acid for different period of time. The water contact angle measurements showed that the hydrophobicity of the treated surface increased by time up to 60 min; however, the contact angles slightly decreased after 60 min with bigger standard deviations. It was proposed that at the early stage of the experiments, amine moieties of APTES molecules tilted towards surface and later they became vertical; however, polymerisation of APTES molecules was seen after a certain reaction time. The results of their work are presented in Figure 2-32.

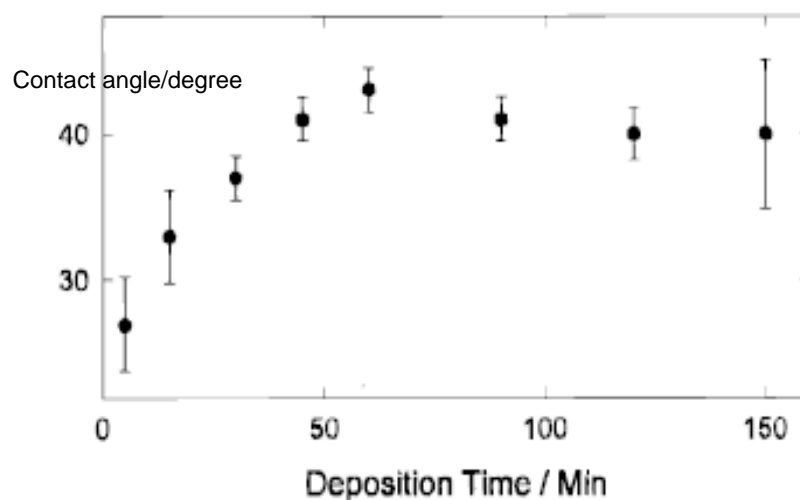


Figure 2-32. Water contact angle measurements for APTES treated surfaces in different time period (247)

Figure 2-33 presents the thickness of the APTES film on the surface in different reaction times. It was reported that the film thickness increased with time from 5 Å to 9 Å. They hypothesised that more APTES molecules attached to the surface when the deposition time increased leading to less tilted molecules on the surface; this results in formation of a thicker film on the surface.

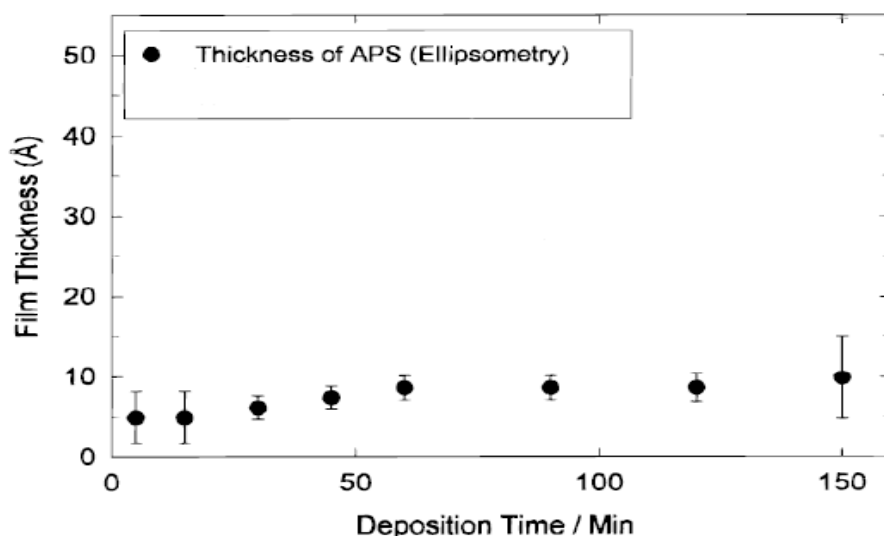


Figure 2-33. Thickness of APTES film in different time period (247)

Heiney et al. (247) eventually postulated that the deposition time played an important role to optimise SAM structure on the surface.

2.8.2.3 Concentration of aminosilanes

Concentration of aminosilanes in the solution affects film formation conformation. It was shown (244, 274, 275) that high concentrations of APTES and APhS in the solution resulted in agglomerations and polymerisations of the molecules before they reached the surface. It was also illustrated (244, 274, 275) that low concentrations led to partially coverage of the surface by APTES and APhS. Figure 2-34 presents topography of the surface treated by 3, 5 and 10 mM concentrations of APTES performed by Zhang et al. (244), which shows the most uniform film formed by the lowest APTES concentration (3 mM).

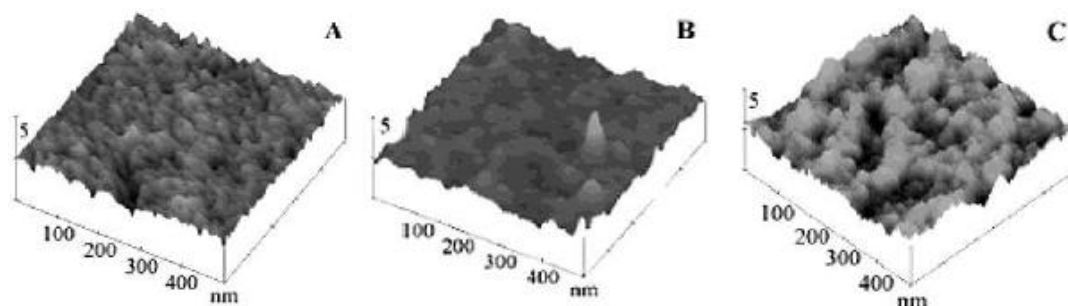


Figure 2-34. Film topography of APTES for different APTES concentrations, A) 3mM, B) 5 mM and C) 10 mM (244)

Wang et al. (276) studied the effects of APTES concentrations on a mica surface to obtain an optimum APTES concentration for SAM formation on the surface. The range of APTES concentrations was between 1% and 10% in toluene solvent. SAM film was obtained by 2% APTES on the mica surface.

2.8.2.4 Solvent

The type of solvent also influences the conformation of APTES on surface (277). Vandenberg et al. (271) deposited 0.4% APTES in different types of solvents at ambient temperature for 15 min. Then these samples were cured for 24 h in three different ways. The thickness of the films was measured by ellipsometry to study the effects of the various solvents. Table 2-5 presents the results of their work for APTES film created in different solvents. The effects of curing are also shown. Different thickness measurements were observed by different solvents. It was also shown that the curing influenced thickness of APTES films on the surface.

Table 2-5. Effect of deposition solvent on APTES film adhesion (271)

APTES thickness (nm)				
Solvent	Initial	24 h water	24 h oven	Oven + water
Toluene	0.9 ± 0.1	0.2 ± 0.1		
Trichloroethylene	0.7 ± 0.1	0.3 ± 0.1	0.6 ± 0.2	1.0 ± 0.3
Xylene	1.8 ± 0.1	0.2 ± 0.1	1.4 ± 0.2	1.7 ± 0.3
Acetone	0.8 ± 0.2	0.2 ± 0.1	0.7 ± 0.2	1.0 ± 0.4
Chloroform	1.0 ± 0.1	0.2 ± 0.1	0.8 ± 0.2	0.9 ± 0.2
Water	0.3 ± 0.1	0.4 ± 0.3	0.5 ± 0.1	0.7 ± 0.2
Ethanol	0.8 ± 0.1	0.1 ± 0.1		

2.8.2.5 Curing

Curing SAM film of aminosilane influences the film structure on surface. The investigation on coverage of the surface by aminosilane molecules showed that in order to create a uniform film on the surface, silanization is not only depends on the condition of experiment such as temperature, concentration, solvent and time) but also the procedure before and after experiment plays an important role (258, 278-280).

Siqueira Petri et al. (258) created 3-aminopropyltrimethoxysilane (APS) SAM in solution phase. 1% APS was immersed in toluene for 4 min at 60 ± 1 °C

and the surface was characterised by Ellipsometry and AFM. Thickness of the APS film was reported $9 \pm 1 \text{ \AA}$, but after post curing process on the treated surface the thickness of the film reduced to 1 \AA . The thickness of APS film obtained by Siqueria et al. (258) was different from the thicknesses reported by Tsukruk et al. (281) and Haller et al. (256) with the values of 5 \AA and 21 \AA , respectively.

Vandenberg et al. (271) also studied the effects of various types of curing on thickness of APTES film formed on the surface. The main results from their work were that different curing methodology resulted in different thickness of film on the surface and curing did not always reduced the thickness.

Table 2-6. Effect of different curing methodologies on thickness of APTES films (271)

APTES thickness (nm)				
Curing condition	APTES film type	No curing	curing	Curing 24 h in H₂O
Air	Thin	1.8 ± 0.6	2.4 ± 0.4	1.5 ± 0.3
	Thick	33 ± 2	38 ± 2	20.5 ± 0.8
Dessicator	Thin	1.8 ± 0.6	1.4 ± 0.2	0.8 ± 0.3
	Thick	33 ± 2	32 ± 3	1.3 ± 0.2
Ethanol	Thin	1.8 ± 0.6	2.4 ± 0.3	0.6 ± 0.3
	Thick			
Oven 200°C	Thin	1.8 ± 0.6	0.7 ± 0.3	0.9 ± 0.2
	Thick	33 ± 2	18 ± 2	17.9 ± 0.9

Chiang et al. (277) employed two different methods (air-dried and heat-cured) to cure the silanized samples. They reported that the air-dried APTES forms one or two siloxane bonds with the surface whereas the heat-cured APTES molecule forms three siloxane bonds with the surface.

Post-treatment of aminosilane SAM films is critical for creation of a uniform film on surface. For instance, when samples were baked after silanization at $100 \text{ }^\circ\text{C}$ and $150 \text{ }^\circ\text{C}$, the percentages of primary amine increased; this presents a film structure with amine groups upward. However, the excessive temperature may result in reduction of primary amine contents due to the reaction between CO_2 - which is adsorbed in ambient before post curing - and amine group of aminosilane; this leads to formation of carbamate (244, 282).

Rinsing with a solvent is used as a post-treatment method to remove the weakly-attached-aminosilane molecules to the other aminosilanes in order to form a uniform thin film. APTES film on the surface was rinsed by AcOH solvent to remove the weak bonded-APTES molecules; this led to a reduction of film thickness from

140 nm to 4 nm (283). It was also shown (284) that aqueous phosphate buffer decreased thickness of APTES film more than 70 Å. Figure 2-35 presents the topography of the surface before and after post curing for the work was performed by Argekar et al. (284).

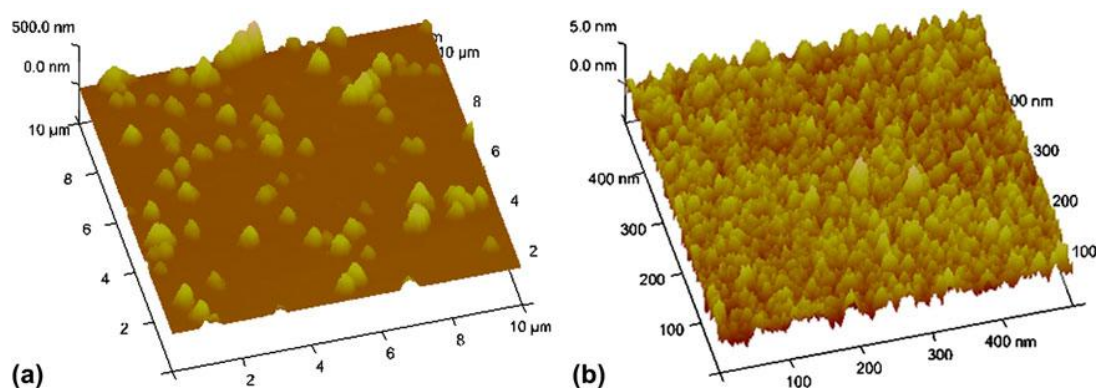


Figure 2-35. AFM images for a) before post treatment b) after post treatment by aqueous phosphate buffer (284)

Siqueira Petri et al. (258) also showed the roughness of the surface increased after silanization process from $1.25 \pm 0.07 \text{ \AA}$ to $2.2 \pm 0.2 \text{ \AA}$ which was in agreement with the results obtained by Tsukruk (281). The both authors suggested increasing the roughness after silanization might originate from the impurities and contamination on the surface.

2.8.3 Comparison between APTES and APhS

In general the factors mentioned above affect surface conformation, however, the molecular structure of APTES and APhS can affect film formation on the surface. Zhang and Srinivasan (244) studied APTES and APhS film formation under the same experimental condition and compared them with each other. 3 mM APTES or APhS layers deposited on silicon based surfaces in the solution of toluene and water (99.9/0.1) for 5 h at the ambient temperature. They reported 88.6% primary amine of APTES deposited on quartz surface whereas higher content (nearly 100%) of primary amine of APhS was observed for the film formed on quartz. they suggested that the rigid structure of APhS may limit the opportunities for hydrogen bonding between APhS and quartz surface. The high resolution of N_{1s} spectra is illustrated in Figure 2-36.

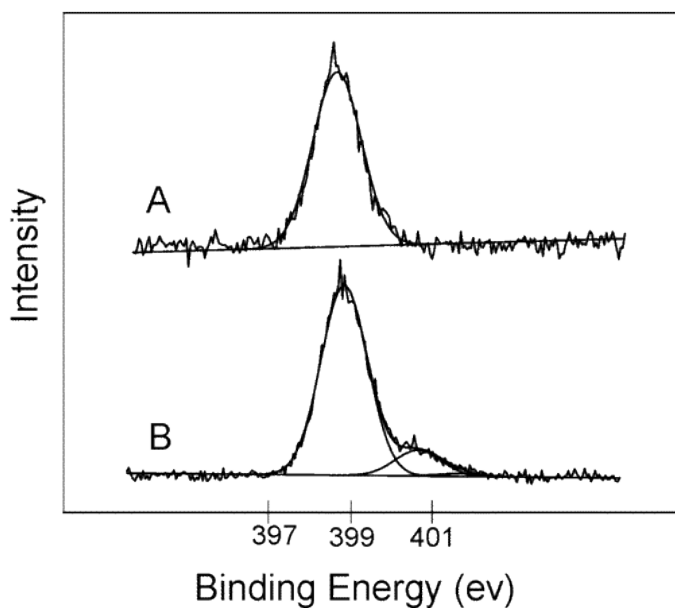


Figure 2-36. High resolution of N_{1s} spectra of quartz treated by A) APhS and B) APTES (244)

Moreover, it was shown that in comparison with APTES the roughness of APhS is smaller and APhS creates smoother film (244, 285-287). The difference between APTES and APhS films can be related to the rigid aromatic structure of APhS resulting in highly dense APhS molecules (244, 285). The phenyl ring of APhS prevents rotating and tilting molecules which result in smoother film with lower thickness. The topography of APTES and APhS films are illustrated in Figure 2-37 which shows a thinner film of APhS. The thickness of APTES and APhS films deposited on silicon dioxide was reported 5 nm and 1 nm, respectively. They suggested the larger aggregation of APTES compared to APhS deposited on the surface owing to more hydrogen bindings for the former.

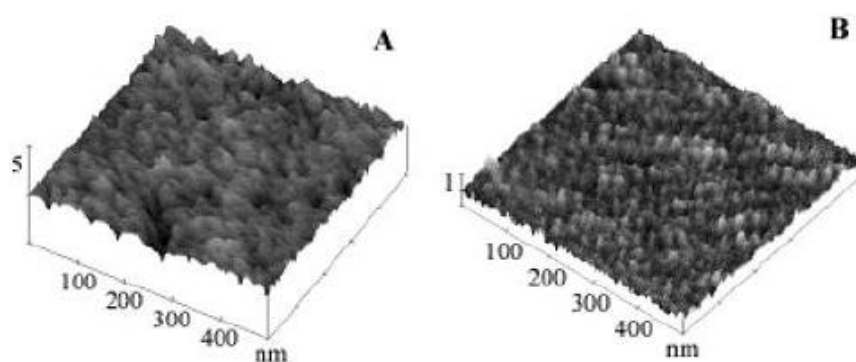


Figure 2-37. Topography of A) APTES and B) APhS film presenting smoother film for APhS (244)

Chapter 3

Methodology and Experimental Techniques

3.1 Introduction

An extensive literature review on silanization of silicon based surfaces has been performed in Chapter 2. One of the main challenges in this project was to find chemicals applicable to reservoir conditions which are able to reduce scale deposition near the wellbore area. Hence, the possible chemicals which could meet the purpose of this research are reviewed firstly in this chapter.

Secondly, the experimental methodology in this project is explained. Two different approaches were employed during this project to study potential of anti scaling surfaces:

- ❖ Employing Quartz Crystal Microbalance (QCM) to measure adsorption of 3-aminopropyltriethoxysilane (APTES) as a function of time in order to create SAM on a quartz surface
- ❖ Coating quartz surfaces with two different aminosilanes followed by running scale tests to evaluate the ability of the treated surfaces in order to reduce adhesion/deposition of calcium carbonate scale

Quartz component is the main composition of the most formation rocks (sandstone formation) in petroleum reservoirs, thus quartz surfaces were chosen as substrates to study aminosilane film formation and deposition of CaCO_3 . Film formation of two types of aminosilanes APTES and p-aminophenyltrimethoxysilane (APhS) on quartz surfaces were studied at different concentrations. Simple brine compositions with two saturation ratios (low and high) were used in scale tests in order to reduce the complexity of the study. Scale deposition tests were carried out in a pseudo-dynamic condition at 80°C .

In order to better understand the behaviour of the treated surfaces by APTES and APhS, the surface composition, roughness and wettability were studied by different techniques such as X-ray Photoelectron Spectroscopy (XPS), surface profiler (NP FLEX) and contact angle measurements, respectively. The results of

calcium carbonate scale deposition on the treated surfaces were analysed by Scanning Electron Microscopy (SEM) and weighing balance to study morphology of CaCO_3 crystals and to measure the amount of scale deposition.

An overview of surface kinetics is provided at the end of this chapter in order to calculate the surface coverage obtained by different concentrations of APTES.

3.2 Organosilanes

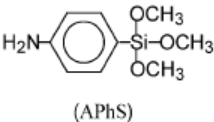

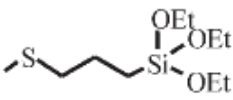
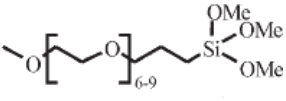
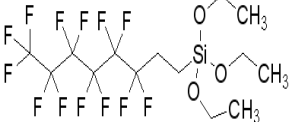
As mentioned, the first stage of this work was to identify chemicals can be applied to the near wellbore area with functions of: i) first, having covalent reaction with formation rock and ii) second, decreasing the tendency of mineral scale deposition on the near wellbore formation rock. The earlier was not fully known at the beginning of the research; however, one of the functionalities of organosilanes is that these chemicals can have a wide range of different types of tails which could be beneficial to this work as effects of different tails on scale deposition could be investigated. In other words, this coating should be semi-permanent (attached on formation rock for a long period) and simultaneously have fewer propensities to inorganic scaling.

Organosilanes were used as coupling agents in order to immobilise other molecules such as protein, enzyme, DNA on different substrates like quartz, glass (212, 213, 288, 289). One of the interesting properties of organosilanes is that these chemicals are able to chemically bond on different types of surface like metals, glass and quartz (206). In addition, organosilanes can have various types of tails which enable them to introduce distinguished physical and chemical properties on surface. Besides, organosilanes were used in the oil and gas industry for different purposes. One of the objectives of using organosilane in the oil field was to immobilize kaolinite in order to increase the adsorption of scale inhibitor on the formation rock (290, 291). This was inspired by the fact that the clay material in the formation rock is the most determining factor in adsorption of scale inhibitor on the rock (143).

Hence, several organosilanes were preliminary studied in this work, which are listed in Table 3-1. The reactivity of these organosilanes with quartz surface was demonstrated in the literature (206, 215, 218, 222, 224, 260, 292). It is seen from Table 3-1 that the major difference among these organosilanes is the tail structure. In addition, they need different solvents in the solution to react with the surface. Amongst the organosilane listed in the table only couple of them are hydrophilic (APTES and APhS). Also, APTES was previously qualified to be applied in oil fields (143, 290, 291). It was very important not to completely alter the

wettability of the formation rock (from hydrophilic to hydrophobic) near the wellbore area due to the fact that it is desirable to have water wet formation rock rather than oil wet in water production zones, APTES and APhS were initially selected to be investigated in this research.

Table 3-1. Different types of organosilanes with the structures, formulas and physical properties

Materials	Solvent	Shape	Wettability
P-aminophenyl trimethoxy silane	Toluene	 (APhS)	Hydrophilic
3-aminopropyl triethoxyl silane	Ethanol+ water		Hydrophilic
3-mercaptopropyl triethoxy silane	Ethanol- Water +acetic acid		Hydrophobic
2-[methoxy (polyethyl enoxy) propyl] trimethoxy silane	Toluene + diluted HCL		Hydrophobic
1H,1H,2H,2H-Perfluoro Octyltriethoxy silane	Toluene		Hydrophobic
Trimethoxy(octadecyl)Silane	Toluene	$\text{CH}_3(\text{CH}_2)_{16}\text{CH}_2-\text{Si}(\text{OCH}_3)_3$	Hydrophobic
Trichloro(1H,1H,2H,2H-perfluorooctyl) silane	Toluene	$\text{CF}_3(\text{CF}_2)_5\text{CH}_2\text{CH}_2-\text{Si}(\text{Cl})_3$	Hydrophobic

3.3 Experimental methodology and materials

The first step was to study the kinetics of APTES film formation to calculate the surface coverage. These results were used to better interpret the film structure formed by aminosilanes on the quartz surface. QCM was employed to measure the rate and amount of adsorption of APTES on the surface as a function of time. By controlling the experimental conditions, this technique helps to create a uniform film on the substrate (212, 213, 215, 285, 288, 289, 293, 294). Prior to apply QCM technique for APTES film formation, distilled water (DW) was tested in QCM to calibrate the instrument; this is shown in Figure 3-1. It is seen that the mass adsorption of DW was constant with respect to time resulting in zero adsorption rate. This experiment was randomly repeated several times to make sure of consistency of the QCM results.

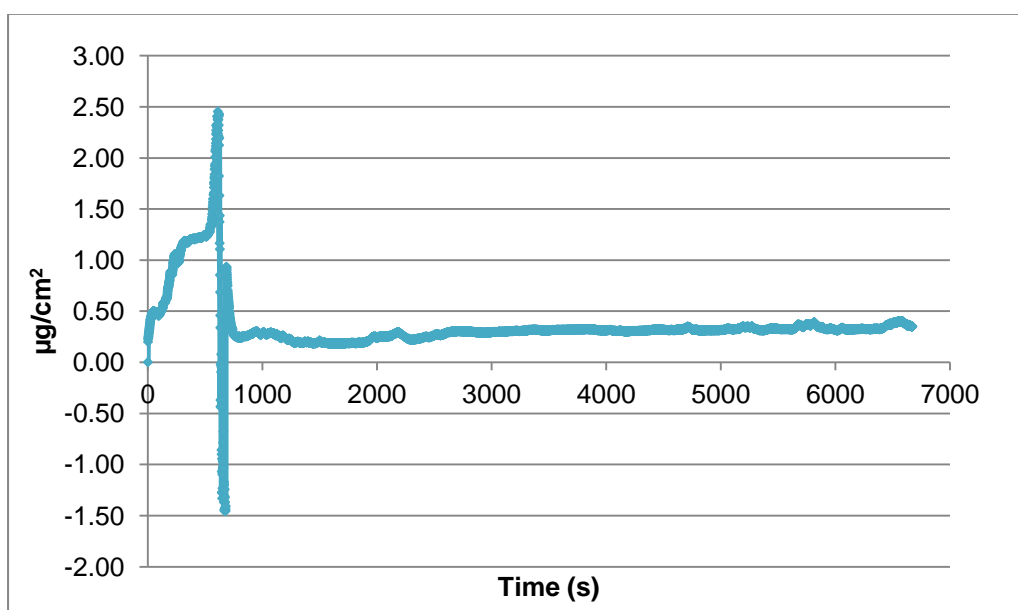


Figure 3-1. DW adsorption on quartz crystal surface as function of time by QCM at ambient temperature

Apart from QCM, quartz single crystal coupons were used as substrates for the film formation in a static condition. Various concentrations of APTES and APhS were utilised to study performance of the treated quartz surfaces on deposition of calcium carbonate. The treated surfaces by APTES and APhS were characterized by different surface characterisation methods in order to assess the relation between scale deposition and the surface properties and to suggest possible film structures on the quartz surfaces. Scale deposition tests were carried out on APTES- and APhS-treated surfaces and also compared with blank quartz surfaces in order to

evaluate the performance of the treated surface. Weighing balance and SEM were employed to measure the amount of scale deposition on the surfaces and to study the morphology of calcium carbonate crystals on the surfaces, respectively.

Ethanol/water and toluene were used as solvents for APTES and APhS in this work, respectively. As mentioned in Chapter 2, different solvents can affect the formation of film on the substrates. In addition, water content influences the structure of film on surfaces. Based on literature review and comparing the previous works, more uniform film formation was shown by using toluene as a solvent compared with ethanol/water. However, more experimental times were generally required for using toluene in the solution to have a uniform film on surfaces. On the other hand, higher concentrations were required in the solution where ethanol/water was used as solvents. In addition, it is more desirable to use a water soluble solvent near the wellbore area in water production zones. Hence, ethanol/water was chosen as a solvent for APTES film formation.

The main purpose of using APhS in this research was that it has the same tail group (-NH₂) as APTES, but different tail structure (benzene ring in APhS and alkoxy in APTES). This could result in useful information in order to understand the behaviour of film conformation on calcium carbonate scale deposition, since the surface composition remained similar for both APTES- and APhS-treated surfaces (only structure is different). The only solvent could be used for APhS experiments was toluene, otherwise the ethanol/water would have been used.

3.3.1 Materials

Crystals of QCM as the substrate for APTES film formation were supplied from Stanford Research System in USA. These crystals were AT-cut quartz crystals, 5 MHz, 1 inch diameter size with circular gold electrode on the centre of both sides. Quartz surfaces also as the rock analogue for studying APTES and APhS film formation and calcium carbonate deposition were provided by PI-KEM in the UK. The quartz surfaces are featured with both sides polished with dimensions of 10x10x0.5 mm.

3-aminopropyltriethoxysilane (APTES) - 99.7% purity - with molecular formula of H₂N(CH₂)Si(OC₂H₅)₃ was supplied from Sigma-Adrich, UK. P-aminophenyltrimethoxysilane (APhS) with molecular formula of C₉H₁₅NO₃Si was provided by Glest, UK.

Ethanol (>99%) with molecular formula of C₂H₆O and toluene (99%) with formula of C₇H₈ was supplied by Fisher, UK.

3.3.2 Experiment methods

Before treating the substrates by aminosilanes, cleaning treatments needed to be carried out in order to first remove contamination from surface and second to improve the functionality of the quartz surface for film formation experiments by creating OH bonds on the surface. Hence, plasma chamber was first used to remove possible contamination from the surface. After that, the substrates were rinsed by DW followed by drying with pressurized air gun. These procedures were followed for both QCM and quartz coupon experiments.

3.3.2.1 APTES film formation study by QCM

Only APTES was employed in QCM for studying the film formation and the kinetics. Different APTES concentrations (2%, 4%, 6% and 8%) in a solution of ethanol and water (95/5 v/v) was used; this was inspired from Janssen et al.'s work (260). 200 ml solution of ethanol and distilled water (95/5 v/v) were prepared. Prior to adding APTES in the solvent the cleaned crystal inside the holder was immersed in the solution. QCM was then run in DW until the mass rate measured by QCM stabilized. After that, a desired amount of APTES was added into the solution. Prior to adding APTES into solution, the same amount of the solvent was extracted. The tests were run for two hours. The experiment time was modified according to the literature (260).

3.3.2.2 Silanization of quartz coupons by APTES and APhS

Two ranges of APTES concentrations were used in silanization experiments on the quartz coupons. The first range was the same as the QCM experiments (2-8%). A wide range of APTES concentrations (also below 1%) used in literature mainly with toluene as a solvent. In addition, it was shown that by applying 2% APTES concentration to the solution a multilayer film was created on the surface rather than SAM (295). Hence, it was attempted to study the possibility of using lower APTES concentrations to create a uniform film in ethanol/water solution in order to reduce the cost of methodology and amount of chemicals used in the oil field for Health Safety Environment (HSE) purposes. Therefore, the second range of concentration was selected between 0.05% and 0.1% (0.05%, 0.1%, 0.15% and 0.2%).

Different APTES concentrations were added and left into a solution of ethanol and water (95/5 v/v) for 5 min followed by immersing a quartz coupon in the

solution for 30 minutes. The total volume of the solution was 5 ml. The experiment was run at the ambient temperature. After that, the treated surfaces were rinsed by ethanol and dried with pressurised air gun.

It was demonstrated (285) that 0.06% APhS in toluene solution for 2 h formed APhS SAM on quartz surface. Hence, a range of concentrations were chosen for APhS film formation from 0.03% to 0.24% (0.03%, 0.06%, 0.12%, 0.18% and 0.24%). This could help to better understand the behaviour of the treated surfaces on calcium carbonate scale deposition. The desired APhS was added to 5 ml solution of toluene and left few min to dissolve in the solution. After that pre-cleaned quartz coupon was immersed in the solution for 2 h. Then, the treated surface was rinsed by toluene and dried by the pressurised air gun. The experimental methodology for APhS film formation was obtained from Puniredd et al. (285).

3.3.2.3 Calcium carbonate scale deposition test

Basic calcium carbonate brines were chosen in the scale experiments. As mentioned before, two different saturation ratios (4.8 and 54.8) were selected. The compositions of the solution are illustrated in Figure 3-2. These tests were carried out at 80°C in the pseudo-dynamic condition. Both silanized and blank surfaces were used in the scale test for comparison the studies to evaluate the ability of the aminosilane-treated surfaces in order to reduce calcium carbonate scale deposition.

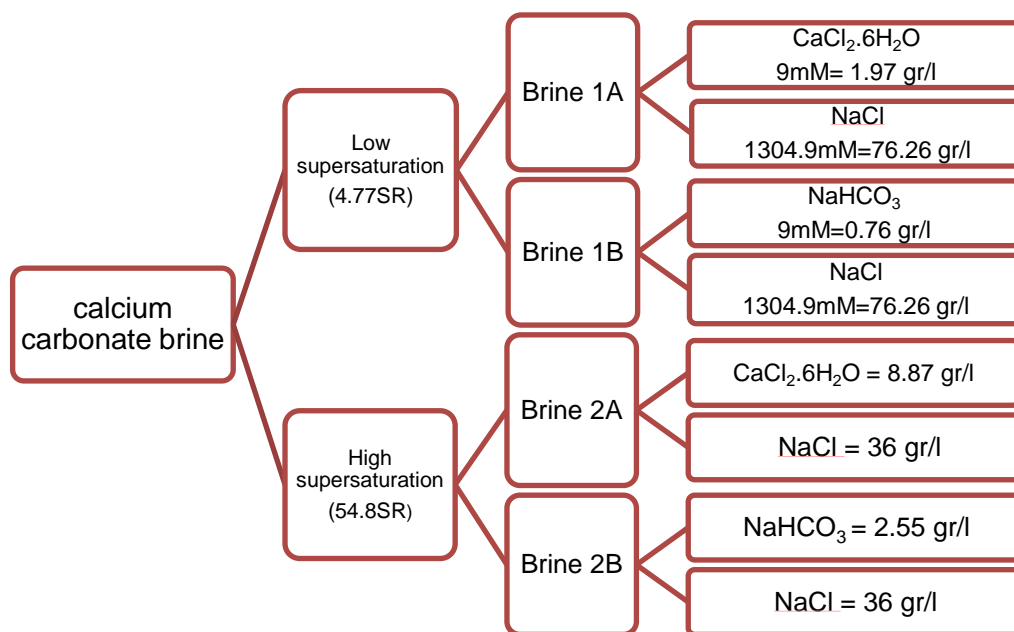


Figure 3-2. Compositions of calcium carbonate brines in scale deposition tests

Brines A and B were heated separately at 80°C. After that, these two brines were mixed by keeping the temperature constant. Immediately, the blank and silanized coupons were immersed in the calcium carbonate brine by means of a holder to stay in the solution vertically in order to eliminate precipitation of crystals on the surface.

A picture of the experimental set up was shown in Figure 3-3. A specific lid was designed for these experiments to stop the evaporation of the water from the solution. Plus, the holder was designed to keep the crystal vertically in the solution without covering the quartz surface exposed to the solution. A magnetic stirring bar was employed in the solution to create a pseudo-dynamic condition. At the same time, the whole beaker and the solution were heated by a hotplate to keep the temperature at 80°C constantly. These experiments were carried out for 24 h.

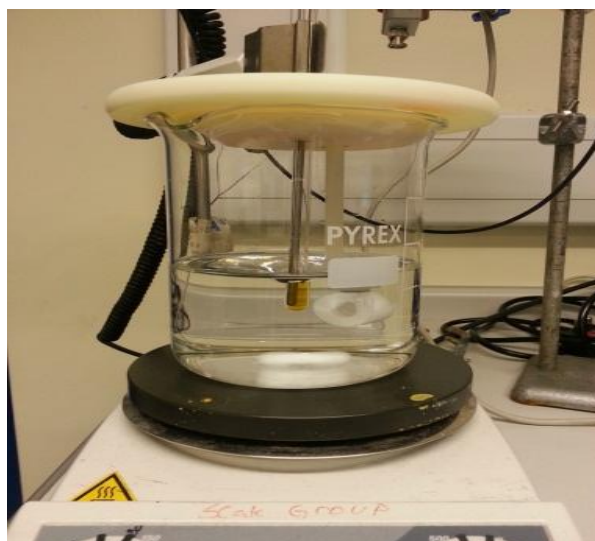


Figure 3-3. The picture of the scale experiment set up

3.4 Characterisation techniques

Different characterisation techniques were employed to study the film kinetics, surface properties, morphology of calcium carbonate scales on the surfaces and the effects of formation film on scale deposition.

3.4.1 Quartz Crystal Microbalance (QCM)

QCM is known as an ultra-sensitive mass sensor. The way QCM works is that frequency of piezoelectric quartz crystal is disturbed by being introduced to a small mass (296). The piezoelectricity of quartz was first observed in 1880's when

the quartz surface was under strain (297, 298). The applications of QCM were for gas adsorption measurements until 1980's. QCM measurement in liquid solution was achieved in mid 1980's for the first time. Since that time, QCM has undergone many modifications to reduce the potential errors in order to improve the measurement reading (299). The piezoelectric quartz crystal generates a voltage when the symmetry of the crystal is disturbed by mechanical stress. Then, the frequency alteration is recorded, which can be converted to mass adsorption on the quartz surface.

In this work, QCM200 model with 5 MHz crystal frequency was used. This QCM was provided by Stanford Research System and is shown in Figure 3-4. The diameter of crystals used in this QCM was 1 inch.



Figure 3-4. QCM200 set up (QCM200 Digital Controller, QCM25 Crystal Oscillator, crystal Holder and Quartz sensors)

QCM is able to measure the kinetics of film during adsorption in liquid or gas phase (300). The quartz crystal is made of AT-cut quartz due to zero frequency drift at the ambient temperature and partially coated by gold as electrodes in the centre. The electrodes are connected to an oscillator and a specified voltage is applied over the electrodes which lead to start vibration of QCM crystal owing to the piezoelectric properties of quartz crystal (301-303). When the deposition starts on the crystal, the increase in mass is detected by the decrease in the frequency of the quartz crystal (304-306). Front and back sides of QCM crystal are shown in Figure 3-5.



Figure 3-5. Front and back sides of QCM crystal

3.4.1.1 Sauerbrey model

The QCM principals based on Sauerbrey equation (Equation 3-1) (307, 308), which shows a linear relation between mass and frequency. This means that a small mass adsorption on the quartz surface results in the change in the frequency of the quartz. It is assumed that mass equally deposits on the detective area of the sensor which leads to shift resonance frequency of the device (309, 310).

$$\Delta f = \frac{-2f_0^2 \Delta m}{A(\mu_q d_q)^{1/2}}$$

Equation 3-1

Δf : measured frequency shift (Hz)

f_0 : resonance frequency (Hz)

Δm : the mass change (g)

A : effective area of the electrode (m²)

μ_q : shear modulus of the quartz (2.947x10¹¹ g·cm⁻¹·s⁻²)

d_q : quartz density (2.648 g/cm³)

QCM has been known as one of the best devices to show the growth of mass as a function of time (288, 289, 311-317). Figure 3-6 presents different mass deposition trends as a function of time.

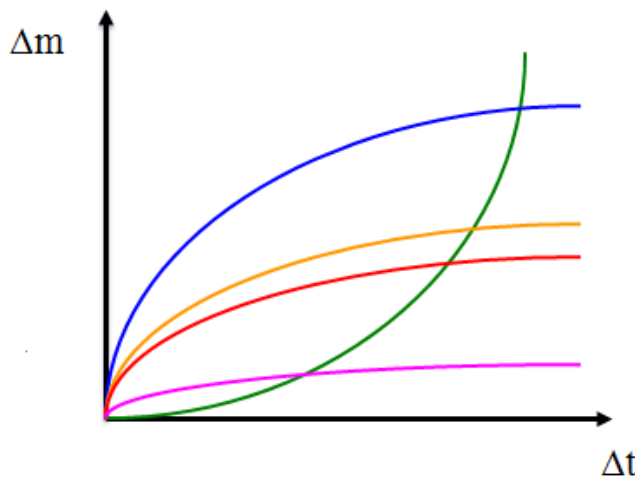


Figure 3-6. A model of QCM's graph showing the rate of deposition as a function of time

Some assumptions are required to be made in order to have an appropriate application of Sauerbrey model, which are presented below:

- The quartz crystal consists of two parallel faces.

- The amplitude loss of quartz vibration is negligible.
- The model is in one dimension.
- The mass adsorption is uniform on the surface
- The weight of electrodes on quartz crystal surface is negligible and the electrodes are completely conductive.
- The electrodes are fully connected to the quartz crystal
- The adsorption mass is much smaller than crystal weight.

In order to correctly apply Sauerbrey model, the density of the solution and viscosity of the loaded layer need to be kept constant. The change in viscosity results in a shift in frequency which needs an appropriate algorithm to remove this effect from measurements (318). Nonetheless, these two parameters change during QCM measurements in a liquid phase (319). These problems were firstly solved by Glassford (320) and later by Kanazawa and Gordon (319), who involved the solution properties allowing prediction of resonance frequency changes. The equation below includes viscosity and density of the solution in Sauerbrey in liquid solution.

$$\Delta f = f_0^{3/2} \left(\frac{\rho_L \eta_L}{\pi \rho_q \mu_q} \right)^{1/2} \quad \text{Equation 3-2}$$

Where:

f_0 = frequency of oscillation of unloaded crystal (Hz)

ρ_q = density of quartz (2.648 g/cm³)

μ_q = shear modulus of quartz (2.947x10¹¹ g·cm⁻¹·s⁻²)

ρ_L = density of liquid in contact with the electrode

η_L = viscosity of the liquid in contact with the electrode

3.4.2 X-ray Photoelectron Spectroscopy (XPS)

Siegbahn et al. developed XPS for the first time in 1960s in Sweden (321). The information about the top layer of a substrate is very important to surface engineers. XPS is known as a strong surface analytical technique, which is able to analyse existing elements on the surface, to provide quantitative composition and to determine the chemical state of film formation on the surface. These features of XPS allow getting a deeper understanding on physical and chemical characteristics of a surface. XPS provides information about few nanometers of the first top layer

of the surface and is generally considered as a non-destructive. In this work, XPS analysis was performed using a VG theta probe ESCA 250 spectrophotometer (Thermo Electron Corporation, West Sussex, UK).

Basically, photoelectric effect is the main mechanism of XPS. When an X-ray photon interacts with a surface an electron is emitted from an atomic energy level or a valence band of which the energy is analysed by the spectrometer; the schematic is shown in Figure 3-7.

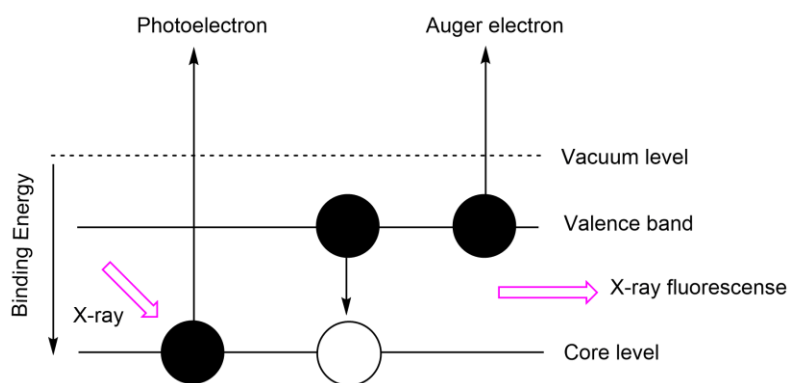


Figure 3-7. Schematic of photoionisation process and the relaxation mechanisms

The binding energy of the emitted electron (BE) is associated with the kinetic energy of the photoelectron (EK) and the photon energy ($h\nu$); this is given in Equation 3-3 where ϕ_s is the spectrometer work function.

$$BE = h\nu - EK - \phi_s$$

Equation 3-3

The X-ray beam is able to penetrate a few micrometers depth of the surface; however, the photoelectron of the 10 atomic layers of the surface can be detected. Thus the detection of surface composition is originated from the top few nanometer of atomic layer. In organic materials, this results in detection of C1s, O1s and N1s (core compositions of organics) from the first 2 to 3 nm of the surface when EK varies between 10 to 1000 electron volt (eV).

3.4.2.1 Qualitative analysis

Available elements on the surface are detected by qualitative analysis of XPS, which is performed by a survey scan spectrum. Each spectrum and chemical shift is related to a unique element; the spectrum can be in range of a fraction of

electron volt to several electron volts. The spectra detection is automatically performed in XPS instrument by using peak identification features, which are later fitted by computer curve fitting software. This routine is normally straightforward and simple, but it becomes complicated in some cases where peaks are overlapping.

Initial-state (the charge of the atom) and final-state (the electronegativity of the atom) effects in XPS are responsible for chemical shifts of detected elements. The occurrence of the shift influenced by the initial-state effects and value of the shift is affected by final-state effects. For example, the binding energy shift of C1s in C-F is 2.9 eV, but this value increases in CF₂ and CF₃ by 5.9 eV and 7.7 eV, respectively (322).

3.4.2.2 Quantitative analysis

Equation 3-4 presents the relationship of the intensity of a photoelectron (I) to the number of atoms of the element per volume (n), the photoelectric ionization (cm²) $\sigma(E_{kin})$, the X-ray flux in photons/cm².s (J), the detection efficiency of each electron transmitted $D(E_{kin})$, analyser transmission (T), angular asymmetry of the intensity of the photoemission from each atom (L), the detected surface area (A), the inelastic mean free path of photoelectrons ($\lambda(E_{kin})$) and the measured angle of emission of electron from surface (Θ) (323, 324).

$$I = n \cdot (J \cdot \sigma(E_{kin}) \cdot D(E_{kin}) \cdot T \cdot L \cdot A \cdot \lambda(E_{kin}) \cdot \cos\theta) \quad \text{Equation 3-4}$$

Thus the number of atoms per cm³ for a specific element can be calculated by Equation 3-5.

$$n = I / (J \cdot \sigma(E_{kin}) \cdot D(E_{kin}) \cdot T \cdot L \cdot A \cdot \lambda(E_{kin}) \cdot \cos\theta) \quad \text{Equation 3-5}$$

3.4.3 Contact angle

Understanding of surface free energies between two entities is important. The strength of the interaction on the surface is dictated by surface energy. Contact angle measurements can be employed with different solvents in order to calculate the surface energy of the substrates (260) by measuring the interface angle between the liquid and solid phases. Wettability is also known to be associated with surface composition and roughness of the surface. Hence, for better understanding of the surface characterization on scale deposition, the mechanism of the interfacial

energies of two surfaces (solid-liquid phase) and effect of surface free energy and the components on its environment are investigated.

The contact angle method is being widely used to describe the surface energy of solids. The higher the contact angle value of water indicates, the more hydrophobic the solid surface becomes; which represents the lower surface energy of the surface. Figure 3-8 presents a water contact angle instrument. In this study, Contact Angle Goniometry 4000 is used to measure the water contact angles.



Figure 3-8. Contact angle measurement instrument

The surface energy of solid phase can be evaluated by the contact angles between the solid and liquid phases on a flat surface. The relation between contact angle and surface energies can be found via Young's equation.

$$\gamma_S = \gamma_{SL} + \gamma_L \cdot \cos \theta$$

Equation 3-6

Where γ_S is the surface energy of solid, γ_{SL} the surface energy of solid/liquid interphases, γ_L the liquid surface tension and θ the contact angle.

In this work, θ is the parameter which is measured in Equation 3-6. Figure 3-9 shows a schematic of a liquid droplet and the parameters involved in Young equation.

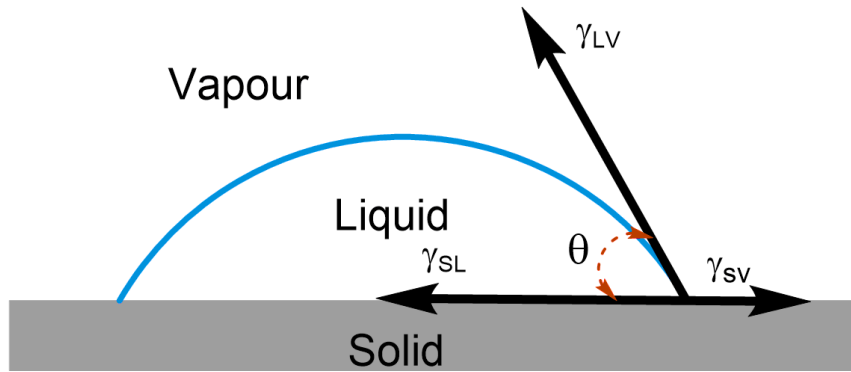


Figure 3-9. Schematic of liquid droplet on a solid surface presenting the Young's equation

3.4.3.1 Surface Profiler-NPFLEX- (roughness measurement)

In order to measure the roughness of the surfaces and study the effects of topography on calcium carbonate scale deposition, a Taylor Hobson surface profiler was employed. The irregularity of substrate originated from peaks and valleys of surface texture is referred to the roughness, which is mainly affected by manufacturing process and the top layer structure of the surface. The deviations from a mean line are measured to evaluate the roughness of the surface; the mean line represents an ideal smooth surface without peaks and valleys. Different parameters are involved in measuring the roughness of a surface, since the surface geometry is so complicated to take into account just one parameter (325). The parameters involved in studying the surface topography are presented in Table 3-2.

Table 3-2. Some of the influencing factors in roughness studies (quoted from (325-327))

Designation parameter	Definition	Formula
S_a Arithmetical mean height	Mean surface roughness	$S_a = \frac{1}{A} \int_A z(x, y) dx dy$
S_q root mean square height	Computes the standard deviation for the amplitudes of the surface (RMS)	$S_q = \sqrt{\frac{1}{A} \iint_A z^2(x, y) dx dy}$
S_{sk} Skewness	Qualifying the symmetry of the height distribution	$S_{sk} = \frac{1}{S_q^3} \left[\frac{1}{A} \iint_A z^3(x, y) dx dy \right]$
S_{ku} kurtosis	Qualifying the flatness of the height distribution	$S_{ku} = \frac{1}{S_q^4} \left[\frac{1}{A} \iint_A z^4(x, y) dx dy \right]$

Root mean square height (S_q) measurements were mainly used in this work; however, Skewness (S_{sk}) helped in some interpretation. S_q computes the standard deviation for the amplitudes of the surface (RMS).

3.4.3.2 Scanning Electron Microscopy (SEM)

SEM is a big microscope with high magnification which employs electrons instead of light to get images with high resolution. This device is capable of capturing pictures with high magnification (100000 times bigger) from a sample which allows us to get more information from the desired surface or particles. SEM produces a beam of electrons on the sample in the chamber which are emitted from a thermal resource with a range of energy between 30 eV and 100 eV. In order to create an image from a sample, incident electrons from the electron column above the chamber cause emission of electrons from the sample leading to detecting the desirable area.

Figure 3-10 shows different parts of a SEM device participating in imaging a sample on a surface. Electron gun exposes the incident electrons in column from above the chamber. Anode plate accelerates electrons attraction and scanning coils diverts the beam to scan over the sample in a rectangular area. Also, there is another part so-called back scattered electron detector which provides the image contrast and topography. Secondary electron detector creates images with high resolution.

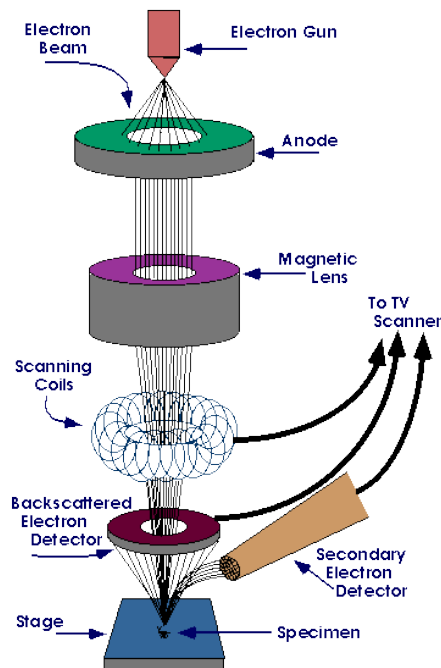


Figure 3-10. Different parts of a SEM device involved in creating a picture

SEM can be applied for different applications such as microstructure studies and film characterisation. The SEM machine used in this study is LEO 1530: Gemini FEGSEM with Oxford Instruments AZtecEnergy EDX system with 80mm X-Max SDD detector - high resolution, low kV, secondary electron imaging

plus EDX capabilities and KE STEM detector. Figure 3-11 shows an image of calcium carbonate crystals taken by SEM.

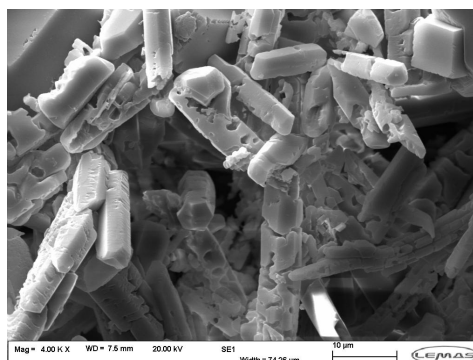


Figure 3-11. SEM image of calcium carbonate crystals

3.5 Film kinetics

Studying kinetics of film formation helps to better understand the parameters involved during adsorption. In order to have an optimum experimental conditions and parameters during formation of Self-Assembled Monolayer (SAM) film on a quartz surface, kinetics of APTES adsorption on crystal quartz surface was studied by QCM. This information helps to understand the best required concentrations of APTES and reaction time to form SAM of APTES on the quartz surface. In addition, the surface coverage formed on the quartz surface by each concentration of APTES. The mechanisms of APTES adsorption on the quartz surface can be also investigated.

SAM technique which self-terminates chemisorption reactions with one layer on the surface under correct experimental conditions is one of the focuses in the literature (212, 213, 288, 289). Different isotherms to describe the adsorption mechanisms of organosilanes on surfaces were studied previously by other researchers (222, 328, 329) who showed that Langmuir isotherm better interpreted the adsorption phenomenon of organosilane molecules on quartz surface. Langmuir adsorption isotherm assumes: i) that the adsorbent surface is completely flat and perfect (homogeneous surface), ii) that all available sites of the surface are equivalent, the adsorbing materials adsorb onto a stationary surface, iv) that each site can accept just one molecule (mono-layer adsorption) and v) that there is no interference between two adjacent adsorbates (294, 328, 330, 331).

The surface coverage is described as the fraction of surface occupied by adsorbate, which is a unitless quantity, Θ ; this gives the Langmuir isotherm (330-332). Thus, the rate of surface coverage is given by

$$\frac{d\theta}{dt} = k_a(1 - \theta)C - k_d\theta$$

Equation 3-7

Where Θ is the fraction of available sites that occupied by adsorbate; $(1 - \Theta)$ is the remaining free available sites; C is the APTES concentration; and k_a and k_d are the adsorption and desorption constants, respectively. Integration of Equation 3-7 results in the surface coverage as function of time.

$$\theta(t) = \frac{C}{C + \frac{k_d}{k_a}} (1 - e^{-(k_a C + k_d)t}) \quad \text{Equation 3-8}$$

This result is simplified by replacing k_{obs} for $k_a C + k_d$ and K' for

$$K' = \frac{C}{C + \frac{k_d}{k_a}}$$

This results in Equation 3-9 giving surface coverage by APTES on the quartz surface as a function of time.

$$\theta(t) = K'(1 - e^{-k_{obs}t}) \quad \text{Equation 3-9}$$

As shown earlier, APTES adsorption on the quartz surface as a function of time can be plotted by QCM. In order to calculate the surface coverage, k_{obs} needs to be calculated from the QCM plots. A Matlab code was written to fit the experimental data and to calculate k_{obs} ; the Matlab code is presented in Appendix A. As $k_{obs} = k_a C + k_d$, a plot of k_{obs} for different APTES concentrations versus C gives a linear trend with a slope indicating adsorption constant (k_a) and an intercept indicating desorption constant (k_d). Thus, equilibrium constant (K_{eq}) is obtained by.

$$K_{eq} = \frac{k_a}{k_d} \quad \text{Equation 3-10}$$

The percentage of the surface covered by APTES is then calculated by

$$\theta = \frac{C}{C + \frac{1}{K_{eq}}} \quad \text{Equation 3-11}$$

Where Θ is the surface coverage (%), C concentration of APTES, and K_{eq} equilibrium constant of the solution.

Chapter 4

Film Formation of APTES on Quartz Crystal

4.1 Introduction

A self-assembled monolayer (SAM) consists of organic molecules that attach on the surface of a substrate in systematic groups (1-3). However, to create a SAM surface the growth process needs to be controlled by controlling experimental condition during film formation to adapt the orientation of the molecules for each specific goal. The Quartz Crystal Microbalance (QCM) was used to study the kinetics of film deposition on the surface (used as analogue for sandstone) for different concentrations of 3-aminopropyltriethoxysilane (APTES). This allowed the adsorption and growth process of APTES on the quartz surface to be examined in detail. This technique can also be used to assess the ability of the treated quartz surfaces to minimise scale; this will be demonstrated in the next chapters.

Various concentrations of APTES (2, 4, 6 and 8% v/v) were added in solutions of ethanol and water to study effect of concentration on film coverage (260). There are different types of isotherm which could be considered to calculate the surface coverage, however, other isotherms such as Tempkin isotherm showed a poor correlation for different concentrations of APTES (222). Since the focus of this research was not specifically on the type of isotherm and based on the

obtained results in the previous works (222, 328, 329), Langmuir isotherm was selected to study the kinetics of film formation. Since one of the assumptions of Langmuir isotherm is that the adsorption is limited to monolayer and the purpose of the project was to create a SAM on quartz crystals, Langmuir isotherm was employed to describe the adsorption of APTES on the surface. Matlab was applied to the experimental results to fit the data to the Langmuir isotherm. From the equations obtained from Matlab, which fit the Langmuir isotherm the equilibrium constant and surface coverage of the quartz crystals at equilibrium were calculated. These data are presented later in the chapter. A simulation of the arrangement of the molecules was also carried out through minimising the energy of the molecules. This was used to estimate the surface area that was occupied by one molecule of APTES in order to estimate the mass of APTES covering the whole surface to provide further evidence of the molecular arrangement. The progress of the chapter is presented in Figure 4-1.

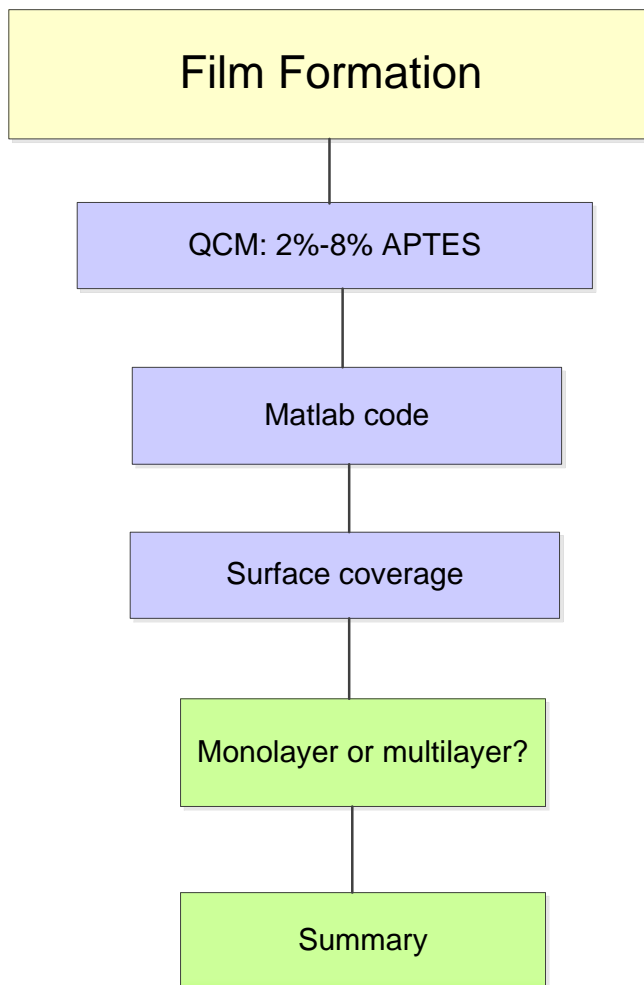


Figure 4-1. Summary of Film Formation, Chapter 4

4.2 Using QCM crystals as surrogate rock surface

As mentioned in Chapter 3, the QCM crystal is partially covered by gold electrode (see Figure 4-12). After treating the crystal by APTES, an investigation was required to understand the possibility of adsorption of APTES on the gold electrode. Hence, X-ray Photoelectron Spectroscopy (XPS) was employed to trace probable APTES reaction on the gold section of crystal by acquiring silicon spectrum at 99.5 eV and gold at 84 and 87 eV (111). Firstly survey of the gold part of crystal was demonstrated that there is no silicon peak at 99.5 eV (Figure 4-2). In addition, there is few percentage of nitrogen which is negligible for XPS analysis.

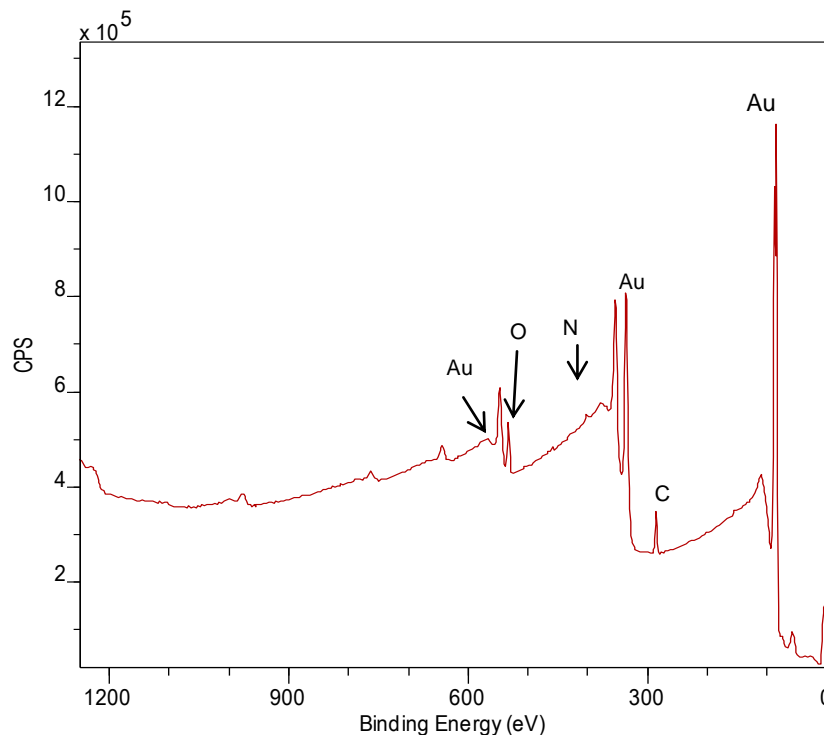


Figure 4-2. Survey spectrums scan of gold section of QCM crystal after 2 h experiment in APTES solution

In addition, the silicon element was scanned in detail to observe any peak related to silicon binding energy around 99.5 eV. As it can be seen in Figure 4-3, no trace of silicon is found.

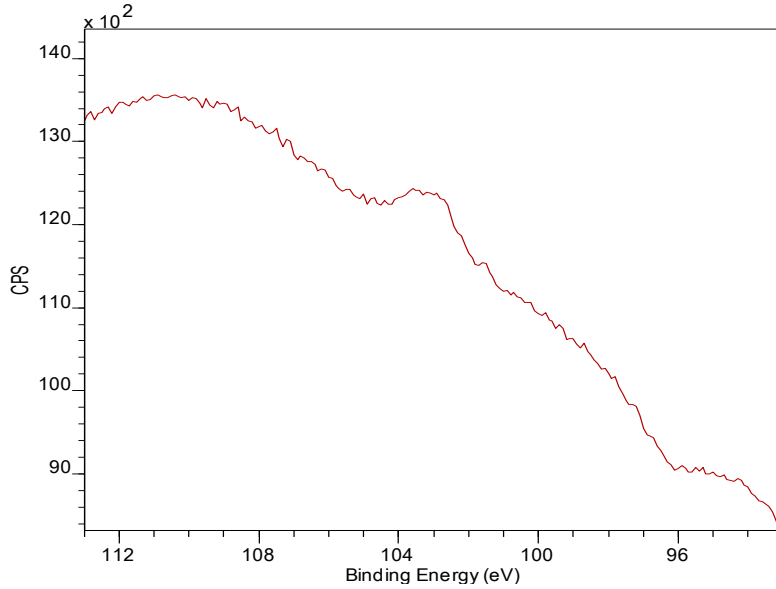


Figure 4-3. Non peak area around binding energy of silicon at 99.5 eV on gold part of crystal

Moreover, the gold spectrum of the survey scan was studied more in detail to observe any possible shifts in binding energy of pure gold; this is presented in Figure 4-4. It is observed that the gold binding energies, 84 and 87 (111), did not shift to either direction which indicates that the gold part of the crystal remains unreacted with APTES.

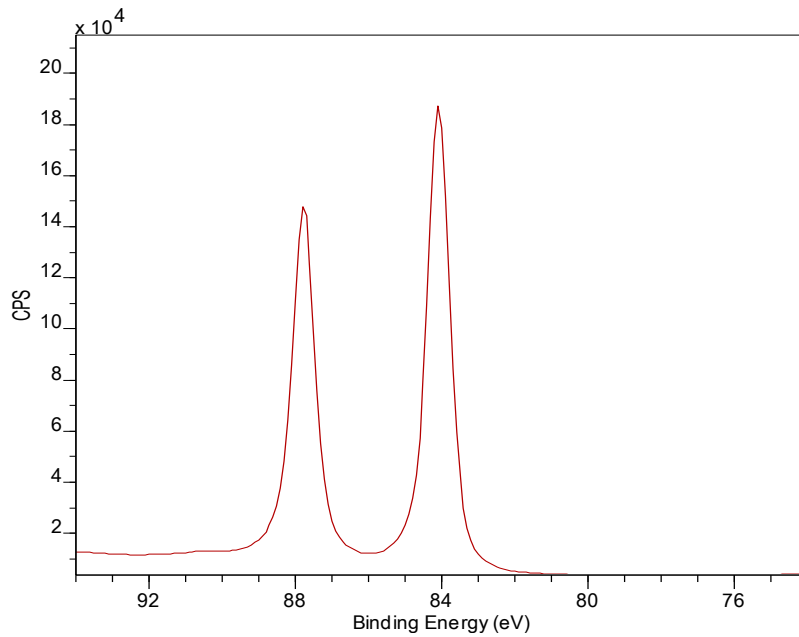


Figure 4-4. A gold spectrum of the survey scans of the QCM electrode

4.3 Film formation kinetics

After assuring no trace of APTES on the gold part of the crystal, APTES film formation on quartz section of crystals was studied. Each experiment was carried out for two hours – each with a different concentration (2-8%) of APTES. The reaction of the molecules on the surface had reached equilibrium when the mass (or frequency of oscillator) versus time stabilizes and reaches a plateau (333). Figure 4-5 illustrates the adsorption trend of various concentrations of APTES on the quartz crystals as a function of time. A sharp growth of APTES on the surface is observed at the initial stage of adsorption for all concentrations. In general, the adsorption of APTES onto the surface increases with concentration of the solution. However, a few experiments did not follow the same trend as expected. This will be discussed later in the chapter.

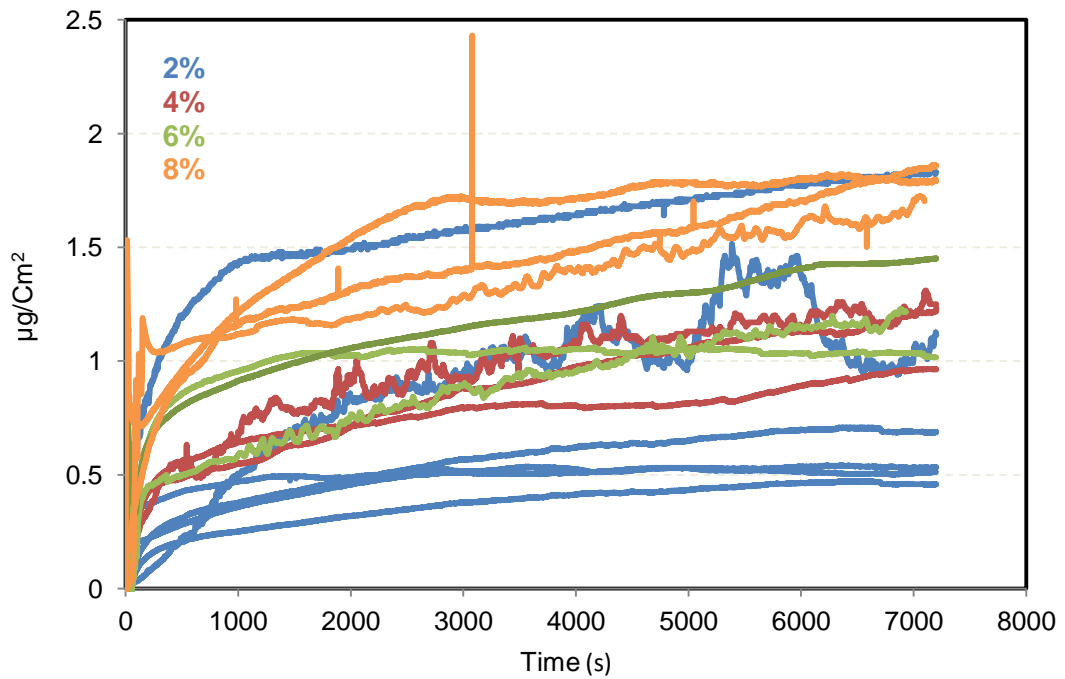


Figure 4-5. Mass growth of APTES on quartz crystals as a function of time by QCM

Maximum mass of APTES adsorbed on QCM crystals after two hours experiment is illustrated in Figure 4-6.

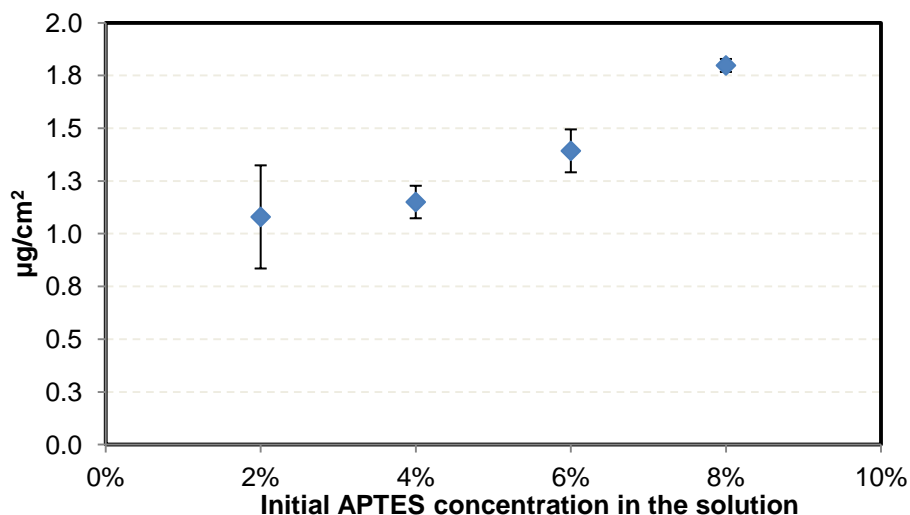
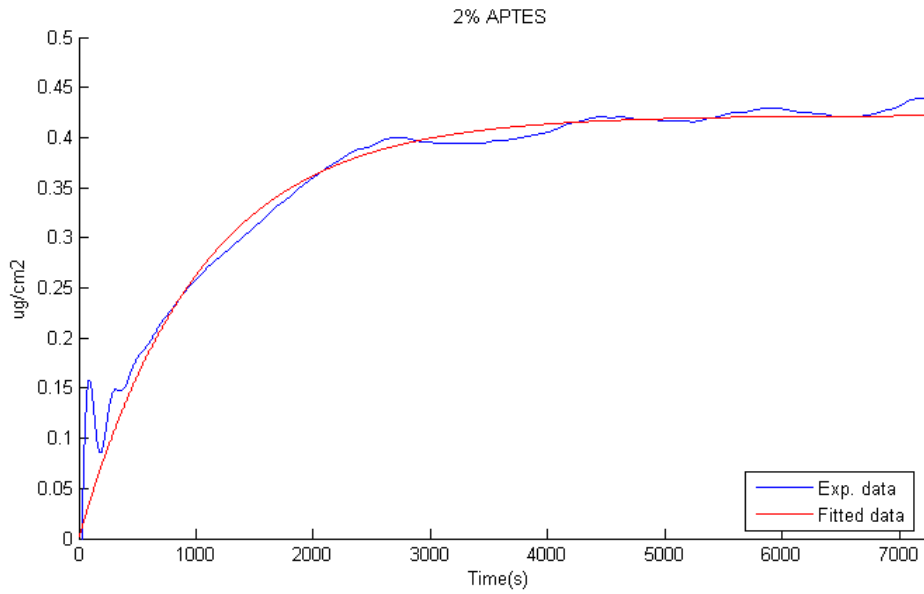


Figure 4-6. Maximum adsorption of APTES on QCM crystal for various concentrations after 2 h experiment on ambient temperature

By increasing APTES concentration in the solution, maximum mass of APTES adsorbed on the surface increases as expected. At this stage, these results may not give any further information; however these with assistance of the surface coverage of APTES calculated by Matlab are valuable to compare with the result obtained by ChemDraw software (the maximum surface area that APTES can occupy in the space which is called relaxation mode) in order to understand the maximum required mass to create a SAM. These comparisons provide comprehensive information about APTES film formation on QCM crystal, which will be discussed later in this chapter.

As mentioned in Chapter 3, the Langmuir isotherm was chosen to interpret the experimental data of QCM with the assumption of having at most one layer of chemical adsorbed on the surface. As described earlier, a code in Matlab was written to fit Langmuir isotherm to the raw data from QCM; samples are illustrated in Figure 4-7 for 2 and 4% (v/v) concentration.

a)



b)

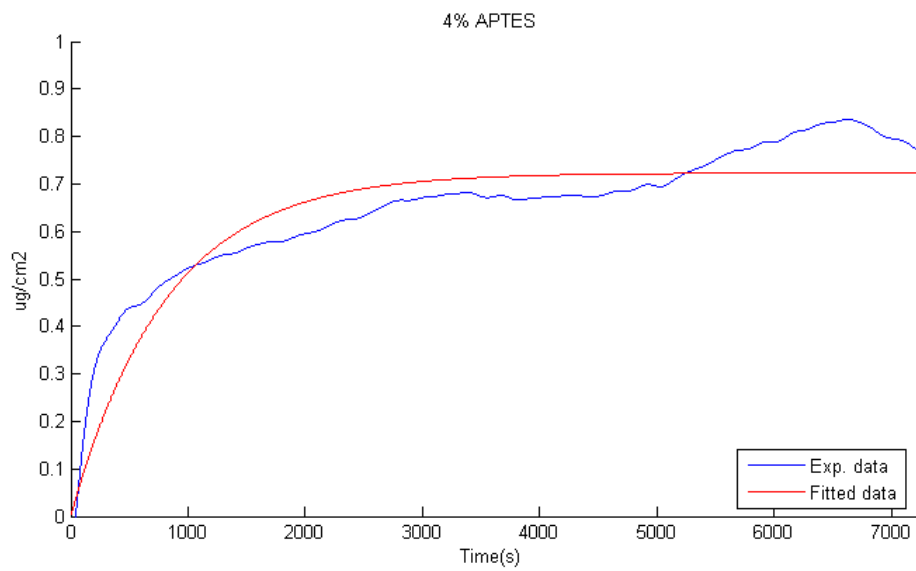
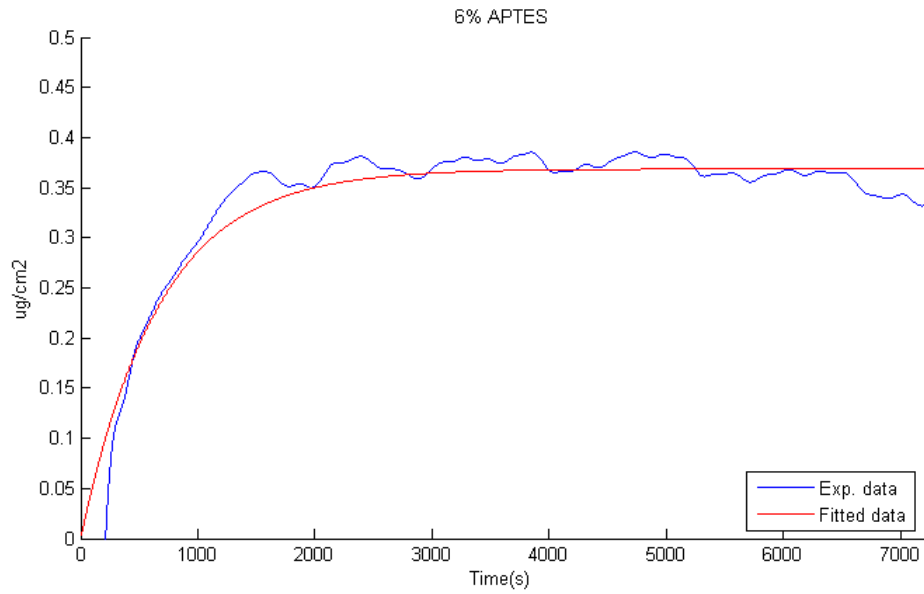


Figure 4-7. Experimental data fitted by Matlab code for a) 2% and b) 4% APTES concentration

And for 6 and 8% APTES, the samples are shown in Figure 4-8.

a)



b)

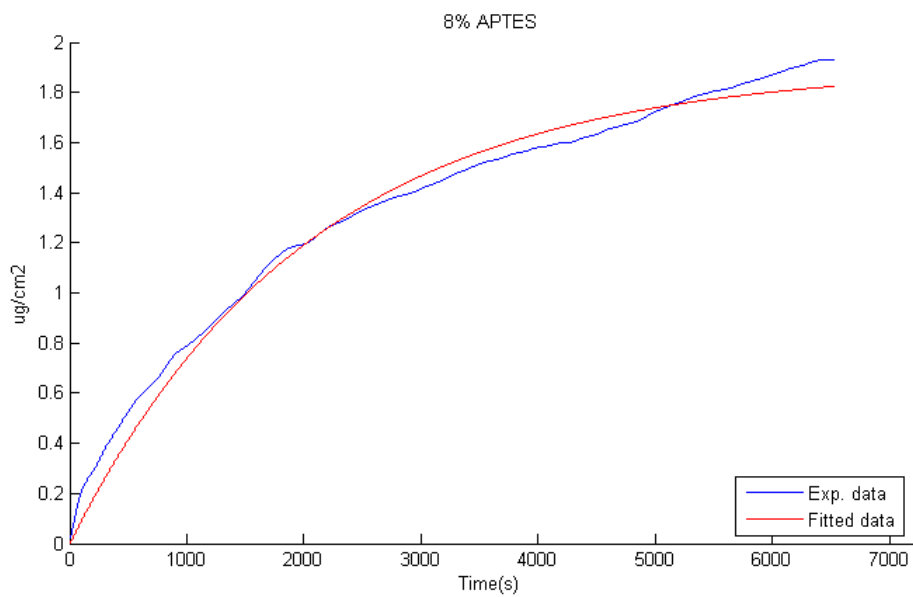


Figure 4-8. Experimental data fitted by Matlab code for a) 6% and b) 8% APTES concentration

Based on equation 4-6 in Chapter 3, K_{obs} was calculated which is illustrated in Table 4-1. By plotting K_{obs} versus APTES concentration, K_{eq} can be found (this was explained in Chapter 3).

Table 4-1. K_{obs} at various concentrations of APTES

Concentration (v/v)	2%	4%	6%	8%
K_{obs}	0.00177 ± 0.00020	0.00292 ± 0.00109	0.00351 ± 0.00118	0.00557 ± 0.00135

K_{eq} (equilibrium constant) (see Chapter 3 for more details regarding the equations) can be used to calculate the surface coverage of APTES at each concentration. The graph of K_{obs} as a function of APTES concentration is presented in Figure 4-9, which gives $K_{obs} = 0.599 C + 0.0004$ with $R^2 = 0.95$. Since K_a and K_d are the slope and y-intercept of the graph, $K_{eq} = 0.0599/0.0004 = 149.8$.

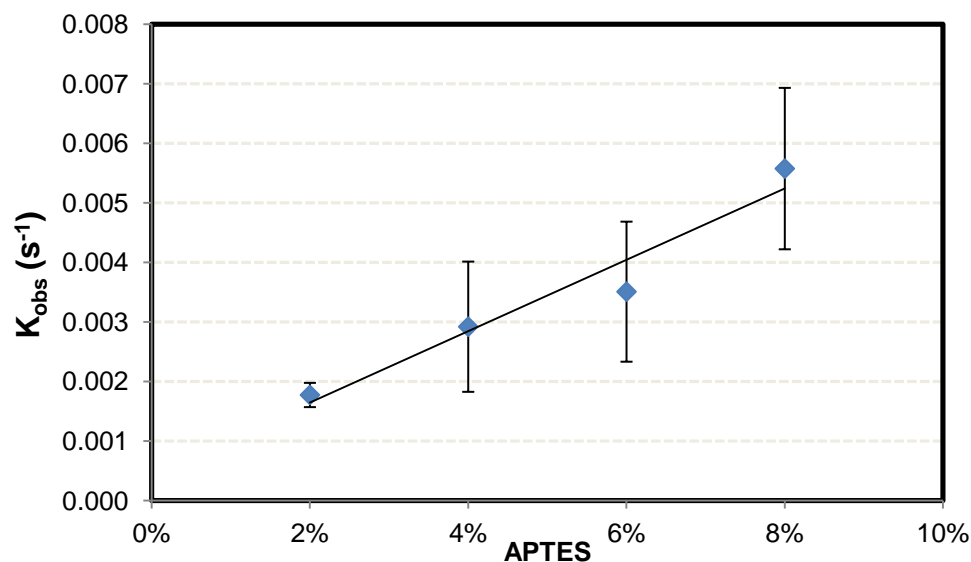


Figure 4-9. Plot of K_{obs} versus APTES concentration at ambient temperature

By substituting in $\Theta = \frac{C}{1 + \frac{1}{K_{eq}}}$, surface coverage of APTES is obtained and

shown in Table 4-2 as expected.

Table 4-2. Mean surface coverage of APTES at each concentration

Concentration (v/v)	2%	4%	6%	8%
Θ	75%	86%	90%	92%

Also, the surface coverage of APTES is illustrated in Figure 4-10 for better demonstration. It is observed that by increasing the concentration more percentage of the crystal surface was covered by APTES.

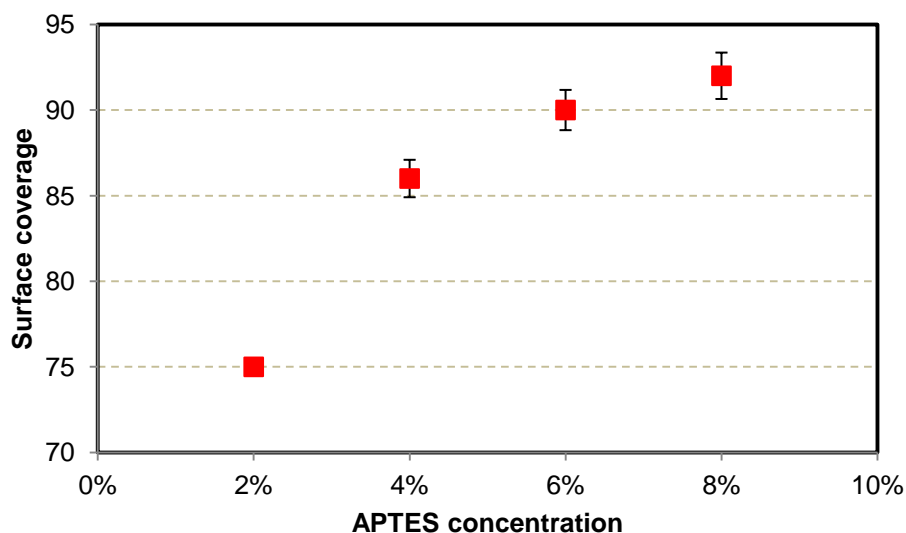


Figure 4-10. Surface coverage of APTES at different concentrations after 2 h experiment at ambient temperature

4.4 Monolayer or multilayers?

To analyse whether or not the film formed on the QCM is a monolayer or multilayered film the molecular area corresponding to the deposited mass can be calculated assuming that the film is a monolayer. Therefore, ChemDraw software was used to model the structure of APTES at the relaxation mode.

APTES molecule structure which is drawn by ChemDraw software is actually based on an energy minimization simulation, where the atoms of the molecules are relaxed until the optimum spatial geometry (exhibiting the minimal intra-molecular energy without considering any other influence factor) is found. The 2D and 3D structure of APTES at relaxation mode of molecule are shown in Figure 4-11.

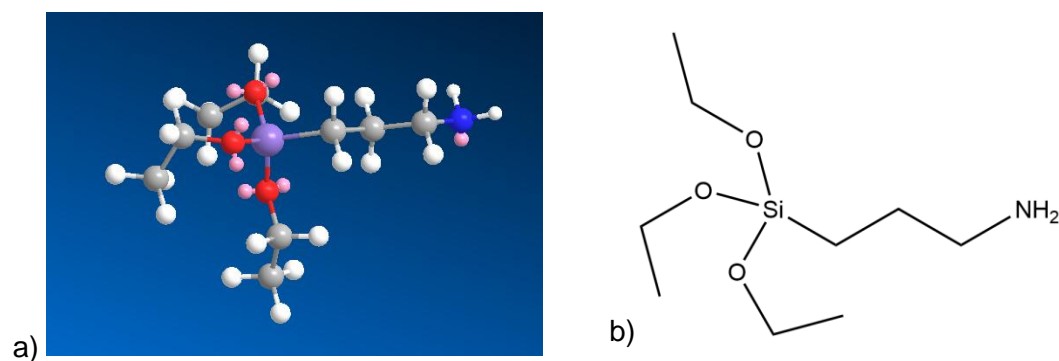


Figure 4-11. Image of relaxation mode of APTES a) 3D and b) 2D – drawn by ChemDraw software

The Chem Draw software is able to calculate the coordinate of each atom of the molecule after energy minimization simulation. An ideal adsorption of APTES on a quartz surface (289, 334, 335) is shown in Figure 4-12.

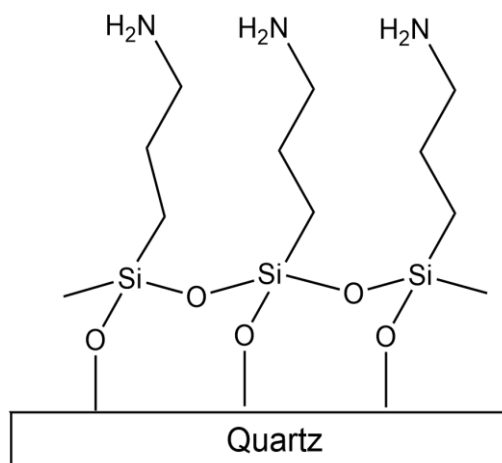


Figure 4-12. An ideal schematic of APTES reaction with a quartz surface

With a reliable presumption, the surface area occupied by one APTES can be estimated by calculation of surface area of the circumscribed of the oxygen triangle. The top view of APTES on a quartz surface is illustrated in Figure 4-13.

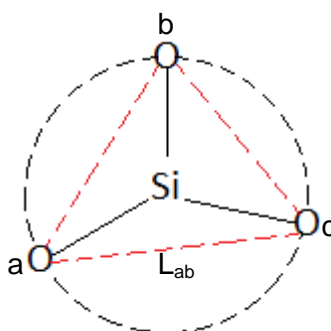


Figure 4-13. Top view of APTES on a quartz surface showing the possible surface area covered by one APTES

Although there is of course a lot of assumptions and uncertainties here, this calculation can indicate what order of magnitude mass is required to have fully coverage of APTES on a crystal surface. The coordinate of the three oxygen atoms in the relaxation mode is given below:

$$a = O_1 = (-3.2582, 0.7244, -0.719)$$

$$b = O_2 = (-4.4988, -1.6354, -0.217)$$

$$c = O_3 = (-3.3522, -0.2553, 1.8174)$$

Substituting the coordinates of individual oxygen atoms in Equation 4-1 gives the lengths of the three bonds of oxygen from each other.

$$\text{Length} = L_{ab} = \sqrt{(x_a - x_b)^2 + (y_a - y_b)^2 + (z_a - z_b)^2} \quad \text{Equation 4-1}$$

Thus the lengths of oxygen triangle are:

$$L_{ab} = 2.712886 \text{ \AA}$$

$$L_{bc} = 2.712591 \text{ \AA}$$

$$L_{ca} = 2.720657 \text{ \AA}$$

When the length of three sides of triangle is known, the radius of the circumscribed of triangle is calculated by substituting the length in Equation 4-2.

$$r = \frac{L_{ab}L_{bc}L_{ca}}{\sqrt{(L_{ab} + L_{bc} + L_{ca})(L_{bc} + L_{ca} - L_{ab})(L_{ab} + L_{ca} - L_{bc})(L_{ab} + L_{bc} - L_{ca})}} \quad \text{Equation 4-2}$$

Therefore,

$$r = 1.5677 \text{ \AA}$$

And the surface area occupied by one molecule of APTES given by

$$A = \pi r^2 = \pi \times (0.07717)^2 = 7.717 \text{ \AA}^2 = 0.07717 \text{ nm}^2$$

With considering the surface area of QCM crystal $5.067 \times 10^{14} \text{ nm}^2$, the number of molecules is:

$$\text{Number of molecules} \sim \frac{\text{Crystal's surface area}}{\text{Molecular area}} = \frac{5.067 \times 10^{14}}{0.07717} = 6.5656 \times 10^{15}$$

The molecular weight of APTES ($\text{C}_9\text{H}_{23}\text{NO}_3\text{Si}$) is 221.369 g/mol, which means that the weight of one APTES molecule is 3.676×10^{-22} , giving:

$$\text{amount of APTES} = 6.5656 \times 10^{15} \times 3.676 \times 10^{-22} = 2.4135 \times 10^{-6} \text{ g}$$

Therefore the mass of APTES required to have a complete uniform coverage by a monolayer film is 0.48 \mu g/cm^2 . This value is less than of the values in Figure 4-5 which were experimentally measured by QCM. The first crude conclusion from the ChemDraw simulation may explain that the adsorption of

APTES on crystal quartz is not a monolayer film; however, ChemDraw calculations involved a lot of assumptions and uncertainties, as the surface area occupied by an individual APTES is a complicated process and it is not the focus of this research. On the other hand the experimental data measured by QCM were reasonably fitted by Langmuir isotherm which assumes a monolayer adsorption on a surface. In addition, it was shown that the crystal surface coverage calculated by Matlab (Table 4-2) was not completed even in high APTES concentration after 2 h. Hence two hypotheses can explain these results.

Since the amount of APTES required to have fully covered surface by ChemDraw simulation was based on a lot of simplifications, a range of mass weight can be considered instead of just one value. Therefore, a range of 0.5-1.5 $\mu\text{g}/\text{cm}^2$ APTES is required to have a complete uniform coverage of the quartz crystal. Then this can indicate that SAM of APTES was obtained in film formation experiments, which is in a good agreement with the results from Matlab. However, the surface coverage calculated by Matlab states an incomplete coverage on the QCM crystal.

On the other hand, another hypothesis, without refusing the explanation mentioned above, could be the sensitivity of APTES polymerisation in aqueous solution. In the absence of water in the solution, silanization corresponds to the amine moieties as the alkoxy groups on APTES can not be hydrolysed (244); whereas uncontrolled polymerisation of APTES can be obtained by excess water in the solution (270, 336). This polymerisation can be in both vertical and horizontal directions (270, 336). Hence, instead of one APTES, polymerised molecules can attach to crystal quartz surface. This does not reject the assumption of monolayer attachment as a layer of polymerised APTES could adsorb on the surface. This is schematically demonstrated in Figure 4-14. Besides, surface morphology and hydrolytic stability of adsorbed APTES are influenced by the purity and the concentration of silane in the solution (337). Aggregation and polymerisation in the solution is directly related to the concentration of APTES, e.g. the higher concentration the more polymerised APTES in the solution (337). On the other hand, the purity of the APTES in the solution along with polymerisation sensitivity increases the complexity of the reaction (111, 337). This was discussed in detail in Chapter 2.

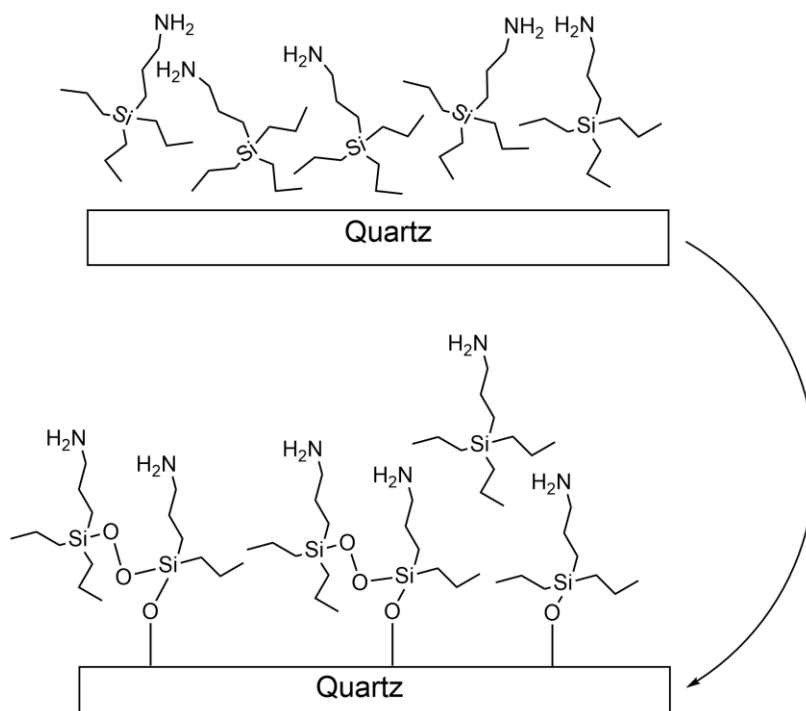


Figure 4-14. Schematic reaction of polymerised APTES

Moreover, the post processing stage of the experiments - rinsing the crystals by water – can remove unstable and weak bonds of polymerised APTES. The effect of water in post processing step is that it can penetrate irregular structured polymers of APTES to break down some siloxane bonds in order to disaggregate the APTES polymers from surface (271, 337). This phenomenon makes the film formation of APTES on the surface even more complicated (337).

4.5 Summary

This chapter presented film formation of APTES on quartz surface. QCM was applied to study the kinetics of film formation. Based on literature (294, 328, 330, 331), Langmuir isotherm was employed to interpret the kinetics of APTES film formation. Matlab code was used to fit the experimental results to Langmuir isotherm. Langmuir equilibrium constant (K_{eq}) was calculated to estimate the surface coverage of the APTES. The summary of this chapter is listed below:

1. The surface coverage of APTES was not completed even at high concentration.
2. By increasing the concentration of APTES in the solution, surface coverage (Θ) increased. 75%, 86%, 90% and 92% surface coverage were calculated from QCM results for 2%, 4%, 6% and 8%, respectively.

3. ChemDraw was applied with a lot of assumption to estimate the required APTES to create SAM on crystal surface. The calculated value was 0.4763 $\mu\text{g}/\text{cm}^2$.
4. The value of required mass calculated by ChemDraw simulation to have SAM was less than maximum weight measured by QCM after 2 hrs. Although even this value is higher than estimated value by ChemDraw, the data obtained from Matlab showed the APTES did not fully cover the surface. This phenomenon was explained by two hypotheses.

Chapter 5

Scale Prevention Performance

5.1 Introduction

In this chapter, the effect of coating materials on deposition and adhesion of calcium carbonate on the treated and un-treated quartz is explored under pseudo-dynamic condition. The objective was to understand the impact of various types of coating chemicals at different concentrations on the deposition of mineral scale. SEM and gravimetric measurements were used to observe and measure scale formation on the treated quartz surfaces and compared with the blank surface. Other characterisation methods were also employed such as XPS, contact angle and roughness which will be discussed in detail in the next chapter. As mentioned in Chapter 3, two simplified brines of calcium carbonate with different saturation ratios (low=4.77 and high=54.80 SR) were used, since the effect of saturation ratio (SR) of a solution on mineral scale formation is well defined in the literature (83, 86, 337). The morphology of calcium carbonate scale deposition on the treated and the blank quartz surfaces was observed under SEM and compared to assess the effect of coating chemical on calcium carbonate formation. In addition, the gravimetric results of scale deposition were measured by microbalance scale.

To treat the quartz surface for scale deposition studies, two types of organosilane (APTES and APhS) were employed. The range of APTES concentrations are from 0.05% to 8%, whereas the selected range of concentration for APhS was from 0.03% to 0.24%. The amount of mineral scale deposition on the quartz surfaces treated by various concentrations of organosilanes was compared with the results from blank surfaces. In addition, the results of the low and high saturation ratios were compared with each other. The work flow of this chapter for investigation of scale deposition\adhesion on the coated and uncoated quartz surfaces is presented in Figure 5-1.

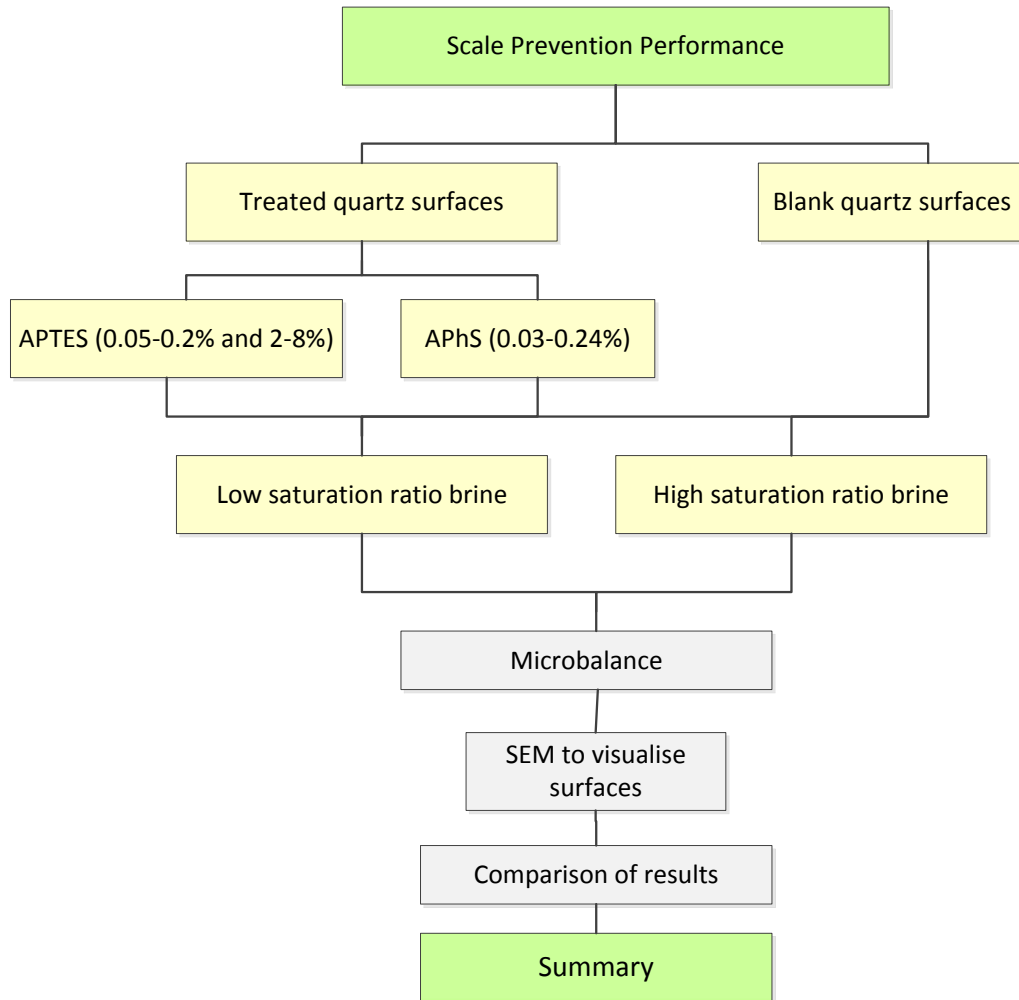


Figure 5-1. Workflow of scale prevention study in this chapter

5.2 The effects of APTES coating on scale deposition

Since two saturation ratios were used for scale deposition tests, the study of the mineral scale prevention performance was divided in two sections: i) in low and ii) high SR solutions. As mentioned above, two ranges of APTES concentration were studied for scale prevention performance tests. The reason for choosing a low range of concentrations is that there is a discussion regarding organosilane concentration to form Self Assembled Monolayer (SAM) on a quartz surface in the literature (244, 260, 271, 285, 338). In order to create SAM, approximate amount of APTES was obtained via the basic calculation by ChemDraw simulation (Chapter 4). This calculation indicated a range of 0.5-1.5 $\mu\text{g}/\text{cm}^2$ is required to create SAM on the quartz surface, which is much lower than the concentration of APTES (2-8% in 5 ml solution). Also, the required time to create SAM of APTES on the surface is critical and was demonstrated (222, 244, 258, 260, 271, 283, 339-342) that APTES formation can be obtained on surface in various experiment times (from 4 min to 24

h). Therefore, it was decided to test the effect of a lower range of APTES concentrations to evaluate whether it is possible to form SAM in 30 minutes.

5.2.1 APTES coating behaviour in low SR= 4.77

Brine composition for saturation ratio of 4.77 was previously presented in Figure 3-4. The mass of calcium carbonate deposition on treated (0.05, 0.1, 0.15, 0.2, 2, 4, 6 and 8%) and non-treated surfaces are illustrated in Figure 5-2. Since the x axis of the graph is shown on a logarithmic scale and the value of scale deposition on the blank surface was considered 0% coating, the graph is not able to show the mass deposition at 0. The amount of mass deposition on the blank surface (0% coating) was 1116.8 μg and is shown by the red line.

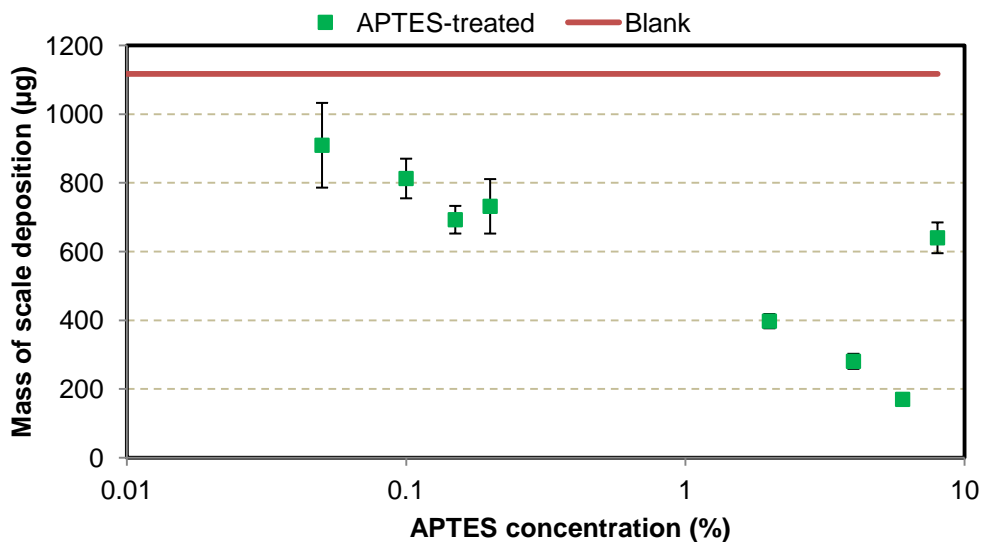


Figure 5-2. Calcium carbonate mass deposition versus concentration at 4.77 SR and 80°C after 24 h experiment

Figure 5-2 shows that the amount of precipitation decreased (except at 8%) by increasing the concentration of APTES in the coating process. As demonstrated in Chapter 4, coverage of the quartz surface increases by adding more APTES in the solution. This may indicate that mass deposition is related to surface coverage i.e. deposition on the treated surfaces decreases when the surface coverage increases. Other factors such as roughness, the orientation of coating chemical during film formation and chemical states of film can affect the propensity of the surface to scale precipitation, which may explain the different behaviour of the surface at 8%. The effect of roughness, surface energy and coating materials on scale deposition has been demonstrated previously (163, 189, 199, 202, 203, 337, 343-345). As discussed in Chapters 2 and 4, creating the SAM on the quartz

surface is a complex process and various factors can influence the film structure and APTES orientation on the surface. This will be discussed in detail in Chapters 6 and 7.

In order to better demonstrate the impact of APTES coatings on the deposition of CaCO_3 scale reduction, Figure 5-2 was re-plotted and is presented in Figure 5-3. This graph shows the surface performance in terms of scale reduction percentage versus APTES concentrations. A clear scale reduction is observed by coating the quartz surface by means of APTES. The maximum performance of the APTES film was 85% at 6% APTES concentration. In general, except from 8%, coating performance improved by increasing the APTES concentration. Although the correlation coefficient ($R^2 = 0.68$) of logarithmic equation of the graph is poor, the performance of scale deposition prevention qualitatively improved by increasing the APTES concentration. Using a linear extrapolation gives correlation coefficient $R^2 = 0.36$.

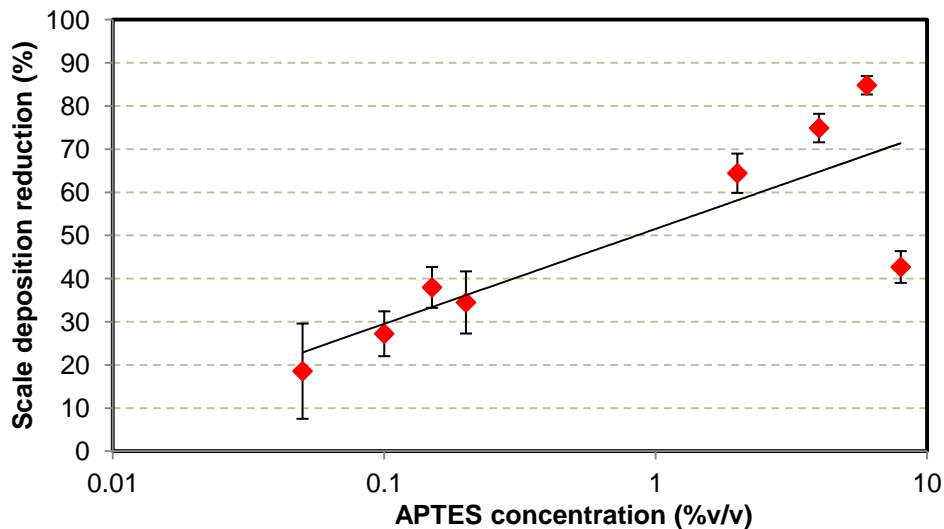


Figure 5-3. The reduction of scale deposition as function of APTES concentration at 4.77SR and 80°C after 24 h experiment

Since the coating material at 8% showed different behaviour from the rest of concentrations, Figure 5-3 was re-plotted without considering the result of 8%. This is presented in Figure 5-4. This graph shows a good correlation between the performance of treated surfaces (0.05-6%) in scale prevention as function of concentration of coating material; the correlation is shown below with coefficient of $R^2 = 0.99$.

$$CP = 12.44\ln(C) + 59.9$$

Equation 5-1

Where CP and C (v/v) are the coating performance in reduction of scale deposition and APTES concentration, respectively. However, $R^2 = 0.88$ is obtained if a linear fit is used to extrapolate the experimental data.

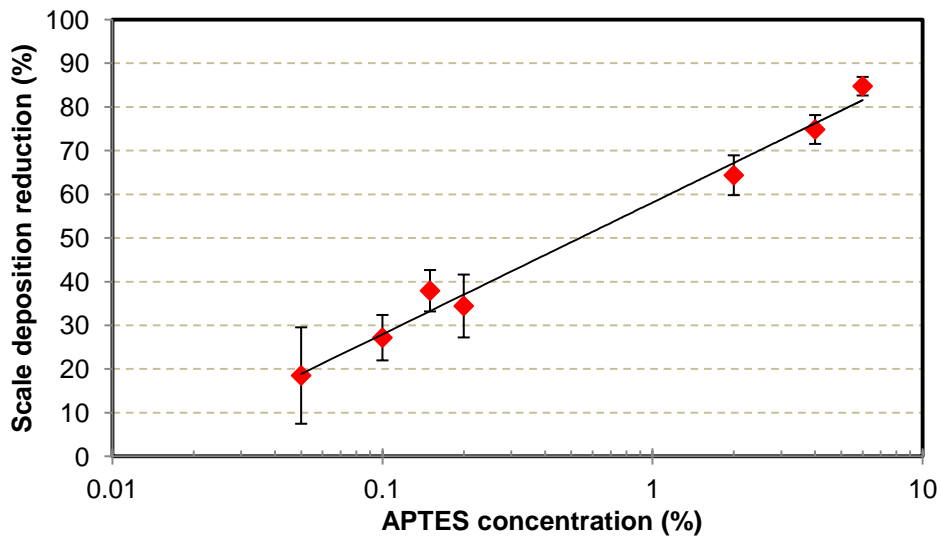


Figure 5-4. The scale deposition reduction as function of APTES concentration at 4.77SR and 80°C with eliminating the value at 8%

Figure 5-4 shows that with eliminating the result of 8% the treated surface performance in scale deposition reduction can be potentially fitted by a logarithmic correlation as function of APTES concentration of which is associated with surface coverage. Higher adsorption of APTES for 8% was observed on the quartz surface in Chapter 4 by QCM, but lower performance is seen by 8% APTES. This may indicate that another factor like the chemical states of adsorbate can be more crucial in explaining the different behaviour of the same film on scale reduction, which will be explained more in detail in Chapter 7.

5.2.1.1 Visualization of calcium carbonate deposited on untreated and APTES-treated quartz surfaces in low SR=4.77

SEM was used to study the aggregation and morphology of calcium carbonate crystals on the uncoated and coated surfaces. Firstly, a lower magnification of SEM image was taken to qualitatively evaluate the amount of deposit formed on the surface; these images are illustrated in Figure 5-5 and Figure 5-6. From visual observation, in comparison with non-treated surfaces, the amount of calcium carbonate deposited on the treated surfaces clearly reduced. The tendency of the coated surface to scaling reduced by increasing the concentration of coating chemicals in the film formation process; this is in good

agreement with the gravimetric results. Although the low magnification images of SEM are not able to quantify the amount of mass deposited on the surface, it can be seen to generally support the gravimetric result. It shows that the amount of scale deposited on treated surface is lower than the blank quartz surface. Besides, the change in morphology of calcium carbonate deposition on the treated surfaces was observed by SEM and compared with the non-treated surface.

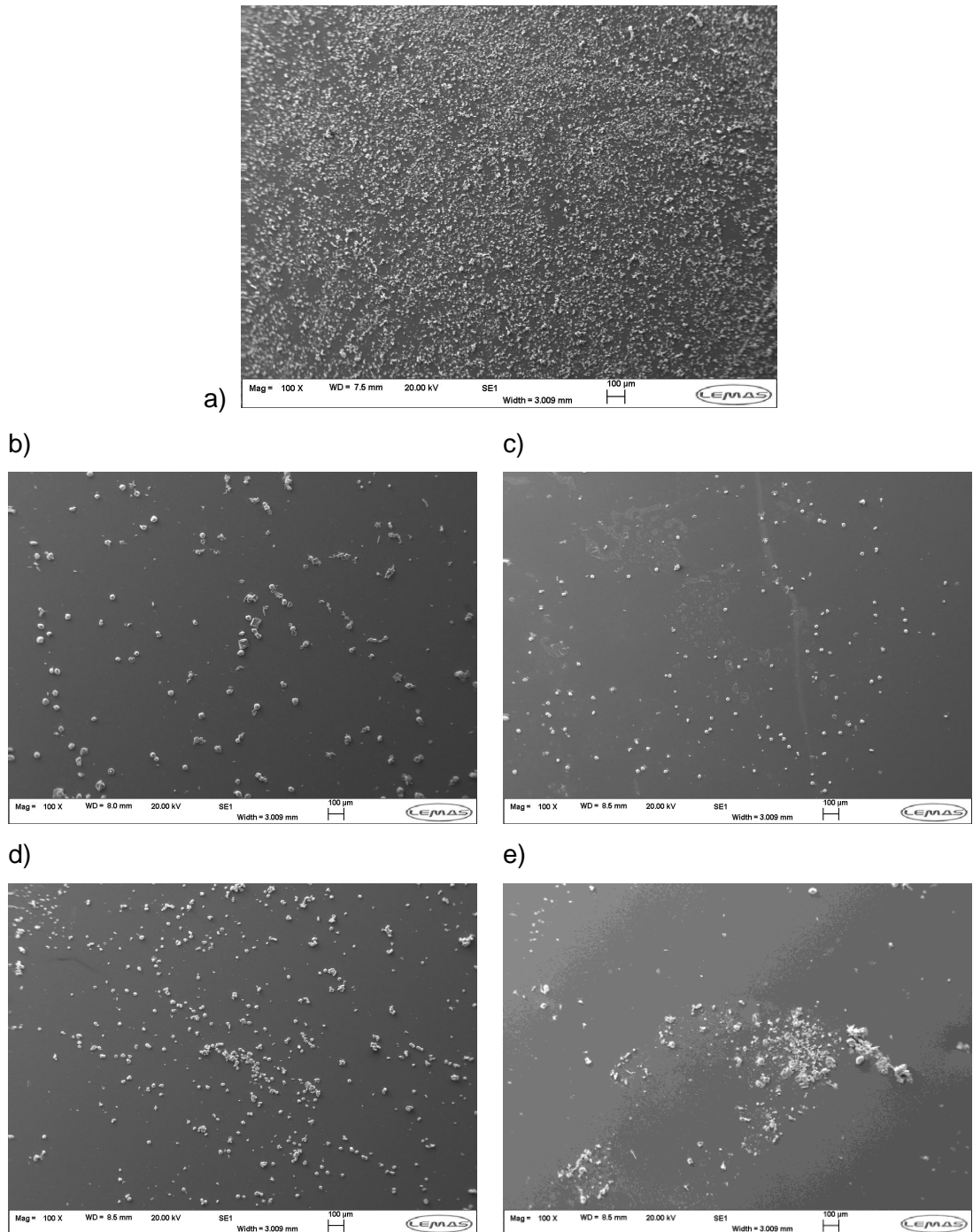


Figure 5-5. Low magnification SEM images of calcium carbonate deposited on a) non-treated quartz surface, b) 0.05%, c) 0.1%, d) 0.15% and e) 0.2% APTES coated quartz surfaces in low SR= 4.77 at 80°C

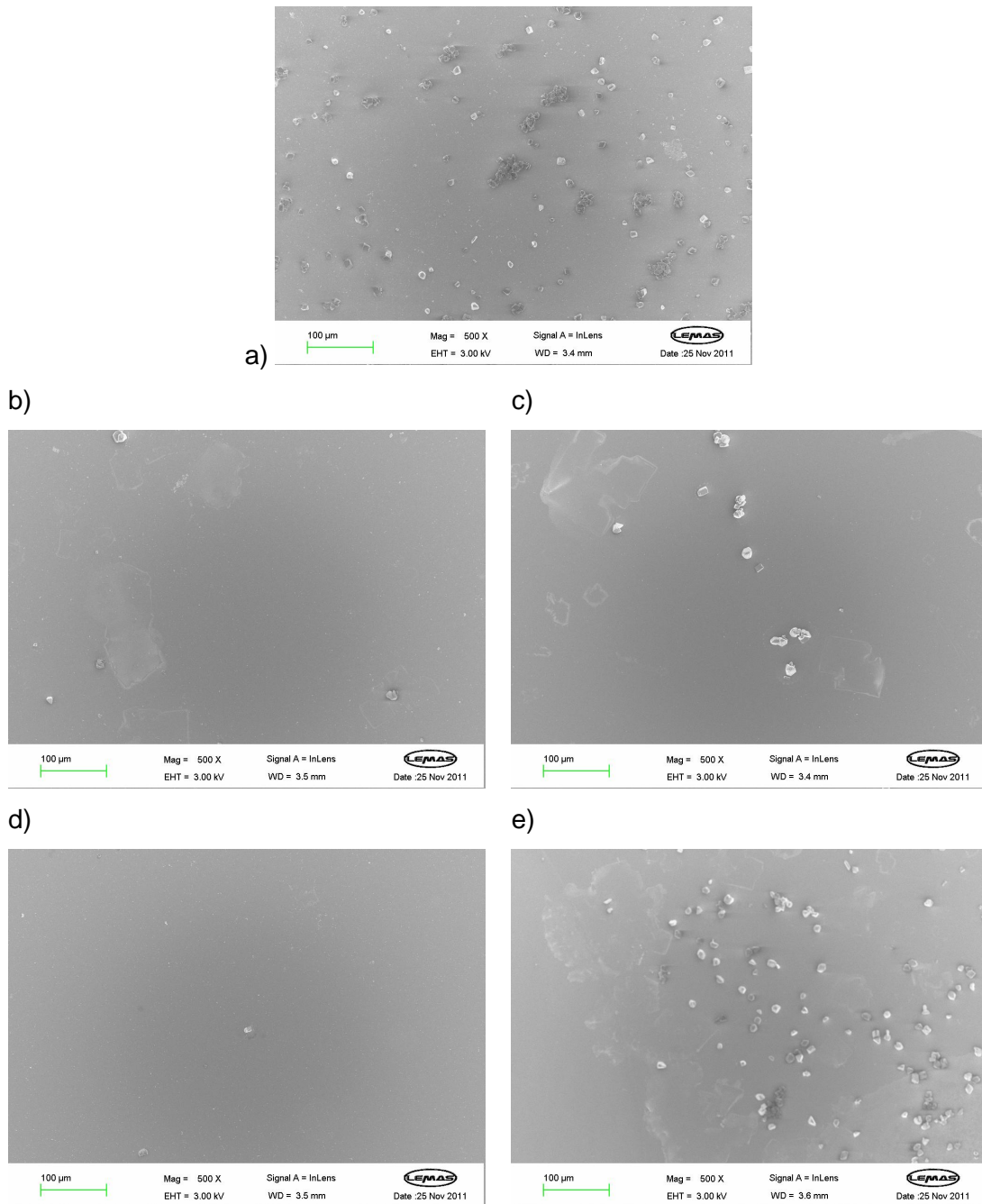


Figure 5-6. Low magnification SEM images of calcium carbonate deposited on a) non-treated quartz surface, b) 2%, c) 4%, d) 6% and e) 8% APTES coated quartz surfaces in low SR= 4.77 at 80°C

The non-treated and treated quartz surfaces behaviour in association with scale deposition in low saturation ratio (4.77) CaCO₃ solution at pseudo-dynamic condition at 80°C can be systematically presented in Figure 5-7. The blue arrow indicates that the efficiency of the surface in terms of scale deposition reduction increases towards the right hand side; this is categorised by orange (lower efficiency) and green (higher efficiency).

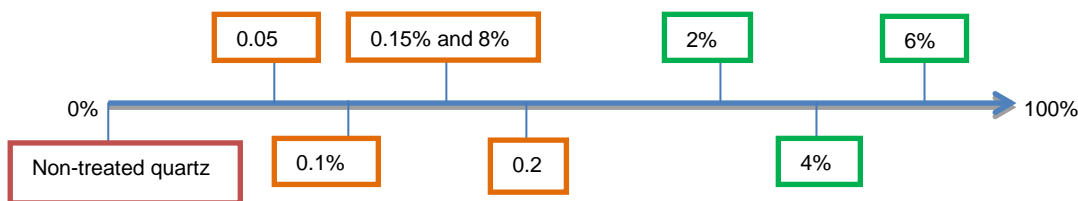


Figure 5-7. Systematic ranking of APTES coating performance in terms of amount of scale deposited on the quartz surface in low SR=4.77

5.2.1.2 Morphology of calcium carbonate deposited on untreated and APTES-treated quartz surfaces in low SR=4.77

As discussed in Chapter 2, the morphology of calcium carbonate can vary at different conditions (95, 198). In order to understand the influence of APTES coating material and the morphology of calcium carbonate, higher magnification images of substrates by SEM were also taken. Figure 5-8 shows the differences between calcium carbonate shapes for the coated (0.05-0.2%) and uncoated quartz surfaces. The observation under SEM for the blank quartz surface shows clusters of calcite whereas the shape of CaCO_3 crystals on the treated surfaces is mainly distorted calcite.

Figure 5-9 also illustrates calcium carbonate morphology on the quartz surfaces coated at the higher range of APTES concentration (2-8%). In comparison with the crystals on the blank surface, the calcium carbonate deposited on the treated surfaces is distorted cubic shapes. It was found that the solution temperature (346, 347), impurity of the solution (346) and the flow rates (346, 347) affect the morphology of the calcium carbonate. In contrast, not much attention was paid on the influence of surface on the morphology of calcium carbonate. Some information (8, 163, 181, 189, 193, 198) is available on the effect of the different surface chemistry, roughness and wettability on the morphology. However, the effect of surface on morphology was not understood clearly. It was shown that the treated surface destroys nucleation sites but does not affect on the crystallisation of calcium carbonate (4). It can be seen from Figure 5-8 and Figure 5-9 that the morphology of CaCO_3 deposited on the treated surface have slightly different shape (distorted at the edges) than on non-treated surfaces.

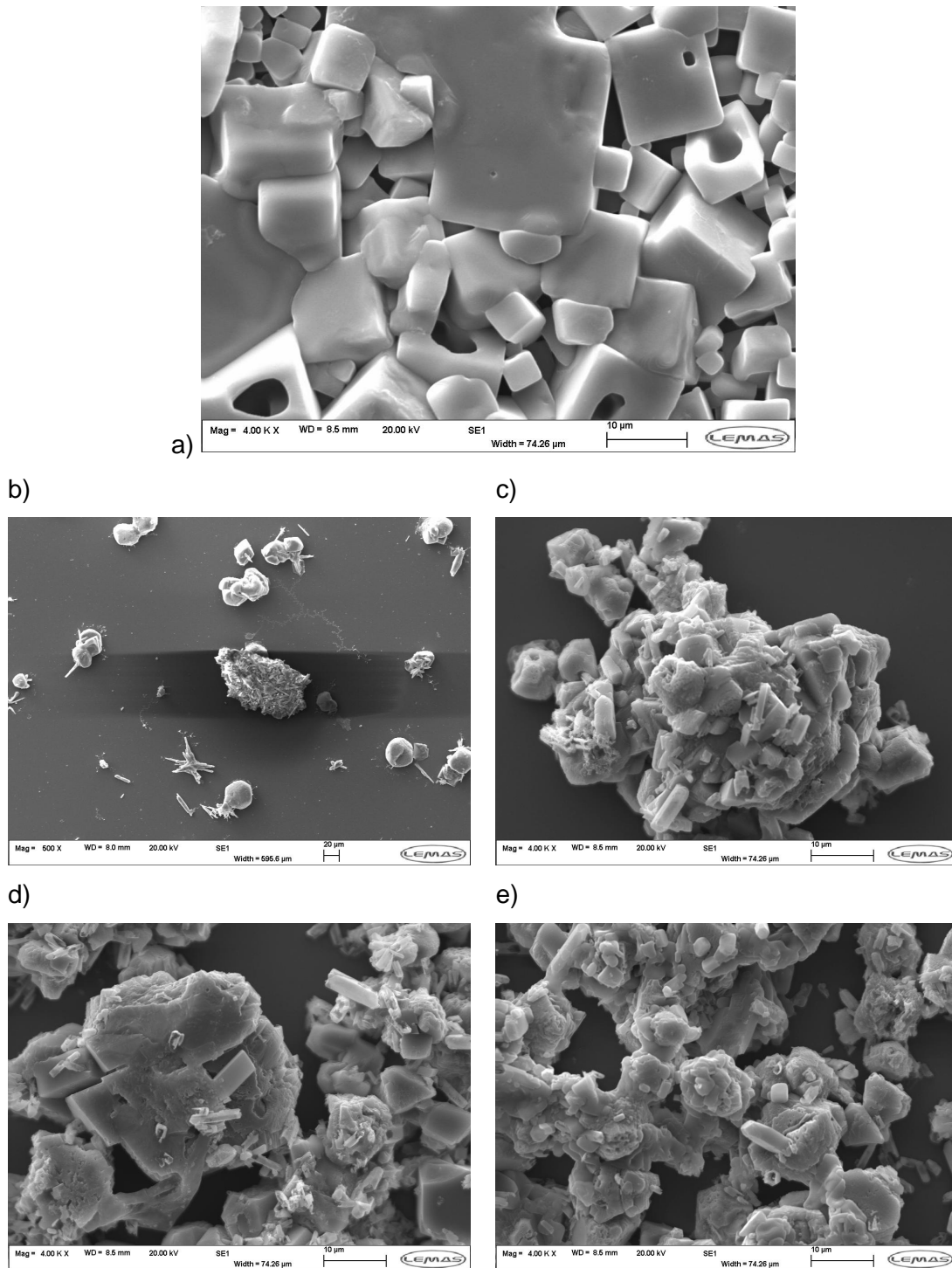


Figure 5-8. High magnification SEM images of calcium carbonate deposited on a) non-treated quartz surface, b) 0.05%, c) 0.1%, d) 0.15% and e) 0.2% APTES coated quartz surfaces in high SR= 4.77 at 80°C

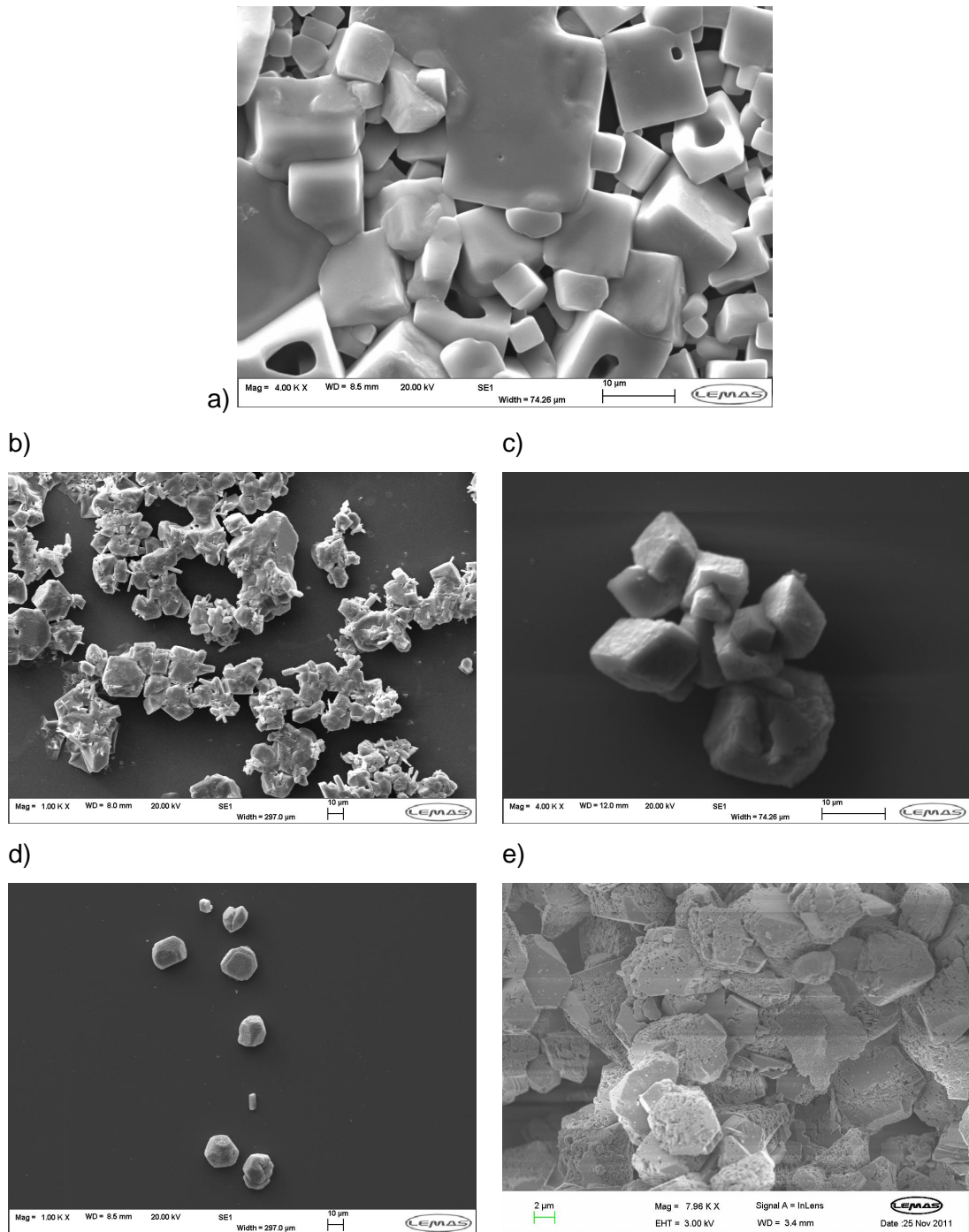


Figure 5-9. High magnification SEM images of calcium carbonate deposited on a) non-treated quartz surface, b) 2%, c) 4%, d) 6% and e) 8% APTES coated quartz surfaces in high SR=4.77 at 80°C

5.2.2 APTES coating behaviour in high SR= 54.8

The performance of the treated quartz surfaces were also studied in high SR=54.8 calcium carbonate solution. This was carried out to understand the performance of the APTES coating at higher SR, since the deposition of CaCO_3 on the surface varies at different saturation ratio solutions (83, 86, 337). The brine composition of SR=54.8 was previously presented in Figure 3-4. The mass of

calcium carbonate deposited on treated and non treated surfaces is illustrated in Figure 5-10. There is a great similarity in the overall trend at low SR as presented before. The amount of calcium carbonate scale deposition on the blank surface (0% coating) was 1500.7 μg . However, the slope of the reduction varies from low SR as expected. This can be owing to the effect of pH values on the surface charge in the solution. When the pH is not controlled during the experiment, this parameter can alter in various manners in different SR solutions. Since the degree of ionisation of the substrate depends on the pH value, and mineral scale deposition is thought to be related to the ionization of the surface (348), the different behaviour of the deposition of CaCO_3 on the treated quartz surface may be resulted from this phenomenon.

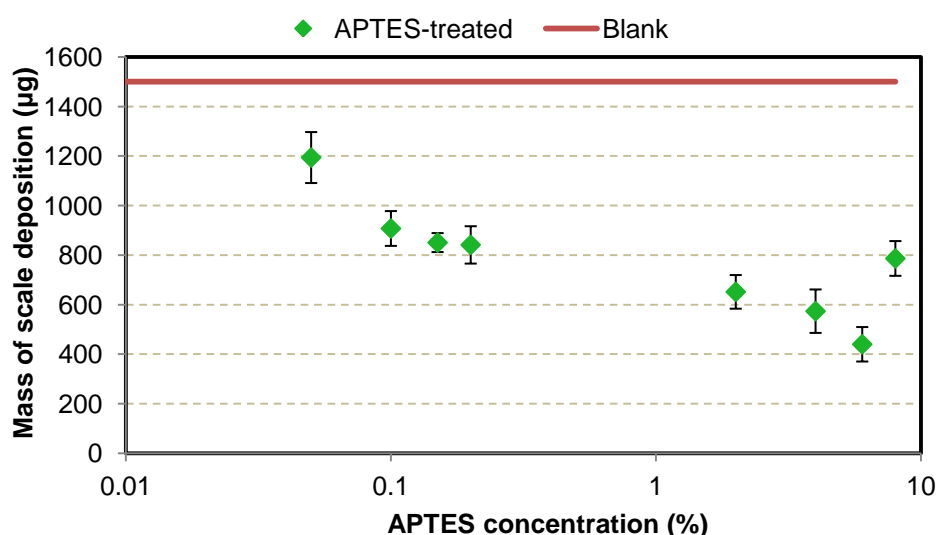


Figure 5-10. The mass of calcium carbonate deposited on the APTES treated surface as a function of concentration at high SR=54.8

In order to better show the performance of coating materials on the amount of CaCO_3 scale reduction on the surface in high SR (54.8), Figure 5-10 was re-plotted and shown in Figure 5-11. This graph shows the mass of calcium carbonate reduction as a function of APTES (%) in coating process. Up to 70% reduction of CaCO_3 scale deposition was obtained at the quartz surface treated by 6% APTES. Moreover, the minimum mass reduction was related to the low range of APTES concentration (0.05%). However, the performance of the treated surface at 8% APTES was not as affected as 2-6% and was as small as the low range of APTES. Although higher adsorption of APTES on the quartz surface was shown for 8% in Chapter 4, the chemical states of adsorbate can be more crucial in explaining the different behaviour of the same film on scale reduction. This will be explained more in detail in Chapter 6. Apart from the importance of surface composition of the

substrate, other surface characteristics such as wettability and roughness can be critical. However, the influence of coating concentration in film formation process on reduction of deposition of scale will be discussed at the end of this chapter.

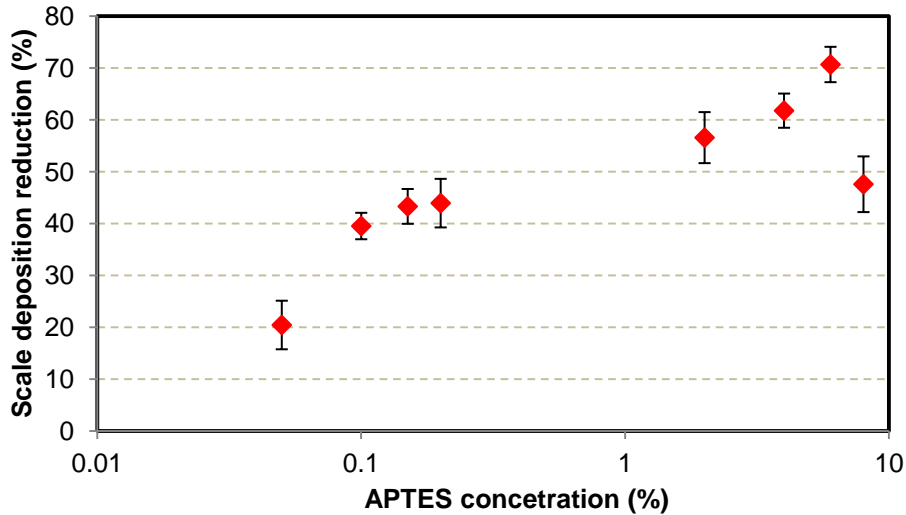


Figure 5-11. The amount of scale deposition reduction as function of APTES concentration at 54.8SR and 80°C

Linear and logarithmic extrapolations were fitted to the experimental data of Figure 5-11 and $R^2=0.36$ and $R^2=0.69$ were obtained; respectively, which show poor fits for both extrapolations; however, better result for logarithmic correlation.

The same as results which obtained for low SR (Figure 5-3), scale results at high SR presented different behaviour at 8% APTES concentration. Thus, Figure 5-11 plotted again and 8% was eliminated to gain the correlation between the performance of treated surfaces (0.05-6%) in terms of scale reduction at high SR; Figure 5-12 illustrates the scale reduction as a function of APTES concentration. the correlation is shown below with coefficient of $R^2 = 0.99$.

$$CP = 12.44\ln(C) + 59.9$$

Equation 5-2

Where CP and C (v/v) are the coating performance in reduction of scale deposition and APTES concentration, respectively. However, $R^2 = 0.88$ is obtained if a linear fit is used to extrapolate the experimental data.

Figure 5-12 presents the same trend as the graph in low SR (Figure 6-4). However, the observed correlation in high SR ($R^2= 0.75$) is quite poor in comparison with correlation in low SR ($R^2= 0.99$).

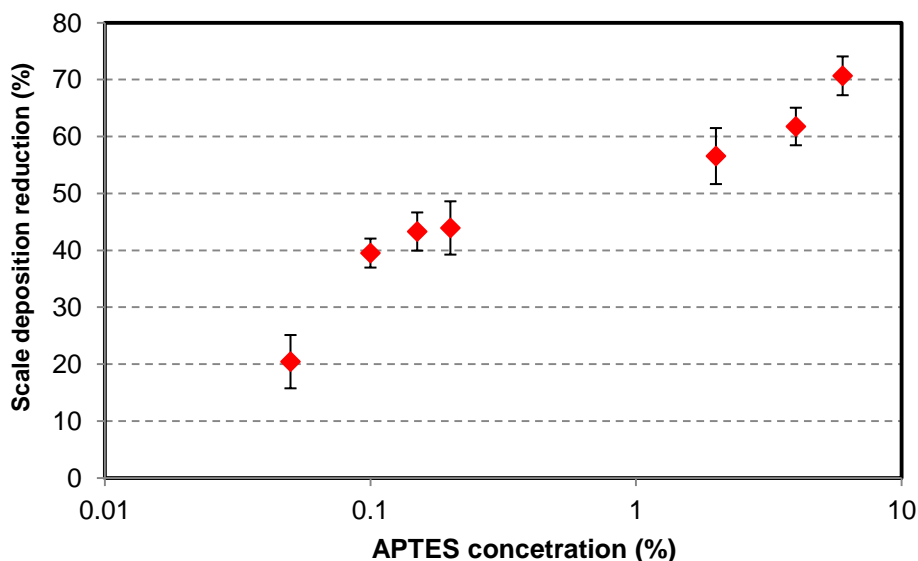


Figure 5-12. The scale deposition reduction as function of APTES concentration at 54.8 SR and 80°C with eliminating the value at 8%

Figure 5-13 shows the performance of the quartz surface in relation to the amount of scale deposition in high SR (54.8) solution. The blue arrow indicates that the efficiency of the surface in terms of scale deposition reduction increases towards the right hand side; this is categorised by orange (lower efficiency) and green (higher efficiency).

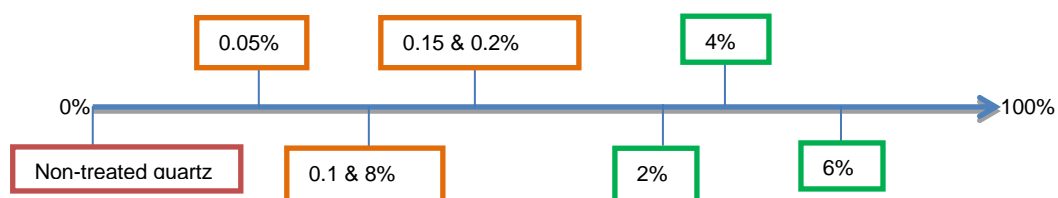


Figure 5-13. Systematic ranking of surface performance coated by APTES in terms of amount of scale reduction on surface in high SR=54.8 at pseudo-dynamic condition at 80°C

5.2.2.1 Visualization of calcium carbonate deposited on untreated and APTES-treated quartz surfaces in high SR=54.8

SEM was again applied to visually observe the amount of mass deposited on the treated and untreated quartz surfaces. Figure 5-14 and Figure 5-15 illustrate lower magnification of SEM images of the quartz surfaces coated by low and high concentrations of APTES, respectively. Compared to the blank surface, the amount of scale on the coated surfaces decreased. Gravimetric results together with SEM images can be schematically presented in terms of the amount of calcium carbonate scale deposition on the surface.

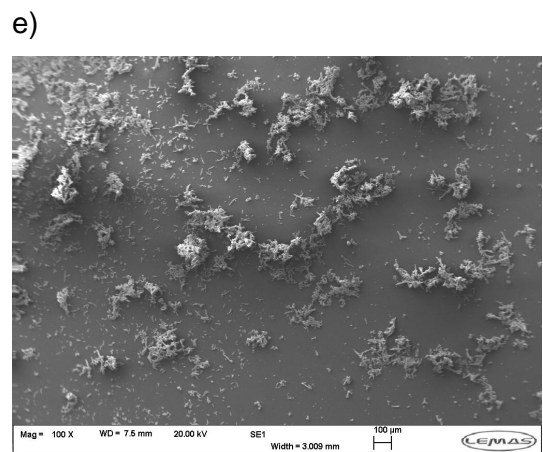
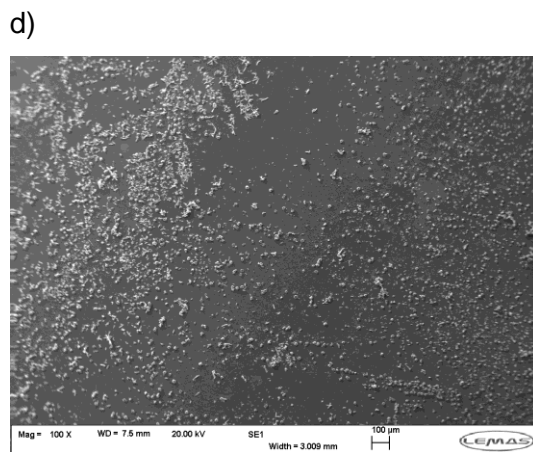
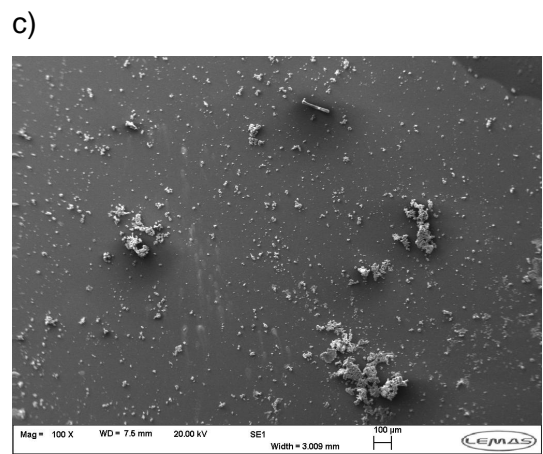
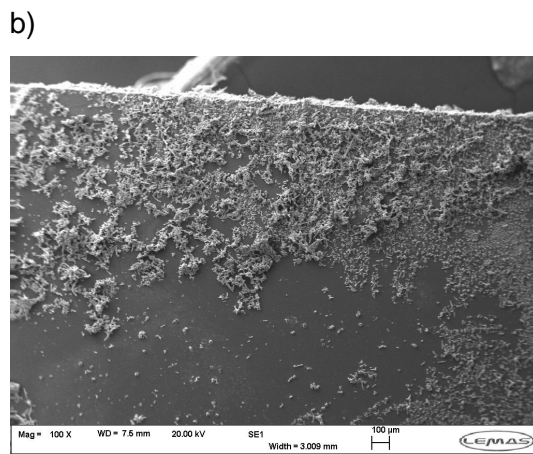
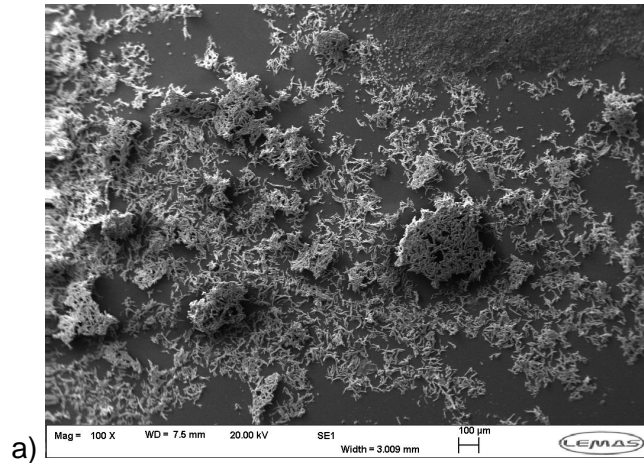


Figure 5-14. Low magnification SEM images of calcium carbonate deposited on a) non-treated quartz surface, b) 0.05%, c) 0.1%, d) 0.15% and e) 0.2% APTES coated quartz surfaces in low SR= 54.8 at 80°C

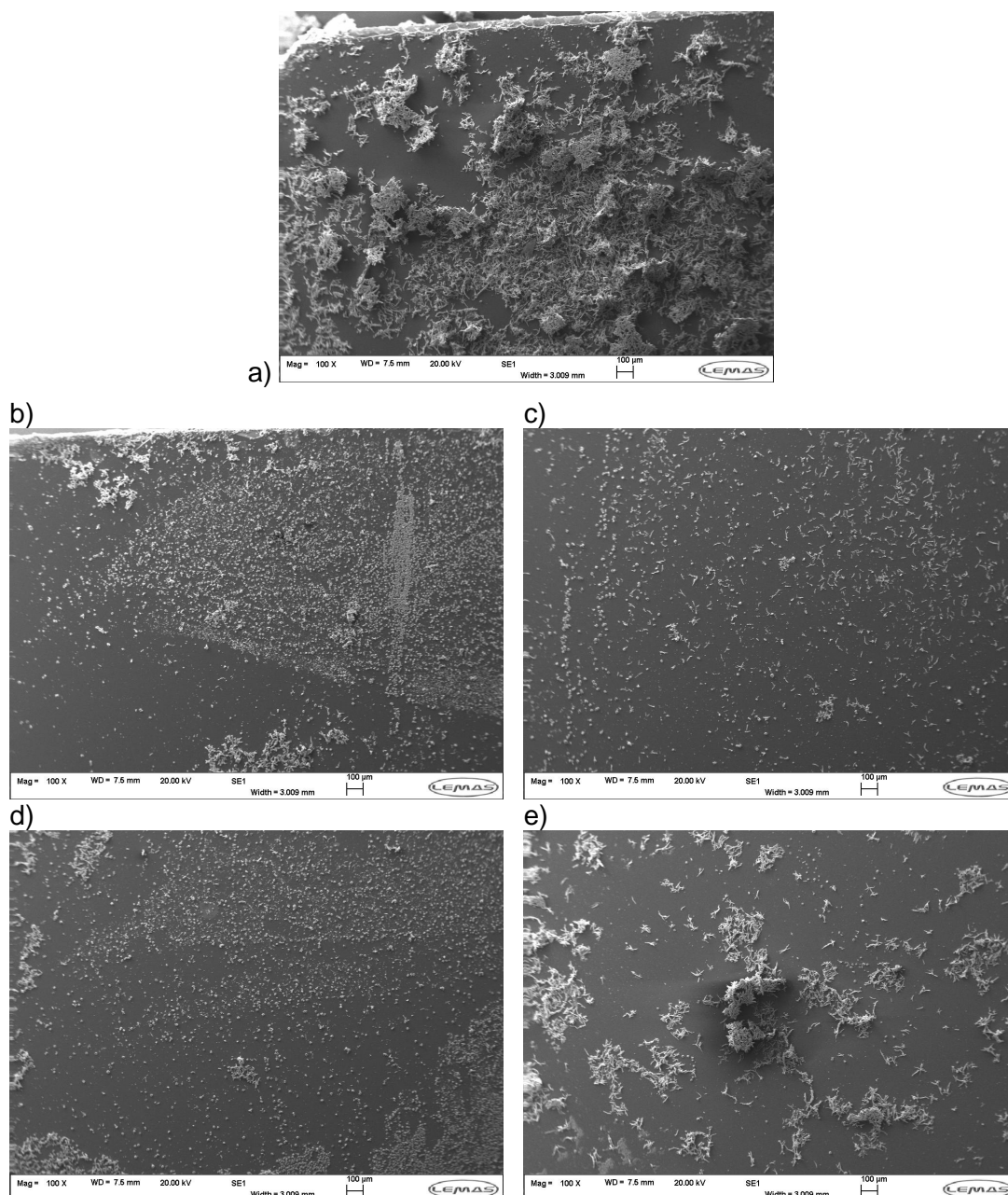


Figure 5-15. Low magnification SEM images of calcium carbonate deposited on a) non-treated quartz surface, b) 2%, c) 4%, d) 6% and e) 8% APTES coated quartz surfaces in low SR= 54.8 at 80°C

5.2.2.2 Morphology of calcium carbonate deposited on untreated and APTES-treated quartz surfaces in high SR=54.8

Also, the influence of the treated quartz surfaces in high SR solution on calcium carbonate in terms of crystal morphology was investigated by SEM. Figure 5-16 and Figure 5-17 show the morphology of the CaCO₃ crystal on the uncoated and coated quartz surfaces at 80°C after 24 h experiment. Figure 5-16 illustrates the changes in crystal shapes for the blank and treated surfaces coated with low concentration of APTES (0.05-0.2%). It can be observed the morphology of

the crystals slightly changed for the blank and treated quartz surfaces in high SR solution compared to low SR. All the images seem to present calcite and aragonite crystals on the surfaces; however, XRD analyses required for studying crystal morphology which can be the subject of future work. The shape of calcium carbonate for untreated and treated surfaces (0.05-0.2%) appears a mixture of long chain and distorted cubic of calcium carbonate crystals. The crystallisation process of the scale deposited on the surfaces was not affected by APTES coating as was seen in section 5.2.1.2. However, the size of the cubic crystals on the blank surface is bigger which may indicate a shorter induction time (163).

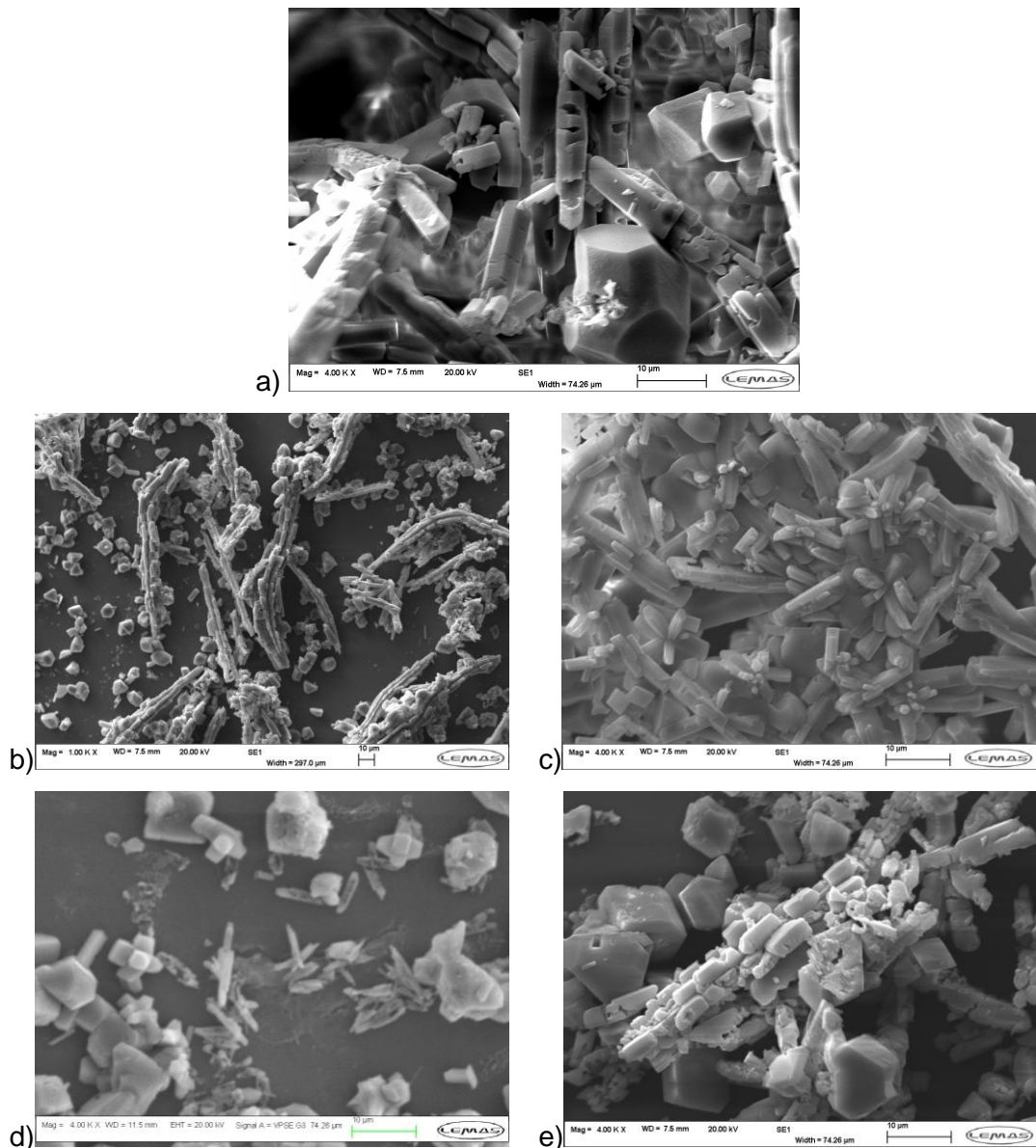


Figure 5-16. High magnification SEM images of calcium carbonate deposited on a) non-treated quartz surface, b) 0.05%, c) 0.1%, d) 0.15% and e) 0.2% APTES coated quartz surfaces in high SR= 54.8 at 80°C

However in Figure 5-17, the shape of calcium carbonate formed on the surfaces treated by 2-8% APTES is different from 0.05-0.2% and shows mainly distorted calcite crystals, except from Figure 5-17e which presents the mixture of long chain and distorted calcite crystals. This is in agreement with gravimetric results as the efficiency of the quartz surface treated by 8% APTES is similar to 0.5-0.2%. This suggests reduction of nucleation sites on the surface by APTES at 2-6% concentration since more matured calcite precipitated on the surface, which indicates more efficient surface coverage by these 2-6% concentrations.

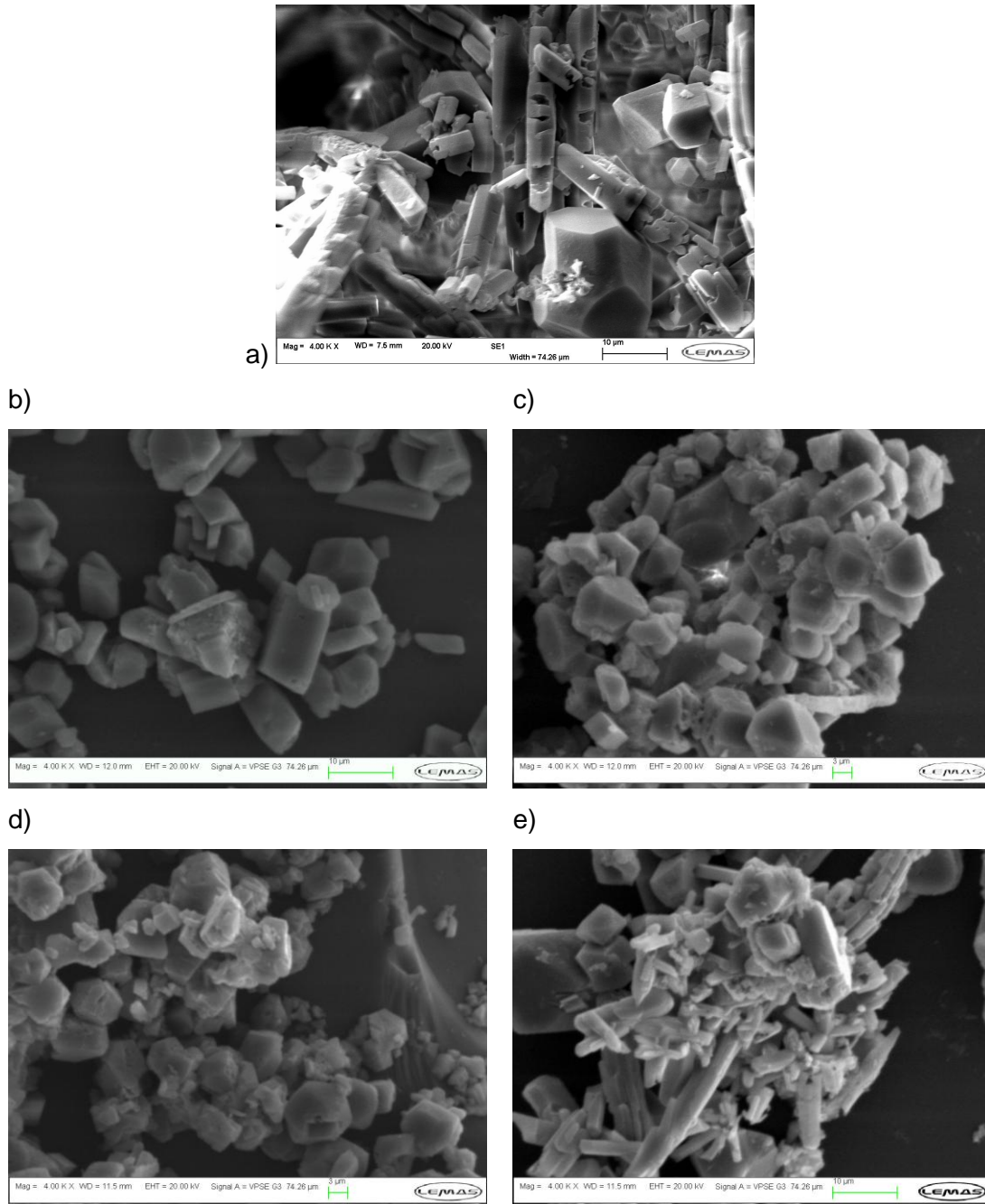


Figure 5-17. High magnification SEM images of calcium carbonate deposited on a) non-treated quartz surface, b) 2%, c) 4%, d) 6% and e) 8% APTES coated quartz surfaces in high SR=54.8 at 80°C

5.3 The effects of APhS coating on scale deposition

Another organosilane used in this research was APhS. As mentioned in Chapter 3, APhS was chosen due to the similarity with APTES in terms of having an amine group at the end of the tail structure and dissimilarity in terms of aromatic group in the middle of molecule structure. The structures of both organosilanes were shown in Chapter 3. According to the literature (244, 285), 3 mM (0.06%) APhS was applied to the quartz surface to create a SAM film on the surface. It is known that the different surfaces with different properties such as roughness, surface energy etc. can influence the calcium carbonate deposition on the surface (4, 163). Thus, the range of APhS concentration from 0.03% to 0.24% was selected to study the performance of the APhS-treated surface on scale deposition reduction. The same saturation ratios (low=4.77 and high=54.8) were employed.

5.3.1 APhS coating behaviour in low SR= 4.77

The same condition applied for the surfaces coated with APTES (the same brine composition as the one used for APTES with SR=4.77) was employed in this section. Gravimetric results after scale deposition test are presented in Figure 5-18. This figure illustrates the weight of mass deposited on the non-treated and treated surfaces as a function of APhS concentration. As is seen in Figure 5-18, compared with the result of blank quartz surface the mass deposition on the treated surfaces by APhS significantly reduced. Figure 5-18 shows that the amount of precipitation decreased by increasing the APhS concentration in the solution up to 0.06% followed by a small increase after 0.06%.

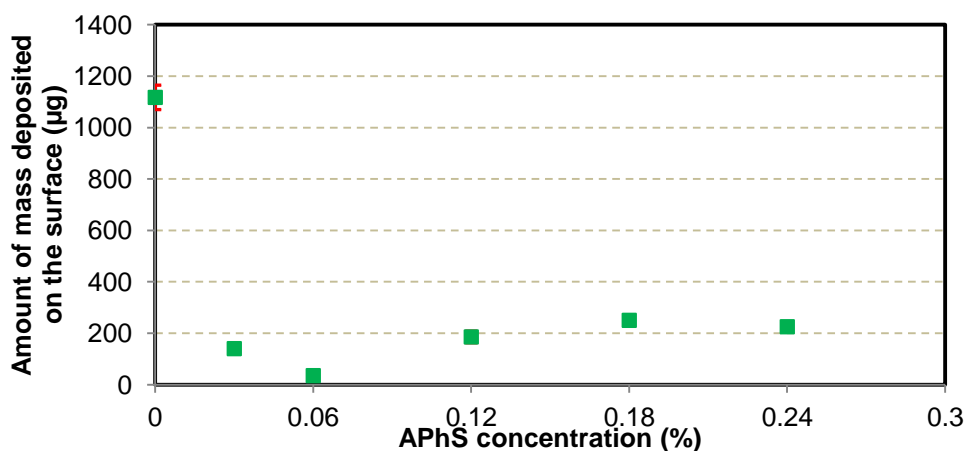


Figure 5-18. The mass of calcium carbonate deposited on the APhS treated surface as a function of concentration at low SR=4.77 (error bars are too small and hidden in the markers)

In Figure 5-18, in comparison with APTES (Figure 5-3) a different trend is observed by APhS. According to the results in Chapter 4, if more surface coverage is obtained by increasing the APhS concentration, the results of Figure 5-18 shows no direct relation between the treated surface performances in reducing scale deposition and APhS concentration in film formation.

With the aim of demonstrating the performance of the surfaces coated with APhS, Figure 5-19 is plotted to present the scale reduction results in terms of percentage. A significant calcium carbonate mass reduction is seen for all APhS-coated surfaces. The minimum and maximum mass reduction is related to 0.06% and 0.18%, respectively. A poor linear regression is fitted to the results from APhS with correlation coefficient of $R^2 = 0.56$.

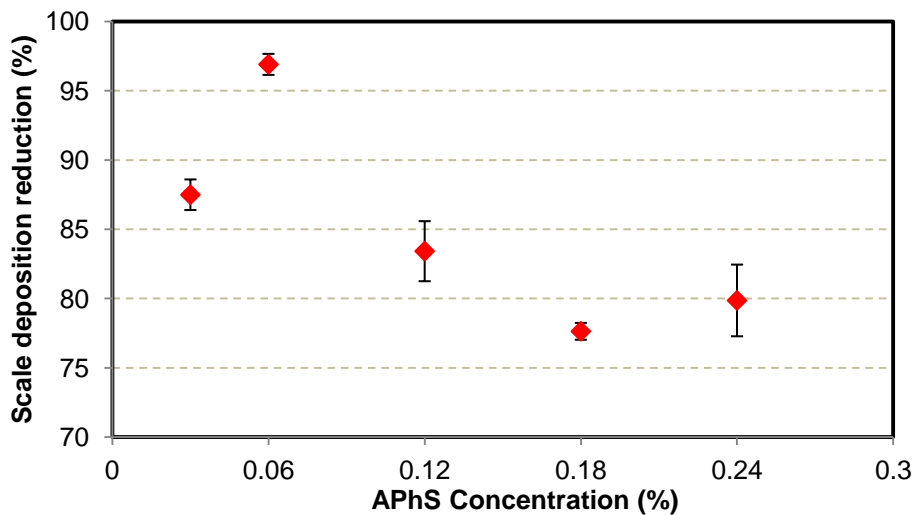


Figure 5-19. The scale deposition reduction as function of APhS concentration at 4.77SR and 80°C

A systematic ranking of the surfaces in terms of the efficiency of scale deposition reduction is presented in Figure 5-20. This schematically illustrates the effect of APhS coating on placing the surfaces in high efficiency zone.

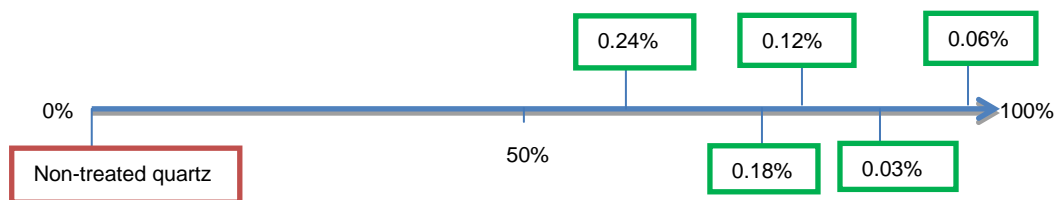


Figure 5-20. Systematic ranking of surface performance in terms of amount of scale reduction on APhS-coated surface in high SR=4.77 at pseudo-dynamic condition at 80°C

5.3.1.1 Visualization of calcium carbonate deposited on untreated and APhS-treated quartz surfaces in low SR=4.77

To support the gravimetric results, SEM was used to visualise the quantity of calcium carbonate formed on the quartz surfaces; this is shown in Figure 5-21. In comparison with the blank surface, the scale deposition on the treated surfaces clearly reduced. From visual observation less scale formation is seen for the treated surfaces with 0.03% and 0.06% APhS concentration where a small number of crystals are counted.

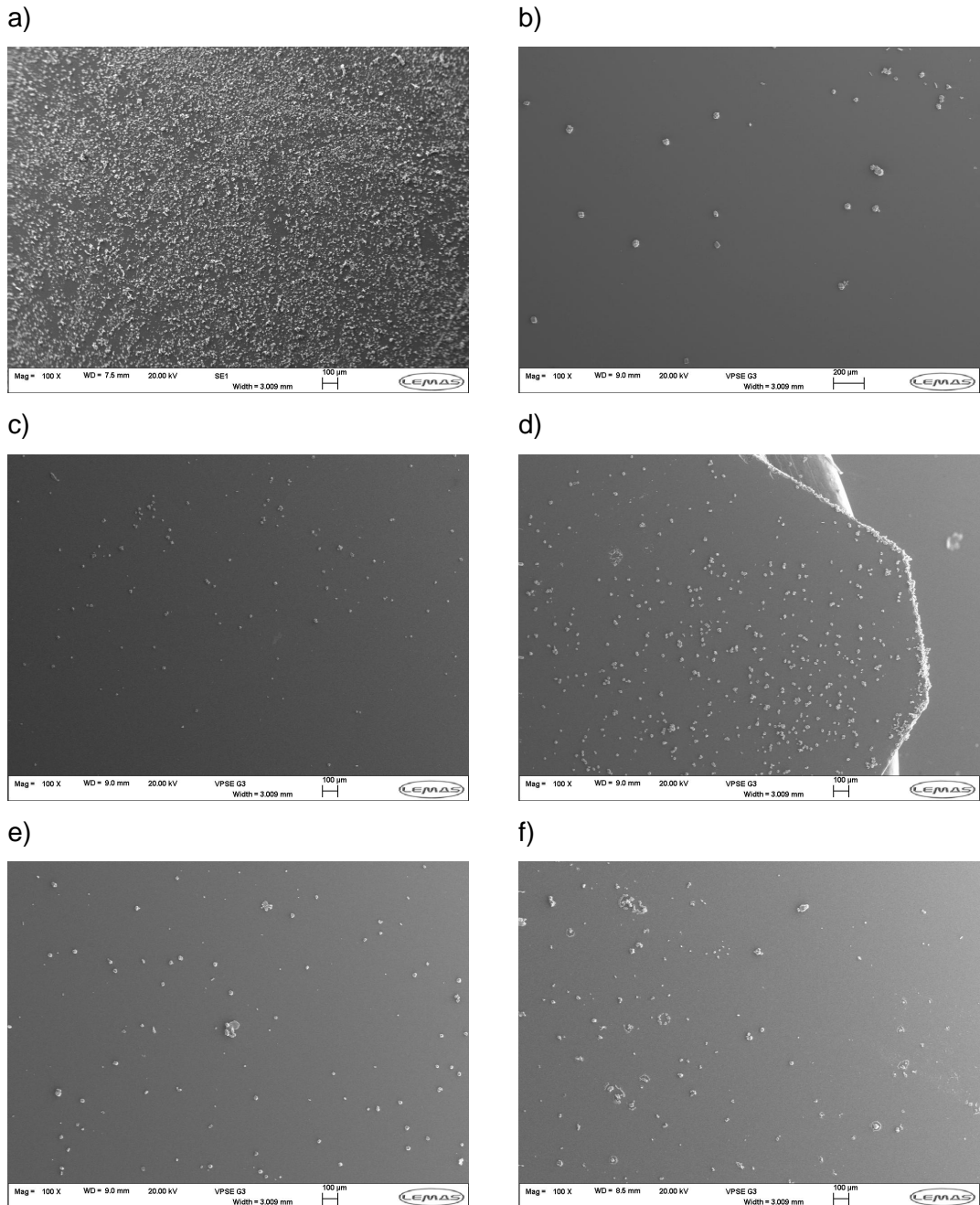


Figure 5-21. Low magnification SEM images of calcium carbonate deposited on a) non-treated quartz surface, b) 0.03%, c) 0.06%, d) 0.12%, e) 0.18% and f) 0.24% APhS coated quartz surfaces in low SR= 4.77 at 80°C

5.3.1.2 Morphology of calcium carbonate deposited on untreated and APhS-treated quartz surfaces in low SR=4.77

Higher magnification images taken by SEM are shown in Figure 5-22 to study the morphology of the crystals on the untreated and treated surfaces. The shape of crystals for all the coated surfaces seems to be distorted calcite whereas the calcium carbonate crystals deposited on the blank quartz surface are clusters of calcite. This suggests the influence of the coating material on crystallisation morphology. The same behaviour as APTES effect in low SR is seen in Figure 5-22, i.e. the APhS coating block the nucleation sites of the quartz surface or reduces the surface energy of the quartz in order to lower tendency of scaling on the surface.

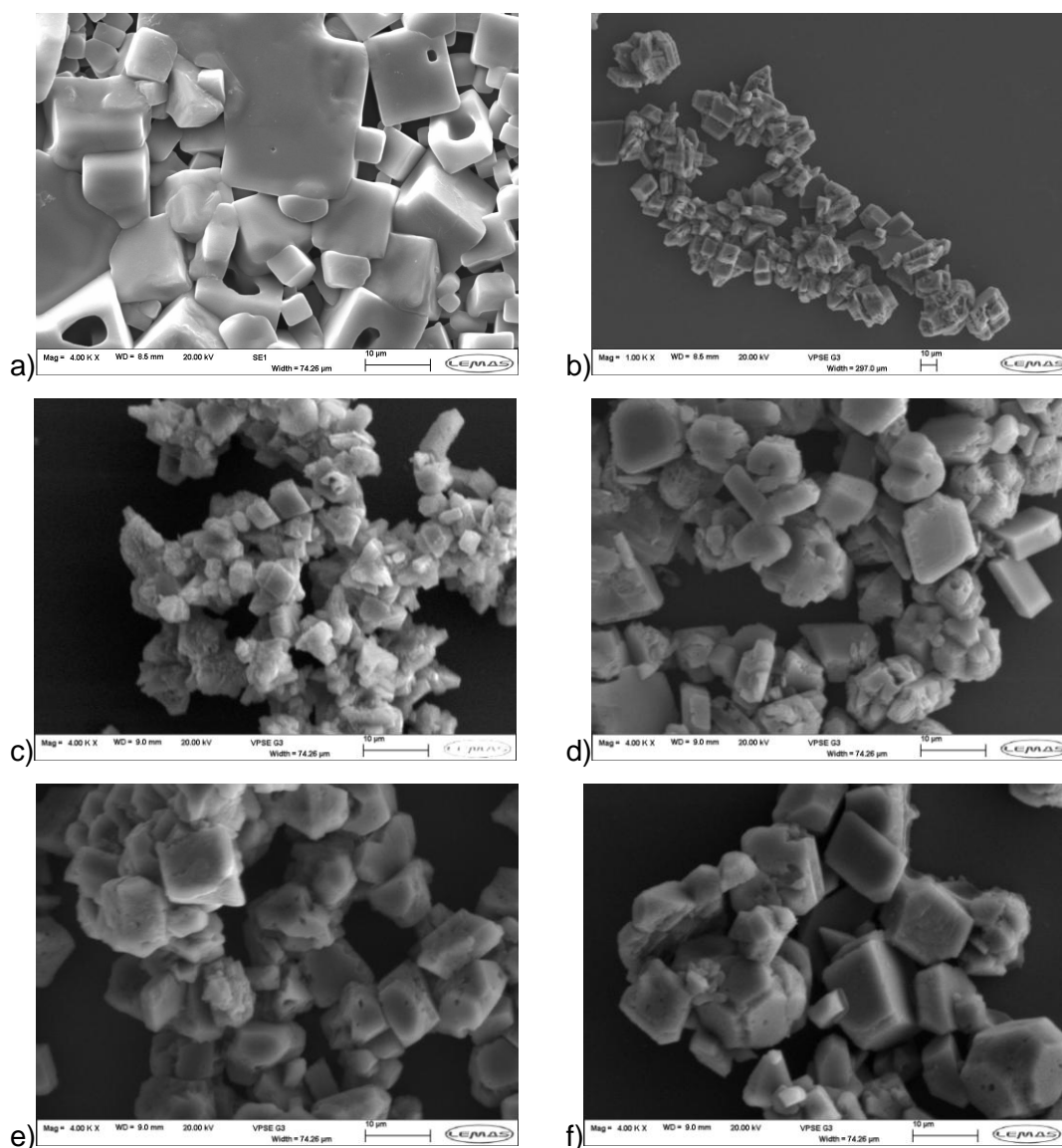


Figure 5-22. High magnification SEM images of calcium carbonate deposited on a) non-treated quartz surface, b) 0.03%, c) 0.06%, d) 0.12%, e) 0.18% and f) 0.24% APhS coated quartz surfaces in low SR = 4.77 at 80°C

5.3.2 APhS coating behaviour in high SR = 54.8

The performance of the treated quartz surfaces were also compared with the untreated surface in high SR=54.8 calcium carbonate solution. The same brine as in the APTES study for high SR was used for APhS. The gravimetric results of the amount of mass deposited on the treated and untreated surfaces are presented in Figure 5-23. It is observed that the amount of mass reduction considerably reduced on the treated surfaces compared with blank surface. The blank surface is shown as 0% concentration in x-axis. The minimum and maximum mass deposited on the APhS-coated surfaces were at 0.06% and 0.03% with 131.3 and 336.7 μg ; respectively, whereas the amount of mass deposited on the blank surface was 1500.7 μg . This indicates the high proficiency of the APhS coating on prevention of calcium carbonate scale deposition even in high SR solution.

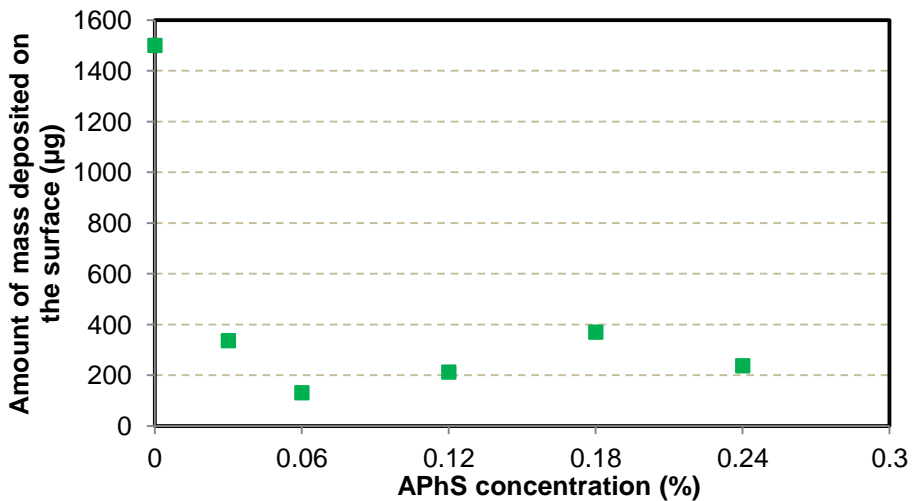


Figure 5-23. The mass of calcium carbonate deposited on the APhS treated surface as a function of concentration at high SR=54.8 (error bars are too small and hidden in the markers)

In order to better illustrate the performance of the surfaces treated by APhS in terms of prevention of scaling on the surface, Figure 5-23 was re-plotted and is shown in Figure 5-24. This graph shows the efficiency of the surface in scale reduction as a function of the coating material concentration. More than 90% scale deposition reduction was obtained by APhS at 0.06% concentration after 24 h experiment at 80°C.

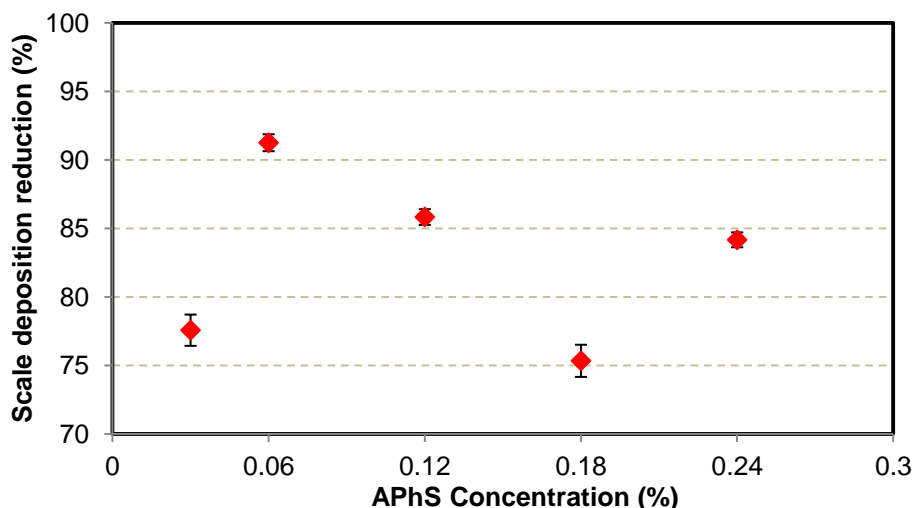


Figure 5-24. Scale deposition reduction as function of APhS concentration at 54.8 SR and 80°C

The impact of different SAM-surfaces on scale reduction was schematically presented in Figure 5-25.

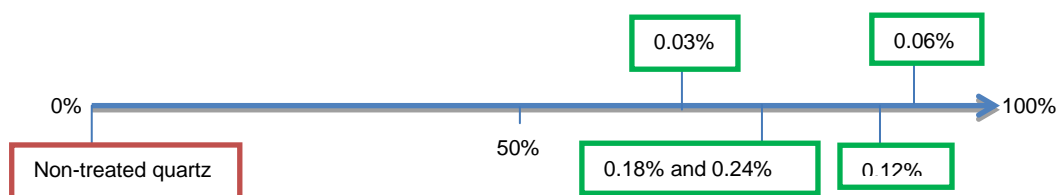


Figure 5-25. Systematic ranking of surface performance in terms of amount of scale reduction on APhS-SAM surface in high SR=54.8 at pseudo-dynamic condition at 80°C

5.3.2.1 Visualization of calcium carbonate deposited on untreated and APhS-treated quartz surfaces in high SR=54.8

SEM was employed to see whether visual observation supports the gravimetric results. On the other hand, as explained before in this chapter, different saturation ratios influence the amount of scale formed on the surface. Thus, the image analysis of calcium carbonate in high SR was carried out in terms of the aggregation and morphology of the crystals. From the results obtained at lower magnification in Figure 5-26, it is quite clear that the amount of CaCO₃ decreased on the treated surfaces. The observation shows compact calcium carbonate clusters and the coverage of the blank surface by mineral scale whereas the treated surfaces present smaller clusters and more isolated crystals.

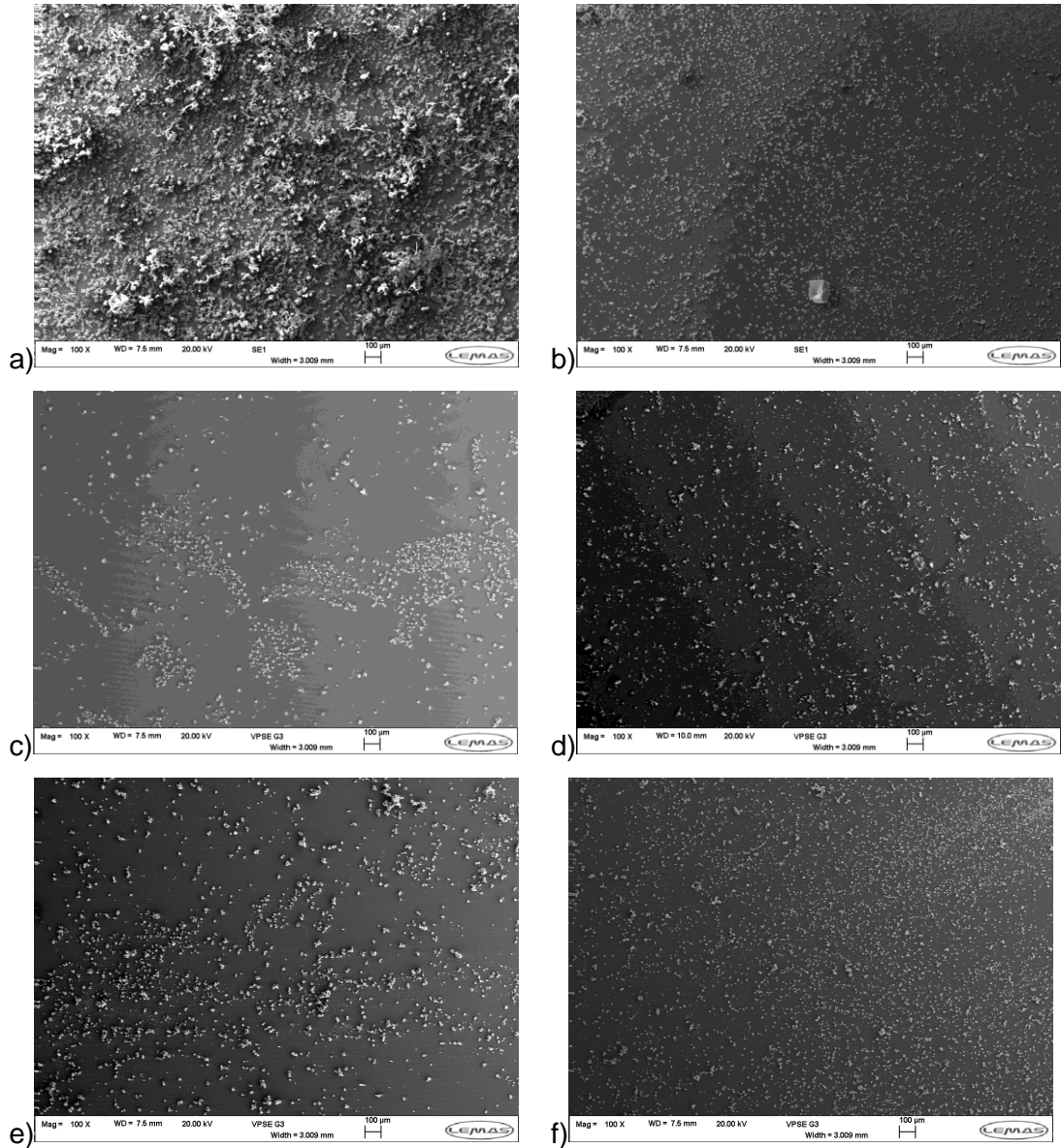


Figure 5-26. Low magnification SEM images of calcium carbonate deposited on a) non-treated quartz surface, b) 0.03%, c) 0.06%, d) 0.12%, e) 0.18% and f) 0.24% APhS coated quartz surfaces in low SR= 54.8 at 80°C

5.3.2.2 Morphology of calcium carbonate deposited on untreated and APhS-treated quartz surfaces in high SR=54.8

In addition, the noticeable observation from a visual point of view is the change of crystals shape for the treated surfaces compared to blank quartz. The shape of calcium carbonate deposited on the blank surface is a mixture of cubic and chain calcite whereas distorted cubic calcite formed on the treated surfaces.

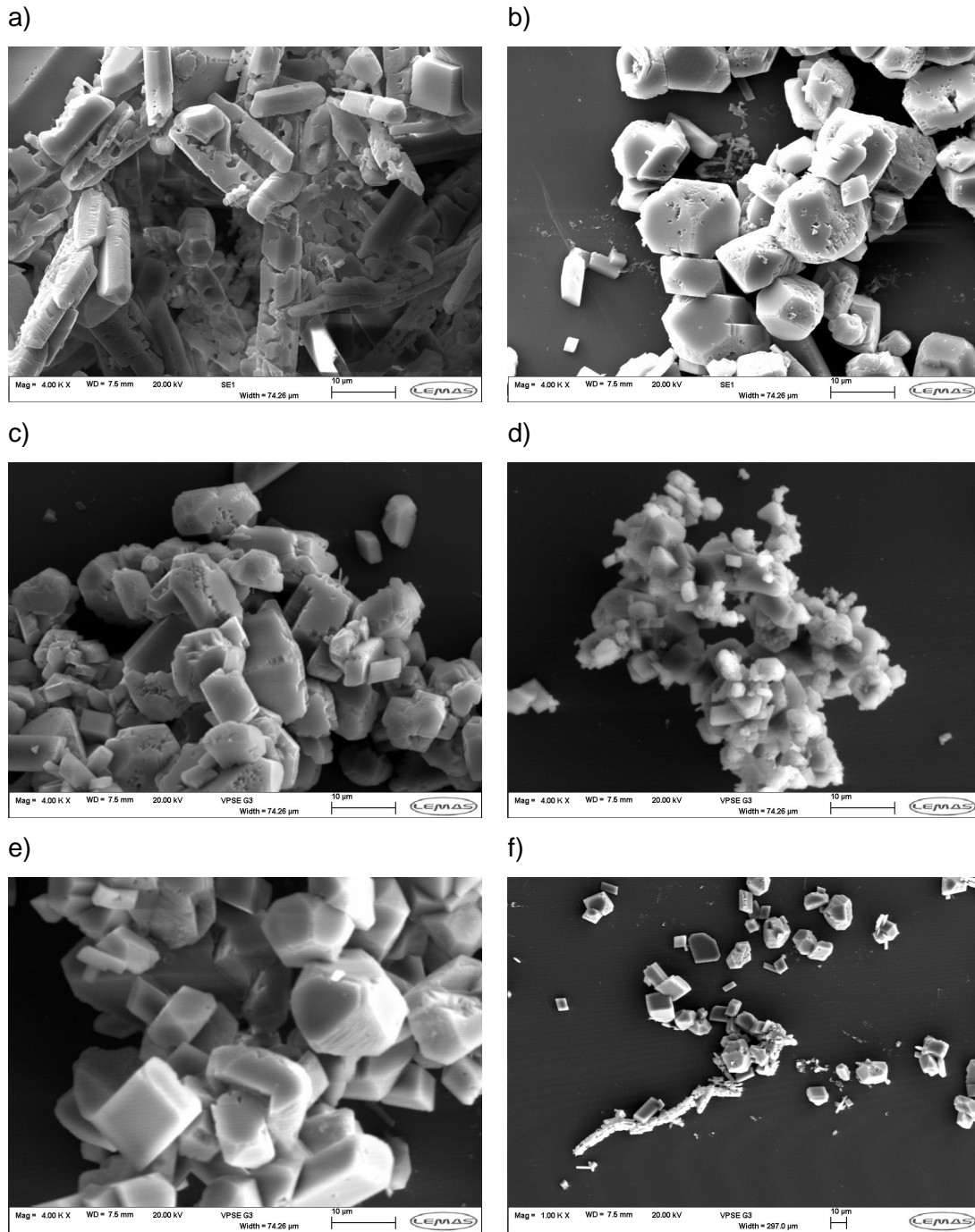


Figure 5-27. High magnification SEM images of calcium carbonate deposited on a) non-treated quartz surface, b) 0.03%, c) 0.06%, d) 0.12%, e) 0.18% and f) 0.24% APhS coated quartz surfaces in low SR= 54.8 at 80°C

5.4 Comparison of APTES and APhS coated surface performances in CaCO₃ deposition reduction

In this section, all the scale test results for APTES and APhS coated surfaces in both low and high saturation ratios are shown in Figure 5-28. The main conclusion can be obtained from the bar chart is that both APTES and APhS

coating materials are able to reduce the tendency of the calcium carbonate crystal to the surface. In general, the efficiency of the APhS coating surfaces was higher than APTES.

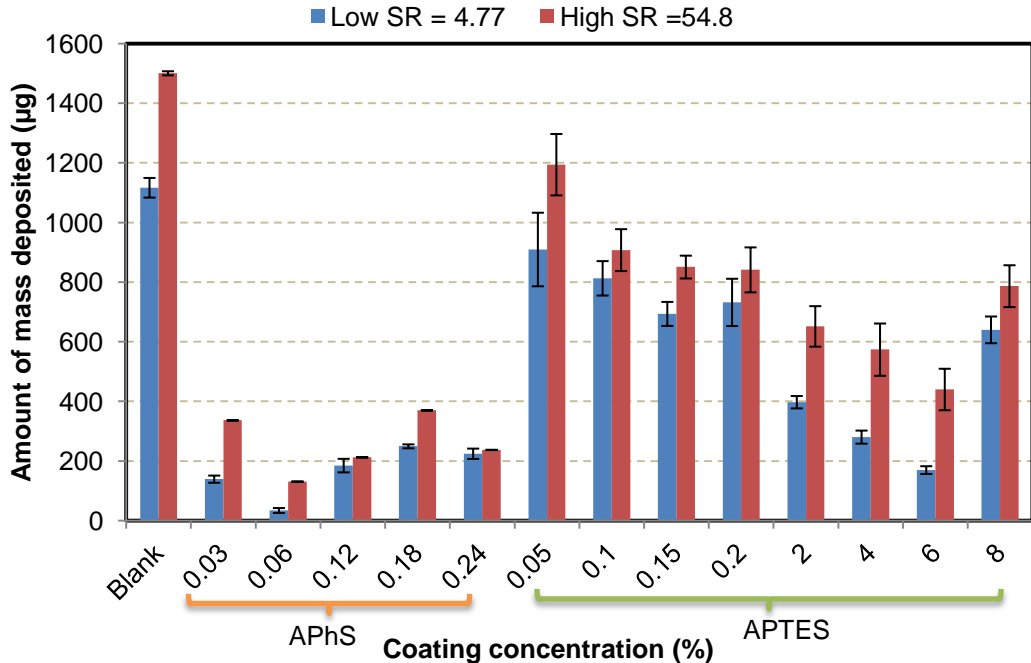


Figure 5-28. Comparison results of the amount of mass deposited on the surface versus coating material concentration in low and high saturation ratio solutions at 80°C after 24 h experiment

Figure 5-29 illustrates the performance of the treated- and untreated-surfaces in terms of calcium carbonate deposition at low and high SR at 80°C. Similar behaviours are observed from the treated surfaces in both low and high SR solutions. Better performances in low and high SR solutions are seen at 0.06% and 6% for APhS and APTES, respectively. The standard deviations for APTES at 0.05-8% are much bigger and cover a bigger range of data; this can be due to the challenges involved in reproducibility of APTES film formation in the presence of water in the solution. The excess of water in the solution of APTES yields more APTES polymerisation leading to less repeatability in the formation of APTES on the surface (244-246, 271, 342). Different film orientation may have led to different surface performance observed in these concentrations. For APhS at 0.12% and 0.24%, same performance can be concluded by considering the standard deviations for these concentrations. Thus, it can be stated that similar behaviour was observed for all concentrations in low and high saturation ratio; however, with slightly better efficiency at low SR solutions.

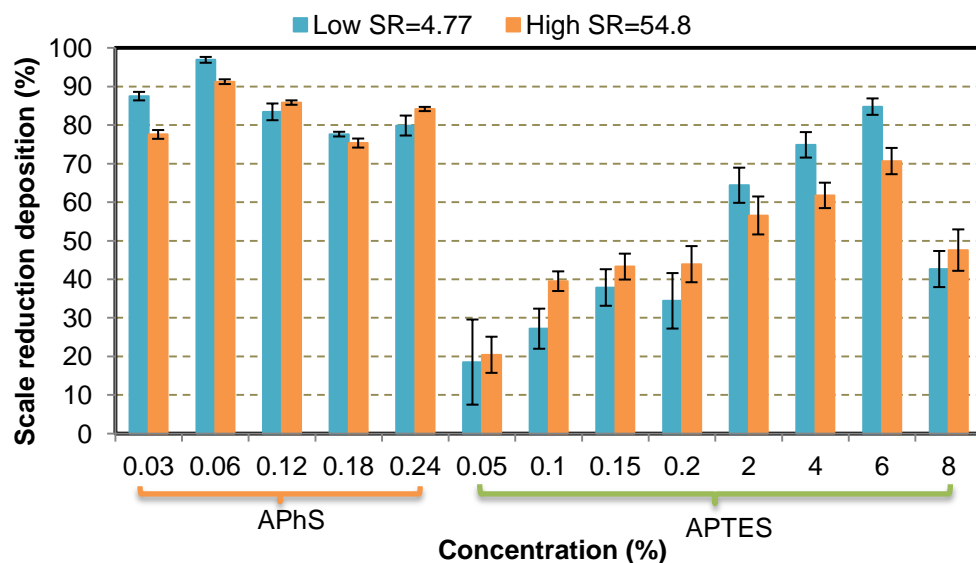


Figure 5-29. Comparison results of the surface performance versus coating material concentration in low and high saturation ratio solutions at 80°C after 24 h experiment

The best performance among all the treated quartz surfaces was obtained at 0.06% APhS coating concentration in both low and high saturation ratio solutions. This could be due to a uniform film formation on the quartz surface by 0.06% APhS as was demonstrated in the literature (244, 285). Since the head group of both materials is amino group (NH₂), it was expected to see the same performance for both APhS and APTES. The superiority of APhS could be owing to the rigid structure of the APhS which prevents tilting the molecule towards surface (244, 285). Also the gravimetric results obtained from APhS-coated quartz surface showed a stable behaviour in terms of mass reduction deposited on the surface in both low and high SR solutions under the same experimental condition (pseudo-dynamic solution at 80°C for 24 h). On the other hand, APTES-coated surfaces demonstrated a bigger range of results; this could be due to either a wider range of concentration applied or the complexity of APTES film formation; the latter was discussed in the literature (244-246, 349).

The reduction of amount of scale deposited on the treated surface is explained by the change of surface chemistry properties after coating. The point of zero charge (PZC) of quartz was shown to be between 2 and 3 (350-352) depending on composition materials, i.e. the quartz surface becomes negative in pH above 2-3, and positive in pH below 2-3. This is schematically shown in Figure 5-30a. Since the pH of the experiments for both low and high SR solutions was 7-8 (calculated by MultiScale™ (111)), the blank quartz surface in aqueous solution became negatively ionised. It was previously demonstrated that a negatively charged surface promotes crystal nucleation leading to growth of

polycrystalline calcium carbonate (163, 348), which favours CaCO_3 growth. On the other hand, aminosilane treated surfaces become positively charged in aqueous solution (275)(see Figure 5-30b) due to presence of an electron pair on the amine group (353). This is based on the fact that amine group can potentially accept protons from Lowry-Brönsted acids and perform as a base (353). Moreover, it was demonstrated (348) that the positively charged surface created an unfavourable substrate for the nucleation of calcium carbonate. Therefore, this explains the performance of the aminosilane-coated surfaces in terms of reducing the amount calcium carbonate deposited. However, it was reported that a neutral surface limits the number of available nucleation sites on the surface and promotes formation of single calcium carbonate crystals (5, 181, 348). Since the APhS-treated surfaces are less positively (towards neutral) charged, better performance of these surfaces in terms of scale deposition reduction may be explained by the fact that APhS might reduce the available sites for crystal nucleation.

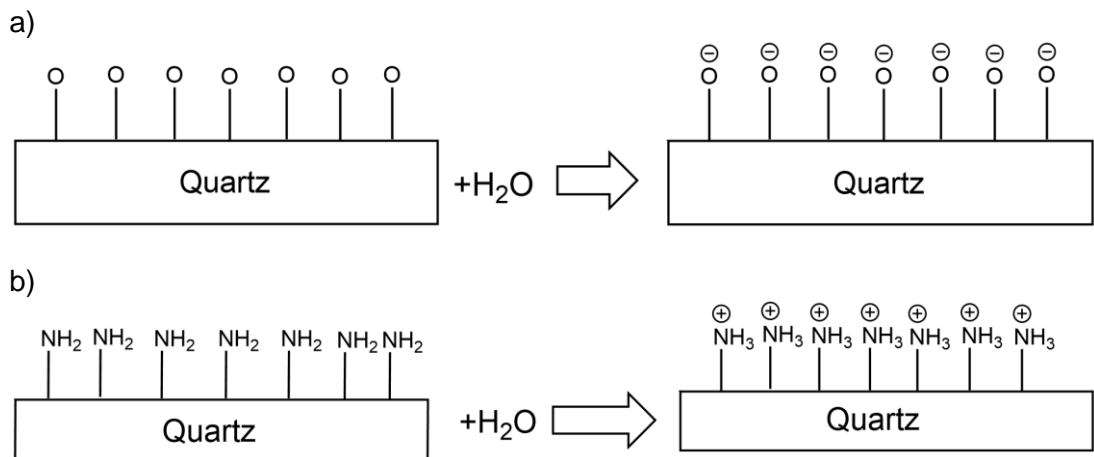


Figure 5-30. Surface charge distribution of a) untreated and b) aminosilane-treated behaviours in aqueous solution

Since the head group of both aminosilane tails is an amine group, it was expected that similar behaviour from both coating materials would be observed. The amine group on the APTES is a much stronger base than on the APhS owing to aromatic structure of APhS (353) leading to more positively charged surface by APTES than APhS. There are two factors that can determine the strength of amine of a base: i) how easy a lone pair attracts a hydrogen ion and ii) how stable the formed pair is. The alkyl group in APTES tends to repel the pair electrons on nitrogen, which introduce more negative charge on the APTES. This makes APTES stronger base with $\text{p}K_b=3.16$. Figure 5-31 illustrates the process of reaction between APTES and water.

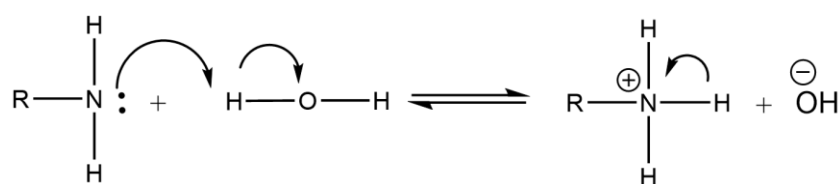


Figure 5-31. The ability of water to stabilize the corresponding ammonium ion is diminished in presence of alkyl group which results in formation of stronger basis and reduction of APTES acidity

On the other hand, in APhS the electron pair in nitrogen interferes with delocalised ring of the phenyl; this creates new delocalised electrons. Thus, the lone pair of nitrogen in APhS would not be fully available to attract a hydrogen ion after interacting with the phenyl ring; i.e. the delocalised electrons are more attractive to the lone pair of nitrogen. Figure 5-32 shows the interaction of electron pair of nitrogen and phenyl ring.

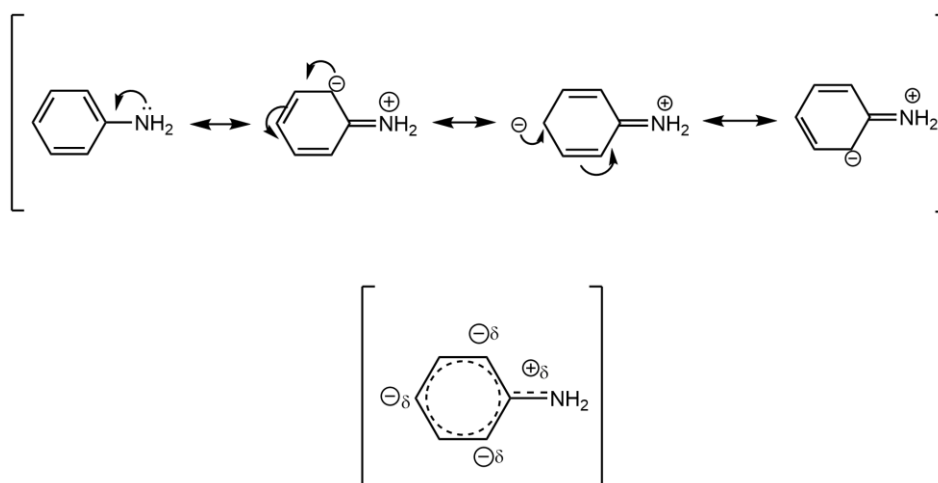


Figure 5-32. The theoretical basis for the diminished basicity of APhS

On the other hand, interaction with hydrogen ion will disrupt the delocalized electrons – which are more stable. This requires more energy and will not occur easily, which makes phenylamine a weaker base with $pK_b=9.38$. The smaller pK_b , the stronger base (353). The interaction between phenyl group and water is shown in Figure 5-33. Since after interaction with water increases the pK_b of APhS, the tendency of APhS in formation of acid increases which may affect the scale reduction on the treated quartz surfaces.

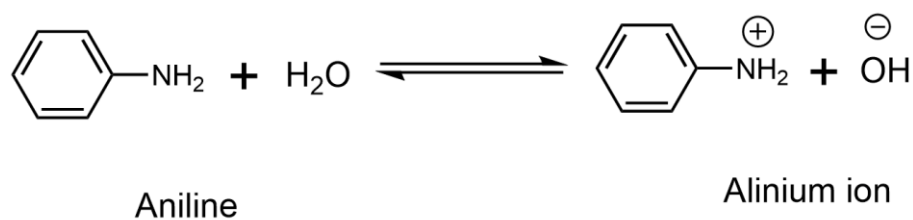


Figure 5-33. Phenyl group of APhS causes creating a molecule with higher pK_b , introducing weaker basis and stronger in acidity

As mentioned in Chapter 2, horizontal and vertical polymerization of APTES molecules in the presence of water complicates the film formation of APTES on quartz surface (245, 246). It was also believed that APTES will be more cross-linked to one another in the presence of water (246, 270). Moreover, the APTES molecules are flexible and can easily tilt towards the surface, which makes an unfavourable film formation (244). This is schematically illustrated in Figure 5-34a, which can explain the wider range of efficiency in terms of scale deposition reduction on APTES-treated surfaces. On the other hand, it was demonstrated (244, 285, 354) that APhS creates a uniform film on a quartz surface due to the rigid structure of benzene. This phenomenon explains the better efficiency of APhS in reducing the amount of calcium carbonate deposited on the coated surfaces compared with APTES which indicates the importance of film orientation on reduction of calcium carbonate scale deposition. The both positive and neutral surfaces do not favour deposition of calcium carbonate scale (348), however, neutral surface influences more on scale reduction which could be one of the factors explain the different performance of APTES. Moreover, the other aspect, which can explain the different behaviour of these aminosilanes, is the structure of the film deposited on the quartz surface. This suggests that the amount of scale deposited on the treated quartz surface is strongly dominated by the structure and the orientation of coating molecule. This can also suggest that in case of a uniform formation of APTES with amine group upward at the surface, the same performance may be resulted. This can be a subject of future work.

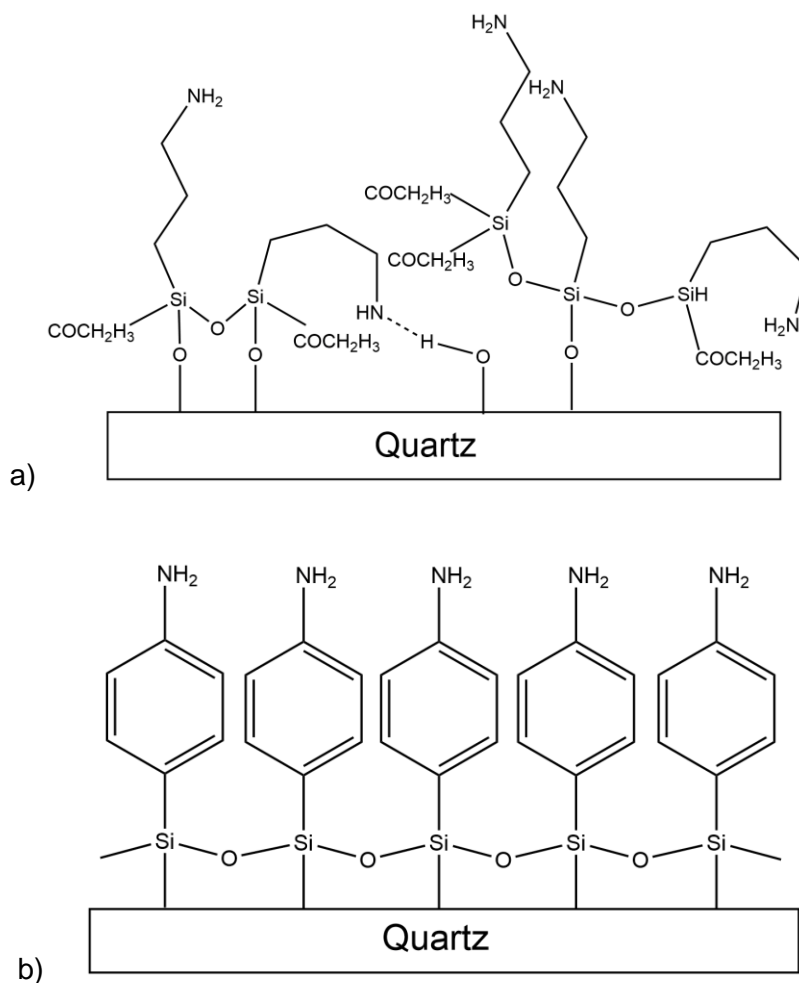


Figure 5-34. Possible schematic of film formation structures of a) APTES and b) APhS on quartz surface

As was mentioned in Chapter 2 and demonstrated in Chapter 4, formation of APTES on a quartz surface is a complicated process and involves a highly-controlled condition. This could be the explanation the larger scatter in the results from scale tests. In Chapter 4, it was shown that the highest surface coverage was obtained at 8% APTES concentration; however the results of 6% were acceptably close to the 8%. As can be seen from Figure 5-28, the best results for both low and high SR in APTES was obtained at 6%. This suggests that the film formation at 6% is more uniform with amine group upwards at the surface than other concentrations. In contrast, at 8% owing to lack of water presented in the solution more amine groups were protonated and reacted with the quartz surface or oriented and bended towards the surface; which can explain the results at 8%. The effect of water was discussed in the literature (244-246, 267, 355). This will be analysed more in detail in Chapter 6, which studies the surface characterisation of treated surfaces and this will be also discussed in Chapter 7.

5.5 Summary

In this chapter, the behaviour of the treated surface in terms of the mass reduction of calcium carbonate on the surface was compared with the un-treated quartz surface. The results of this chapter are important as it presents the main objective of the research, i.e. the potential for coating internal surface of rock to reduce/prevent scale deposition/adhesion. This plays a critical role for further investigations of the idea in terms of creating less favourable surface in near wellbore area to reduce the severity of the scale deposition in production loss of the well. Various concentrations of APTES and APhS were applied to the quartz surface in coating process. Microbalance and SEM were employed to measure and observe the amount and morphology of the scale deposited on the surface. Some major and minor conclusions of the chapter are presented below:

1. The amount of calcium carbonate scale deposited on the surface coated by APTES and APhS significantly reduced in comparison with uncoated quartz surface.
2. Up to 95% of scale deposition reduced on the 0.06% APhS-coated surface for both low and high SR, where the minimum efficiency was observed on 0.05% APTES-coated surface.
3. Compared to APTES, the amount of scale deposited on the surfaces treated by APhS were more stable and much lower.
4. The amount of calcium carbonate scale deposited on the all surfaces were higher in high (54.8) SR than low (4.77) SR.
5. Morphology of the calcium carbonate crystals were slightly changed on the treated surfaces in comparison with the untreated quartz surface. Distorted crystals were observed on treated surfaces in low SR solutions, whereas distorted and chain crystals were dominant in high SR solution.
6. The reduction of calcium carbonate scale deposition on the treated-surfaces can be related to lower number of available sites on the surfaces by forming aminosilane films.
7. The feasibility of a proactive scale management by creating unfavourable rock surface for scale deposition in near wellbore area was demonstrated in this chapter.

Chapter 6

Film Characterisation and Surface Properties of APTES and APhS Coating

6.1 Introduction

In this chapter, physicochemical properties of two different organosilane films on quartz surface are studied in order to better understand the results of scale tests (Chapter 5). As shown in Chapter 4, various concentrations of the APTES and APhS were applied to create a film on the quartz surface subsequently the effect of this coating on reduction of scale deposition on the treated quartz substrates was assessed. The objective of this chapter is to employ a wide range of surface characterisation techniques to comprehensively analyse the surfaces of Chapter 5 after formation of the film. Film composition, roughness and surface energy of APTES and APhS were analysed by XPS, contact angle measurements and 3D optical profilometry, respectively. Each coating chemical was studied using each of the surface characterisation methods, before the results are compared together.

Firstly, XPS was employed to characterise the chemical properties of the treated surface. This was performed by monitoring the concentration and binding energy of nitrogen. Figure 6-1 illustrates APTES and APhS molecular structures with primary amine on the tail of the molecules. As mentioned in Chapter 2, since most of rock analogue is quartz (SiO_2), the organosilane group was chosen to interact with quartz surface. After film formation procedure, it was expected Si head group bonds to the quartz surface and primary amine of the molecules cover the top layer of the surface.

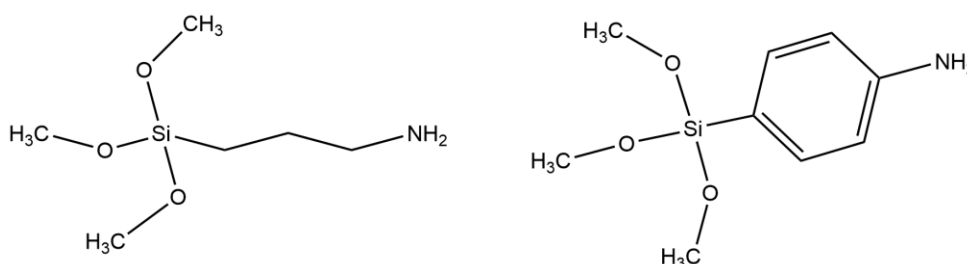


Figure 6-1. APTES and APhS molecular structures

Secondly, the physical properties of the treated surface were analysed by studying the wettability and the roughness of the surface. Static contact angles of the surfaces were measured using a water droplet. In addition, the topography of the treated and untreated surfaces was measured by optical profilometry. The map of analysis to approach the objective of this chapter is presented in Figure 6-2.

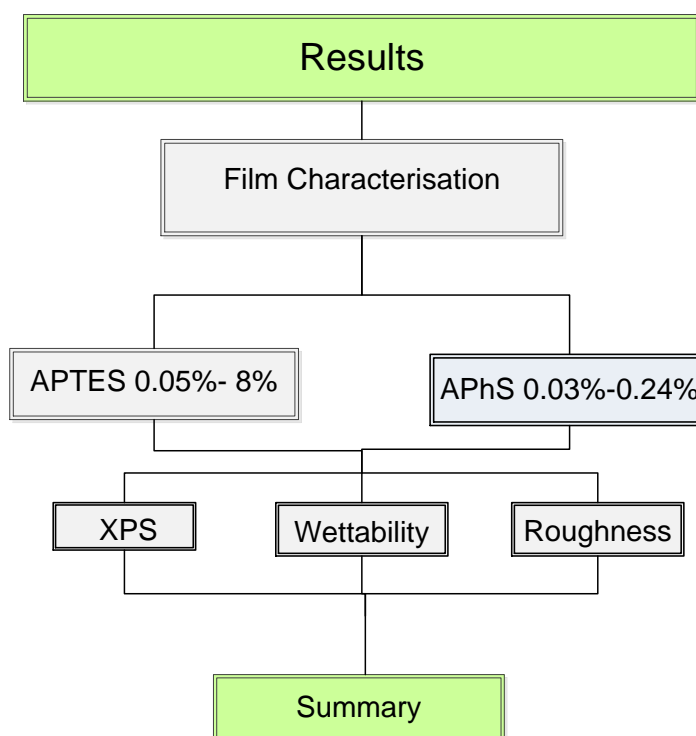


Figure 6-2. Summary of Film Characterisation analyses in Chapter 6

6.2 X-ray Photoelectron Spectroscopy results of APTES- and APhS-treated surfaces

XPS is capable of detecting and quantifying the elements on the surface as well as identifying chemical states of the constituent elements by showing a clear binding energy fingerprint. This section investigates the chemical state and shifts of treated surfaces by XPS. (C1s) hydrocarbon peak at 284.8 eV is used as a reference for all binding energies. The presence of APTES and APhS on the quartz surface were confirmed by N1s peak (398.7-402 eV (222, 244, 285, 356-359)) and the more intense C1s peak (284.8 eV) in the survey scan of XPS. If the ethoxy groups (-OCH₂CH₃) of APTES and APhS groups react to the quartz surface, the free amine group on the head of aminosilanes can be detected at 398.7-399.6 eV by XPS(222, 244, 285, 356-359). However, some amine moieties can have hydrogen bonding with each other and the surface and become protonated; this can

be observed by XPS at 400-402 eV (222, 244, 285, 356, 359). The degree of protonation as well as nitrogen presentation detected by XPS can be used to explain the different behaviour of the APTES- and APhS- treated surfaces with respect to scale deposition observed in Chapter 5. Before analysing N1s binding energy for the treated surfaces, a survey scan was acquired on a bare quartz surface to detect the main composition of quartz surface. The survey scan of the blank quartz surface is presented in Figure 6-3.

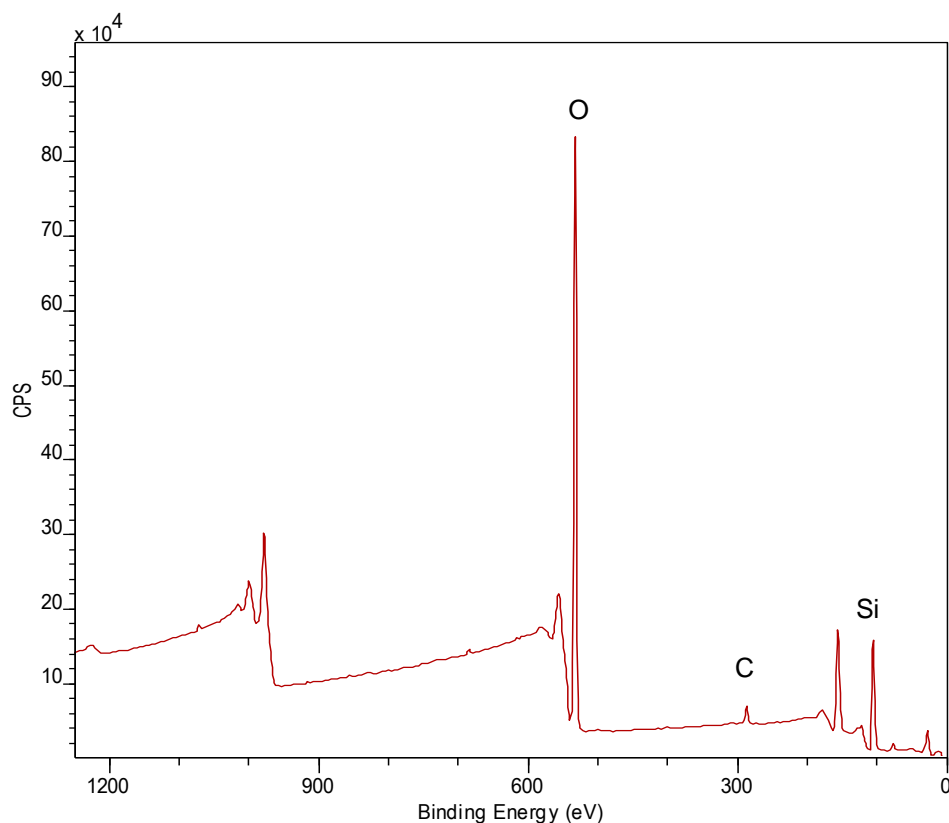


Figure 6-3. A survey scan of the blank quartz surface showing main composition of the surface

Silicon, oxygen, carbon are observed in the survey scan of the untreated quartz surface in Figure 6-3 as main compositions; these are the common elements between the quartz, APTES and APhS. Based on APTES and APhS molecular structure, the only element that can differentiate the survey scan of coating materials is nitrogen. Therefore, surveys scan of the treated surfaces were acquired to detect the nitrogen peak. Figure 6-4 illustrates a survey of APhS coating surface presenting the N1s spectrum around 399 eV (244, 356-359) for the surface coated by 0.06% APhS; this N1s peak is related to amine group of APhS.

After detecting the amine on the treated surfaces, the C1s high resolution spectra were analysed before studying the N1s spectra. The binding energy at

284.8 eV was referred to C1s (360). Figure 6-5 illustrates the high resolution of C1s of the blank and 0.06% APhS-treated surfaces.

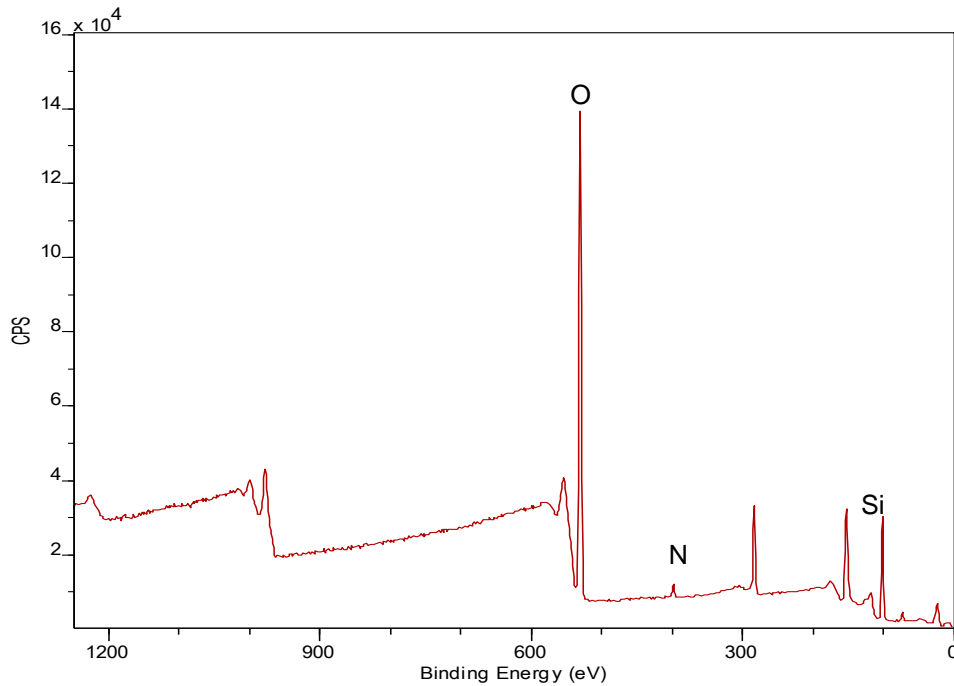


Figure 6-4. A survey scan of the treated quartz surface by 0.06% with the main compositions

Two components at 284.8 and 285.7 eV are observed in Figure 6-5a, which are referred to C-H and C-O, respectively (244). During silanization of aminosilane on the treated surface, the -O-CH₃ peak component disappeared by condensation of the silane with the hydroxyls of the substrate to create Si-O-Si (244). Then the C-O peak is replaced by a C-N peak component at 285.7-286 eV which indicates the presence of the aminosilane on the quartz surface (244). Figure 6-5b shows the C1s binding energy of C-H and C-N of the surface coated by 0.6% APhS.

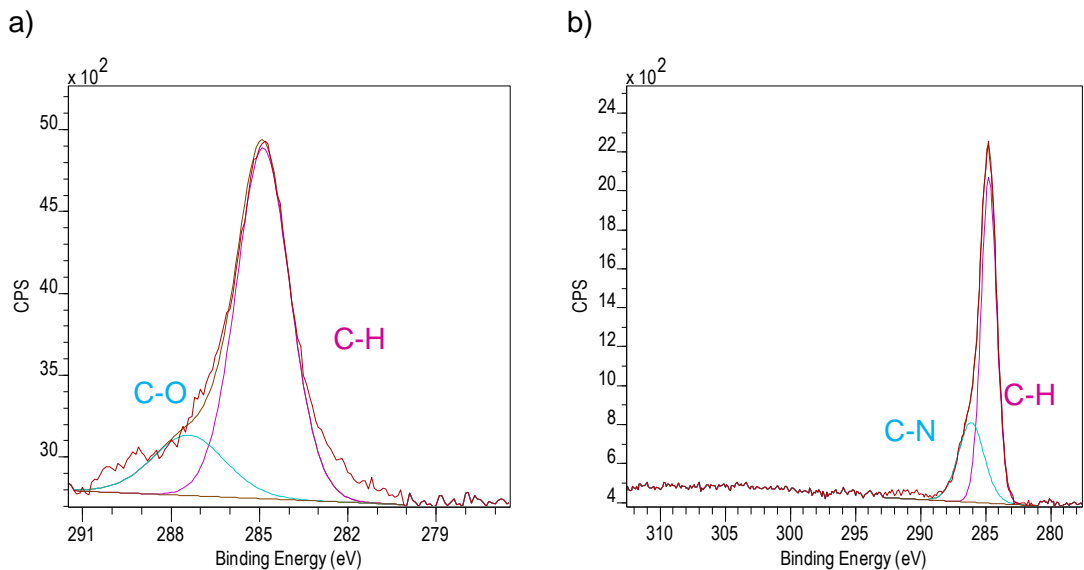


Figure 6-5. C1s high resolution spectra of the a) bare quartz and b) treated quartz by 0.6% APhS

The N1s spectra were analysed in detail to study the possible composition which occurs while APTES or APhS reacting with the quartz surface in the solution. The information obtained from the N1s peak presents the chemical state of the amino group of APTES or APhS affecting mineral scale deposition during the scale test. As mentioned in Chapter 5, in comparison with the blank quartz surface, the coated surfaces with APTES and APhS made a clear reduction of calcium carbonate deposition and adhesion; however, each concentration of APTES and APhS behaved differently in relation to the amount of scale deposited on the surface. Thus investigating the chemical states and binding energy shifts of N1s spectra of the different concentrations can be a useful method to interpret the different behaviour of the coated surfaces. Although the binding resolution of some chemicals are greater than the relative chemical shifts owing to intrinsic width of molecule peak (361), high resolution spectra of some molecules are able to distinguish between the chemical shifts. Hydrogen-bonded/protonated amine can be postulated to exist from free amine groups on the surface; this was demonstrated in the literature (222, 244, 285, 356-359, 362). However, hydrogen-bonded and protonated amine cannot be separated (356) by high resolution N1s spectrum on amine.

6.2.1 Chemicals states and binding energy shifts of APTES-treated surface

High resolution N1s spectra of the quartz surfaces treated by 0.05%, 0.1%, 0.15% and 0.2% APTES are presented in Figure 6-6. As mentioned, in N1s spectrum the free NH_2 can be observed between 398.7 and 399.6 eV. The hydrogen-bonded or protonated amines can be also observed ~ 400 eV. Figure 6-6a shows that the high resolution N1s spectrum consists of two peaks centred at 399.3 and 401.7 eV with the ratio of 1:1.4 for 0.05% concentration. The former presents the primary amine group and the latter indicates the hydrogen-bonded or protonated amine of APTES on the surface. Figure 6-6b illustrates three peaks for 0.1% APTES at 399.2 eV, 401.3 eV, and 403.4 eV. The lowest-binding energy in N1s high resolution spectra refers to the primary amines, the middle peak to the hydrogen binding and the highest-binding energy to the protonated amines (356, 363-365).

Hydrogen-bonded and protonated amines are considered H-bonded/protonated amine ($\text{---NH}_2/\text{NH}_3^+$) in this study, since it is difficult to distinguish between H-bonded and protonated amines by XPS due to the fact that

in most cases the relative chemical shifts of protonated and H-bonded amines are below the energy resolution (366). Thus, the ratio between NH_2 and $\text{---NH}_2/\text{NH}_3^+$ was 1:1.9 for the surface treated by 0.1%. The detected peaks for 0.15% and 0.2% in Figure 6-6c and Figure 6-6d are 399.4/401.8 eV and 399.2/401.5 eV for primary and H-bonded/protonated amines with the ratios of 1:1.5 and 1:1.2, respectively. The higher percentage of peaks at >400 eV indicates that higher number of APTES were protonated or hydrogen bonded during the coating process.

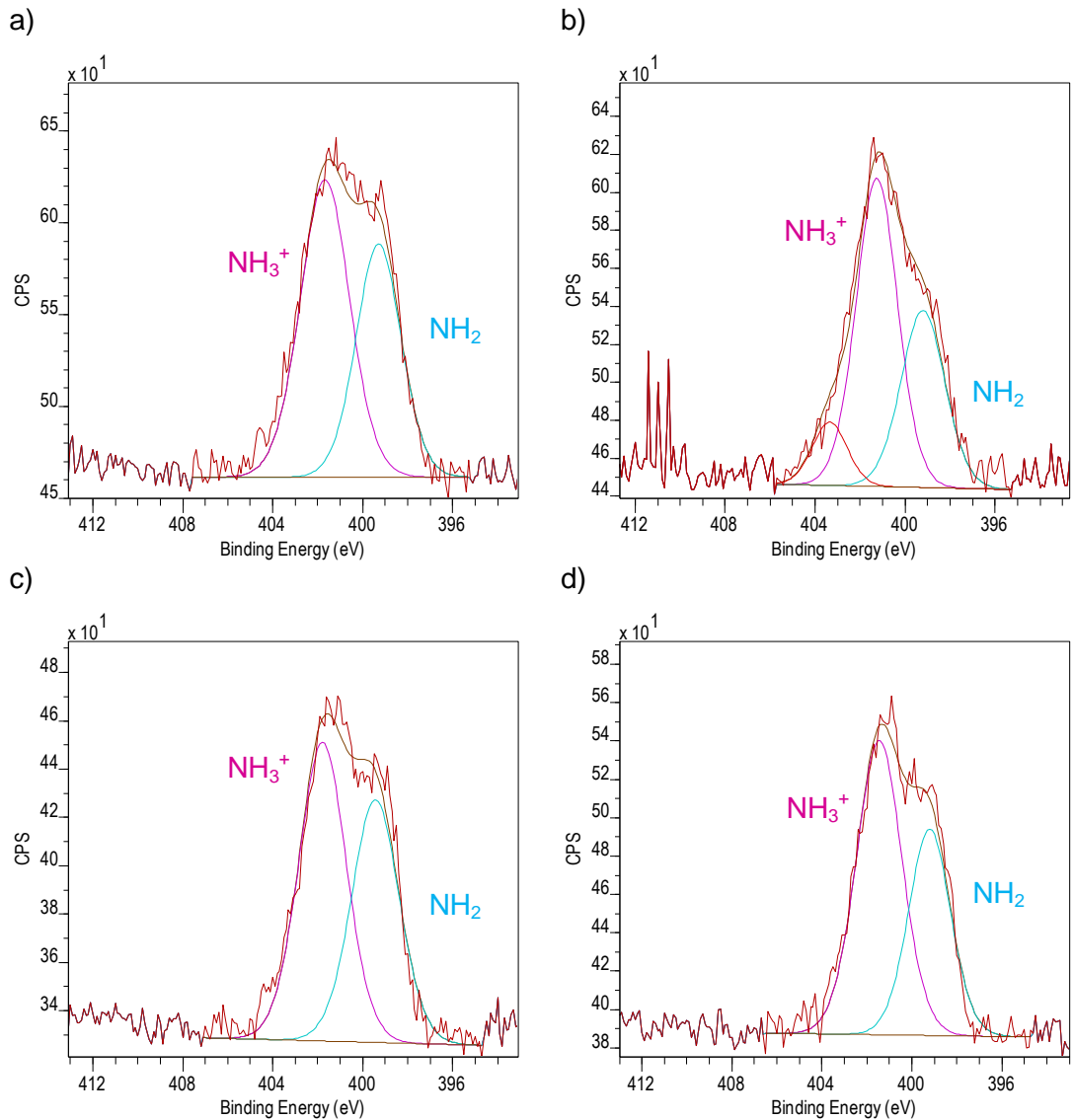


Figure 6-6. High resolutions N1s spectra of the quartz surfaces coated with a) 0.05%, b) 0.1%, c) 0.15% and d) 0.2% APTES

The ratio of $\text{NH}_2/\text{NH}_3^+$ for the coated surfaces by APTES (0.5%-0.2%) is presented in Table 6-1.

Table 6-1. Ratio of primary amines to hydrogen/protonated amines on the treated surfaces by APTES (0.05%-0.2%)

APTES concentration (%)	0.05	0.1	0.15	0.2
NH ₂ /NH ₃ ⁺	1:1.4	1:1.9	1:1.5	1:1.2

The percentages of NH₂, ---NH₂/NH₃⁺ and nitrogen of each concentration (0.05-0.2%) are presented in Figure 6-7. In general, all the concentrations show a higher percentage of H-bonded/protonated amine on the surface around 60% with a lower percentage of primary amine (~40%). Although silanization on the quartz surface does not happen without introducing water to the solution, excess of water results in hydrogen-bonds and protonation of amino moieties on the surface (245, 246, 270, 355, 367). This indicates that lowering the concentration of APTES in the solution led to more H-bonded/protonated amines, while polymerised aminosilane competes with alkoxy groups. The more H-bonded/protonated amines on the surface the more weak bonds on the surface, which may result in dissociation of aminosilane in water from surface. The concentration of nitrogen detected by XPS increased by APTES concentration indicating higher amount of APTES on quartz surface.

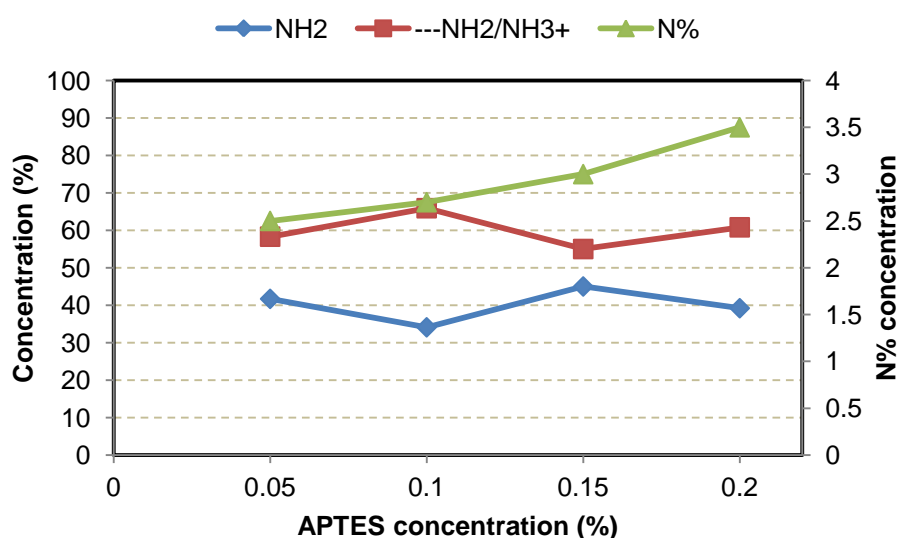


Figure 6-7. Percentage of free amine and H-bonded/protonated amines of the quartz surfaces treated by different concentrations of APTES

Another range of APTES concentrations to create a SAM film on the quartz surface was 2-8%. Figure 6-8 displays high resolution N1s spectra collected at 2%, 4%, 6% and 8% APTES. The binding energies of hydrogen bonded/protonated and primary NH₂ for 2% APTES were observed at 400.9 eV and 399.5 eV; respectively, with NH₂/NH₃⁺ ratio of 2.7:1. In the image b of Figure 6-8, the N1s peak presents a higher percentage of free amine for the quartz surface coated by 4% APTES than

by 2% at 398.7 eV, whereas a small shift is seen at 399.7 eV detecting hydrogen bonding/protonation between APTES and the quartz surface. This spectrum shows a lower percentage of protonated APTES than the free amines where the ratio of free amine to the H-bonded/protonated amine is 3.4:1. In comparison with 2% and 4% APTES, a higher percentage of N1s high resolution spectrum was acquired for the primary NH_2 component (398.8 eV) at 6% APTES. The amine shift at 400.2 eV is related to H-bonded/protonated amine on the surface with the proportion of 1:9 to the primary amine. The surface treated by 8% APTES showed highest H-bonded and protonated amines which is attributed to the higher binding energy signal at 400.3 eV for N1s high resolution (see Figure 6-8d), and the lower binding energy signal at 399.5 is related to primary amine, with the ratio of 1.9:1, respectively. The decrease in percentage of free amines at 8% could be resulted from the lack of required water in order to hydrolysing APTES solution (244-246). The sensitivity of water concentration on APTES adsorption on the surface was discussed in the literature (244-246, 270, 355, 367).

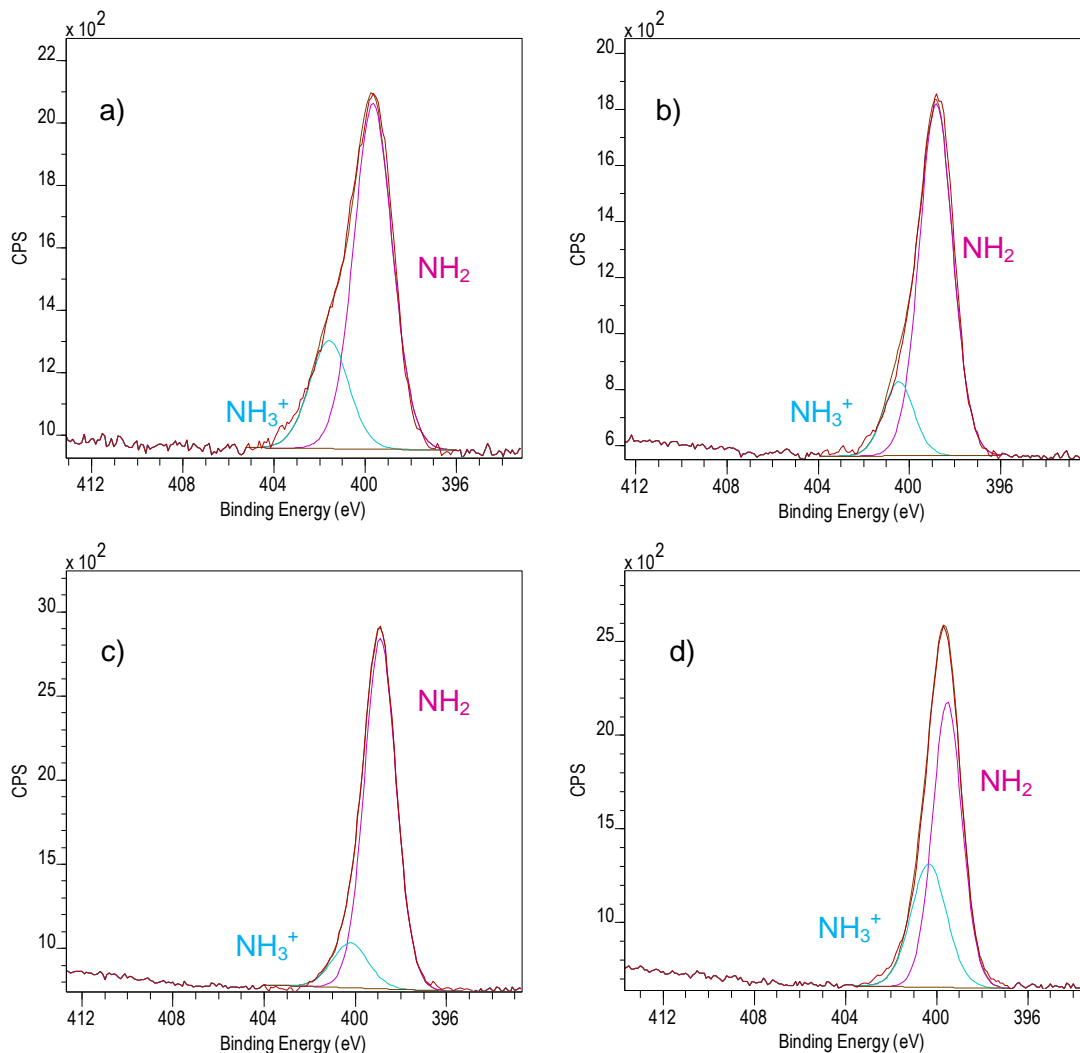


Figure 6-8. High resolutions N1s spectra of the quartz surfaces coated with a) 2%, b) 4%, c) 6% and d) 8% APTES

The ratio of $\text{NH}_2/\text{NH}_3^+$ for the treated quartz surfaces by APTES (2%-8%) is presented in Table 6-2.

Table 6-2. Ratio of primary amines to hydrogen/protonated amines on the treated surfaces by APTES (2%-8%)

APTES concentration (%)	2	4	6	8
$\text{NH}_2/\text{NH}_3^+$	2.7:1	3.4:1	9:1	1.9:1

The percentages of the primary, H-bonded/protonated amines and nitrogen for the surfaces of which treated by 2-8% APTES are shown in Figure 6-9. The same trend as low-range APTES for nitrogen percentage is observed for high-range; the nitrogen content increased by concentration indicating more amount of APTES on quartz surface. Among all concentrations, higher percentage of free NH_2 is seen for the quartz surface treated by 6% APTES, which indicates more uniform and less oriented film formation on the quartz surface. As shown in Chapter 4, the highest surface coverage was obtained by 8% APTES in the solution, however the lowest primary amine was observed at 8%. This can be explained by orientation and polymerisation of APTES at 8% on the quartz surface. The quartz surface treated by 4% APTES has the second highest primary amine followed by 2% with 72.7%. Primary amine content increased by concentration except from 8%, which indicates the number of siloxane bonds increased up to a APTES concentration of 6% suggesting an upright conformation.

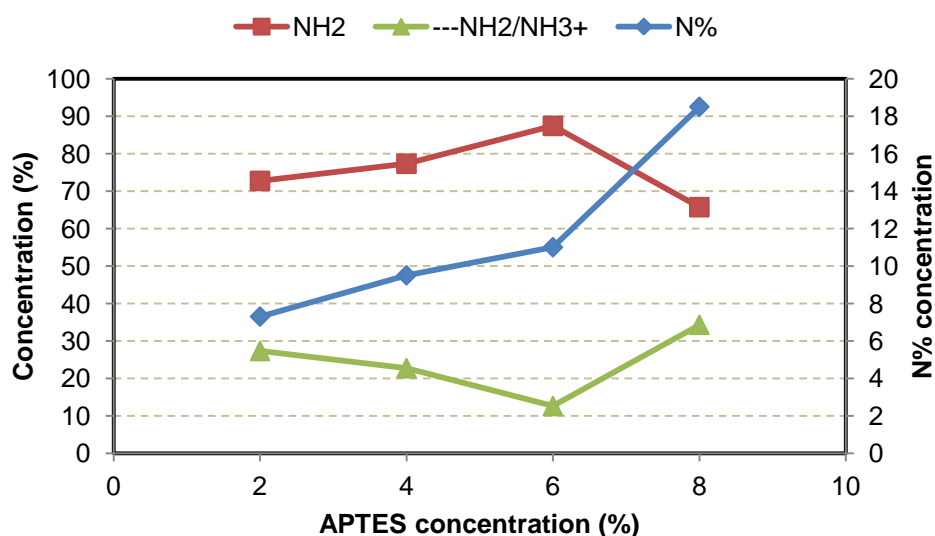


Figure 6-9. Percentage of free amine and hydrogen bonded/protonated amine of the quartz surfaces coated with different concentrations of APTES

6.2.2 Chemicals states and binding energy shifts of APhS-treated surface

APhS films were also characterised by XPS to study the chemical states of the film treated on the quartz surfaces. The wide scan and the high resolution C1s spectrum for the surfaces treated by APhS were similar to the surfaces coated by APTES (244) which were illustrated in Figure 6-4 and Figure 6-5. The N1s spectra for the surfaces treated by different percentage of APhS were presented in Figure 6-10. There were two or three binding energies for all the surfaces treated by APhS with the primary amine group in majority at low-energy signal and H-bonded/protonated amines at high-energy signals appearing like a shoulder next to the free amine peak (356, 359, 368-370). As observed in N1s high resolution spectra, there are two peaks for 0.03% and 0.06% APhS which the low-binding signal is attributed to the primary amines and the high-binding signal attributed to the H-bonding/protonated amines. Whereas, there are three peaks for 0.12%, 0.18% and 0.24% APhS that the lowest-binding energy in N1s high resolution spectra refers to the primary amines, the middle peak to the hydrogen binding and the highest-binding energy to the protonated amines (356, 363-365). The lowest concentration of APhS (0.03%) showed a high percentage of free amine and the ratio between the primary amines at 399 eV and the H-bonded/protonated amine at 400.5 eV is 6.7:1.

At 0.06% APhS, the N1s high resolution showed the highest percentage of primary amine among the quartz surfaces treated by different concentrations of APhS and proportion of the peak detected at 399.2 eV and H-bonding/protonated amine peak at 401.9 eV was 46.6:1, which indicates that the majority of APhS in the solution underwent covalent bonds via methoxy groups. According to the literature (244, 285, 354), 0.06% APhS is able to create a uniform film on the quartz surface which was demonstrated by high content of primary amine in XPS. This is in agreement with the XPS result of 0.06% in this work which may similarly indicate a SAM film formed on quartz surface. The quartz treated by 0.12% APhS (image c) presents a low-energy signal at 398.7 eV for the primary NH_2 , the middle signal at 400.1 eV referring to the hydrogen bonding of amine and the higher-energy signal relating the protonated amine. The ratio between NH_2 and $\text{---NH}_2/\text{NH}_3^+$ was 3.6:1 for the surface treated by 0.12% APhS which shows a reduction of the primary amine compare to 0.03% APhS. The N1s spectrum at 0.18% showed peaks at 399.7 eV for the free NH_2 , at 401.5 eV for H-bonded and at 402.8 eV for NH_3^+ . The ratio of primary to H-bonded/protonated amines is 4.3:1. There were also three binding energy signals for N1s high resolution spectrum of 0.24% APhS at 399.4

eV, 401 eV, and 402.6 eV referred to primary, hydrogen bonded and protonated amines; respectively, with the proportion of 5.2:1 (NH_2 to $\text{---NH}_2/\text{NH}_3^+$).

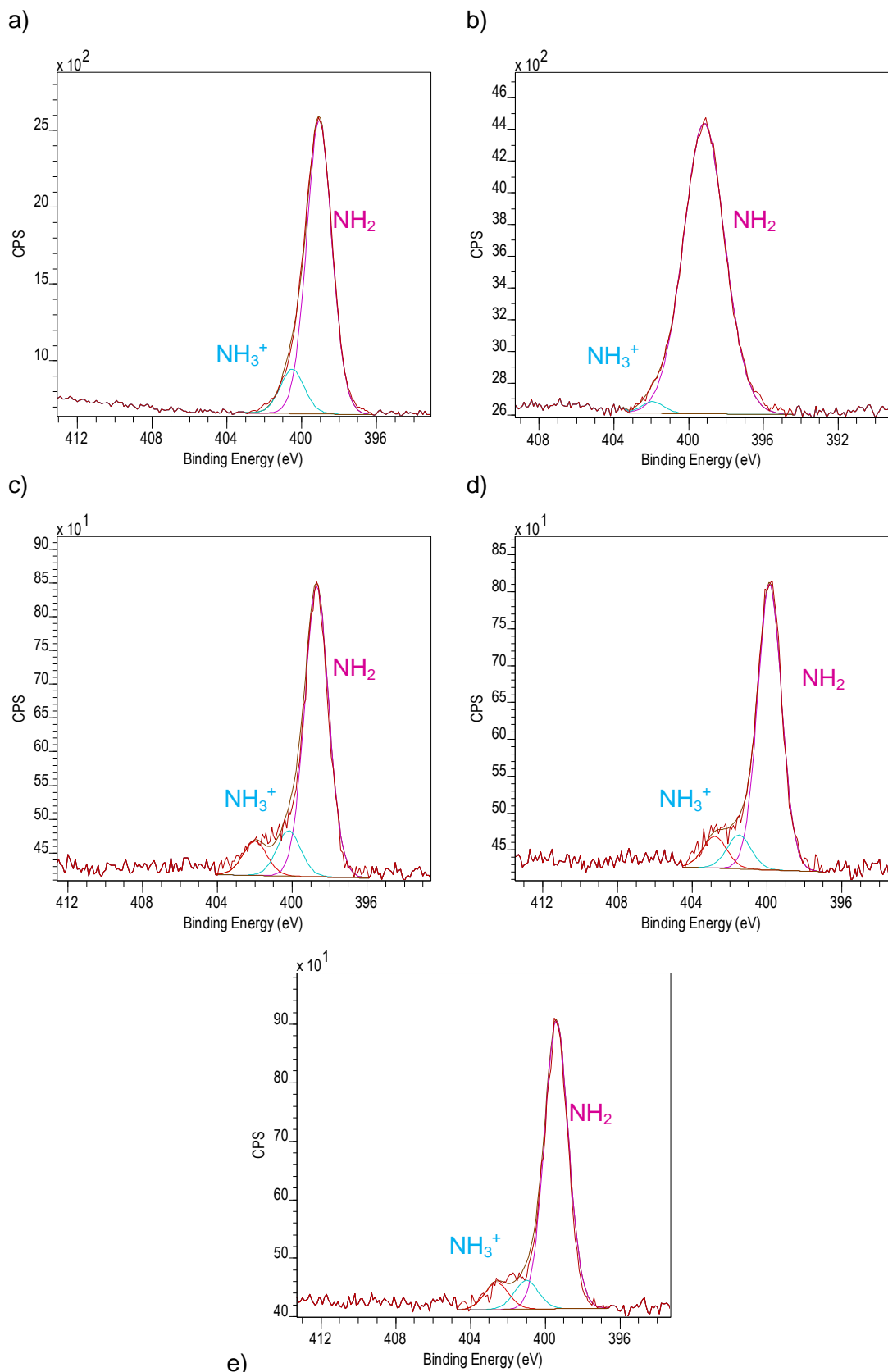


Figure 6-10. High resolutions N1s spectra of the quartz surfaces coated with a) 0.03%, b) 0.06%, c) 0.12%, d) 0.18% and e) 0.24% APTES

The ratio of $\text{NH}_2/\text{NH}_3^+$ for the treated surfaces by APTES (0.06%-0.24%) is presented in Table 6-3.

Table 6-3. Ratio of primary amines to hydrogen/protonated amines on the treated surfaces by APhS (0.06%-0.24%)

APhS concentration (%)	0.03	0.06	0.12	0.18	0.24
$\text{NH}_2/\text{NH}_3^+$	6.7:1	46.6:1	3.6:1	4.3:1	5.2:1

Figure 6-11 presents the percentage of the primary, H-bonded/protonated amines and nitrogen for the surfaces of which treated by various concentrations of APhS. It is observed that percentage of nitrogen increased by concentration indicating more APhS molecules on quartz surface. In general, the percentage of primary amine is higher than H-bonded/protonated amines in all the APhS concentrations. Among APhS concentrations the highest ratio of primary amine was recorded for the surface treated by 0.06% APhS with 97.9% which is in agreement with Puniredd's results (285). Moreover, Zhang and Srinivasan (244, 354) demonstrated 0.06% (3 mM) APhS concentration gives a uniform SAM film with nearly 100% primary amine. Therefore, the XPS results of APhS may suggest: i) formation of a uniform SAM film at 0.06% and ii) the film formed at 0.03% and 0.12-0.24% underwent H-bonding or protonation.

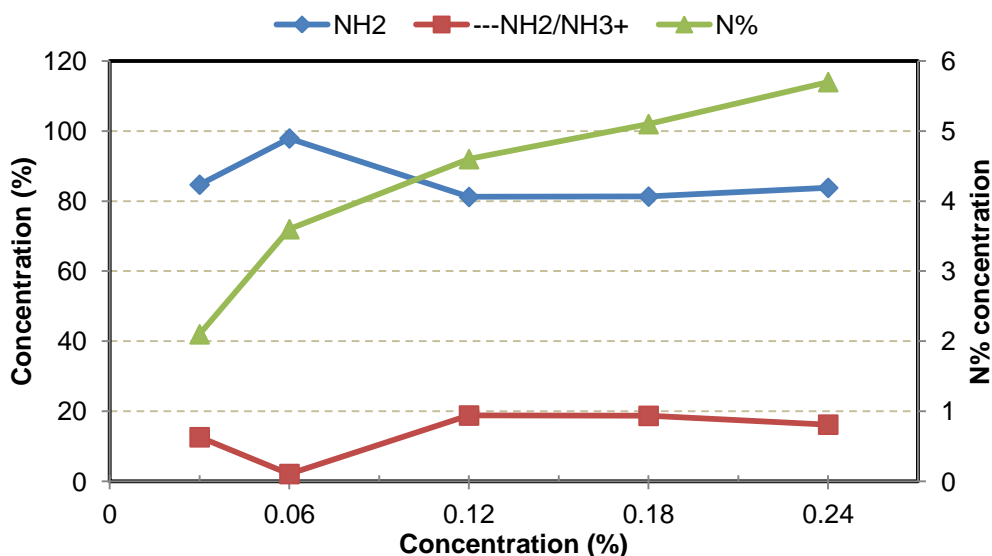


Figure 6-11. Percentage of free amine and hydrogen bonded/protonated amines of the quartz surfaces coated with different concentrations of APhS

6.2.3 Comparison of film characterization of APTES- and APhS-treated surfaces by XPS

In sections 6.2.1 and 6.2.2, the N1s chemical states of APTES and APhS was individually illustrated. In this section, it is attempted to compare the binding

energy shift of N1s of APTES and APhS together and to interpret the different behaviour of these aminosilanes on the quartz surface at different concentrations. Figure 6-12 shows the percentages of nitrogen on the quartz surfaces for APTES and APhS as well as primary and H-bonded/protonated amine percentages. The graph shows that by increasing the concentration of coating materials in the solution, the adsorption of APTES and APhS on the quartz surface increased. The higher range of APTES concentrations showed higher percentage of primary amine on the surface compared to the lower APTES concentrations with highest primary amine at 6%, which may indicate a SAM on the surface at 6% APTES. In general, a high content of primary amine was observed for all APhS concentrations compare with APTES; this behaviour was previously demonstrated (244). This is due to the effect of rigid benzene ring in APhS which prevents orientation of the amine group towards the surface in order to create H-bonds (244, 285). It was previously reported (244, 285, 371, 372) that the required concentration of APhS to create a SAM on quartz surface is 0.06%, which is in agreement with our results as the highest percentage of primary amine was obtained at 0.06% APhS. It was also demonstrated (244, 285, 354) that almost 100% primary amine was obtained by APhS at different conditions. However, there is a little information regarding potential effects of APhS concentration on the chemical states of amine on the surface. Besides, the APhS film formation was performed in toluene and it was shown (225, 270) that toluene prevents the flip-flop phenomena of organosilane during film formation. This can explain the higher content of primary amine by APhS. In this study, 98% primary amine was obtained at 0.06% APhS which indicates a uniform surface morphology; this was shown by Zhang and Srinivasan (354). Lower nitrogen percentage obtained at 0.03% may suggest an incomplete coverage compare with 0.06-0.24%. Lower content of primary amine at 0.12-0.24% with higher concentration of nitrogen may suggest polymerisation of APhS and formation of H-bonded on the surface.

Higher percentages of H-bonded/protonated amine were obtained in low range (0.05-0.2%) of APTES concentrations. Low primary amine content at low APTES concentrations (0.05-0.2%) can be due to higher concentration of water in the solution. The amount of water, film deposition time, aminosilane purity and post-curing process are the important elements to form a uniform layer of aminosilane on quartz surface (206, 245, 246). For example, it was demonstrated that curing the treated surface at a temperature higher than 100°C will increase the percentage of primary amine on the surface by breaking the hydrogen bond from the surface and re-silanization on the quartz surface (244, 245, 267, 287, 373). Post curing by

temperature was skipped in this research since the application of this work is in oil fields and applying post-curing process to formation rock will be impossible. It was also demonstrated (218, 374) that loose aminosilane can be liberated by alcohol or water rinsing immediately after silanization process, which was used in this study. In this work, the experiment conditions were constant for all experiments for APTES except from the concentration. Since the presence and amount of water in the solution were demonstrated to be a determining factor in formation of a uniform film of APTES on the quartz surface (206, 244-246, 270, 375), it can be stated that the difference in water concentrations resulted in various components percentages of nitrogen for different APTES concentrations. Although silanization does not happen on surface without presence of water, the excess of water also results in formation of polymerised aminosilanes (244-246). As can be seen from Figure 6-12, high concentration of H-bonded/protonated amines were obtained in low APTES concentrations which may indicate that APTES were mainly polymerised in the solution and later deposited on the quartz surface. The impact of water is promoted in case of APTES deposition owing to self-catalysing the formation of both chemisorbed and polymerised APTES by the aminopropyl group (376). Amine moieties can compete with alkoxy groups to react with the surface (355) leading to formation of H-bonded/protonated amines on the surface. The amount of H-bonded/protonated amines is influenced by the amount of water in the solution (245). It can be concluded that in low percentage of APTES due to higher concentration of water in the solution, mainly polymerised APTES adsorbed on the substrate with or without amine moieties tilting towards the quartz surface.

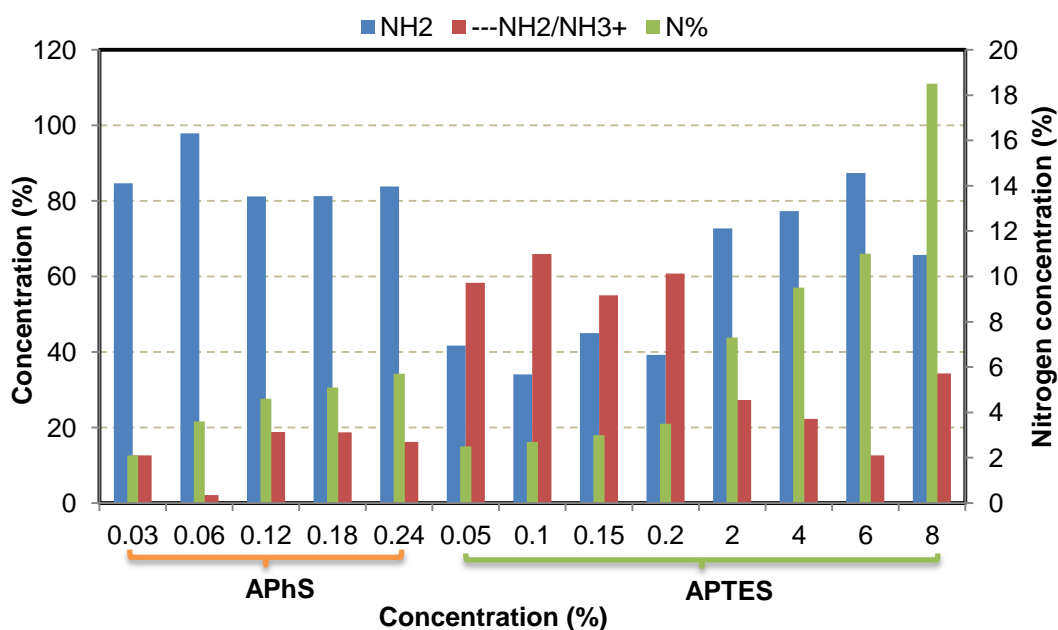


Figure 6-12. Percentage of primary amines, hydrogen bonded/protonated amines and total percentage of nitrogen for the quartz crystals treated by APTES and APhS

On the contrary to low concentration (0.05-0.2%) of APTES, diverse binding energy signals were observed in high APTES concentrations (2-8%); i.e. the bigger value of the components is attributed to primary amine. The highest primary amine was obtained at 6% APTES concentration with 87.4%. The second and the third highest primary amine were gained at 4% and 2% with 77.3 % and 72.7%, respectively. It is observed that when the APTES concentration increases from 6% to 8%, primary amine content decreases. However, from 2% to 6% the percentage of primary amine increased indicating a film with most of the primary amines upward. This indicates that APTES molecules mostly created siloxane bonds with quartz surface presenting free amines upward. Although the percentage of primary amines for 2-8% is higher than H-bonded/protonated amines and the experiments carried out under the same conditions, the amount of water plays a critical role in the relative percentage of H-bonded/protonated amines. As it is shown in Figure 6-9, the minimum concentration of $\text{--NH}_2/\text{NH}_3^+$ was obtained at 6% APTES suggesting the optimum quantity of water was presented at this concentration. The primary amine content increased by the APTES concentration; however the opposite behaviour was seen at 8% APTES with 65.7% primary amine (the lowest among 2-8%). This may indicate that at 2-6% APTES, the adsorption occurred in the shape of monomers, dimers or small aggregates; whereas at 8% APTES monomers polymerised before adsorbing on the quartz surface forming large aggregated polymers of APTES. This phenomenon might cause non-uniform and less-ordered structure of APTES molecules deposited at 8%. This can be discussed more in detail by roughness measurements, which will be studied in this chapter. Zhang and Srinivasan (244) showed lower percentage of primary amines by increasing the concentration of APTMS (instead of ethoxy groups in APTES, APTMS consists of three methoxy groups) from 3 mM to 10 mM in solution of toluene for 5 h (they believe that 3 mM (~0.07%) is the optimum concentration of APTMS to form a SAM film in toluene solution for 5 h). This is in agreement with our results with assumption of 6% APTES in ethanol/water solution for 30 min creates a SAM film of APTES on quartz surface, increasing the concentration from 6% to 8% gives lower primary amine on the surface. Zhang and Srinivasan (244) also demonstrated that various primary amine contents can be achieved at different experiment times under the same condition. It was shown (244) that the maximum (~85%) primary NH_2 was obtained after 5 h experiment in 5 mM (~0.12%) in toluene solvent at room temperature. The results of this work show that by changing the type of solvent from toluene to ethanol/water and increasing the APTES concentration to 6% at ambient temperature, even higher primary amine

content (87.4%) in 30 min experiment can be achieved. This also suggests that higher percentage of primary amine can be gained even at low range of APTES concentration (0.05-0.2%) by increasing the experiment time; this can be the subject of future work.

It was previously demonstrated that the percentage of primary amine decreases by increasing the concentration of APTES in anhydrous toluene solution (244). As mentioned above, anhydrous toluene can decay the flip-flop phenomenon in formation of APTES on quartz surface and it was also demonstrated (244) that a trace amount of water in toluene solution can give a high amount of free amine on the surface. However, in this study ethanol/water solution was employed as it was attempted to use a solution of which can be applied to oil fields. SAM on different substrates was also obtained by higher concentrations of aminosilanes in various solutions with different silanization time (258, 260, 267, 271, 341, 377-380). As mentioned above and in Chapter 2, there is a wide range of work presenting formation of aminosilane on different substrates in various conditions (concentration, temperature, post-processing, type of solution, concentration of solution, time, etc.); this was not the focus of this work. The attempt was to use a simple process to create SAM on quartz surface in order to modify the surface properties of formation rock to prevent/reduce mineral scale deposition.

6.3 Wettability and surface energy results of APTES- and APhS-treated surfaces

As explained in Chapter 3, the wettability of quartz surface is altered after treating by APTES and APhS. Thus, the static contact angles were measured to compare the behaviour of the treated quartz surfaces. Figure 6-13 shows some of the images taken before and after film formation of aminosilanes showing that the APTES and APhS decreased the hydrophilicity of quartz surface. The relevant contact angle for the blank quartz surface is observed in image (a) showing that the water droplet almost spread on the surface and create a flat droplet on quartz whereas the treated surfaces by APTES and APhS create a droplet with higher contact angles.

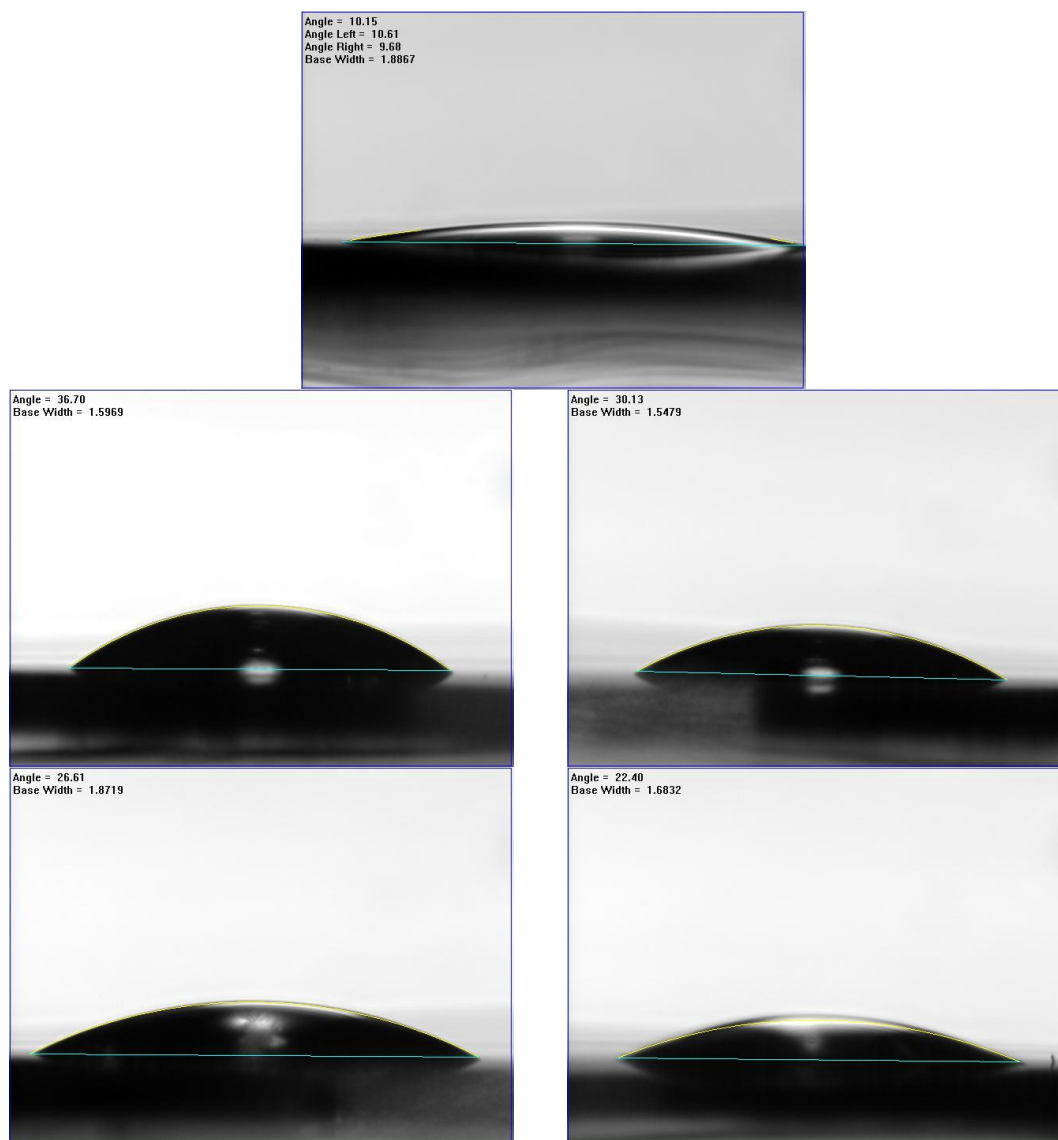


Figure 6-13. Contact angle measurements for a) blank quartz surface and b-e) treated surfaces by APTES

6.3.1 Surface energy of treated surfaces by APTES

Figure 6-14 illustrates the water contact angles of the untreated and treated surfaces by APTES at different concentrations. The low value of contact angle of blank surface is due to using plasma chamber to remove the contamination from the surface; this was also observed by previous work (255). The decrease of hydrophilicity of treated surface is associated to presence of alkyl chain of APTES introducing more hydrophobic properties to the bare quartz surface (255). The graph shows that the water contact angle of the surface decreased for the higher range of APTES (2-8%) whereas the quartz surfaces coated by low ranges of APTES (0.05-0.2%) show a higher contact angle. Water contact angles of APTES films on substrate are related to several aspects such as amino, ethoxy and silanol

groups in the film, solvent, degree of cross-linking and water content. The higher contact angle of the low range of APTES is the result of high amine protonation, which means more hydrophobic character of APTES at low concentrations.

It was previously shown that the presence of H-bonded/protonated amine decreased wettability of aminosilane SAM of surface (222, 255, 259, 339, 381). As shown in XPS results high percentages of H-bonded/protonated amines were observed at low APTES concentrations (0.05-0.2%). This may indicate that most of the APTES molecules - which bonded to surface - formed H-bonded/protonated amines instead of undergoing siloxane bonds. An increase in contact angles due to tilted amines to the surface was shown previously (255, 259). It was also reported that the hydrophobicity of methyl-terminated silane surfaces are higher than surfaces covered by amino group (342). The reasons made above to explain the behaviour of treated quartz surfaces by low range of APTES could also clarify the water contact angle measurements gained for the surfaces coated by high APTES concentration.

As seen in Figure 6-14, the contact angles obtained at high concentrations decreased which can be related to the primary amine content at these concentrations. Since the increase of H-bonding/protonation of amine groups decreases the wettability of the surface (222, 255, 259, 339, 381); thus, increase of primary amine groups promote the decrease of contact angles compare to the low range of APTES. According to the XPS results in high APTES concentrations, the percentage of primary amine increased by APTES concentration from 2% to 6% which is in agreement with the results obtained from the contact angles. The contact angles at 8% slightly increased owing to the higher concentration of H-bonded/protonated amines acquired from XPS results. Although 8% shows the lowest percentage of free amine among 2-8% APTES and it is expected to see the highest contact angle for 8% compared to 2-6%, the contact angle measured for 8% presented a lower contact angle compare to 2 and 4%. This result suggests that the structure of film formed by 8% should be different from the low ranges (0.05-0.2%) of APTES. Since contact angle measurements show the surface tension of the top layer of film, this suggests the aggregates and polymerised APTES molecules containing the primary amines on the top layer.

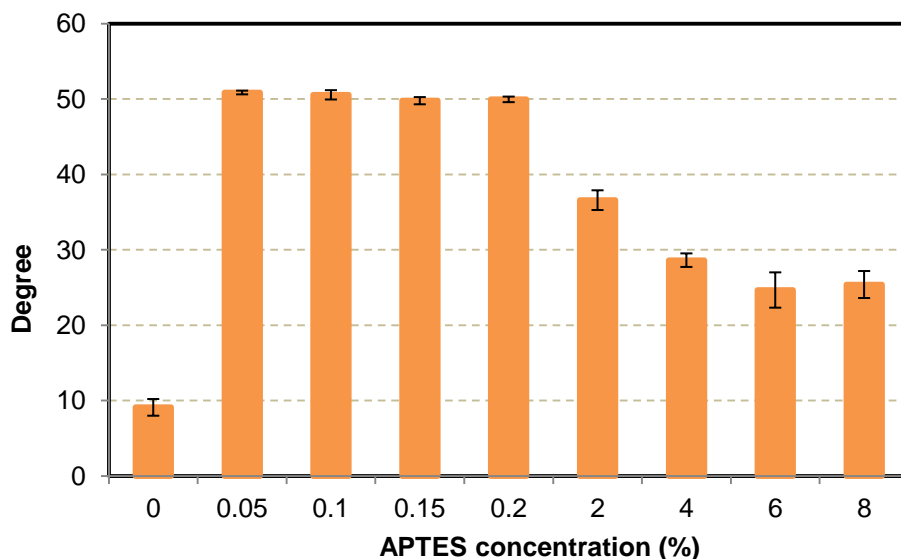


Figure 6-14. Static water contact angles for the quartz surfaces treated by different concentrations of APTES

6.3.2 Surface energy of treated surfaces by APhS

The wettability of the quartz surface treated by APhS was also studied by water contact angle measurements; this is presented in Figure 6-15. It is observed that the hydrophilicity of the treated surfaces by APhS also decreased with respect to the bare quartz surface; however this reduction is higher than APTES-treated surfaces. The higher contact angles related to APhS-coated surfaces could be referred to the different type of solvent of which was used in the experiments. As mentioned in Chapter 3, the solvent used in APhS solution is toluene which is hydrophobic while the solvent of APTES solution was ethanol/water. It was previously illustrated that various types of solvent result in different contact angles (382). Moreover, the structure of APhS contains a benzene ring which increases the hydrophobicity of the molecule; thus these two factors can cause the APhS-treated surface to be more hydrophobic than the APTES-treated surface. Figure 6-15 shows a similar contact angles for 0.03, 0.12, 0.18 and 0.24% APhS-coated surfaces around 75 degree whereas a lower contact angles were measured for 0.06% APhS (~69 degree). As mentioned, the higher primary amine presents the more uniform film formed on the surface which leads to lower contact angles among other concentrations. This supports the results from XPS that showed the highest primary amine among APhS concentrations was obtained at 0.06%. The contact angle results for other concentrations are in the same range, which shows the same surface energy for these concentrations.

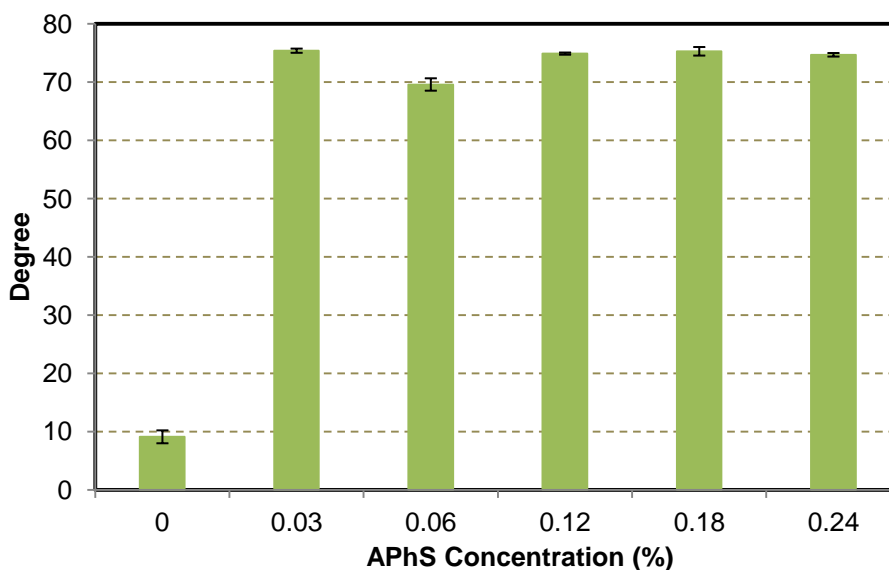


Figure 6-15. Static water contact angles for the quartz surfaces treated by different concentrations of APhS

6.4 Topography of surfaces treated by APTES and APhS

As expected, the aminosilane film deposition influences the chemical states, wettability and roughness of the quartz surfaces. The surface energy and the chemical components of the coating materials were studied earlier in this chapter. Thus, the roughness of the surfaces was measured to study the effect of aminosilanes on topography of the surface after coating. This was performed by several measurements for each sample using Talysurf profiling (non-contact method) system to analyse the data obtained by NP FLEX. More information regarding Talysurf profiling system was presented in Chapter 3. Figure 6-16 shows the topography of untreated and treated (0.2% and 6% APTES, and 0.06% APhS) quartz surfaces. First, roughness of each aminosilane surface is separately analysed followed by a comparison study between APTES and APhS.

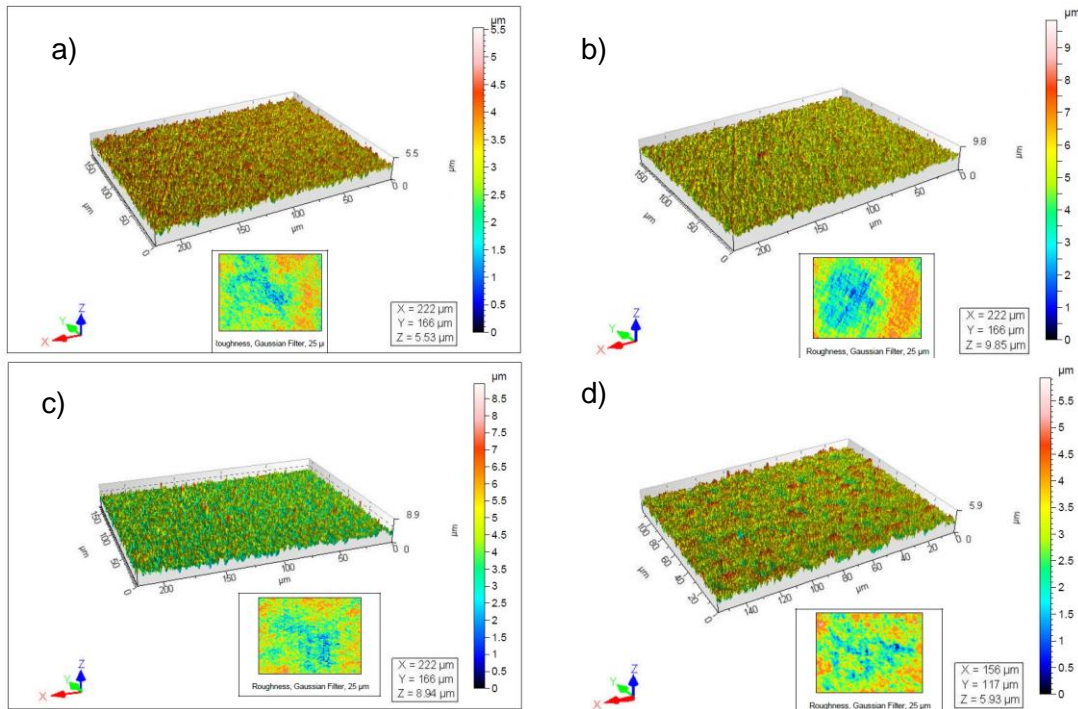


Figure 6-16. Topography images of a) untreated quartz and b) surface treated by 0.2% APTES c) surface treated by 6% APTES and d) surface treated by 0.06% APTES

6.4.1 Roughness of APTES-treated surfaces

Root-Mean-Square (rms) roughness (R_{rms}) of each sample for all the APTES-treated and untreated surfaces was measured, which is shown in Figure 6-17. The red line and two green dashed lines show mean R_{rms} and standard deviation of blank quartz surface, respectively. In comparison with the blank quartz surface, the roughness of all the treated surfaces increased. Among the treated surfaces, the R_{rms} increased from 0.05% to 0.15% and levelled off up to 4% followed by an increase for 6% to 8%.

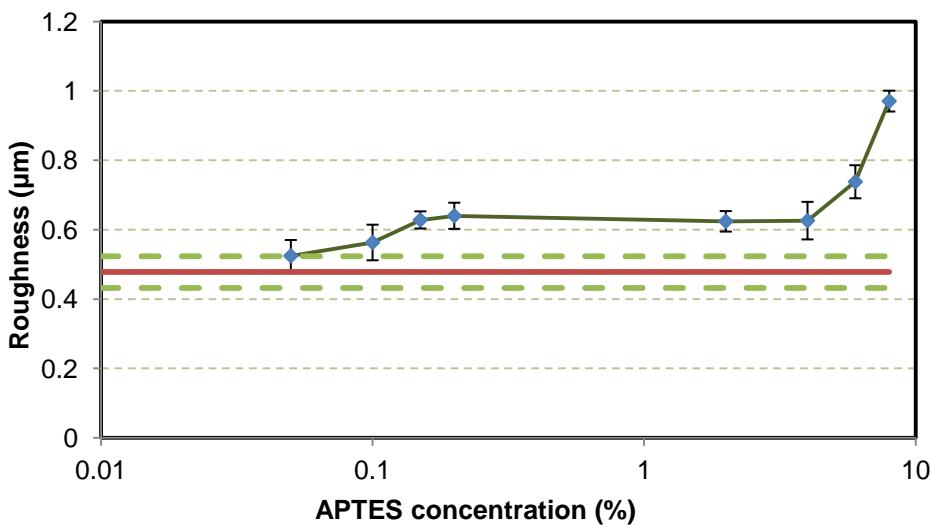


Figure 6-17. Roughness (rms) of blank and the treated surfaces treated by APTES in 30 min at ambient temperature

Figure 6-18 shows the skewness values of APTES-treated and un-treated quartz surfaces, which vary for different concentrations. The red line and two green dashed lines show mean skewness and standard deviation of un-treated quartz surface, respectively. More information regarding skewness was provided in Chapter 3. Generally, the positive skewness indicates that the peaks are higher than the valleys are deep (327) and vice versa. The value of skewness decreased from 0.05% to 0.2% and increased for higher range of APTES (2, 6 and 8%) except from 4% with the maximum at 8%. The first observation from the skewness results is that the surfaces (0.15, 0.2 and 2%) with the same R_{rms} values can have totally different roughness profile.

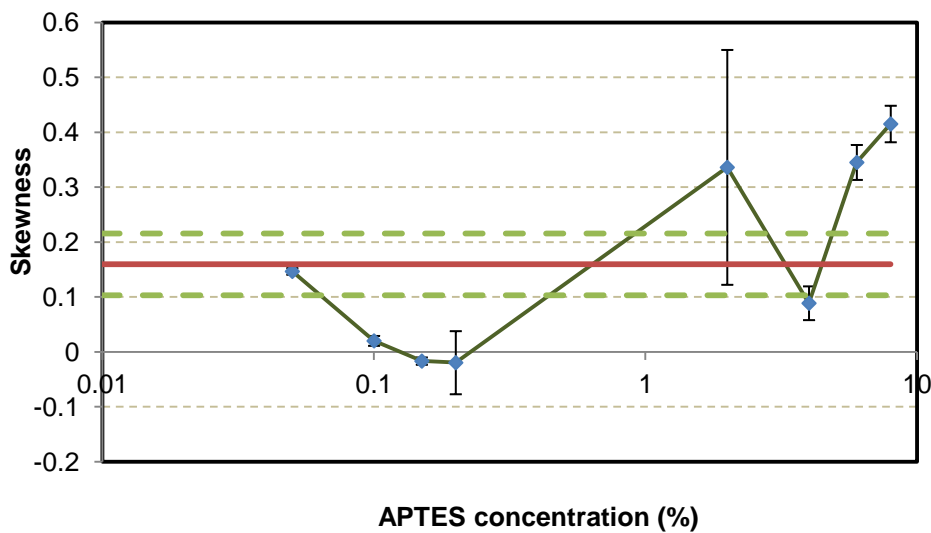


Figure 6-18. Skewness of APTES-treated surfaces after 30 min silanization in ambient temperature

It was previously demonstrated that the R_{rms} of APTES- and APTMS-treated surface increased after formation of SAM on substrates (255, 259, 275, 383), which is in agreement with the results in Figure 6-17. The R_{rms} gradually increased from 0.05% to 0.2%; however, the skewness decreased leading to more homogenous surfaces. This may suggest that the low ranges of APTES concentrations filled more valleys of the quartz surfaces. However, slightly increase of roughness (R_{rms}) for the quartz surfaces coated by 0.05-0.2% APTES could be due to adsorption of some polymerised APTES molecules on the surface.

Figure 6-17 illustrates that R_{rms} at 2% and 4% is in the same range as low APTES concentrations (0.05-0.2%), on the other hand Figure 6-18 shows higher skewness for 2% and 4% APTES. This may indicate better surface coverage obtained by 2% and 4% APTES comparing to low concentrations (0.05-0.2%). Figure 6-17 shows higher roughness values for 6% and 8% APTES coated

surfaces which could be due to increase in the number of APTES clusters on the quartz surface. However, the number of polymerised APTES molecule should be significantly higher for the surface treated by 8% since the increase in the roughness value from 6% to 8% APTES is more significant than from 4% to 6%.

Therefore, it can be stated that aggregation of APTES molecules on the quartz surface increased by APTES concentration in the solution of ethanol/water where 30 min silanization at ambient temperature was used. In addition, with considering the R_{rms} and skewness, it can also be stated that APTES molecules initially formed on valleys with some clusters on peaks for up to 0.2% APTES which may suggest incomplete formation of APTES on the quartz surface. On the other hand, more surface coverage and clusters can be concluded for 2-8%. It was previously demonstrated that R_{rms} of APTMS increased by concentration (244). This may be due to the fact that in higher concentrations of APTES in presence of water the probability of forming polymerised APTES before reaching the surface is higher. Also, the chance of originating a uniform APTES film on surface is higher in low concentrations at desired time (244).

6.4.2 Roughness of APhS-treated surfaces

The same procedures were followed for APhS-treated surfaces. R_{rms} of APhS-treated and untreated surfaces are illustrated in Figure 6-19. The red line and two green dashed lines show mean R_{rms} and standard deviation of blank quartz surface, respectively. The roughness of 0.03-0.24% APhS-treated surfaces increased in comparison with the blank quartz surface, except from R_{rms} of 0.12% which remained constant. By considering the standard deviation for 0.03-0.12%, similar roughness may be concluded.

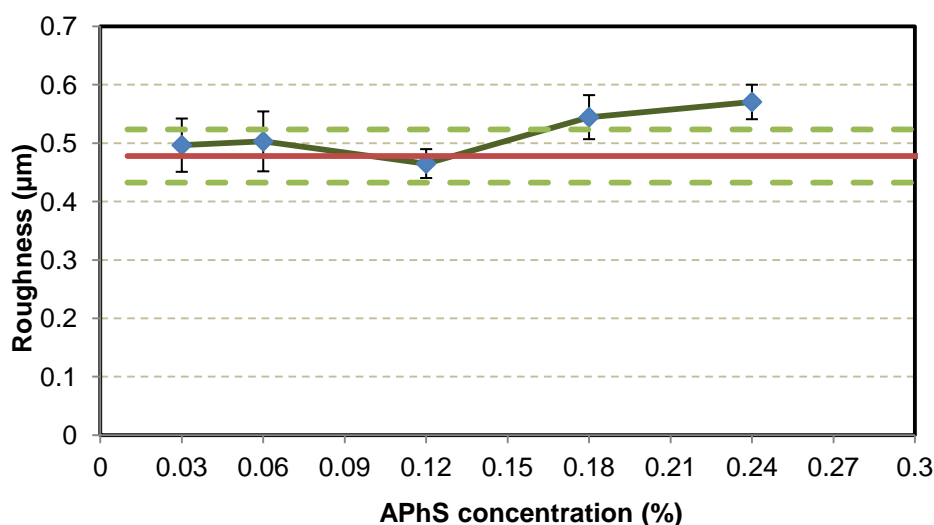


Figure 6-19. Roughness (rms) of blank and APhS-treated surfaces after 2 h silanization in ambient temperature

Figure 6-20 presents skewness values of APhS-treated surfaces after 2 h silanization at ambient temperature. The red line and two green dashed lines show mean skewness and standard deviation of un-treated quartz surface, respectively. The graph shows approximately the same skewness for 0.06-0.18% indicating homogenous surfaces in terms of height of peaks and depth of valleys. However, slightly larger skewness values were obtained at 0.03% and 0.24% compare with the rest of APhS-treated surfaces. By considering the standard deviation of skewness values, the same roughness profile for APhS treated surfaces can be assumed.

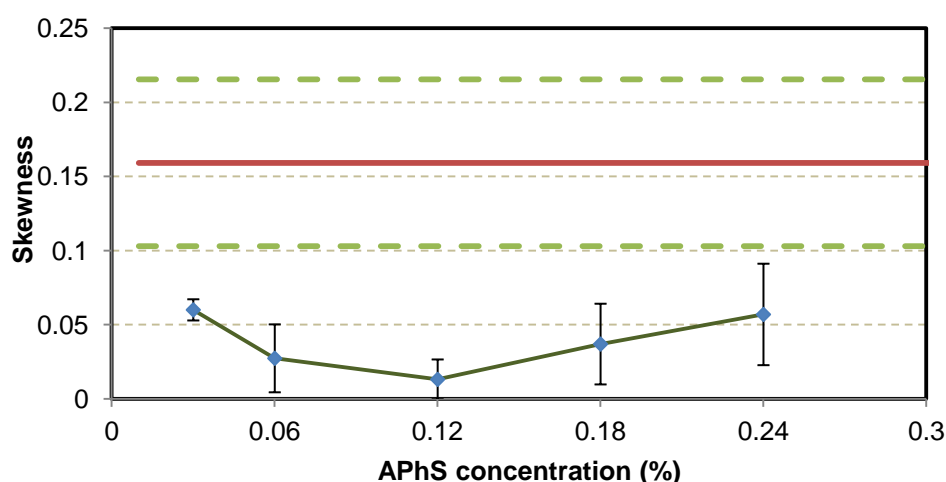


Figure 6-20. Skewness of APhS-treated surfaces after 2 h silanization in ambient temperature

From the R_{rms} results of APhS-treated quartz surfaces, a uniform formation of APhS film on the quartz surface for 0.03-0.12% APhS surfaces can be suggested, which can be an indication of a SAM formation of APhS on quartz surface by 0.06-0.12%. On the other hand, some clusters of APhS molecules might adsorb on the surfaces treated by 0.18% and 0.24% due to the higher values of roughness.

6.4.3 Comparison results of roughness of APTES- and APhS-treated surfaces

Figure 6-21 shows R_{rms} values of untreated and treated quartz surfaces. APhS-treated surfaces showed smoother surface compare with APTES-treated surfaces; this could be due to formation of SAM of APhS with lower aggregation of molecules on the quartz surface. It was previously demonstrated (244, 384) that a SAM of APhS on surface created a smoother surface compare with APTES.

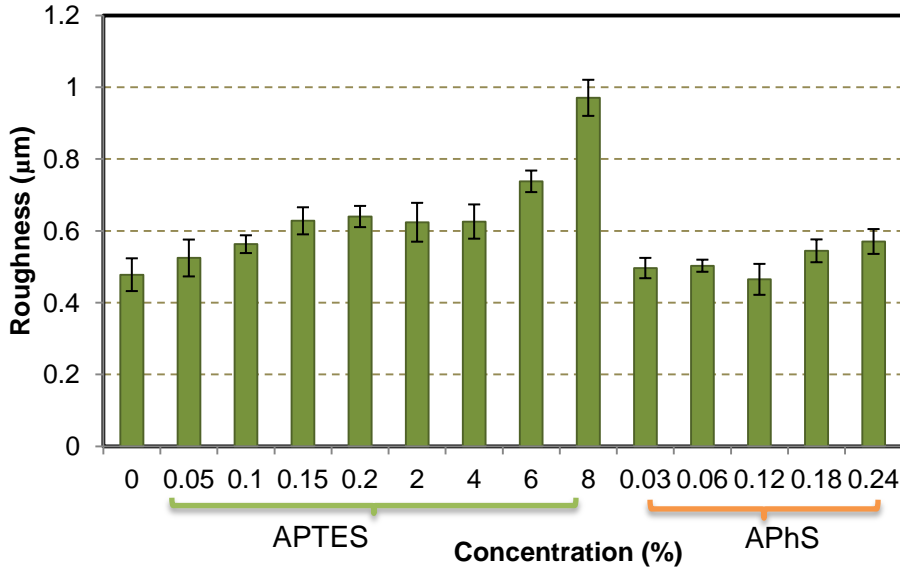


Figure 6-21. Roughness (rms) of blank, APTES- and APhS-treated surfaces

Figure 6-22 illustrates skewness values of blank and treated surfaces for APTES and APhS. It shows more homogeneous surfaces for all APhS concentrations and low concentrations of APTES compare with higher concentrations of APTES. This may be due to lower clusters in the surfaces treated by APhS and low-concentration APTES.

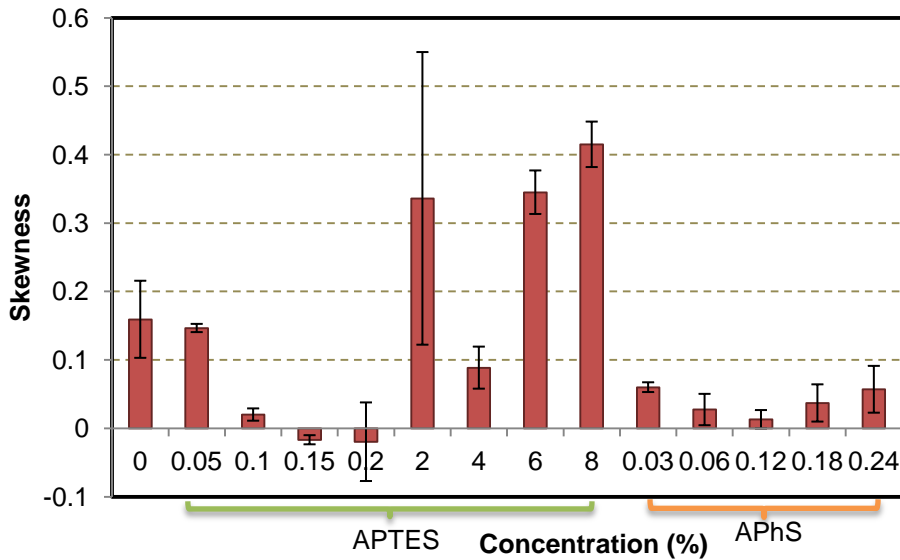


Figure 6-22. Skewness of blank, APTES-treated APhS-treated surfaces

6.5 Structure of APTES and APhS film formation on quartz surface

Aminosilanes are usually employed to create a SAM film via Si-O-Si bonds with free amines upward for further derivatizations- this is the ideal structure.

Various concentrations of APTES (0.05-0.2% and 2-8%) and APhS (0.03-0.12%) were applied to create a SAM film on quartz surface with silanization times of 30 min and 2 h; respectively, at ambient temperature. Different performance was observed for different aminosilanes at each concentration. XPS, contact angle and roughness measurements were employed to study APTES and APhS film formations on quartz surface in order to investigate the behaviour of new films on reduction of calcium carbonate deposition. Thus, the film characterisation's results were analysed to suggest the possible film structures for the treated surfaces which are separately discussed in detail for each concentration.

6.5.1 Possible APTES film structures on quartz surface

The conformation of APTES on quartz surface is related to the density of APTES attached on the surface and the type of bonding (267). Upright conformation (ideal reaction) can be achieved when APTES molecules attach on quartz surface via siloxane bonds. However, attraction between primary amine to silanol oxygen on the quartz surface can introduce a tilted conformation. Both conformations are shown in Figure 6-23a and b. APTES molecules are also able to crosslink with each other, which is highly sensitive to concentration of water in the solution. This decreases the repeatability of formation of SAM on the surface. Besides, APTES molecules can physisorb to quartz surface through hydrogen bonding; this interaction is not stable and can easily be removed by post processing like washing by ethanol and water. The schematic of hydrogen bonding of APTES to quartz surface is shown in Figure 6-23c.

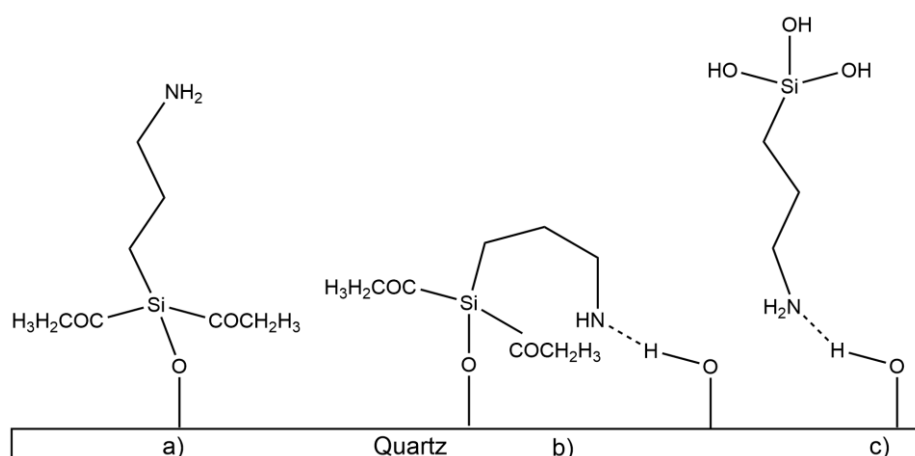


Figure 6-23. Various APTES conformations on quartz surface: a) upright and b) tilted conformations, and c) hydrogen bonding

6.5.1.1 APTES film structure on quartz surface at low concentrations (0.05-0.2%)

The XPS results of 0.05-0.2% APTES showed higher content of H-bonded/protonated amines than primary amine. This indicates that a large number of APTES molecules experienced H-bonding/protonation with the quartz surface at amino end leading to a low percentage of free amines; the schematic structure is depicted in Figure 6-23b and c. Although higher concentration of water in low range of APTES concentration results in polymerisation of molecules, the size of polymers is small due to low concentration of APTES. In addition, the results of surface energy on low APTES concentrations illustrated higher contact angles ($\sim 50^\circ$) compare with high APTES concentrations, which shows the tendency of the treated surfaces in low concentration towards more hydrophobic surface. As demonstrated in the literature (222, 255, 259, 339, 381), higher content of H-bonded/protonated amine on surface results in an increase in water contact angles. This is due to exposure of alkyl chain of APTES to the exterior. Thus, this may be an indication of that a significant amount of hydrogen bonded/protonated amine tilted towards surface (Figure 6-23b). Moreover, the roughness results of surfaces treated by low concentration of APTES compare with high concentration of APTES, showed smaller size of aggregation due to low concentration of aminosilane. This indicates more protonated amine horizontally bended towards surface. Therefore, based on film characterisation results, the possible film structure on quartz surface of which treated by low concentration of APTES is presented in Figure 6-24.

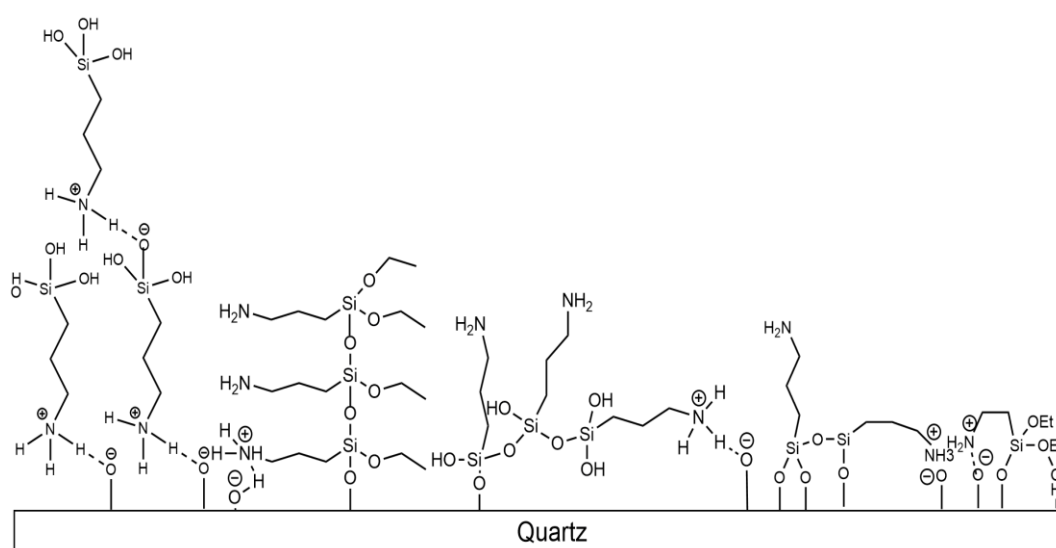


Figure 6-24. Schematic structures of deposited aminosilanes on quartz surface at low range of APTES (0.05-0.2%)

6.5.1.2 APTES film structure on quartz surface at high concentrations (2-8%)

Since the film characterisation results of high APTES concentrations showed different behaviour, possible film structures are separately discussed for 2-6% and 8%. The XPS results of 2-6% APTES showed higher content of primary amine with the maximum value at 6% indicating a large number of APTES underwent siloxane bonds (Figure 6-23a). The nitrogen percentage also increased by APTES concentration suggesting more surface coverage (compact layers) or some polymerisations of APTES on the quartz surface. Also, the wettability of the surfaces treated by 2-6% APTES decreased by increasing the concentrations – which is in agreement with XPS results – referring to a SAM film of APTES on the quartz surface. On the other hand, the roughness results showed slightly rougher surface at 6% compare with 2% and 4% indicating some aggregation on substrate. Therefore, the schematic structure at 2-6% APTES is depicted in Figure 6-25.

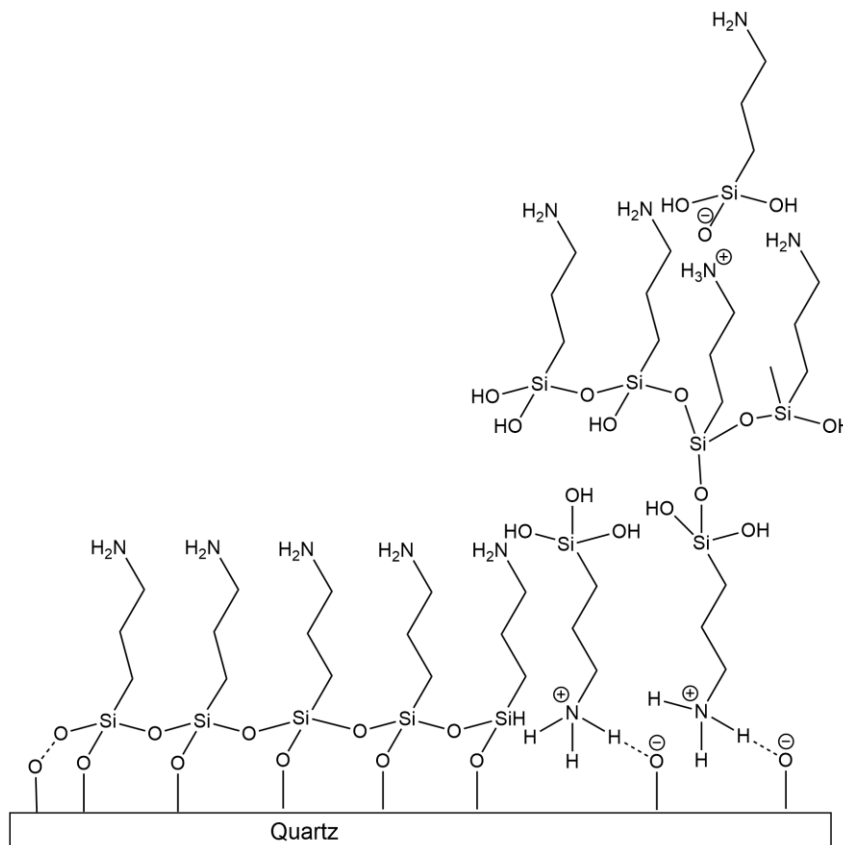


Figure 6-25. Schematic structures of 2-6% APTES film formed on quartz surface

In contrast to 2-6% APTES, the XPS result of 8% showed a decrease in content of primary and increase in percentage of H-bonded/protonated amines,

which indicates that compare to 2-6% a larger number of APTES experienced H-bonding and protonation. In addition, the percentage of nitrogen detected by XPS dramatically increased from 6 % to 8% which may suggest the presence of polymerised APTES or aggregation on quartz surface. The wettability of the surface treated by 8% decreased compare with 6% which is due to higher content of H-bonded/protonated amine moieties on the surface. However, the contact angle values of 8% did not show the same wettability of the low-range APTES (0.05-0.2%). Thus, this suggests that a significant amount of H-bonded/protonated amine occurred in the shape of Figure 6-23c rather than bended amine toward the surface (Figure 6-23b). Moreover, the roughness results illustrated rougher surface compare with 2-6% which indicates more aggregation on the quartz surface. This suggests a rougher surface at 8% compare with 2-6% with more polymerized APTES of which might or might not undergo H-bonding with another APTES molecule. The schematic possible structure of APTES film at 8% is presented in Figure 6-26.

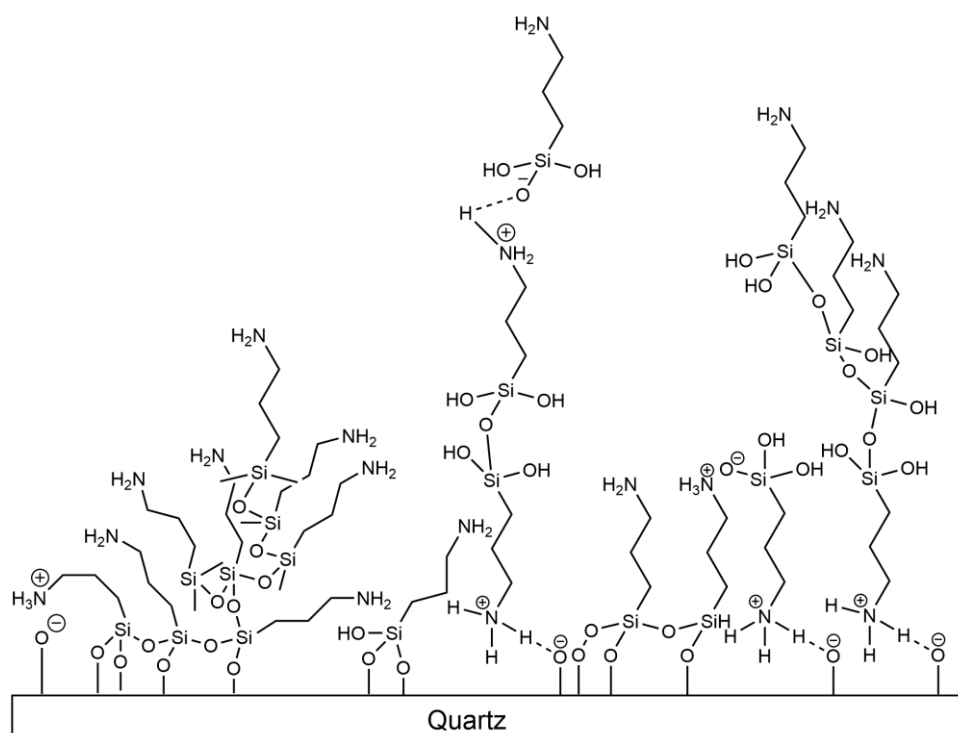


Figure 6-26. Schematic structures of 8% APTES film possibly formed on quartz surface

6.5.2 Possible APhS film structures on quartz surface

In contrast to APTES film formation, APhS molecules showed more consistent results with the concentrations. The XPS results of APhS illustrated that a large number of APhS experienced siloxane bonds with the quartz surface. The maximum primary amine was obtained at 0.06% indicating a uniform SAM film of

APhS at this concentration. For other concentrations of APhS some H-bonding/protonation occurred during SAM. Moreover, the wettability measurements of APhS-treated surfaces showed slightly more hydrophilic surface at 0.06% compare with other concentrations. The slightly higher contact angles at 0.03% and 0.12-0.24% are owing to the presence of H-bonded/protonated amine moieties on quartz surface. The roughness measurements of APhS illustrated smoother surfaces compare with the surfaces treated by APTES. However, the roughness of 0.18% and 0.24% APhS is slightly higher than 0.03-0.12%. This suggests some polymerisation on 0.18% and 0.24% APhS surfaces. Therefore, the possible schematics of APhS formation on quartz surface for different concentrations are presented in Figure 6-27.

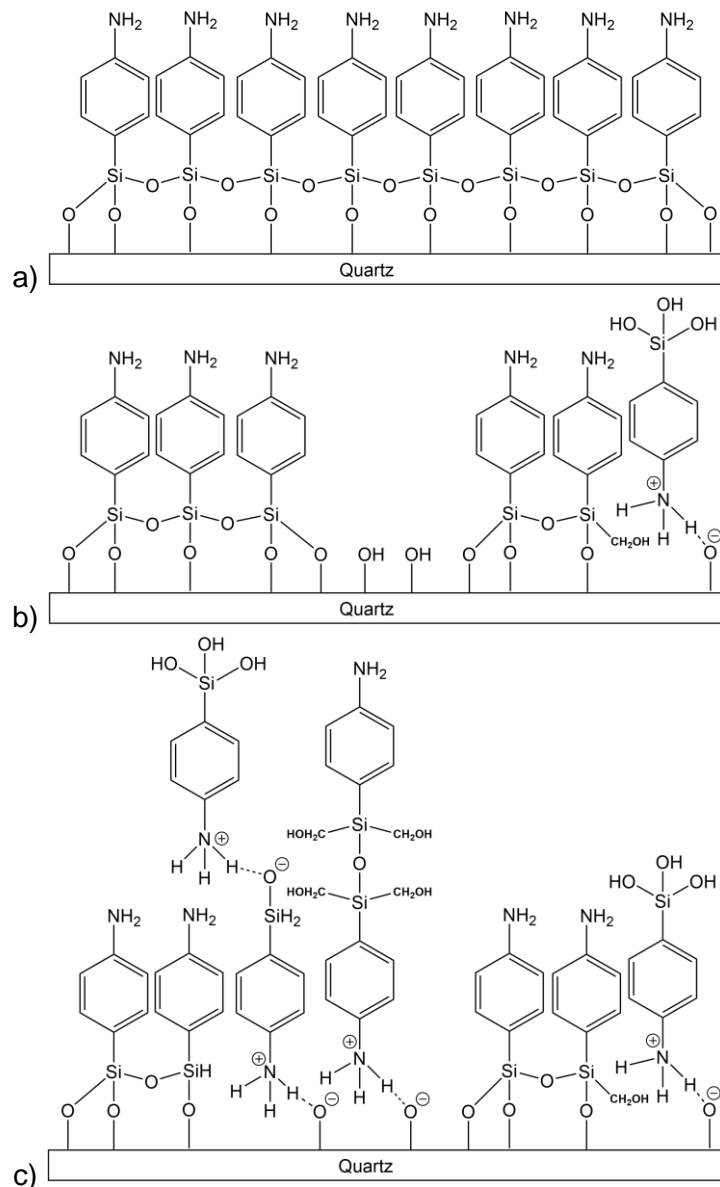


Figure 6-27. Schematics of possible APhS conformation on quartz surface at a) 0.06%, b) 0.03% and c) 0.12-0.24% concentrations

6.6 Summary

Two different aminosilanes – APTES and APhS – were applied to quartz surface in order to create a SAM film of which would be able to reduce amount of mineral scale deposition. To fully understand the tendency of the treated surfaces to calcium carbonate, APTES and APhS films on the substrates were characterised by XPS, contact angle and roughness measurements. The results obtained by characterization methods were used to introduce the possible film structure and orientation on quartz surface at different concentrations of APTES and APhS. Some major and minor conclusions of the chapter are presented below.

1. Higher primary amine content was obtained at the higher ranges of APTES concentration compare with the lower ranges. The maximum primary amine (~87.4%) for APTES molecule was obtained at 6%.
2. Primary amine percentage increased from 2% to 6% APTES and decreased at 8%.
3. More than 80% free amines were observed by APhS at all the concentrations with the maximum of ~98% at 0.06%.
4. Two ranges of wettability were measured for APTES film formation. Higher contact angles were obtained by the low-range concentrations compare with the higher ranges.
5. Wettability of the surface treated by APTES increased from 2% to 8% concentrations.
6. The water contact angle measurements of APhS molecule showed higher values compared with APTES.
7. Among APhS film formations, wettability of 0.06% APhS was slightly higher.
8. Roughness (rms) of APTES-treated surfaces increased by concentration with the maximum at 8%.
9. The surfaces treated by APhS showed smoother surfaces compare with the treated by APTES.
10. Roughness values of APhS-treated surfaces also increased by concentration.
11. Different film structures were suggested according to the characterization results.

Chapter 7

Discussion

7.1 Introduction

Recently attention on the effects of surfaces in scale deposition has increased. Mechanisms of mineral scale formation on the surfaces have become the focus of most research. The question related to scale formed on surface is whether mineral scale is precipitated from the bulk or, at the same time, nucleated and grown on from the surface. So far, studies have been focused on the different coatings on stainless steel and polymer surfaces to reduce mineral scale deposition (3-6, 8, 181, 187, 189, 193, 196, 199, 202, 203, 337, 343, 344); these surfaces are mainly used in used in safety valves and pipelines. However, scaling does not occur only in production system (well, pipelines, safety valves, etc.). Other areas may encounter scale problems; the reservoir near the wellbore area can have scale and this causes reduction in hydrocarbon production. Generally, squeeze treatments are performed to protect the near wellbore area from mineral scale deposition. However, this methodology involves many challenges such as safety and environmental issues, formation damage, etc. and is a costly treatment due to the cost of chemicals, pumping jobs, delivering the chemical to offshore platforms and main importantly deferred/loss production owing to 24 h shut in period.

The objective of this work was to introduce and develop a new methodology in order to reduce the risk of scale deposition in near wellbore area. In order to achieve an anti scale rock surface, the properties of the formation rock are needed to be altered. Surface compositions, roughness and surface energies of different substrates were reviewed (see Chapter 2) in order to understand physical and chemical properties of the surface in relation to mineral scale deposition. Since there is no access to the near wellbore to alter the physical properties of the formation rock, the only solution is to remotely change the surface chemistry of the near wellbore area. Hence, the focus was to form a film on the rock surface which is capable of i) reacting strongly with rock surface and ii) reducing mineral scale adhesion on surface. In addition to these two features, it must be thin enough not to

block oil flow paths and it should bond to the rock surface in-situ from the applied solution.

Two types of aminosilanes with different concentrations were employed to create a SAM film on the quartz surface (analogous to formation rock since the main composition of rock is quartz) in order to reduce scale deposition. The kinetics of film formation on quartz crystal was studied by QCM and the surface coverage by applying different APTES concentrations (2-8%) was calculated by considering the Langmuir isotherm; this was performed in Chapter 4. The maximum surface coverage (92%) was obtained by 8% APTES in the solution. In Chapter 5, the effect of treated quartz surfaces by APTES and APhS on reduction of scale deposition was compared with each other and the blank quartz. A clear scale reduction on the surfaces was observed via gravimetric and SEM results. No direct correlation was observed between the performance of the surface in terms of reduction of scale deposition and the concentration of APTES and APhS in solution. The best performances were obtained at 0.06% and 6% among all concentrations of APhS and APTES; respectively, in both low SR=4.77 and high SR=54.8. In order to comprehensively understand the behaviour of the treated surfaces in scale deposition, the film created on quartz surfaces was characterised by XPS, water contact angle and roughness measurements; this was widely discussed in Chapter 6. Possible film structures on the surface according to characterisation results were proposed at the end of Chapter 6. Therefore, the aim of this chapter is to interpret the results of Chapter 6 in terms of film structure proposed in the previous chapter. In addition, related literature is discussed in detail to support the results observed in Chapter 5. The performances of APTES and APhS films are separately discussed in this chapter and a short comparison between APTES and APhS will also be provided at the end (a detail comparison in terms of film structure and scale performance were provided in Chapter 6 and 5, respectively). It is worth mentioning that this is the first study that investigates possible film formation on rock surfaces near the wellbore area in order to reduce mineral scale deposition.

7.2 The performance of the quartz surface treated by APTES in reduction of calcium carbonate scale deposition

In Chapter 5, performance of various surfaces treated by different concentrations of APTES in terms of reduction of calcium carbonate scale deposition was illustrated in Figure 5-3 and Figure 5-4. A good correlation between APTES concentration and surface efficiency in reduction of scale deposition was

presented without considering the performance of the surface at 8% APTES (see Figure 5-4 and Equation 5-1). However, by taking the result of 8% APTES into account the correlation coefficient reduced from $R^2=0.99$ to $R^2=0.68$. This indicates that other factors such as roughness and wettability may influence the performance of the surfaces treated by APTES. Before jumping into studying effects of roughness and wettability on the performances of surfaces treated by APTES, more investigation on effects of surface composition on reduction of scale deposition is required. As demonstrated in Chapter 6, apart from nitrogen concentration, the chemical states of nitrogen formed on the surface are important and play a critical role in film deposition in order to have the desired film conformation (Figure 6-27a). Thus, the efficiency of the surfaces treated by APTES in terms of reduction of calcium carbonate scale deposition in low $SR=4.77$ solution was plotted as a function of concentration of primary amine; this is illustrated in Figure 7-1. This obviously shows a better correlation in comparison with Figure 5-3.

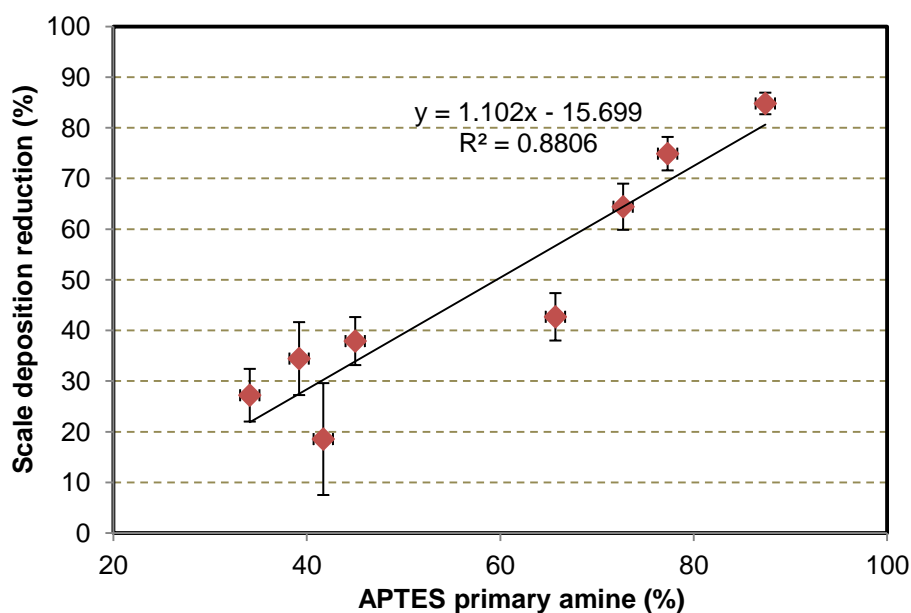


Figure 7-1. Behaviour of surfaces treated by different APTES concentrations in reduction of calcium carbonate scale deposition at 80°C and after 24 h experiment at $SR=4.77$ as a function of primary amine contents

Figure 7-1 shows a fairly good linear fit between surface efficiency in terms of reduction in calcium carbonate scale deposition and concentration of primary amines of the surfaces treated by different APTES concentrations (0.05-8%) with a correlation coefficient of $R^2=0.88$.

Although a lower correlation coefficient was obtained in Figure 7-1 in comparison with Figure 5-4, a wider range of experiments is included by using primary amine concentrations instead of APTES concentrations. Practically the

amount of scale deposition on the surfaces treated by APTES is directly related to the percentage of film structure of which has upright conformation (Figure 6-25a).

Figure 7-2 illustrates the behaviour of surfaces treated by APTES in terms of reduction of mineral scale deposition in high SR=54.8 solution at 80°C for 24 h experiments. A linear correlation was also fitted to the experimental data with $R^2=0.72$ which is lower than in the low SR=4.77 solution.

There is not much information regarding effects of an APTES film on scale adhesion and precipitation in literature, but effects of surface composition on scale precipitation will be discussed at the end of this chapter.

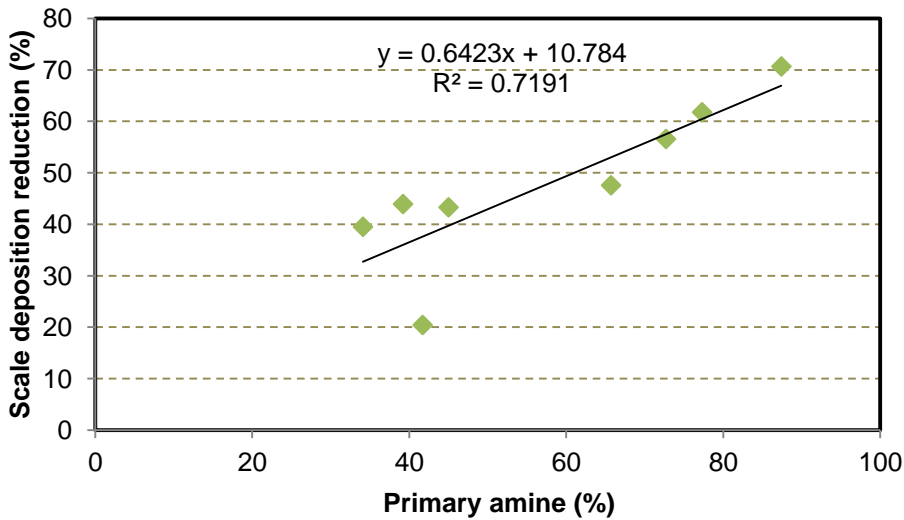


Figure 7-2. Behaviour of surfaces treated by different APTES concentrations in reduction of calcium carbonate scale deposition at 80°C and after 24 h experiment at SR=54.8 as a function of primary amine contents

However, other features like coverage, roughness and wettability of film formation may also influence the performances of treated surfaces in reduction of calcium carbonate scale deposition. Figure 7-3 presents the performance of quartz surfaces treated by various concentrations of APTES (0.05-8%) as a function of contact angle measurements. The graph shows no correlation between contact angles and the performance of APTES film formation on quartz surface in reduction of calcium carbonate scale. However, two distinguished areas can be extracted from Figure 7-3, which are separated by two coloured circles (blue and amber). Better performance of surfaces with lower water contact angles are observed compared with the surfaces with more hydrophobicity tendency. However, this is in contrast with biofouling study (197) that has shown better performance in hydrophobic surface due to their non-sticky properties.

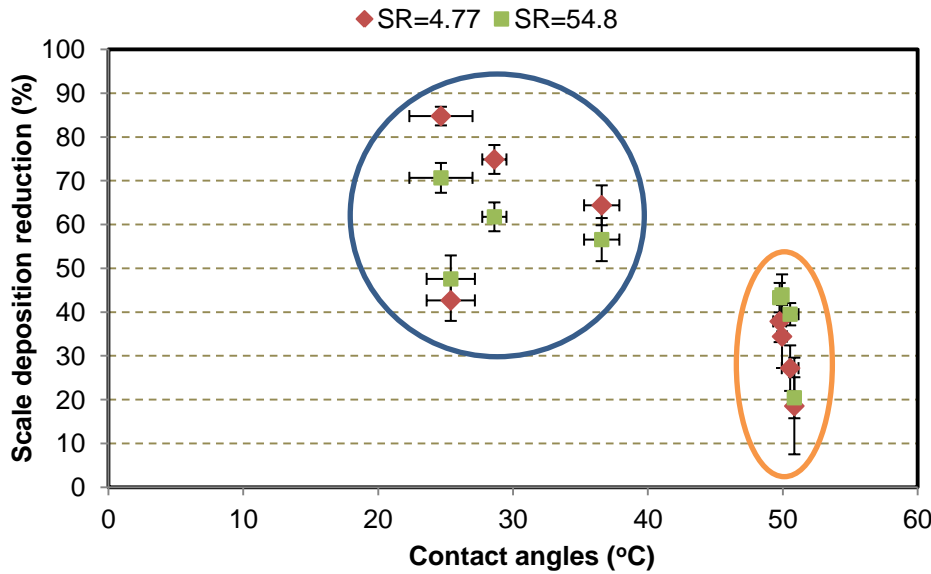


Figure 7-3. Behaviour of surfaces treated by different APTES concentrations in reduction of calcium carbonate scale deposition at 80°C and after 24 h experiment as a function of contact angles

Related literature regarding effects of wettability of surface in scale adhesion will be discussed later in this chapter. In order to understand the effects of roughness on calcium carbonate scale deposition, the efficiency of the surfaces treated by APTES versus roughness is plotted in Figure 7-4. This graph illustrates that the performance of the APTES-treated surfaces increased by roughness except from the performance of the surface with ~1 μm related to 8% APTES.

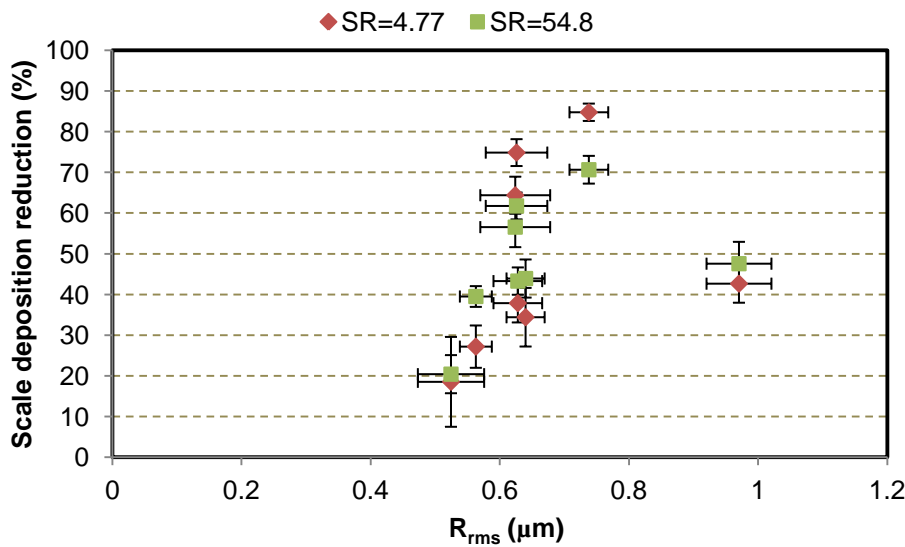


Figure 7-4. Behaviour of surfaces treated by different APTES concentrations in reduction of calcium carbonate scale deposition at 80°C and after 24 h experiment as a function of surface roughness

It was previously demonstrated (193, 199) that scale deposition on stainless steel surface increased by roughness, which is in contrast with results of this work. It is observed in Figure 7-4 that the amount of scale deposited on the treated surfaces decreased where the roughness increased. However, the performance of the surface treated by 8% APTES in reduction of scale deposition decreased, which can be due to increasing roughness.

It is clear that the performance of the surfaces treated by various APTES concentrations could not be correlated with wettability and roughness (physical properties), on the other hand, it can be related to primary amine content (chemical properties). Although Figure 7-1 and Figure 7-2 contained the whole range of APTES concentrations, poor correlation coefficients were obtained by relating the surface performance just to primary amine content. Thus, an attempt was made to correlate the performance of the APTES film formations in reduction of calcium carbonate scale deposition with both physical and chemical properties.

From the figures in the previous pages, it can be stated that the main contribution on the performance of the surfaces treated by APTES in reduction of calcium carbonate scale deposition is primary amine content as expected. It was also shown in Chapter 6 that different APTES conformation resulted in different roughness and wettability measurements. It was also demonstrated (260) that solvent used in the film formation process influences the wettability of the film formed on the surface. Since different solvents may be employed in film formation process, it was attempted to eliminate the effects of wettability as a main factor which influences the performance of the treated surfaces. Besides, it can be found in the literature (69, 70, 76) that the wettability of a surface can be associated with roughness and topography of the surface. As shown, the major influence of the efficiency of the surface is due to surface chemistry (composition and more specifically conformation of film created); therefore, primary amine content was emphasised more with positive impact followed by the concentration of APTES in film formation process since the surface coverage influenced the performance of the surface (Chapter 5).

It was also demonstrated that a wide range of APTES concentrations was employed to create a uniform SAM on the surface (244). Although the higher surface coverage in this study was obtained at 8%, it was also illustrated that with a simple calculation an acceptable surface coverage can be obtained even with applying lower concentrations (see Chapter 4). Therefore, the average of higher range of APTES concentrations (4% APTES) was used as a reference concentration that gives an acceptable surface coverage. Roughness of the treated

surface was another parameter, which was taken into account for predicting correlation. Since it was generally shown (178, 198, 199, 203) that the higher roughness, the higher scale deposition on surface; the impact of roughness on the performance of the APTES-treated surfaces was considered negative in the correlation. The correlation is formulated in form of the equation below.

$$CP \sim [primary\ amine\ content] [APTES\ concentrations] [roughness] \quad \text{Equation 7-1}$$

Where CP is the coating performance in terms of reduction of scale deposition. In order to use the values of primary amine contents, APTES concentrations and roughness in the equation above; some normalisations were required in order to have the same unit in both sides of the equation. Coating performance, CP, and primary amine content, PA, are unitless, and the unit of roughness (R_{rms}) is metres. APTES concentration (C_N) can have different units depending on usage. Therefore, R_{rms} and C_N are normalised as below:

- ❖ R_{rms} : (Roughness of treated surfaces)/(roughness of the blank surface)
- ❖ C_N : (Concentration of aminosilanes in the solution)/(the concentration that gives SAM)

It was assumed that the film performance can be correlated to PA, C_N and R_{rms} by the equation below:

$$CP = a.PA^b + c.C_N + d.(R_{rms} - 1)^2 \quad \text{Equation 7-2}$$

The constants: a , b , c and d , were determined using least-square fitting and Microsoft Excel and listed in Table 7-1.

Table 7-1. Calculated constants in Equation 7-2

a	b	c	d
0.62	1.1	0.55	-20

This gives an equation which can be fitted to the experimental data and includes both physical and chemical properties of the film created on the quartz surface.

$$CP = 0.62PA^{1.1} + 0.55C_N - 20(R_{rms} - 1)^2 \quad \text{Equation 7-3}$$

The CP obtained by Equation 7-3 is plotted in Figure 7-5 versus the experimental results for APTES film on quartz surface at SR=4.77. The graph shows how far the purple rhombic ('Estimation' values) are from the experimental data (the red squares and line). The correlation coefficient was also calculated $R^2=0.89$, which shows slightly higher value compared with the correlation obtained by Figure 7-1 ($R^2=0.88$). Although Equation 7-3 could slightly improve the linear fit for the experimental data, it considers more parameters in the equation which may be useful for a wider range of data later when all the experimental results of both APTES and APhS are studied together.

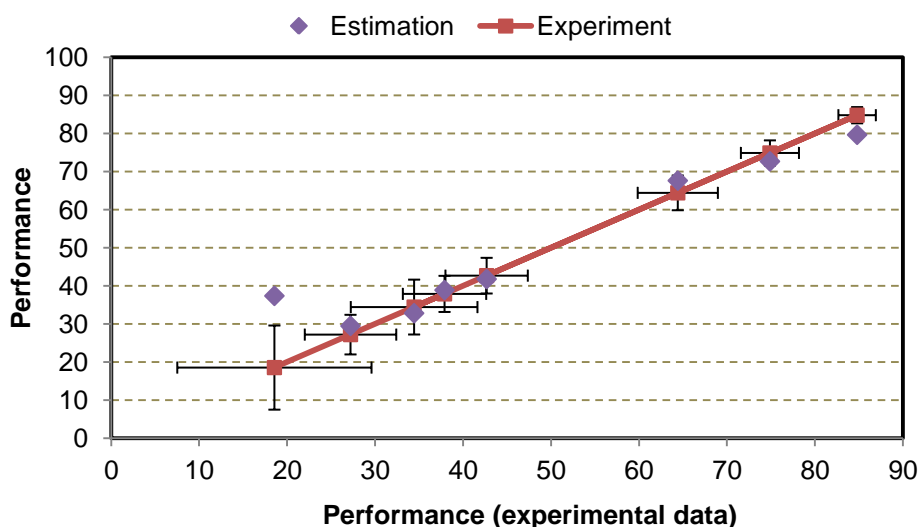


Figure 7-5. Experimental and estimated data versus experimental data for the surfaces treated by different APTES concentrations at 80°C and after 24 h experiment in SR=4.77 solution

The same procedure was followed for SR=54.8 in order to assess Equation 7-3 in predicting the performance of the treated surface by primary amine contents, normalised APTES concentration and roughness; this is presented in Figure 7-6. The correlation coefficient $R^2=0.46$ was obtained from the estimated data according to Equation 7-3, which is much lower than formulating the performance as a function of just primary amine content (Figure 7-2). However, both low and high SR solutions were correlated by one correlation (Equation 7-3).

Figure 7-6 together with Figure 7-5 indicate that the APTES film tendency can be related to the primary amine content which is associated to conformation of the film created on the quartz surface (Figure 6-24, Figure 6-25 and Figure 6-26). This was expected since the wettability and topography of the surfaces treated by APTES were correlated to the film formation structures, which was extensively discussed in Chapter 6.

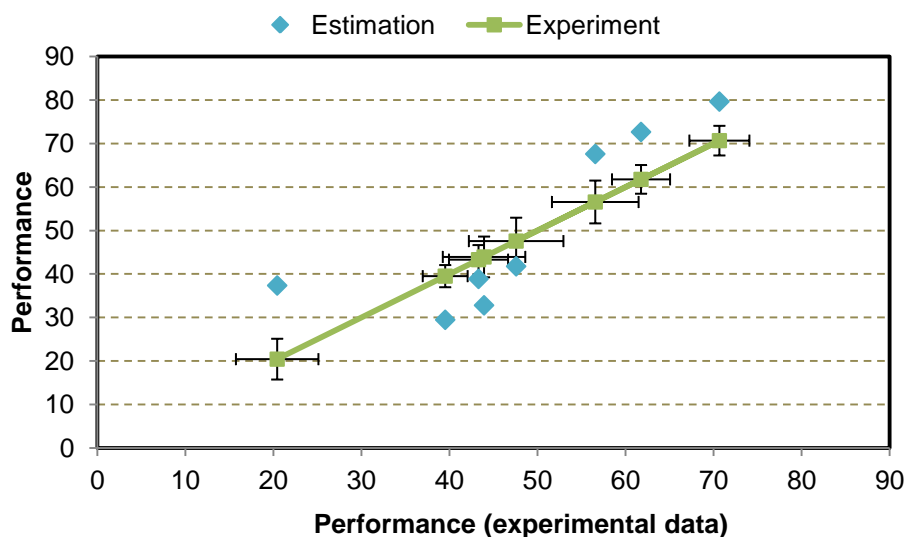


Figure 7-6. Experimental and estimated data versus experimental data for the surfaces treated by different APTES concentrations at 80°C and after 24 h experiment in SR=54.8 solution

Although it was demonstrated that the primary amine content is the dominant factor interpreting the APTES film performance, there are two concentrations (0.05% and 8%) that need more discussion since they do not follow the trend (the higher primary content, the better surface in scale reduction).

At 0.05% APTES concentration, 41.7% primary amine was measured by XPS; however, 18.5% and 20.4% efficiency were achieved by 0.05% APTES, respectively. Although the contact angle and roughness measurements of 0.05% are in the same range of 0.1-0.2% and the primary amine content of 0.05% APTES is higher than 0.1-0.2%, the performance of the quartz surface treated by 0.05% APTES is much lower at this concentration compared with 0.1-0.2%. This can be explained by the concentration of APTES in the solution meaning that the created film on the quartz surface covered much less percentage of the surface remaining more part of the surface without APTES film. On the other hand, the concentration of nitrogen measured by XPS at 0.05 is in the same range of nitrogen percentage measured by XPS for 0.1-0.2% APTES (see Figure 7-6). This may indicate more polymerisation on the quartz surface with many sites left uncovered on the surface, which is due to excess of water presenting in the solution (see Chapter 6).

The performance of the quartz surface treated by 8% APTES showed lower performance in reduction of scale deposition compared with 2-6%, which can be explained by low primary amine content. On the other hand, at 8% APTES higher primary amine content was measured compared with low range of APTES concentrations (0.05-0.2%), but gave almost as low efficiency as 0.15-0.2%. This can be explained by conformation of the film created by 8%, which was illustrated in

Figure 6-26. Higher roughness measurement was observed at the surface treated by 8% APTES (see Figure 6-17), which can be another reason of the lower efficiency of this surface. It was previously demonstrated that higher surface roughness value resulted in more scale deposition on the surface (178, 198, 199, 203).

Therefore, it can be stated that the tendency of the APTES film to calcium carbonate scale deposition is mainly related to the film conformation which is originated from the chemical states of the components on the surface.

7.3 The performance of the quartz surface treated by APhS in reduction of calcium carbonate scale deposition

The same approach as the APTES is followed to investigate the effects of surface chemistry and composition as well as roughness and wettability on reduction of calcium carbonate scale deposition on the surfaces treated by various concentrations of APhS (0.06-0.24%). Figure 7-7 illustrates the performance of the surfaces treated by various concentrations of APhS in reduction of calcium carbonate scale deposition as a function of primary amine contents. The graph shows that the efficiency of the treated surfaces increased by free amine percentage. The experimental data was fitted by a linear equation with correlation coefficient $R^2=0.83$.

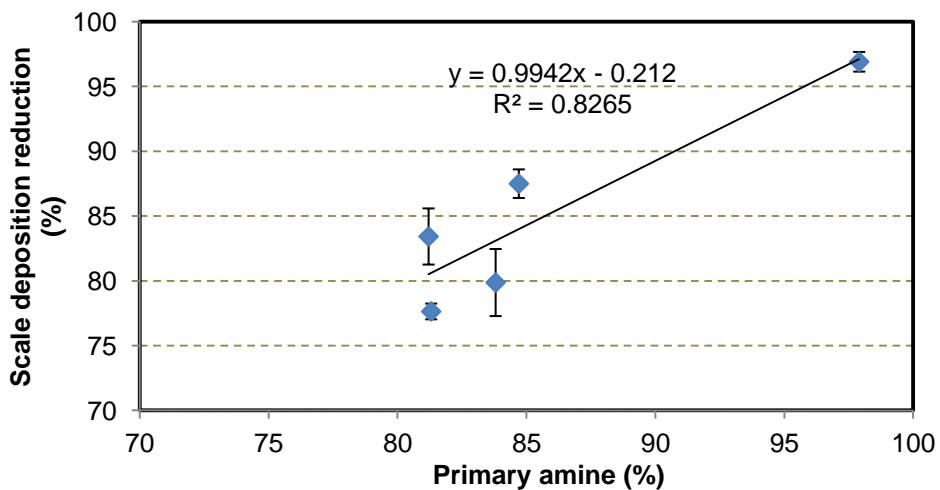


Figure 7-7. Behaviour of surfaces treated by different APhS concentrations in reduction of calcium carbonate scale deposition at 80°C and after 24 h experiment at SR=4.77 as a function of primary amine contents

In comparison with APTES results in low SR=4.77 solution, the correlation coefficient R^2 for APhS is lower, which could be due to a lower number of

experiments for APhS. However, compared with Figure 5-19 a better correlation was obtained when performance of the surfaces treated by APhS was plotted as a function of primary amine contents. Thus this again indicates that the tendency of the surfaces treated by aminosilanes can be interpreted by the primary amine content which represents the conformation of the film formed on the quartz surfaces.

Figure 7-8 shows the tendency of the quartz surface treated by APhS to calcium carbonate scale deposition in high SR=54.8 solution. Compared with low SR=4.77, the correlation fitted the experimental data is poorer with correlation coefficient $R^2=0.49$. However, in comparison to Figure 5-18, scale deposition on the APhS-treated surface in high SR=54.8 was fitted much better by using primary amine percentage, which again represents the film conformation (Figure 6-27). The experimental data in Figure 7-8 is linearly correlated to the equation below.

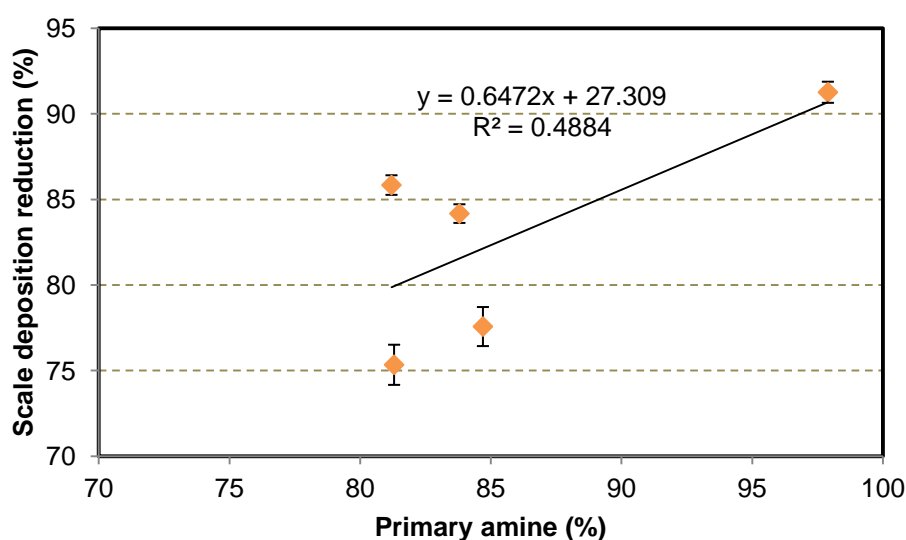


Figure 7-8. Behaviour of surfaces treated by different APhS concentrations in reduction of calcium carbonate scale deposition at 80°C and after 24 h experiment at SR=54.8 as a function of primary amine contents

Figure 7-9 presents performance of the surfaces treated by different APhS concentrations as a function of wettability of the treated surfaces. The graph clearly shows no relation between water contact angle measurement and the behaviour of the surfaces treated by APhS. However, the surface with more hydrophilic tendency demonstrated better performance in terms of reduction of calcium carbonate scale deposited on the quartz surface.

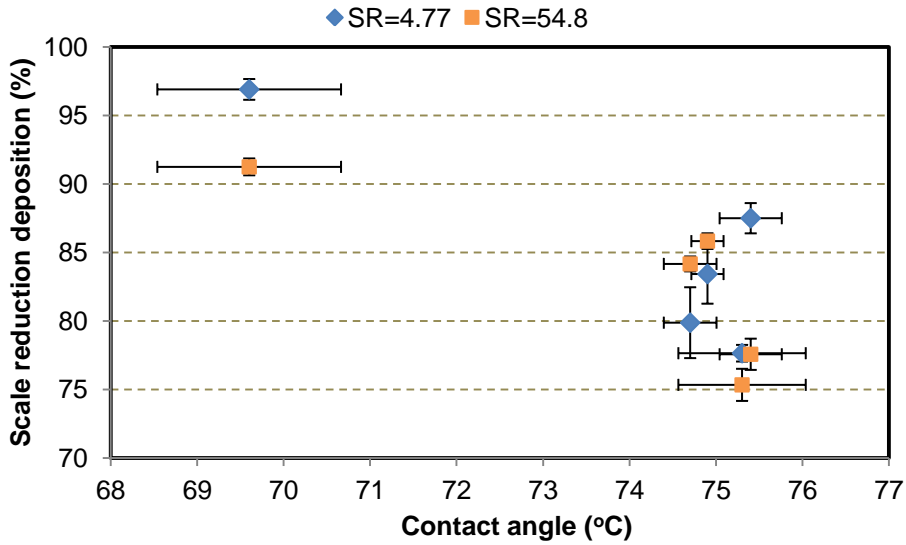


Figure 7-9. Behaviour of surfaces treated by different APhS concentrations in reduction of calcium carbonate scale deposition at 80°C and after 24 h experiment as a function of contact angles

Figure 7-10 illustrates the tendency of the surface to calcium carbonate scale deposition with respect to roughness (R_{rms}) of the created films. It is observed that roughness of APhS film on quartz surface is not the determining factor. The graph shows random behaviour of surface topography to tendency of calcium carbonate scale deposition.

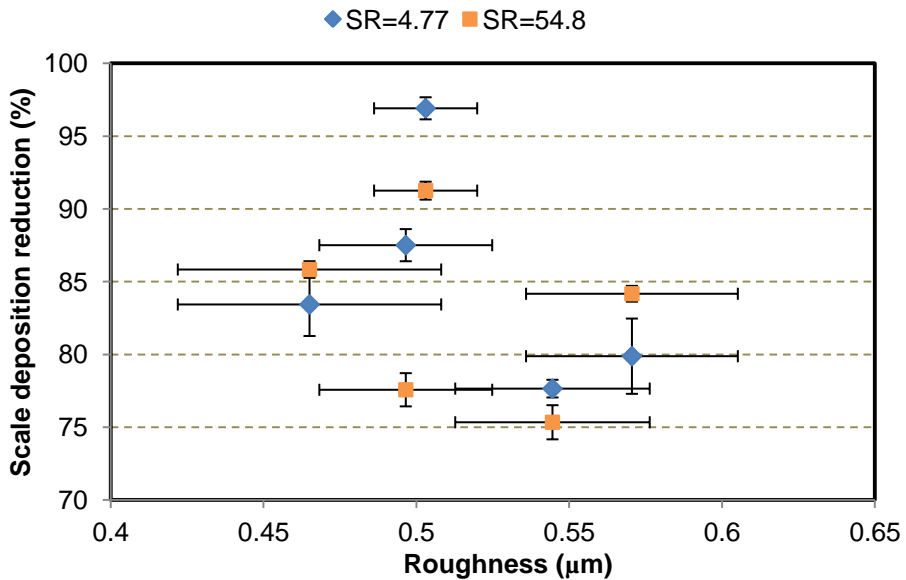


Figure 7-10. Behaviour of surfaces treated by different APhS concentrations in reduction of calcium carbonate scale deposition at 80°C and after 24 h experiment as a function of surface roughness

The same assumptions as APTES were made for APhS in order to include the influence of all properties: primary amine contents, roughness and APhS

concentrations in one correlation which could fit the experimental data for high and low SR solutions. Figure 7-11 shows the estimated and experimental values versus experimental data for the surfaces treated by APhS in SR=4.77 solution. Equation 7-3 was used to estimate the performance of the surfaces treated by APhS in reduction of scale deposition as function of primary amine content, normalised APhS concentration and normalized R_{rms} . Correlation coefficient $R^2 = 0.75$ was obtained from Equation 7-3 which is slightly lower compared with the graph fitted just by primary amine percentages ($R^2=0.83$). Although the correlation coefficient obtained by Equation 7-3 is lower, the same correlation was employed to interpret all data both for APTES and APhS.

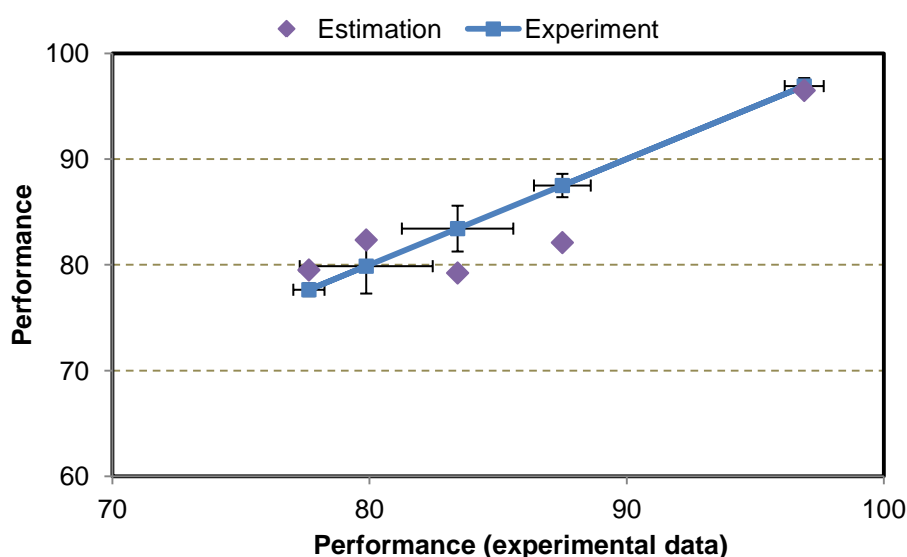


Figure 7-11. Experimental and estimated data versus experimental data for the surfaces treated by different APhS concentrations at 80°C and after 24 h experiment in SR=4.77 solution

The same procedures were followed for high SR=54.8 solution to correlate the experimental data to all properties, which is illustrated in Figure 7-12. The correlation coefficient $R^2=0.32$ was obtained from Equation 7-3 for APhS film in high SR=54.8 solution which is much lower than Figure 7-8 with $R^2=0.49$. However, both correlations are poor enough to be eliminated as predicting formulas for APhS film in high SR=54.8 solution. It is possible to use another correlation which can give predicted values much closer to real values for APhS in high SR=54.8 solution. The equation is given below with $R^2=0.67$; however, the attempt was to interpret all experimental results with one correlation.

$$CP = 0.62PA^{1.1} + 0.55C_N - 20(R_{rms} - 1)^2 \quad \text{Equation 7-4}$$

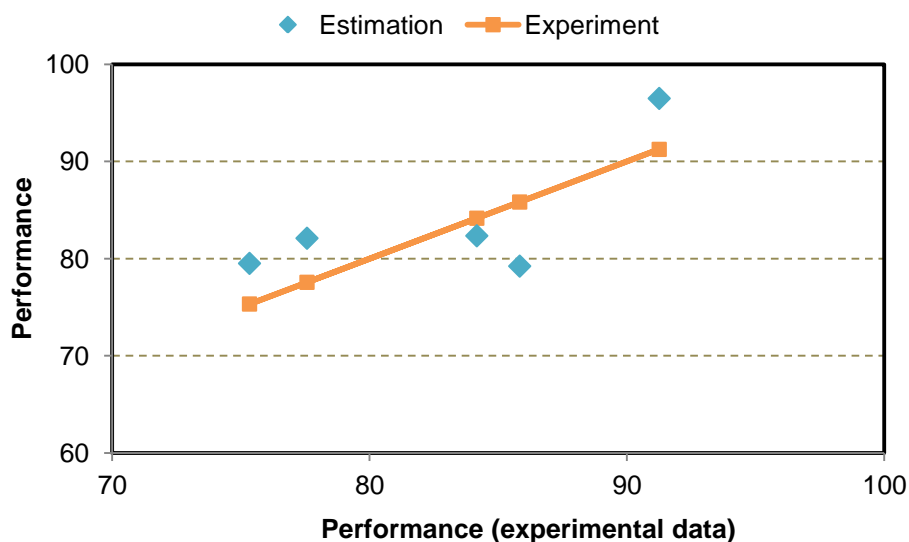


Figure 7-12. Experimental and estimated data versus experimental data for the surfaces treated by different APhS concentrations at 80°C and after 24 h experiment in SR=54.8 solution

7.4 Comparison of APTES and APhS film performances in reduction of calcium carbonate scale deposition

Effects of wettability, roughness and film conformation of each aminosilane (APTES and APhS) on reduction of calcium carbonate scale deposition were separately shown earlier in this chapter. In this section, the influences of these properties on amount of CaCO_3 deposition on the surfaces treated by APTES and APhS are compared together. Figure 7-13 presents the performance of the all surfaces treated by APTES and APhS versus the wettability of the each treated surfaces in both high and low SR solutions. No correlation can be concluded from Figure 7-13; however, three areas can be distinguished from the graph. The first area is separated by a red ellipse which covers a wider range of performance (~42-85%) and contact angles (25-36°); this area is related to APTES with high concentrations (2-8%). The second area is the amber ellipse related to APTES with low concentrations (0.05-0.2%) and shows the lowest performance. However, a narrower range of contact angles was covered by this range of APTES concentrations. And, the third category is the purple ellipse associated to the APhS film which shows the best performance among all the results in terms of reduction of scale deposition on surface. One conclusion from Figure 7-13 is that wettability of treated surfaces by APTES and APhS is clearly not the dominant factor in reduction of CaCO_3 on the surfaces.

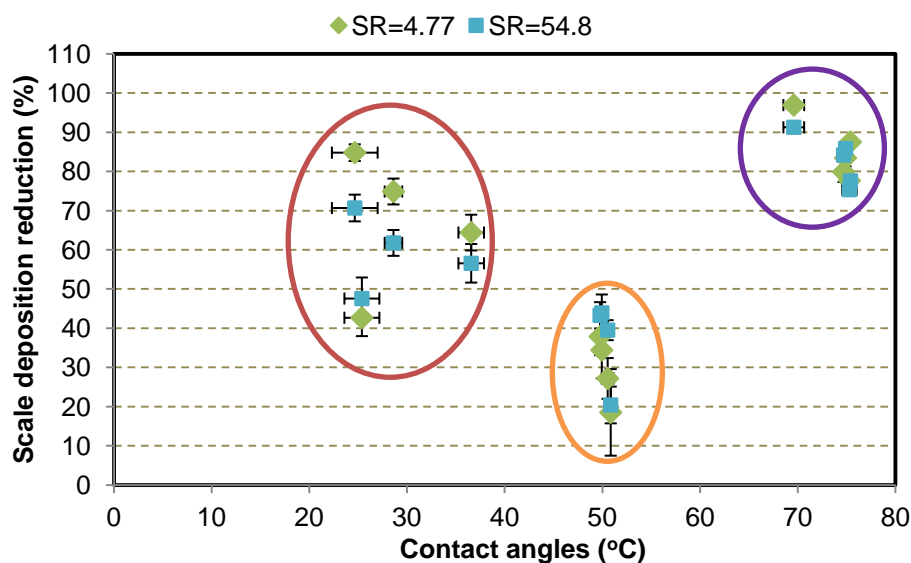


Figure 7-13. Behaviour of surfaces treated by different APTES and APhS concentrations in reduction of calcium carbonate scale deposition at 80°C and after 24 h experiment as a function of contact angles

In Chapter 2, it was shown that scaling on surface can be related to wettability of the surface. It was previously illustrated that hydrophobic surfaces have shown better performance in biofouling research due to their non-stick characteristics (197). In biofouling study, it is believed that the fouling components are formed in the bulk solution and then stick to the surface, thus the study was focused on only deposition (197); hence the lower surface energy, the lower adhesion and fouling deposition. On the other hand, in other study, hydrophilic surfaces generally showed better performance in scaling (4) as the scaling process is a combination of crystallisation from the surface and adhesion together (29), which may suggest that the surface energy may not be a key factor to control the scaling. However, it can clearly be stated that, in this study, scaling cannot be related to wettability of the surfaces treated by APhS and APTES films.

Figure 7-14 shows the performance of the treated surfaces by APTES and APhS in reduction of scale deposition as a function of roughness (R_{rms}), which illustrates no correlation between roughness and the performance of the surfaces in reduction of scale deposition. It can be seen that the highest roughness gave a performance that stayed in the middle and the small range of roughness gave a wide range of performance.

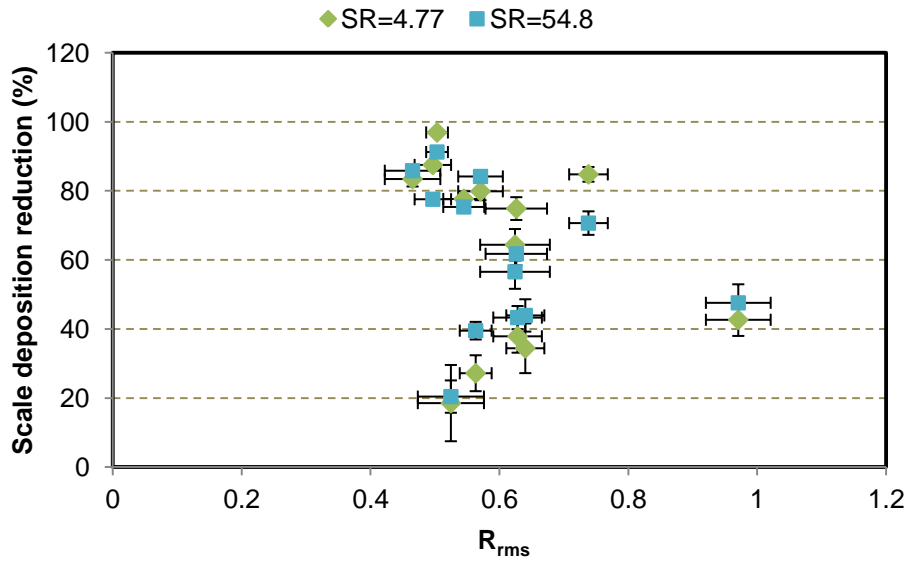


Figure 7-14. Behaviour of surfaces treated by different APTES and APhS concentrations in reduction of calcium carbonate scale deposition at 80°C and after 24 h experiment as a function of film roughness (R_{rms})

The relationship between roughness of a surface and its tendency to scale deposition has been previously studied (199, 337, 343) and it was also demonstrated that the scale formed on the smooth surface has been removed easier compared with the rough surface. However, random behaviour in terms of scaling deposition was also observed previously (4, 193). This study also showed that no correlation can be associated with roughness of the surface treated by different concentrations of APTES and APhS.

It was demonstrated earlier in this chapter that the dominant property in reduction of calcium carbonate scale deposition is the primary amine content, which is directly related to film structure created on the surface. Figure 7-15 illustrates the performance of the treated-surfaces as function of primary amine contents for all experiments (APTES and APhS) in low SR=4.77 solution. It is observed that the performance of the surfaces treated by APTES and APhS in reduction of scale deposition increased by primary amine contents no matter which aminosilane was used to treat the quartz surface. A linear extrapolation between primary amine percentages and the performance of the surfaces with correlation coefficient $R^2=0.93$ is shown in Figure 7-15.

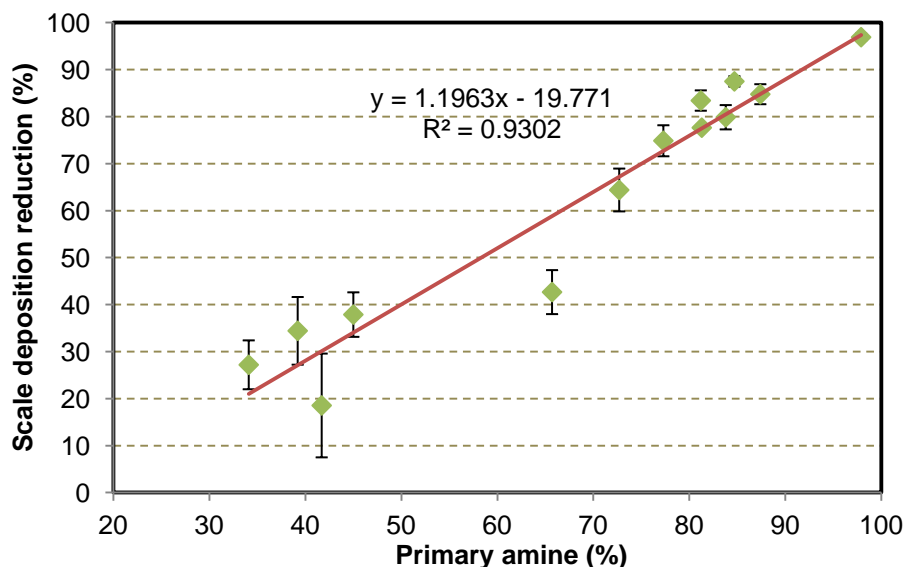


Figure 7-15. Behaviour of surfaces treated by all APTES and APhS concentrations in reduction of calcium carbonate scale deposition at 80°C and after 24 h experiment at SR=4.77 as a function of primary amine contents

Figure 7-16 illustrates the efficiency of the surfaces treated by APTES and APhS in reduction of calcium carbonate scale deposition as function of free amine percentage (%) in high SR=54.8 solution. A linear correlation was fitted to the experimental data with correlation coefficient $R^2=0.81$.

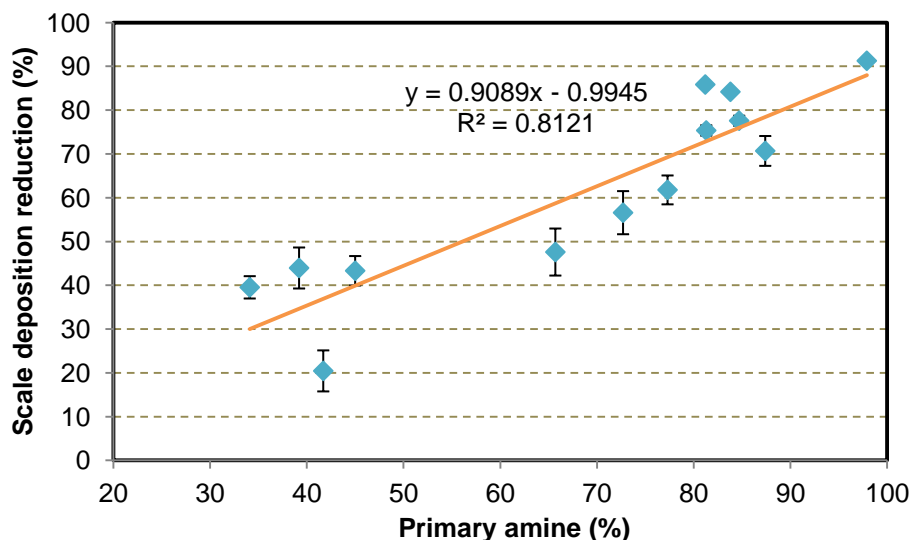


Figure 7-16. Behaviour of surfaces treated by all APTES and APhS concentrations in reduction of calcium carbonate scale deposition at 80°C and after 24 h experiment at SR=54.8 as a function of primary amine contents

Both Figure 7-15 and Figure 7-16 showed an improved correlation coefficient R^2 compared with the related graphs for individual APTES and APhS in

low and high SR solutions owing to an increased number of data in graph; however, each of them provides different contents in their equations.

Equation 7-3 was again employed to involve roughness, aminosilane concentrations and primary amine contents to predict the efficiency of the surfaces treated by APTES and APhS in terms of scale reduction. Figure 7-17 shows the efficiency of the treated surfaces (experimental data) and the estimated data from Equation 7-3 versus experimental data with correlation coefficient $R^2=0.94$, which indicates an improvement in correlation coefficient compared with Figure 7-15.

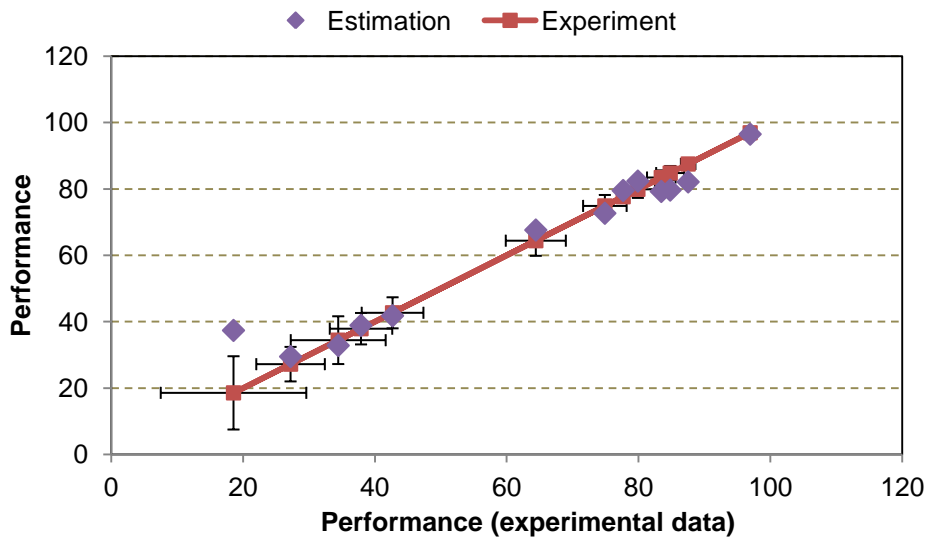


Figure 7-17. Experimental and estimated data versus experimental data for the surfaces treated by different APTES and APhS concentrations at 80°C and after 24 h experiment in SR=4.77 solution

The same procedure was followed for high SR=54.8 solution, which is presented in Figure 7-18 with $R^2=0.82$. The graph shows no improvement in correlation coefficient compared with Figure 7-16, but all parameters are involved in predicating the equation. Although no modification in the equation was shown in Figure 7-18 even by adding more complication, it applies the same equation (Equation 7-3) as used in low SR=4.77 solution.

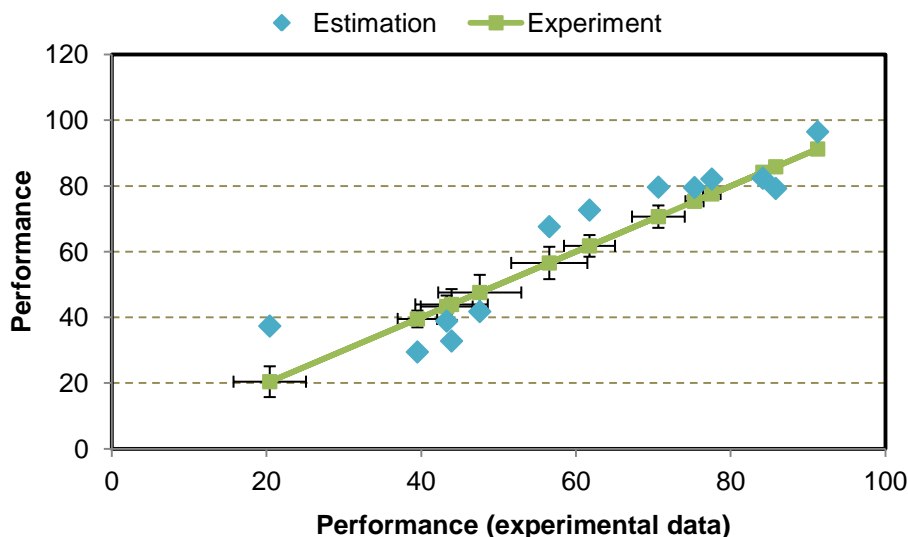


Figure 7-18. Experimental and estimated data versus experimental data for the surfaces treated by different APTES and APhS concentrations at 80°C and after 24 h experiment in SR=54.8 solution

The purpose of using one equation (Equation 7-3) for all Figure 7-5, Figure 7-11, Figure 7-17 and Figure 7-18 was to extrapolate all experimental data with a universal equation. However, these graphs can be correlated with separate equations to predict the efficiency of the treated surfaces with higher accuracy. With comparing all results together, it is obvious that the primary amine is the determining factor that can explain the behaviour of the treated surfaces. It was shown in Chapter 6 that the film structures on the quartz surfaces mainly related to primary amine contents. It can be stated that film structure created on the quartz surfaces is the dominant factor to reduce the amount of calcium carbonate scale deposited on the surfaces.

The saturation ratio of a solution influences the induction time and amount of deposition on surface (163). It was observed from Figure 5-29 that the surfaces treated by APTES and APhS behave differently in reduction of calcium carbonate scale deposition in low SR=4.77 and high SR=54.8 solutions. Some surfaces performed slightly better in low SR=4.77 and some the opposite. The reason may be due to the different degrees of surface charge induced in different SR solutions. It was also shown that different surface charges can result in different amount of scale deposition (5, 344, 348). Then, it can be stated that the treated surfaces behaved differently in different SR solutions since solutions can go through various pH profiles during the experiment when the pH is not controlled. This might lead to different performance of surface in reduction of scale deposition. It was demonstrated that pH of a solution affects the degree of ionisation of the substrates (348).

It was previously shown that different properties such as roughness, surface energy and surface chemistry can affect the efficiency of the surfaces in reduction of scale deposition and interfere the influence of each other (3, 4, 178, 198, 199, 203). Mineral scale deposition on stainless surface was demonstrated to be controlled by roughness of the surface instead of the surface material (4, 193). However, film formation on stainless surfaces treated by PPCA showed an improvement on performance of the surface in reduction of scale deposition (4-6, 181). Although low surface energy is generally related to low scale deposition on surface (203), it was demonstrated that it cannot correlate the tendency of all surfaces towards scaling (3-5, 202). Some studies showed that the scale deposition on the surface is owing to reduction of active sites by chemical treatment (4-6). It was illustrated (4, 5, 181) that negatively charged stainless steel surface was replaced by non-charged surface by PPCA treatment resulting in reduction of scale deposition on the surface.

The similar hypothesis is thought to be occurred in formation of APTES and APhS films on the quartz surfaces. The number of active sites was reduced due to formation of APTES and APhS on the surfaces since the negative surface charged quartz became slightly positive towards un-charged surfaces by forming APTES and APhS. It was shown that positive charged surface un-favour the nucleation of calcium carbonate scale on surface and neutral surfaces limits the number of available sites for scale crystallisation (348). Thus, it is thought that the APTES and APhS films make the quartz surfaces un-charged with slightly positively charged resulting in good surfaces to have fewer tendencies to scale crystallisation and adhesion.

Eroini, V. (4) has also shown no change in amount of calcium carbonate scale deposition on non-eroded and eroded DLC and PTFE surfaces due to importance of the surface chemistry of these surfaces; however, it was also shown that the surfaces coated by ceramic and polymer showed lower influences by coating materials. The performance of DLC surfaces in reduction of scale deposition was related to the low surface energy in fouling studies (6, 184-187); on the other hand, not always lower surface energy led to lower scale deposition on surface (196, 202). It was also shown that surface energy has a significant effect on adhesion of surface on the surface (8, 187, 203); in contrast, insignificant effect (Figure 7-13) was seen on the performance of the surfaces by surface energy in this study as different results obtained by hydrophobic and hydrophilic surfaces.

As shown in Chapter 5, the morphology of calcium carbonate scale deposited on the APTES- and APhS-treated surfaces slightly changed compared

with the blank quartz surface. This indicates that APTES and APhS films have minor effects on the morphology of the CaCO_3 crystal shapes. However, the impact of the films on scale deposition can be related to reduction of nucleation sites on the quartz surface. This behaviour was also observed previously (4) when PPCA was used to treat stainless steel. On the other hand, surface chemistry influenced the morphology of the scale formed on the surface due to different surface charged (348). It was shown that negative charged and neutral surfaces favoured polycrystalline and single-crystal scale on the surface; in contrast, positively charged substrates limited the nucleation of calcite from the surface. Although it was shown in the literature (3, 4, 189, 205, 345, 348, 385-387) that surface composition, roughness and wettability of the surface can alter morphology of scale deposited on the surface, this difference was observed to be negligible in this study.

7.5 Immunizing near wellbore area from CaCO_3 deposition/adhesion by SAM formation

The main contribution of this work is to demonstrate the potential of applying new methodology (separately or in assistance of) in addition to squeeze treatment of scale inhibitor to protect the near wellbore production from precipitation of calcium carbonate. The idea was to illustrate whether it is possible to create a thin layer on wellbore grain surface that does not have any tendencies to deposition of calcium carbonate scale since the CaCO_3 is one of the major issues in near wellbore area. The first step is to prove the concept by demonstrating the potential of some chemicals to reduce the scale deposition. This can be employed with assistance of another methodology used in the oil and gas industry such as squeeze treatment. However, in future, other chemicals may be introduced in order to completely create an anti-scale formation rock.

Squeeze treatments are generally used to protect mainly the near wellbore area and production packers in the well from mineral scale deposition by injecting a massive amount of SI into the near wellbore area: the schematic is shown in Figure 7-19. The SI is released from the near wellbore into the solution during the production to inhibit the production system from scale deposition. This is an effective method to mitigate the scale issue in downhole; however, some disadvantages are involved in the squeeze treatment such as high cost of each treatment due to cost of chemical itself, production loss due to shut-in period and pumping jobs; and damage introduced to the formation by pumping SI. An

alternative methodology to secure the near wellbore area from scaling can benefit the oil and gas industry.

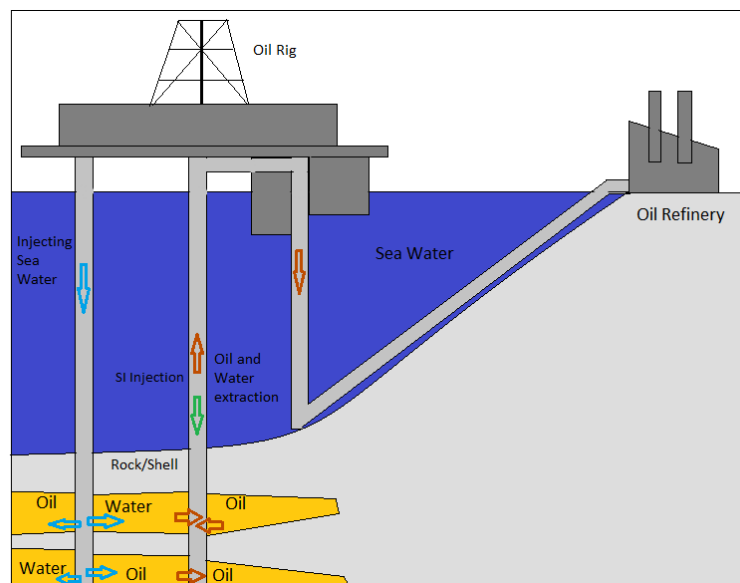


Figure 7-19. SI injection Schematic in an oil well using squeeze treatment

Different surface coatings on metal surfaces have been previously studied in terms of reduction of mineral scale deposition (3, 4, 61, 178, 179, 181, 182, 388, 389). It was illustrated that scaling process on various substrates was influenced by different properties of surfaces such as roughness, wettability and surface chemistry of which impacts are different for each coating (3, 4, 61, 178, 179, 181, 182, 388, 389). Mitigating the mineral scale issues by coating the surface of pipeline and more importantly the critical places like downhole safety valves can be an alternative or an assistance methodology to prevent scaling by SI. On the other hand, no alternative for protecting the near wellbore area has been introduced so far. Therefore, this research focused on introducing and developing a novel methodology to reduce the potential of scale deposition in the near wellbore by creating an anti-scale surface on formation rock. In contrast to coating of pipelines, the idea generated in this research must be performed remotely since there is no access to formation rock, and also the thickness of the new surface introduced to the formation rock is crucial in order not to block the oil path. In addition, the durability of the treatment plays an important role in order to make the methodology cost effective for industrial use. Hence, a covalent bond between the rock surface and the treatment is essential for the purpose of creating an anti-scale surface.

As discussed in the literature chapter, organosilanes are the first choice since the silicon can covalently react with the formation rock - the quartz part of the rock since the majority of the most formation rock consists of quartz - and different

tails can be looked at for interaction between mineral scale deposition and the tail of the treatment. Different tails of organosilane introduce different physical and chemical properties on the formation rock which benefits for this study. Since a hydrophobic surface is not an advantage for oil production, two hydrophilic organosilanes were chosen to study further. In addition, one of these organosilane (APTES) is used in the oil and gas industry for enhanced SI adsorption (290, 291, 390) and immobilising fine migration. The other organosilane (APhS) used in this study has the same tail-end but with different internal tail structure; this was employed to investigate the effects of the structure of organosilane on reduction of scale deposition due to mainly the rigidity of APhS. In order to achieve the purpose of this research, the study was divided into three main chapters: the kinetics of aminosilanes film formation, the behaviour of the treated surfaces with regards to amount of calcium carbonate scale deposition and characteristics of the film formations in order to understand the performance of the film in reduction of amount of CaCO_3 deposition. Here, the results of each chapter individually discussed.

7.5.1 Kinetics of APTES film formation on quartz surface

A SAM technique by using QCM was employed to study the kinetics of APTES film formation on the quartz surface. Four different concentrations (2-8%) were used to study the adsorption and growth of APTES on the substrate. In order to explain the growth and adsorption process, Langmuir isotherm was employed by using a Matlab code to extrapolate the experimental data. In addition, to estimate the required mass of APTES to create a SAM film, ChemDraw software was applied to calculate the maximum occupied space by one molecule of APTES. It was shown that the APTES surface coverage increased by initial concentration of APTES in the solution; however, this trend did not illustrate a linear increment (Figure 4-10). By considering the standard deviation of the results at 6 and 8%, the same surface coverage (more than 90%) can be concluded from the QCM results for APTES. Even though the experiments were carried out in 2 h, the most majority of the coverage was gained in first 2000 sec, which indicates the importance of performing the treatment in high concentrations of APTES in a solution of containing high water content. Generally, aminosilanes SAM was performed in a solution with toluene and very low water content in the solution (246, 277) and the process was implemented in a longer period (from 2 to 24 h). In this study, instead of toluene, ethanol was used in solution along with higher concentrations of water in order to make the treatment more acceptable in the oil and gas industry and more

importantly shorten the film formation procedure in order to reduce the cost by losing lower hydrocarbon production due to shut-in period of wells.

ChemDraw software was used to estimate the amount of APTES molecules required to create a SAM on the quartz surface. This estimation was utilized to understand whether the APTES mass on quartz substrate measured by QCM is in a range of creation of SAM. According to ChemDraw, the amount of APTES molecules are required to form a SAM on quartz surface was calculated $\sim 0.5 \mu\text{g}/\text{cm}^2$. This amount is slightly lower than the mass measured by QCM for 2-6% and at 8% the maximum adsorption is higher compared with other concentrations. These adsorption values are after 2 h experiment; however, in scale deposition tests 30 min experimental time was used for APTES. This should be sufficient enough to create a SAM of APTES on quartz surfaces, which can be observed from Figure 4-5. As a result, Chapter 4 showed that formation of an APTES film on quartz surface in a solution of water and ethanol by different concentrations of APTES (2-6%) is achievable. In addition, formation of polymerized APTES film on quartz surface might be possible owing to high APTES concentration. A schematic of APTES film on a substrate is presented Figure 7-20.

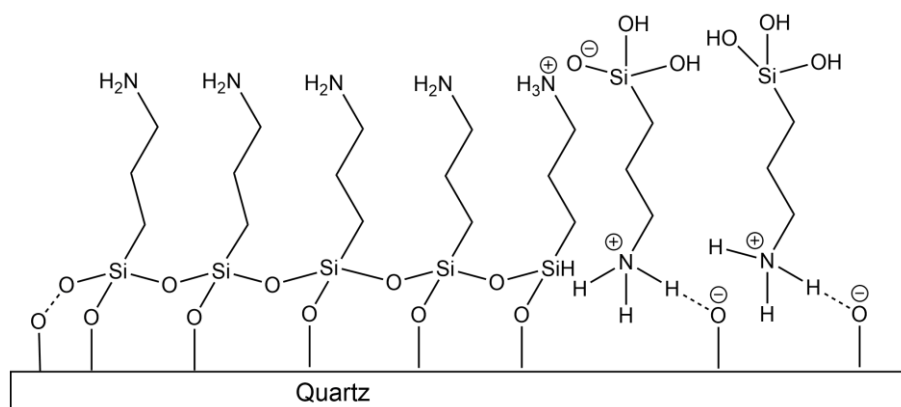


Figure 7-20. Schematic structure of APTES film

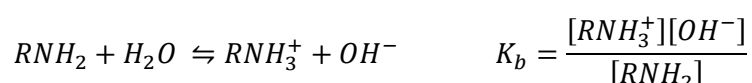
7.5.2 Treatments performance in reduction of scale deposition

Two different aminosilanes (APTES and APhS) with different concentrations (0.5-8% and 0.05-0.24%, respectively) were used to treat the quartz surfaces to demonstrate the tendency of the treatments to scale deposition. Two SRs (low=4.77 and high=54.80) of calcium carbonate solutions were also used to monitor the effect of SR on scaling on the treated surfaces. The results of Chapter 5 were significantly important, since the performance of the treated surface in reduction of CaCO_3 deposition was highly important to prove the idea of creation of anti-scale rock surface. Therefore, the main contribution of this chapter is to

demonstrate the potential of remotely treating internal formation rock surface in order to reduce the risk scale deposition in near the wellbore. However, the results obtained in this work can be applied to idealised lab conditions and the remote creation of the film within the rock pores has not yet been proven.

In general, APhS treatment showed better performance compared with APTES owing to rigid structure of APhS (244, 285) and possibly due to creating a neutral layer on the quartz substrate. The performance of APTES treated surfaces enhanced by increasing the solution concentration except from 8% which had a significant reduction in performance. The maximum performance for APTES treatments was at 6% with 85% and 70% reduction of calcium carbonate scale in low SR=4.77 and high SR=54.8; respectively, compared with the blank quartz surface. For APhS treatments, maximum reduction occurred at 0.6% APhS treatment with 97% and 92% in low SR=4.77 and high SR=54.8, respectively. In contrast to the previous work on reduction of mineral scale on different coatings that showed changes in morphology of scale on coating surfaces (3, 4, 163, 391), morphology of the CaCO₃ deposition on APTES- and APhS-treated was slightly influenced by the treatment compared with the blank surfaces.

The full explanation of APTES- and APhS-treated surfaces tendency to scale deposition was given at the end of Chapter 5. It was discussed that the main effect of APTES and APhS treatments in reduction of CaCO₃ deposition is altering the surface chemistry of the blank quartz by changing the negatively charged quartz surface to the positively (towards neutral) charged surface after treatment. Amines are weak bases and they can react with water.



The reaction is more towards the left hand-side of arrow. Anilines undergo the same types of reaction with much smaller K_b (acid dissociation constant) than alkyl amines, this leads to lower ionization in water for anilines. Aromatic amines are more stabilized in comparison to their ammonium ions than aliphatic amines compared to theirs. This phenomenon states that APhS treatment on quartz surface could be neutral and APTES treatment slightly positive. This can also be one of the reasons that APhS-treated surface performed better than APTES-treated quartz surfaces; this was extensively discussed in section 5.4.

The effect of surface charge on reduction of scale deposition was previously demonstrated (344, 348). Wang (62) studied the effect of polyphosphinocarboxylic

acid (PPCA) treatment on reduction of mineral scale deposition. They believed that the reduction of mineral scale deposition on the substrate was owing to a decrease on active nucleation sites by adsorption of PPCA on the surface. They also hypothesized that the carboxylic group of PPCA interacted with the metal surface leading to creation of non-charged surface on the metal, which resulted in reduction of calcium carbonate scale deposition on the metal surface. On the other hand, Martinod et al. (5, 344) illustrated that interaction of PPCA directly to the metal surface is doubtful since both species were negative in the solution. They believed that PPCA first interacted with a positive charge ion and then reacted with the metal surface. Although Wang et al. (62) and Martinod et al. (5) postulated different hypotheses to explain the interaction of PPCA to the metal surface, their attempts to interpret the reason of reduction in calcium carbonate scale deposition owing to creation of neutral surface by formation of a PPCA film on the metal surface. This behaviour was also observed by formation of aminosilanes film on the quartz surface. Aminosilane-treated quartz surfaces became slightly positive charged but more towards a neutral surface. It was also illustrated that a positive charged surface discourages nucleation of calcium carbonate scale on the surface and a neutral surface reduces the number of available nucleation sites on the substrate (348). It was demonstrated in this study that the APhS treatment performed better in most cases and the reason is due to rigid conformation of APhS compared to APTES and weaker positively charged (neutral) of the surfaces by APhS. Schematics of APTES and APhS film conformation are presented in Figure 7-22 and Figure 7-23.

7.5.3 Characterisations APTES and APhS films on the quartz surfaces

The objective of Chapter 6 was to study physicochemical properties of APTES- and APhS-treated quartz surfaces in order to fully comprehend the tendency of the treatments to calcium carbonate scale deposition. In addition, these characterisations used to understand the structures and conformations of the films formed on the quartz surfaces. Surface chemistry, roughness and surface energy analyses were performed by XPS, 3D surface profiler and contact angle goniometry, respectively. The main contribution of this chapter is to explicate APTES and APhS film structures based on roughness, surface chemistry and energy analyses. The results of Chapter 6 was very important in this research since the film conformations suggested in this chapter could explain the behaviour of the

treatments in reduction of CaCO_3 deposition. Ideal conformations of APTES and APhS on quartz surface are illustrated in Figure 7-21.

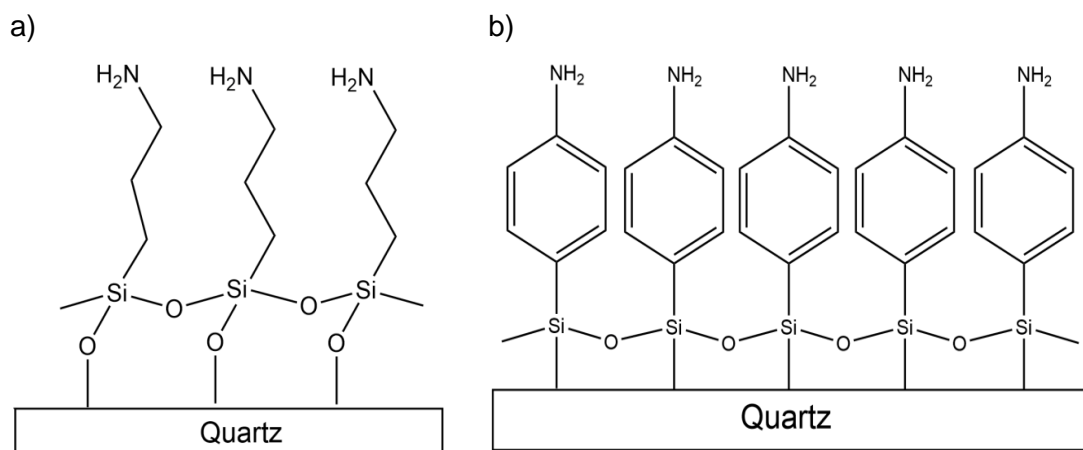


Figure 7-21. Schematic structures of ideal silanization of a) APTES and b) APhS

Different surface characterisation are used for aminosilane studies in literature to show that the conformation created on the surface is as much close to ideal structures (Figure 7-21). In general, formation of a SAM layer on quartz surface in a solution of toluene and aminosilanes (244) was shown more desirable since is closer to the idea conformation (amino group upward). However, it was shown in this study that a desirable conformation is also possible to achieve in certain solution of water and ethanol (APTES treatment). In comparison to Zhang and Srinivasan (244) who carried out the formation of APTES on quartz surface in toluene and obtained 88.6% primary amine content after 5 h, in this work higher primary amine content (87.4%) in shorter time (30 min) was achieved. The purpose, here, was to demonstrate the possibility of applying aminosilanes to formation rock the near wellbore area by means of a solution of which more feasible for the oil and gas industry.

The closest film formation to ideal conformation by APTES was obtained by 6% APTES in ethanol/water solution; this was demonstrated by the primary amine content (86%). The best performance was also seen in 6% APTES among all APTES concentrations which is in agreement with results of the surface characterisations. The lowest contact angle (24°) among other APTES concentrations was also measured on the quartz surface treated by 6% APTES which confirmed the results of XPS. Lower contact angle is obtained by a creation

of uniform layer of aminosilane in comparison with a non-uniform layer with H-bonded/protonated amine on the surface; this was previously illustrated (255, 259, 342). The roughness measurements of APTES-treated surface was also shown to be an agreement with the XPS results of which primary amine detection is the main objective of using XPS. The maximum value of roughness was measured at 8% followed by 6% APTES among other APTES concentrations. This indicated some aminosilanes polymerised before attaching to the surface. However, the most uniform APTES layer was obtained by 6% among other concentrations and this was shown by the results of scale test that illustrated that the highest reduction of CaCO_3 scale deposition at 6% among other APTES concentrations (0.05-8%) in both low $\text{SR}=4.77$ and high $\text{SR}=54.8$ solutions. The APTES film formation was obtained in this work by 6% APTES in water/ethanol after 30 min experiment at ambient temperature is presented in Figure 7-22.

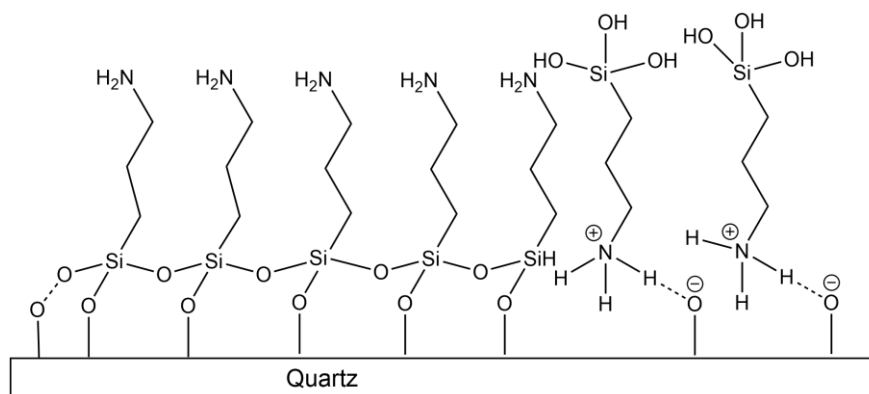


Figure 7-22. Schematic structure of 6% APTES film formed on quartz surface

All APhS treatments showed generally better performance in comparison with APTES treatments; however, the highest reduction was obtained at 0.06% APhS. More than 97.9% primary amine was measured by XPS for 0.06% APhS. Higher contact angle measurements were shown by APhS treatments compared with APTES, which could be due to different solvent (382) or the benzene rings of APhS molecules. However, the lowest contact angle was measured at 0.06% among all concentrations of APhS in both low $\text{SR}=4.77$ and high $\text{SR}=54.8$ solutions. Fairly consistent roughness (R_{rms}) was measured for all APhS treatments, but lower than APTES treatments. The lower roughness measurements are owing to a more uniform treatment of APhS in comparison with APTES; this was previously shown that the treatment of APhS on quartz surface resulted in more uniform surfaces (244, 392). The APhS film was formed in this research in solution of 0.06 APhS and toluene after 2 h experiment at ambient temperature is illustrated in Figure 7-23.

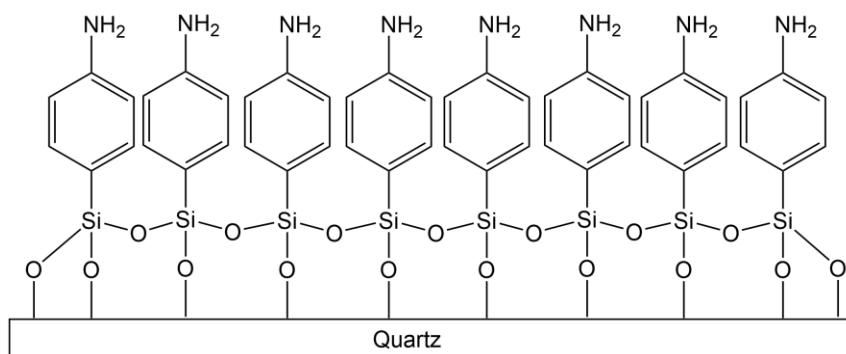


Figure 7-23. Schematic of possible APhS conformation on quartz surface at 0.06%

It can be stated that properties of surface treated by aminosilane (APTES and APhS in this work) such as wettability and roughness are completely dependent on the structure and orientation of the treatments which can be studied by measuring the primary amine content by XPS. In addition, the reduction of calcium carbonate scale deposition on the quartz surfaces is mainly correlated to primary amine content which represents conformation of the film on the substrate; this was shown earlier in this chapter. Since the physical properties of APTES and APhS surfaces such as roughness and wettability are embedded in the chemical property (surface composition) of the film, it can be emphasised that in this work the chemical property of the film is dominant.

Chapter 8

Conclusion and Future Work

8.1 Summary of the results

The main objective of this study was to investigate other possible mitigation actions in order to reduce the risk of scaling near the wellbore area, which simultaneously does not introduce any additional damage to the formation like squeeze treatment. A new methodology was tested by coating internal grain of near wellbore in order to reduce the tendency of scaling to the rock formation. The feasibility of this idea was demonstrated by film formation and scale experiments. The purpose, here, was not to develop the methodology to be ready for implementation in an oilfield; however, it was attempted to firstly demonstrate the potential of the idea and to secondly comprehend the surface characterisation of the films to help further development in future. The method changes the surface chemistry of the internal rock surface to reduce the tendency of scaling on the surface. The main results of each chapter are presented below.

8.1.1 Chapter 4: kinetics of film formation on quartz surface

The kinetics of APTES-films on quartz crystal surfaces at different concentrations (2-8%) in a solution of ethanol and water (95/5 v/v) was studied. Self-Assembled Monolayers (SAMs) of APTES on quartz substrates were investigated by Quartz Crystal Microbalance (QCM). Langmuir isotherm was used to interpret the adsorption of 3-aminopropyltriethoxysilane (APTES) molecules on crystal quartz surfaces.

- Although a complete surface coverage of APTES on crystal quartz surfaces was not achieved, a reasonable coverage of APTES molecules up to 91% was obtained.

- ChemDraw simulation was applied to estimate the amount of APTES required forming a SAM layer on crystal quartz surfaces. It was shown that

approximately $0.5 \mu\text{g}/\text{cm}^2$ is required to create an APTES film on the quartz surface.

- It was demonstrated that it is possible to create a SAM of APTES on quartz surface in 30 minutes in solution of ethanol and water (95/5 v/v) at ambient temperature.

8.1.2 Chapter 5: performance of APTES- and APhS-treated surfaces

In this chapter, the tendency of APTES and p-aminophenyltrimethoxysilane (APhS) treatments to CaCO_3 scale deposition was studied in both low $\text{SR}=4.77$ and high $\text{SR}=54.8$ solutions at 80°C . Different concentrations of APTES (0.5-8%) and APhS (0.03-0.24%) was used to treat the quartz surface for scale experiments. The amount of calcium carbonate scale deposition on treated surfaces was measured by microbalance to compare with the blank quartz surface.

- The amount of CaCO_3 deposition on treated quartz surface significantly reduced compared with the blank surface.
- 95% and 91% of calcium carbonate deposition reduced using the 0.06% APhS in low= 4.77 and high= 54.8 SR solutions, respectively.
- Generally better performance was seen by APhS treatment in both low= 4.77 and high= 54.8 SR solutions.
- The treated quartz surface by 6% APTES reduced the amount of CaCO_3 deposition by 86% and 70% in low= 4.77 and high= 54.8 SR solutions, respectively.

8.1.3 Chapter 6: Characterisation of APTES and APhS treatments

Various characterization methods were employed in Chapter 6 to better understand the results of scale tests in Chapter 5. Surface compositions, wettability and roughness of the treatments were analyzed by X-ray Photoelectron Spectroscopy (XPS), contact angle measurement and 3D optical profilometer;

respectively. Based on the results of this chapter, the film structure of each concentration for both APTES and APhS treatments were proposed.

- Generally, higher primary amine content was observed by APhS treatments than APTES with the maximum of 98% and 87.4%, respectively.
- Higher primary amine content was seen with higher ranges (2-8%) of APTES concentrations. In addition, two ranges of wettability were measured for APTES-treated quartz with hydrophilic surface for lower ranges (2-8%).
- Due to APhS structure and use of hydrophobic solvent, higher contact angle was observed for APhS-treated quartz.
- Smoother substrates were observed by APhS treatments than APTES.
- Based on primary amine, roughness and wettability of the treated surfaces, the possible film structures on the quartz surface for both APTES and APhS for all concentrations were described in Chapter 7.

8.1.4 Chapter 7: Discussion

The main objective of Chapter 7 was to discuss the interpretation of Chapter 6 in order to explain the results of Chapter 5.

- It was shown that the main characteristic of the surface enabling the interpretation of the tendency of CaCO_3 scale deposition is primary amine content. Although other properties such as wettability and roughness affected the scale deposition, the effects of these characteristics can be neglected.
- Film conformation on the quartz surface is capable of explaining the behavior of the treated surfaces in reduction of CaCO_3 scale deposition.
- The main contributions of each Chapter were discussed in this chapter.

8.2 Suggestions for future work

The feasibility of protecting the near wellbore by creating an-anti scale rock surface has been demonstrated in this research. The preliminary results are promising and show the potential of applying this technique near the wellbore.

However, more investigations are required before using this technique in an oil field. Hence, the main future work in order to develop the technology for field applications is listed below into two main groups.

8.2.1 The formation of anti-scale films on the surface

1. Formation of APTES and APhS films on a representative rock surface and evaluating the characteristics of the film .
2. Applying APTES and APhS films at higher range of temperatures (80-100°C) followed by analyzing the properties of the formed films.
3. Applying the APTES and APhS in more acceptable and close to the injection fluid in the oil and gas industry.
4. Investigating the effects of the experiments time. For example, increasing the time of APTES formation with lower concentrations and comparing the results with the results of this work.
5. Employing Atomic Force Microscopy (AFM) technique to better understand the film formed on the surface.
6. Considering other chemicals as anti-scale treatments on the surface.
7. Applying anti-scale chemicals in a QCM with ability of flowing the chemicals.

8.2.2 The tendency of mineral scale to the treated surface

1. Running core flood tests to assess the treated films on the rock surface in terms of scale reduction.
2. Testing the behavior of the treated surface to scale deposition in a longer time.
3. Investigating the treated surfaces to the other scale deposition such as BaSO_4 .
4. Employing XRD technique to better study the morphology of the scale deposited on the surfaces.
5. Studying the scale tendency in dynamic experiments like coreflood experiment.
6. Investigating the durability of the films by removing the scale from the surface and repeat the scale tests.
7. Employing CT- or micro CT-scan to monitor the scale deposition in-situ in a dynamic condition.

Chapter 9 Reference

1. Hughes, B. Mineral Scale in the Oilfield. Houston: bakerhughes.com, 2011.
2. Tantayakom, V., Fogler, H.S., Charoensirithavorn, P., Chavadej, S. Kinetic Study of Scale Inhibitor Precipitation in Squeeze Treatment. *Crystal Growth & Design*. 2004, 5(1), pp.329-335.
3. Cheong, W.C. Biomimetic Approach to Anti-Fouling Surfaces. PhD thesis, The University of Leeds, 2010.
4. Eroini, V. Kinetic study of calcium carbonate formation and inhibition by using an in-situ flow cell. PhD thesis, 2011.
5. Martinod, A.C. An integrated study of CaCO₃ formation and inhibition. PhD thesis, The University of Leeds, 2008.
6. Wang, Z. Aspect of surface energy and adhesion. PhD thesis, The University of Leeds, 2006.
7. Jaouhari, R., Benbachir, A., Guenbour, A., Gabrielli, C., Garcia-Jareno, J., Maurin, G. Influence of water composition and substrate on electrochemical scaling. *Journal of the Electrochemical Society*. 2000, 147(6), pp.2151-2161.
8. Zhao, Q., Liu, Y., Wang, C., Wang, S., Muller-Steinhagen, H. Effect of surface free energy on the adhesion of biofouling and crystalline fouling. *Chemical Engineering Science*. 2005, 60(17), pp.4858-4865.
9. Yang, Q.F., Ding, J., Shen, Z.Q. Investigation on fouling behaviors of low-energy surface and fouling fractal characteristics. *Chemical Engineering Science*. 2000, 55(4), pp.797-805.
10. Moghadasi, J., Jamialahmadi, M., Müller-Steinhagen, H., Sharif, A., Ghalebabor, A., Izadpanah, M.R., Motaie, E. Scale Formation in Iranian Oil Reservoir and Production Equipment During Water Injection. In: 2003/1/1/. SPE: Society of Petroleum Engineers.
11. Jordan, M.M., Sjuraether, K., Collins, I.R., Feasey, N.D., Emmons, D. Life Cycle Management of Scale Control within Subsea Fields and its Impact on Flow Assurance, Gulf of Mexico and the North Sea Basin. In: 2001/1/1/. SPE: Society of Petroleum Engineers.
12. Kalfayan, L. Production Enhancement with Acid simulation. Tulsa: Penn Well, 2008.
13. Reddy, M.M., Nancollas, G.H. The crystallization of calcium carbonate : I. Isotopic exchange and kinetics. *Journal of Colloid and Interface Science*. 1971, 36(2), pp.166-172.
14. Tantayakom, V., Sreethawong, T., Fogler, H.S., de Moraes, F.F., Chavadej, S. Scale inhibition study by turbidity measurement. *Journal of Colloid and Interface Science*. 2005, 284(1), pp.57-65.
15. Eroini, V., Kapur, N., Neville, A., Euvrard, M. Preventing Scale Formation Using Modified Surfaces. In: 13-17 March 2011. NACE International.
16. Kazemi, N., Wilson, M., Kapur, N., Fleming, N., Neville, A. Preventing Adhesion of Scale on Rock by Nanoscale Modification of the Surface. In: SPE International Oilfield Nanotechnology Conference, 12-14 June 2012, Noordwijk, The Netherlands. Society of Petroleum Engineers, 2012.
17. Brecevic, L., Kralj, D. On calcium carbonates: from fundamental research to application. *Croatica Chemica Acta*. 2007, 80(3-4), pp.467-484.
18. Hasson, D., Bramson, D., Limoni-Relis, B., Semiat, R. Influence of the flow system on the inhibitory action of CaCO₃ scale prevention additives. *Desalination*. 1997, 108(1-3), pp.67-79.
19. CHEN, T. New Insights Into the Mechanisms of Calcium Carbonate Mineral Scale Formation and Inhibition. PhD thesis. 2005, Heriot-Watt University, Edinburgh, UK, p.15.

20. Tlili, M.M., Ben Amor, M., Gabrielli, C., Joiret, S., Maurin, G., Rousseau, P. Characterization of CaCO₃ hydrates by micro-Raman spectroscopy. *Journal of Raman Spectroscopy*. 2002, 33(1), pp.10-16.
21. Mukkamala, S.B., Anson, C.E., Powell, A.K. Modelling calcium carbonate biomineralisation processes. *Journal of Inorganic Biochemistry*. 2006, 100(5–6), pp.1128-1138.
22. Morizot, A., Neville, A., Hodgkiess, T. Studies of the deposition of CaCO₃ on a stainless steel surface by a novel electrochemical technique. *Journal of Crystal Growth*. 1999, 198–199, Part 1(0), pp.738-743.
23. Abdel-Aal, N., Satoh, K., Sawada, K. Study of the adhesion mechanism of CaCO₃ using a combined bulk chemistry/QCM technique. *Journal of Crystal Growth*. 2002, 245(1–2), pp.87-100.
24. Meyer, H.J. The influence of impurities on the growth rate of calcite. *Journal of Crystal Growth*. 1984, 66(3), pp.639-646.
25. Konno, H., Nanri, Y., Kitamura, M. Effect of NaOH on aragonite precipitation in batch and continuous crystallization in causticizing reaction. *Powder Technology*. 2003, 129(1–3), pp.15-21.
26. Sabbides, T.G., Koutsoukos, P.G. The crystallization of calcium carbonate in artificial seawater; role of the substrate. *Journal of Crystal Growth*. 1993, 133(1–2), pp.13-22.
27. Luft, J.R., DeTitta, G.T. A method to produce microseed stock for use in the crystallization of biological macromolecules. *Acta Crystallographica Section D-Biological Crystallography*. 1999, 55, pp.988-993.
28. Larson, T.E.a.A.M.B. Calcium Carbonate Saturation Index and Alkalinity Interpretations. American Water Works Association. 1942, 34(11).
29. Chen, T. NEW INSIGHTS INTO THE MECHANISMS OF CALCIUM CARBONATE MINERAL SCALE FORMATION AND INHIBITION. PhD thesis, Heriot-Watt University, 2005.
30. Sohnle, O., Mullin, J.W. Method for Determination of Precipitation Induction Periods. *Journal of Crystal Growth*. 1978, 44(4), pp.377-382.
31. E., N.A. Kinetics of Precipitation. Pergamon: Oxford, 1964.
32. Mullin, J.W. *Crystallization*, 2nd ed. Butterworths London, 1972.
33. He, S., Oddo, J.E., Tomson, M.B. The Nucleation Kinetics of Calcium Sulfate Dihydrate in NaCl Solutions up to 6 m and 90°C. *Journal of Colloid and Interface Science*. 1994, 162(2), pp.297-303.
34. Sohnle, O., Mullin, J.W. Interpretation of crystallization induction periods. *Journal of Colloid and Interface Science*. 1988, 123(1), pp.43-50.
35. He, S.L., Oddo, J.E., Tomson, M.B. The Inhibition of Gypsum and Barite Nucleation in NaCl Brines at Temperatures from 25-Degrees-C to 90-Degrees-C. *Applied Geochemistry*. 1994, 9(5), pp.561-567.
36. Lancia, A., Musmarra, D., Prisciandaro, M. Measuring induction period for calcium sulfate dihydrate precipitation. *Aiche Journal*. 1999, 45(2), pp.390-397.
37. Sohnle, O., Mullin, J.W. Precipitation of calcium carbonate. *Journal of Crystal Growth*. 1982, 60(2), pp.239-250.
38. Nancollas, G.H., Liu, S.T. CRYSTAL-GROWTH AND DISSOLUTION OF BARIUM SULFATE. *Society of Petroleum Engineers Journal*. 1975, 15(6), pp.509-516.
39. Pernot, B., Euvrard, M., Simon, P. Effects of iron and manganese on the scaling potentiality of water. *Journal of Water Services Research and Technology-Aqua*. 1998, 47(1), pp.21-29.
40. Pernot, Euvrard, Simon. Effects of iron and manganese on the scaling potentiality of water. *Aqua*. 1998, 47(1), pp.21-29.
41. H., R. *Chemical water treatment: principle practice*. VCH PUB ed. Cambridge, 1996.

42. Garside, J., Davey, R.J. SECONDARY CONTACT NUCLEATION - KINETICS, GROWTH AND SCALE-UP. Chemical Engineering Communications. 1980, 4(4-5), pp.393-424.
43. Nancollas, G.H. Kinetics of crystal growth from solution. Journal of Crystal Growth. 1968, 3-4, pp.335-339.
44. Hahuest, M., Kleber, W. Ein Beitrag zur Kinetik der Fallungskristallization. Kolloid Z. 1959, 162, pp.36-40.
45. Mullin, J.W. Crystallisation. 4th ed. London: Butterworths & Co, 2001.
46. Ben Amor, M., Zgolli, D., Tlili, M.M., Manzola, A.S. Influence of water hardness, substrate nature and temperature on heterogeneous calcium carbonate nucleation. Desalination. 2004, 166(1-3), pp.79-84.
47. Khamskii, E. Crystallization from Solutions. New York: Kluwer Academic Publishers, 1969.
48. V., K.E. Crystallization From Solutions. Consultants Bureau: New York, 1969.
49. Chalmers, B. Principles of Solidification. Huntington: Robert E. Krieger Co., 1964.
50. H., N.G. Physical chemical studies of its formation and prevention. Symposium on 'Chemicals in the Oil Industry. 1985, pp.143-150.
51. Botsaris, G.D. 'Industrial Crystallization'. New York: Plenum Press, 1976.
52. Estrin, J. 'Preparation and Properties of Solid State Materials'. New York: Marcel Dekker, 1976.
53. Garside, J., Larson, M.A. DIRECT OBSERVATION OF SECONDARY NUCLEI PRODUCTION. Journal of Crystal Growth. 1978, 43(6), pp.694-704.
54. Klepetsanis, P.G., Lampeas, N., Kioupis, N., Koutsoukos, P.G. The effect of mineral deposits on stainless steel. 1995.
55. Söhnel, O.G.J. Precipitation : basic principles and industrial applications. Oxford [England]; Boston: Butterworth-Heinemann, 1992.
56. Nancollas, G.H., Purdie, N. The kinetics of crystal growth. Quarterly Reviews, Chemical Society. 1964, 18(1), pp.1-20.
57. Levi, A.C., Kotrla, M. Theory and simulation of crystal growth. Journal of Physics-Condensed Matter. 1997, 9(2), pp.299-344.
58. Mott, N.F. THEORY OF CRYSTAL GROWTH. Nature. 1950, 165(4191), pp.295-297.
59. Amjad, Z. Mineral scale formation and inhibition. Plenum Press, New York. 1995, pp.33-46.
60. Todd, A.C., Yuan, M. D. Barium and Strontium Sulfate Solid Solution Formation in Relation to North Sea Scaling Problems SPE Production Engineering. 1990, 5(3), pp.279-285.
61. Reddy, M.M., Nancolla, G.H. CRYSTALLIZATION OF CALCIUM CARBONATE .1. ISOTOPIC EXCHANGE AND KINETICS. Journal of Colloid and Interface Science. 1971, 36(2), pp.166-&.
62. Wang, Z. Mineral scale formation -aspect of surface energy and adhesion. PhD thesis, University of Leeds, 2006.
63. Packham, D.E. Handbook of Adhesion. Harlow Longman: New York, 1992.
64. Oliveira, R. Understanding adhesion: A means for preventing fouling. Experimental Thermal and Fluid Science. 1997, 14(4), pp.316-322.
65. Adamczyk, Z., Weronki, P. Application of the DLVO theory for particle deposition problems. Advances in Colloid and Interface Science. 1999, 83(1-3), pp.137-226.
66. Ninham, B.W. On progress in forces since the DLVO theory. Advances in Colloid and Interface Science. 1999, 83(1-3), pp.1-17.
67. Comyn, J. Adhesion science. The Royal Society of Chemistry, 1997.
68. Wenzel, R.N. Resistance of solid surfaces to wetting by water. Industrial and Engineering Chemistry. 1936, 28, pp.988-994.

69. Wenzel, R.N. SURFACE ROUGHNESS AND CONTACT ANGLE. *Journal of Physical and Colloid Chemistry*. 1949, 53(9), pp.1466-1467.
70. Cassie, A.B.D. CONTACT ANGLES. *Discussions of the Faraday Society*. 1948, 3, pp.11-16.
71. Fürstner, R., Barthlott, W., Neinhuis, C., Walzel, P. Wetting and Self-Cleaning Properties of Artificial Superhydrophobic Surfaces. *Langmuir*. 2005, 21(3), pp.956-961.
72. Ji, J., Fu, J.H., Shen, J.C. Fabrication of a superhydrophobic surface from the amplified exponential growth of a multilayer. *Advanced Materials*. 2006, 18(11), pp.1441-+.
73. Zhang, J.L., Li, J.A., Han, Y.C. Superhydrophobic PTFE surfaces by extension. *Macromolecular Rapid Communications*. 2004, 25(11), pp.1105-1108.
74. Quere, D. Non-sticking drops. *Reports on Progress in Physics*. 2005, 68(11), pp.2495-2532.
75. Kwok, D.Y., Lam, C.N.C., Li, A., Leung, A., Wu, R., Mok, E., Neumann, A.W. Measuring and interpreting contact angles: a complex issue. *Colloids and Surfaces a-Physicochemical and Engineering Aspects*. 1998, 142(2-3), pp.219-235.
76. Furstner, R., Barthlott, W., Neinhuis, C., Walzel, P. Wetting and self-cleaning properties of artificial superhydrophobic surfaces. *Langmuir*. 2005, 21(3), pp.956-961.
77. Ledion J., L.P., Labbe J. P. Determination du caractere incrustant d'une eau par un essai d'entartrage accelere. 1985.
78. Ellis, A.J. THE SOLUBILITY OF CALCITE IN CARBON DIOXIDE SOLUTIONS. *American Journal of Science*. 1959, 257(5), pp.354-365.
79. Kralj, D., Vdovic, N. The influence of some naturally occurring minerals on the precipitation of calcium carbonate polymorphs. *Water Research*. 2000, 34(1), pp.179-184.
80. Cheng, B., Lei, M., Yu, J., Zhao, X. Preparation of monodispersed cubic calcium carbonate particles via precipitation reaction. *Materials Letters*. 2004, 58(10), pp.1565-1570.
81. Matsumoto, M., Fukunaga, T., Onoe, K. Polymorph control of calcium carbonate by reactive crystallization using microbubble technique. *Chemical Engineering Research and Design*. 2010, 88(12), pp.1624-1630.
82. Feng, B., Yong, A.K., An, H. Effect of various factors on the particle size of calcium carbonate formed in a precipitation process. *Materials Science and Engineering a-Structural Materials Properties Microstructure and Processing*. 2007, 445, pp.170-179.
83. Chen, T., Neville, A., Yuan, M. Calcium carbonate scale formation—assessing the initial stages of precipitation and deposition. *Journal of Petroleum Science and Engineering*. 2005, 46(3), pp.185-194.
84. Koutsoukos, P.G., Kontoyannis, C.G. PRECIPITATION OF CALCIUM-CARBONATE IN AQUEOUS-SOLUTIONS. *Journal of the Chemical Society-Faraday Transactions I*. 1984, 80, pp.1181-1192.
85. L., C.J. The effect of supersaturation and flow condition on the initiation of scale formation. *Transactions of The Institution of Chemical Engineers*. 1964, 42, pp.T24-T34.
86. Amor, M.B., Zgolli, D., Tlili, M.M., Manzola, A.S. Influence of water hardness, substrate nature and temperature on heterogeneous calcium carbonate nucleation. *Desalination*. 2004, 166(0), pp.79-84.
87. Turner, C.W., Smith, D.W. Calcium carbonate scaling kinetics determined from radiotracer experiments with calcium-47. *Industrial & Engineering Chemistry Research*. 1998, 37(2), pp.439-448.
88. Bohnet, M., Augustin, W. EFFECT OF SURFACE-STRUCTURE AND PH-VALUE ON FOULING BEHAVIOR OF HEAT-EXCHANGERS. 1993.

89. Augustin, W., Bohnet, M. INFLUENCE OF THE RATIO OF FREE HYDROGEN-IONS ON CRYSTALLIZATION FOULING. *Chemical Engineering and Processing*. 1995, 34(2), pp.79-85.
90. Kjellin P., H.K., Nyden M. A: *Physicochemical and Engineering Aspects*. 2001.
91. Yu, J.G., Lei, M., Cheng, B., Zhao, X.J. Facile preparation of calcium carbonate particles with unusual morphologies by precipitation reaction. *Journal of Crystal Growth*. 2004, 261(4), pp.566-570.
92. Oddo, J.E., Tomson, M.B. SIMPLIFIED CALCULATION OF CaCO₃ SATURATION AT HIGH-TEMPERATURES AND PRESSURES IN BRINE SOLUTIONS. *Journal of Petroleum Technology*. 1982, 34(7), pp.1583-1590.
93. Dyer, S.J., Graham, G.M. The effect of temperature and pressure on oilfield scale formation. *Journal of Petroleum Science and Engineering*. 2002, 35(1-2), pp.95-107.
94. Rice University, 2001.
95. Kitamura, M. Controlling factor of polymorphism in crystallization process. *Journal of Crystal Growth*. 2002, 237-239, Part 3(0), pp.2205-2214.
96. Han, Y.S., Hadiko, G., Fuji, M., Takahashi, M. Factors affecting the phase and morphology of CaCO₃ prepared by a bubbling method. *Journal of the European Ceramic Society*. 2006, 26(4-5), pp.843-847.
97. Zhou, G.T., Zheng, Y.F. Chemical synthesis of CaCO₃ minerals at low temperatures and implication for mechanism of polymorphic transition. *Neues Jahrbuch Fur Mineralogie-Abhandlungen*. 2001, 176(3), pp.323-343.
98. F., L. *Sedimentary Carbonate Minerals*. Berlin: Springer, 1973.
99. Given, R.K., Wilkinson, B.H. KINETIC CONTROL OF MORPHOLOGY, COMPOSITION, AND MINERALOGY OF ABIOTIC SEDIMENTARY CARBONATES. *Journal of Sedimentary Petrology*. 1985, 55(1), pp.109-119.
100. Euvrard, M., Filiatre, C., Crausaz, E. A cell to study in situ electrocrystallization of calcium carbonate. *Journal of Crystal Growth*. 2000, 216(1-4), pp.466-474.
101. Chen, T., Neville, A., Yuan, M. Influence of Mg²⁺ on CaCO₃ formation-bulk precipitation and surface deposition. *Chemical Engineering Science*. 2006, 61(16), pp.5318-5327.
102. Chen, T., Neville, A., Yuan, M. Assessing the effect of on scale formation-bulk precipitation and surface deposition. *Journal of Crystal Growth*. 2005, 275(1-2), pp.e1341-e1347.
103. Amjad, Z. *Mineral scale formation and inhibition*. New York: Plenum Press, 1995.
104. Cailleau, P. Importance de l'ion Mg⁺⁺ sur la croissance cristalline des carbonates de calcium en milieu libre. thesis, Montpellier, 1978.
105. Alexanderson. *The Mediterranean Basins as Natural Sedimentation Laboratories*. Dowdon ed. Stroudsburg: Hutchinson & Ross, 1980.
106. Kinsmann, D.J.J.P. *Symp. Chem of Sedimentary and Diagenetic Processes, Mineral. Soc. Great Britain and Ireland*, 1973.
107. Devos, O., Jakab, S., Gabrielli, C., Joiret, S., Tribollet, B., Picart, S. Nucleation-growth process of scale electrodeposition - influence of the magnesium ions. *Journal of Crystal Growth*. 2009, 311(18), pp.4334-4342.
108. Wada, N., Yamashita, K., Umegaki, T. EFFECTS OF DIVALENT-CATIONS UPON NUCLEATION, GROWTH AND TRANSFORMATION OF CALCIUM-CARBONATE POLYMORPHS UNDER CONDITIONS OF DOUBLE DIFFUSION. *Journal of Crystal Growth*. 1995, 148(3), pp.297-304.
109. Wada, N., Yamashita, K., Umegaki, T. Effects of silver, aluminum, and chrome ions on the polymorphic formation of calcium carbonate under conditions of double diffusion. *Journal of Colloid and Interface Science*. 1998, 201(1), pp.1-6.

110. Zeppenfeld, K. Prevention of CaCO₃ scale formation by trace amounts of copper (II) in comparison to zinc (II). *Desalination*. 2010, 252(1–3), pp.60-65.
111. Kaasa, B. MultiScale 7.1(C). Petrotech Norway. 2007.
112. Cavano, R.R. Understanding Scaling Indices And Calculating Inhibitor Dosages. In: 2005/1/1/. NACE: NACE International.
113. Prisyazhniuk, V.A. Prognosticating scale-forming properties of water. *Applied Thermal Engineering*. 2007, 27(8-9), pp.1637-1641.
114. Pitzer, K.S. ELECTROLYTE THEORY - IMPROVEMENTS SINCE DEBYE AND HUCKEL. *Accounts of Chemical Research*. 1977, 10(10), pp.371-377.
115. Pitzer, K.S. Thermodynamics of electrolytes. I. Theoretical basis and general equations. *The Journal of Physical Chemistry*. 1973, 77(2), pp.268-277.
116. Pitzer, K.S., Mayorga, G. Thermodynamics of electrolytes. II. Activity and osmotic coefficients for strong electrolytes with one or both ions univalent. *The Journal of Physical Chemistry*. 1973, 77(19), pp.2300-2308.
117. Ziauddin, W.W.F.M. Formation, Removal, and Inhibition of Inorganic Scale in the Oilfield Environment. Society of Petroleum Engineers, 2008.
118. Crabtree, M., et al. Fighting scale - Removal and prevention. *Oilfield Review*. 1999, pp.30-45.
119. Johnson, A., Eslinger, D., Larsen, H. An Abrasive Jetting Scale Removal System. In: 1998/1/1/. SPE: Society of Petroleum Engineers.
120. Martel, A.E.a.M.C. Chemistry of Metal Chelate Compounds. New York: Prentice-Hall. 1952.
121. Frenier, W.W., Wilson, D., Crump, D., Jones, L. Use of Highly Acid-Soluble Chelating Agents in Well Stimulation Services. In: 2000/1/1/. SPE: Society of Petroleum Engineers.
122. Geiger, G.E. Improve corrosion and deposition control in alkaline cooling water systems. *Hydrocarbon Processing*. 1996, 75(1), pp.93-98.
123. Thomas, P.A.a.M.A.M. A current review of polymeric structures and their practical significance in cooling water treatment in corrosion. In: NACE, Houston. 1985.
124. Colfen, H., Qi, L.M. A systematic examination of the morphogenesis of calcium carbonate in the presence of a double-hydrophilic block copolymer. *Chemistry-a European Journal*. 2001, 7(1), pp.106-116.
125. Warner, P.A.a.J. Green Chemistry: Theory and Practice. Oxford University Press., 1998.
126. Alford, D., Wheeler, A.P., Pettigrew, C. Biodegradation of thermally synthesized polyaspartate. *Journal of environmental polymer degradation*. 1994, 2(4), pp.225-236.
127. Estievenart, C., Kohler, N., Ropital, F., Fiaud, C. Mechanisms of Scale and Corrosion Inhibition by Polyaspartates. In: 2004/1/1/. NACE: NACE International.
128. Martinod, A., Euvrard, M., Foissy, A., Neville, A. Progressing the understanding of chemical inhibition of mineral scale by green inhibitors. *Desalination*. 2008, 220(1–3), pp.345-352.
129. Kavanagh, A.M., Rayment, T., Price, T.J. Inhibitor effects on calcite growth at low supersaturations. *Journal of the Chemical Society, Faraday Transactions*. 1990, 86(6), pp.965-972.
130. Verraest, D., Peters, J., Bekkum, H., Rosmalen, G. Carboxymethyl inulin: A new inhibitor for calcium carbonate precipitation. *Journal of the American Oil Chemists' Society*. 1996, 73(1), pp.55-62.
131. Kerver, J.K., Heilhecker, J.K. Scale Inhibition by the Squeeze Technique. 1969.
132. Ghorbani, N. Nanotechnology Enhanced Squeeze Treatments for Efficient Oilfield Scale Management. PhD thesis, University of Leeds, 2012.

133. Yuan, M.D., Sorbie, K.S., Todd, A.C., Atkinson, L.M., Riley, H., Gurden, S. The Modelling of Adsorption and Precipitation Scale Inhibitor Squeeze Treatments in North Sea Fields. In: SPE International Symposium on Oilfield Chemistry, 2-5 March 1993, New Orleans, Louisiana. 1993 Copyright 1993, Society of Petroleum Engineers, Inc. This paper was prepared for presentation at the SPE International Symposium on Oilfield Chemistry held in New Orleans, Louisiana, U.S.A., March 2-5, 1993.
134. Sorbie, K.S., Jiang, P., Yuan, M.D., Chen, P., Jordan, M.M., Todd, A.C. The Effect of pH, Calcium, and Temperature on the Adsorption of Phosphonate Inhibitor Onto Consolidated and Crushed Sandstone. In: SPE Annual Technical Conference and Exhibition, 10/03/1993, Houston, Texas. 1993 Copyright 1993, Society of Petroleum Engineers, Inc., 1993.
135. Pardue, J.E. A New Inhibitor for Scale Squeeze Applications. In: SPE International Symposium on Oilfield Chemistry, 01/01/1991, Anaheim, California. 1991, 1991.
136. Kahrwad, M., Sorbie, K.S., Boak, L.S. Coupled Adsorption/Precipitation of Scale Inhibitors: Experimental Results and Modeling. *Spe Production & Operations*. 2009, 24(3), pp.481-491.
137. Sorbie, K.S., Yuan, M.D., Chen, P., Todd, A.C., Wat, R.M.S. The Effect of pH on the Adsorption and Transport of Phosphonate Scale Inhibitor Through Porous Media. In: SPE International Symposium on Oilfield Chemistry, 03/02/1993, New Orleans, Louisiana. 1993 Copyright 1993, Society of Petroleum Engineers, Inc. This paper was prepared for presentation at the SPE International Symposium on Oilfield Chemistry held in New Orleans, Louisiana, U.S.A., March 2-5, 1993.
138. Sorbie, K.S. A General Coupled Kinetic Adsorption/Precipitation Transport Model for Scale Inhibitor Retention in Porous Media: I. Model Formulation. In: SPE International Conference on Oilfield Scale, 26-27 May 2010, Aberdeen, UK. Society of Petroleum Engineers, 2010.
139. Tantayakom, V., Fogler, H.S., Charoensirithavorn, P., Chavadej, S. Kinetic study of scale inhibitor precipitation in squeeze treatment. *Crystal Growth & Design*. 2005, 5(1), pp.329-335.
140. Rabaioli, M.R., Lockhart, T.P. Solubility and phase behavior of polyacrylate scale inhibitors. *Journal of Petroleum Science and Engineering*. 1996, 15(2-4), pp.115-126.
141. Przybylinski, J.L. Adsorption and Desorption Characteristics of Mineral Scale Inhibitors as Related to the Design of Squeeze Treatments. In: SPE International Symposium on Oilfield Chemistry, 02/08/1989, Houston, Texas. 1989, 1989.
142. Øystein Bache, Svante Nilsson. Ester Cross-Linking of Polycarboxylic Acid Scale Inhibitors as a Possible Means to Increase Inhibitor Squeeze Lifetime. International Symposium on Oilfield Scale, 26-27 January 2000, Aberdeen, United Kingdom. 2000, pp.60190-MS.
143. Jordan, M.M., Sorbie, K.S., Jiang, P., Yuan, M., Todd, A.C., Taylor, K. Mineralogical Controls on Inhibitor Adsorption/Desorption in Brent Group Sandstone and Their Importance in Predicting and Extending Field Squeeze Lifetimes. In: European Production Operations Conference and Exhibition, 15-17 March 1994, Aberdeen, United Kingdom. 1994 Copyright 1994, Society of Petroleum Engineers, Inc., 1994.
144. Graham, G.M. A Mechanistic Examination of the Factors Influencing Downhole BaSO₄ Oilfield Scale Inhibitors and the Design of New Species. PhD thesis, Heriot-Watt University, 1995.
145. Shen, D., Zhang, P., Kan, A.T., Fu, G., Alsaiani, H.A., Tomson, M.B. Control Placement of Scale Inhibitors in the Formation With Stable Ca-DTPMP Nanoparticle Suspension and its Transport Porous Media. SPE International Oilfield Scale Conference, 28-29 May 2008, Aberdeen, UK. 2008.

146. Zhang, H.,Mackay, E.J.,Chen, P.,Sorbie, K.S. Non-Equilibrium Adsorption and Precipitation of Scale Inhibitors: Corefloods and Mathematical Modelling. In: International Oil and Gas Conference and Exhibition in China, 11/07/2000, Beijing, China. Copyright 2000, Society of Petroleum Engineers Inc., 2000.
147. Vetter, O.J. The Chemical Squeeze Process Some New Information on Some Old Misconceptions. SPE Journal of Petroleum Technology. 1973, 25(3), pp.339-353.
148. Durham, D.K. Equations for Prediction of Scale Inhibitor Return After Squeeze Treatment. In: SPE California Regional Meeting, 03/23/1983, Ventura, California. 1983 Copyright 1983 Society of Petroleum Engineers of AIME, 1983.
149. King, G.E.,Warden, S.L. Introductory Work in Scale Inhibitor Squeeze Performance: Core Tests and Field Results. In: SPE International Symposium on Oilfield Chemistry, 02/08/1989, Houston, Texas. 1989 Copyright 1989, Society of Petroleum Engineers, 1989.
150. do Rosario, F.F.,Khalil, C.N.,Bezerra, M.C.M.,Rondinini, S.B. Process for the controlled fixing of scale inhibitor in subterranean formations. EP 0 781 729. 1997.
151. Hen, J. A Method for the Inhibition of Scale Deposition and Composition Therefor. WO/1994/003706. 1994.
152. Kan, A.T.,Fu, G.M.,Tomson, M.B.,Al-Thubaiti, M.,Xiao, A.J. Factors affecting scale inhibitor retention in carbonate-rich formation during squeeze treatment. Spe Journal. 2004, 9(3), pp.280-289.
153. Gdanski, R.D. Formation Mineralogy Impacts Scale Inhibitor Squeeze Designs. In: Europec/EAGE Conference and Exhibition, 9-12 June 2008 2008, Rome, Italy. Society of Petroleum Engineers, 2008.
154. Bates, C.I.,Collins, I.R.,Ravenscroft, P.D. Coated products and use thereof in oil fields 1997.
155. Collins, I.R.,Cowie, L.G.,Nicol, M.,Stewart, N.J. Field Application of a Scale Inhibitor Squeeze Enhancing Additive. Spe Production & Operations. 1999, 14(1), pp.21-29.
156. Bourne, H.M.,Booth, S.L.,Brunger, A. Combining Innovative Technologies To Maximize Scale Squeeze Cost Reduction. In: SPE International Symposium on Oilfield Chemistry, 16-19 February 1999, Houston, Texas. Society of Petroleum Engineers, 1999.
157. Jordan, M.M.,Sorbie, K.S.,Yuan, M.D.,Taylor, K.,Hourston, K.E.,Ramstad, K.,Griffin, P. Static and Dynamic Adsorption of Phosphonate and Polymeric Scale Inhibitors Onto Reservoir Core From Laboratory Tests to Field Application. In: SPE International Symposium on Oilfield Chemistry, 01/01/1995, San Antonio, Texas. 1995 Copyright 1995, Society of Petroleum Engineers, Inc., 1995.
158. Meyers, K.O.,Skillman, H.L.,Herring, G.D. Control of Formation Damage at Prudhoe Bay, Alaska, by Inhibitor Squeeze Treatment. SPE Journal of Petroleum Technology. 1985, 37(6), pp.1019-1034.
159. Tomson, M.B.,Fu, G.,Watson, M.A.,Kan, A.T. Mechanisms Of Mineral Scale Inhibition. In: International Symposium on Oilfield Scale, 01/01/2002, Aberdeen, United Kingdom. Copyright 2002, Society of Petroleum Engineers Inc., 2002.
160. Jordan, M.M.,Sorbie, K.S.,Chen, P.,Armitage, P.,Hammond, P.,Taylor, K. The Design of Polymer and Phosphonate Scale Inhibitor Precipitation Treatments and the Importance of Precipitate Solubility in Extending Squeeze Lifetime. In: International Symposium on Oilfield Chemistry, 01/01/1997, Houston, Texas. 1997.

161. Baraka-Lokmane, S., Sorbie, K.S. Effect of pH and scale inhibitor concentration on phosphonate-carbonate interaction. *Journal of Petroleum Science and Engineering*. 70, pp.10-27.
162. Graham, G.M., Boak, L.S., Sorbie, K.S. The Influence of Formation Calcium and Magnesium on the Effectiveness of Generically Different Barium Sulphate Oilfield Scale Inhibitors. *Spe Production & Operations*. 2003, (1), pp.28-44.
163. Wu, Z., Davidson, J.H., Francis, L.F. Effect of water chemistry on calcium carbonate deposition on metal and polymer surfaces. *Journal of Colloid and Interface Science*. 2010, 343(1), pp.176-187.
164. Sheikholeslami, R. Composite fouling - inorganic and biological: A review. *Environmental Progress*. 1999, 18(2), pp.113-122.
165. Li, Q., Elimelech, M. Organic Fouling and Chemical Cleaning of Nanofiltration Membranes: Measurements and Mechanisms. *Environmental Science & Technology*. 2004, 38(17), pp.4683-4693.
166. Elimelech, M., Xiaohua, Z., Childress, A.E., Seungkwan, H. Role of membrane surface morphology in colloidal fouling of cellulose acetate and composite aromatic polyamide reverse osmosis membranes. *Journal of Membrane Science*. 1997, 127(1), pp.101-109.
167. Jucker, C., Clark, M.M. Adsorption of aquatic humic substances on hydrophobic ultrafiltration membranes. *Journal of Membrane Science*. 1994, 97(0), pp.37-52.
168. Pronk, P., Infante Ferreira, C.A., Witkamp, G.J. Prevention of fouling and scaling in stationary and circulating liquid-solid fluidized bed heat exchangers: Particle impact measurements and analysis. *International Journal of Heat and Mass Transfer*. 2009, 52(15-16), pp.3857-3868.
169. Cowling, M.J., Hodgkiess, T., Parr, A.C.S., Smith, M.J., Marrs, S.J. An alternative approach to antifouling based on analogues of natural processes. *Science of The Total Environment*. 2000, 258(1-2), pp.129-137.
170. Cheng, Y.H., Zou, Y., Cheng, L., Liu, W. Effect of the microstructure on the properties of Ni-P deposits on heat transfer surface. *Surface and Coatings Technology*. 2009, 203(12), pp.1559-1564.
171. Su, X.J., Zhao, Q., Wang, S., Bendavid, A. Modification of diamond-like carbon coatings with fluorine to reduce biofouling adhesion. *Surface & Coatings Technology*. 2010, 204(15), pp.2454-2458.
172. Muthukumar, T., Aravinthan, A., Lakshmi, K., Venkatesan, R., Vedaprakash, L., Doble, M. Fouling and stability of polymers and composites in marine environment. *International Biodeterioration & Biodegradation*. 2011, 65(2), pp.276-284.
173. Zhao, Q., Wang, S., Müller-Steinhagen, H. Tailored surface free energy of membrane diffusers to minimize microbial adhesion. *Applied Surface Science*. 2004, 230(1-4), pp.371-378.
174. Krishnan, S., Wang, N., Ober, C.K., Finlay, J.A., Callow, M.E., Callow, J.A., Hexemer, A., Sohn, K.E., Kramer, E.J., Fischer, D.A. Comparison of the Fouling Release Properties of Hydrophobic Fluorinated and Hydrophilic PEGylated Block Copolymer Surfaces: Attachment Strength of the Diatom *Navicula* and the Green Alga *Ulva*. *Biomacromolecules*. 2006, 7(5), pp.1449-1462.
175. Liu, C.X., Zhang, D.R., He, Y., Zhao, X.S., Bai, R. Modification of membrane surface for anti-biofouling performance: Effect of anti-adhesion and anti-bacteria approaches. *Journal of Membrane Science*. 2010, 346(1), pp.121-130.
176. Premathilaka, S., Hyland, M., Chen, X., Bansal, B. A study of the effects of surface chemistry on the initial deposition mechanisms of dairy fouling. *Food and Bioproducts Processing*. 2006, 84(C4), pp.265-273.

177. Chambers, L.D., Stokes, K.R., Walsh, F.C., Wood, R.J.K. Modern approaches to marine antifouling coatings. *Surface & Coatings Technology*. 2006, 201(6), pp.3642-3652.
178. Ledion, J., Braham, C., Hui, F. Anti-scaling properties of copper. *Journal of Water Supply Research and Technology-Aqua*. 2002, 51(7), pp.389-398.
179. Macadam, J., Parsons, S.A. Calcium carbonate scale control, effect of material and inhibitors. *Water Science and Technology*. 2004, 49(2), pp.153-159.
180. Müller-Steinhagen, H., Zhao, Q. Investigation of low fouling surface alloys made by ion implantation technology. *Chemical Engineering Science*. 1997, 52(19), pp.3321-3332.
181. Labille, S., Neville, A., Graham, G.M., Boak, L.S. An Assessment of Adhesion of Scale and Electrochemical Pre-treatment for the Prevention of Scale Deposition on Metal Surfaces. In: *International Symposium on Oilfield Scale*, 30-31 January 2002, Aberdeen, United Kingdom. Copyright 2002, Society of Petroleum Engineers Inc., 2002.
182. Singh, B.P., Besra, L., Bhattacharjee, S. Factorial design of experiments on the effect of surface charges on stability of aqueous colloidal ceramic suspension. *Colloids and Surfaces a-Physicochemical and Engineering Aspects*. 2002, 204(1-3), pp.175-181.
183. Moritz, T., Benfer, S., Arki, P., Tomandl, G. Investigation of ceramic membrane materials by streaming potential measurements. *Colloids and Surfaces A: Physicochemical and Engineering Aspects*. 2001, 195(1-3), pp.25-33.
184. Kazi, S.N., Duffy, G.G., Chen, X.D. Mineral scale formation and mitigation on metals and a polymeric heat exchanger surface. *Applied Thermal Engineering*. 2010, 30(14-15), pp.2236-2242.
185. Rosmaninho, R., Santos, O., Nylander, T., Paulsson, M., Beuf, M., Benezech, T., Yiantsios, S., Andritsos, N., Karabelas, A., Rizzo, G., Mueller-Steinhagen, H., Melo, L.F. Modified stainless steel surfaces targeted to reduce fouling - Evaluation of fouling by milk components. *Journal of Food Engineering*. 2007, 80(4), pp.1176-1187.
186. Ren, X.G., Li, T.F., Zhao, Q. Effect of surface treatment on flow boiling heat transfer coefficient in CaSO₄ containing water. *Chinese Journal of Chemical Engineering*. 2006, 14(1), pp.122-126.
187. Zhao, Q., Wang, X. Heat transfer surfaces coated with fluorinated diamond-like carbon films to minimize scale formation. *Surface and Coatings Technology*. 2005, 192(1), pp.77-80.
188. Frenier, W.W., Ziauddin, M. Formation, Removal, and Inhibition of Inorganic Scale in the Oilfield Environment. Society of Petroleum Engineers, 2008.
189. Cheong, W.C., Gaskell, P.H., Neville, A. Substrate effect on surface adhesion/crystallisation of calcium carbonate. *Journal of Crystal Growth*. 2013, 363(0), pp.7-21.
190. Li, W., Wu, P. Biomimetic synthesis of monodisperse rosette-like calcite mesocrystals regulated by carboxymethyl cellulose and the proposed mechanism : An unconventional rhombohedra-stacking route. *CrystEngComm*. 2009, 11(11), pp.2466-2474.
191. Henderson, G.E., Murray, B.J., McGrath, K.M. Controlled variation of calcite morphology using simple carboxylic acids. *Journal of Crystal Growth*. 2008, 310(18), pp.4190-4198.
192. Forster, M., Augustin, W., Bohnet, M. Influence of the adhesion force crystal/heat exchanger surface on fouling mitigation. *Chemical Engineering and Processing*. 1999, 38(4-6), pp.449-461.
193. Bargir, S., Dunn, S., Jefferson, B., Macadam, J., Parsons, S. The use of contact angle measurements to estimate the adhesion propensity of calcium

- carbonate to solid substrates in water. *Applied Surface Science*. 2009, 255(9), pp.4873-4879.
194. Zettler, H.U., Weiss, M., Zhao, Q., Müller-Steinhagen, H. Influence of surface properties and characteristics on fouling in plate heat exchangers. *Heat Transfer Engineering*. 2005, 26(2), pp.3-17.
 195. Wang, Z., Neville, A., Meredith, A. How And Why Does Scale Stick - Can The Surface Be Engineered To Decrease Scale Formation And Adhesion? In: 2005/1/1/. SPE: Society of Petroleum Engineers.
 196. Parsons, S.A., MacAdam, J. Scaling On Heat Transfer Surfaces: Chemical Versus Non-chemical Control. In: 28 March-1 April 2004. NACE International, 2004.
 197. Callow, M.E., Fletcher, R.L. THE INFLUENCE OF LOW SURFACE-ENERGY MATERIALS ON BIOADHESION - A REVIEW. *International Biodeterioration & Biodegradation*. 1994, 34(3-4), pp.333-348.
 198. Keysar, S., Semiat, R., Hasson, D., Yahalom, J. Effect of Surface Roughness on the Morphology of Calcite Crystallizing on Mild Steel. *Journal of Colloid and Interface Science*. 1994, 162(2), pp.311-319.
 199. Herz, A., Malayeri, M.R., Müller-Steinhagen, H. Fouling of roughened stainless steel surfaces during convective heat transfer to aqueous solutions. *Energy Conversion and Management*. 2008, 49(11), pp.3381-3386.
 200. Quddus, A., Al-Hadrami, L.M. Influence of Solution Hydrodynamics on the Deposition of CaSO₄ Scale on Aluminum. *Journal of Thermophysics and Heat Transfer*. 2011, 25(1), pp.112-118.
 201. Kukulka, D.J., Devgun, M. Fouling surface finish evaluation. *Applied Thermal Engineering*. 2007, 27(7), pp.1165-1172.
 202. Förster, M., Augustin, W., Bohnet, M. Influence of the adhesion force crystal/heat exchanger surface on fouling mitigation. *Chemical Engineering and Processing: Process Intensification*. 1999, 38(4-6), pp.449-461.
 203. Rankin, B.H., Adamson, W.L. Scale formation as related to evaporator surface conditions. *Desalination*. 1973, 13(1), pp.63-87.
 204. Gedert, T., Bialuch, I., Augustin, W., Scholl, S. Extending the Induction Period of Crystallization Fouling Through Surface Coating. *Heat Transfer Engineering*. 2009, 30(10-11), pp.868-875.
 205. Cheong, W.C., Neville, A., Gaskell, P., Abbott, S. Using Nature to Provide Solutions to Calcareous Scale Deposition.
 206. Ulman, A. Formation and structure of self-assembled monolayers. *Chemical Reviews*. 1996, 96(4), pp.1533-1554.
 207. Swalen, J.D., Allara, D.L., Andrade, J.D., Chandross, E.A., Garoff, S., Israelachvili, J., McCarthy, T.J., Murray, R., Pease, R.F., Rabolt, J.F., Wynne, K.J., Yu, H. MOLECULAR MONOLAYERS AND FILMS. *Langmuir*. 1987, 3(6), pp.932-950.
 208. Love, J.C., Estroff, L.A., Kriebel, J.K., Nuzzo, R.G., Whitesides, G.M. Self-assembled monolayers of thiolates on metals as a form of nanotechnology. *Chemical Reviews*. 2005, 105(4), pp.1103-1169.
 209. Bigelow, W.C., Pickett, D.L., Zisman, W.A. OLEOPHOBIC MONOLAYERS .1. FILMS ADSORBED FROM SOLUTION IN NON-POLAR LIQUIDS. *Journal of Colloid Science*. 1946, 1(6), pp.513-538.
 210. Vuillaume, D., Boulas, C., Collet, J., Davidovits, J.V., Rondelez, F. Organic insulating films of nanometer thicknesses. *Applied Physics Letters*. 1996, 69(11), pp.1646-1648.
 211. Li, Y.S., Wang, Y., Tran, T., Perkins, A. Vibrational spectroscopic studies of (3-mercaptopropyl)trimethoxysilane sol-gel and its coating. *Spectrochimica Acta Part a-Molecular and Biomolecular Spectroscopy*. 2005, 61(13-14), pp.3032-3037.

212. Kerman, K., Ozkan, D., Kara, P., Meric, B., Gooding, J.J., Ozsoz, M. Voltammetric determination of DNA hybridization using methylene blue and self-assembled alkanethiol monolayer on gold electrodes. *Analytica Chimica Acta*. 2002, 462(1), pp.39-47.
213. Tlili, A., Abdelghani, A., Hleli, S., Maaref, M.A. Electrical characterization of a thiol SAM on gold as a first step for the fabrication of immunosensors based on a quartz crystal microbalance. *Sensors*. 2004, 4(6-7), pp.105-114.
214. Avseth, P., Dvorkin, J., Mavko, G., Rykkje, J. Rock physics diagnostic of North Sea sands: Link between microstructure and seismic properties. *Geophysical Research Letters*. 2000, 27(17), pp.2761-2764.
215. Nuzzo, R.G.A., D. L. J. Reversibly, non-covalent bound surface coating. 1983.
216. Allara, D.L., Nuzzo, R.G. Spontaneously organized molecular assemblies. 1. Formation, dynamics, and physical properties of n-alkanoic acids adsorbed from solution on an oxidized aluminum surface. *Langmuir*. 1985, 1(1), pp.45-52.
217. Allara, D.L., Nuzzo, R.G. Spontaneously organized molecular assemblies. 2. Quantitative infrared spectroscopic determination of equilibrium structures of solution-adsorbed n-alkanoic acids on an oxidized aluminum surface. *Langmuir*. 1985, 1(1), pp.52-66.
218. Wasserman, S.R., Tao, Y.T., Whitesides, G.M. STRUCTURE AND REACTIVITY OF ALKYL SILOXANE MONOLAYERS FORMED BY REACTION OF ALKYL TRICHLOROSILANES ON SILICON SUBSTRATES. *Langmuir*. 1989, 5(4), pp.1074-1087.
219. Banga, R., Yarwood, J., Morgan, A.M., Evans, B., Kells, J. FTIR and AFM Studies of the Kinetics and Self-Assembly of Alkyltrichlorosilanes and (Perfluoroalkyl)trichlorosilanes onto Glass and Silicon. *Langmuir*. 1995, 11(11), pp.4393-4399.
220. Silberzan, P., Leger, L., Ausserre, D., Benattar, J.J. Silanation of silica surfaces. A new method of constructing pure or mixed monolayers. *Langmuir*. 1991, 7(8), pp.1647-1651.
221. Monticelli, F., Toledano, M., Osorio, R., Ferrari, M. Effect of temperature on the silane coupling agents when bonding core resin to quartz fiber posts. *Dental Materials*. 2006, 22(11), pp.1024-1028.
222. Kowalczyk, D., Slomkowski, S., Chehimi, M.M., Delamar, M. Adsorption of aminopropyltriethoxy silane on quartz: An XPS and contact angle measurements study. *International Journal of Adhesion and Adhesives*. 1996, 16(4), pp.227-232.
223. Lieberzeit, P.A., Greibl, W., Stathopoulos, H., Dickert, F.L., Fischerauer, G., Bulst, W.E. Covalently anchored supramolecular monolayers on quartz surfaces for use in SAW sensors. *Sensors and Actuators B-Chemical*. 2006, 113(2), pp.677-683.
224. Kallury, K.M.R., Brennan, J.D., Krull, U.J. Depth Profiling Of Functionalized Silane Films On Quartz And Silicon Substrates And Of Urease Immobilized On Such Films By Angle-Resolved X-ray Photoelectron-Spectroscopy. *Analytical Chemistry*. 1995, 67(15), pp.2625-2634.
225. Touzi, H., Sakly, N., Kalfat, R., Sfihi, H., Jaffrezic-Renault, N., Rammah, M.B., Zarrouk, H. Grafting of anion exchanging groups on SiO₂/Si structures for anion detection in waters. *Sensors and Actuators B-Chemical*. 2003, 96(1-2), pp.399-406.
226. Petitjean, M., Proust, N., Chapeaublanc, J.-F., Perrin, J. Improvement of the SiO₂ deposition by 185 nm photolysis of N₂O and SiH₄ by addition of neopentane. *Applied Surface Science*. 1992, 54, pp.453-459.
227. Sagiv, J. Organized monolayers by adsorption. 1. Formation and structure of oleophobic mixed monolayers on solid surfaces. *Journal of the American Chemical Society*. 1980, 102(1), pp.92-98.

228. Choudhury, T.R., Moosa, A.A., Cushing, A., Bestwick, J. Patients' attitudes towards the presence of medical students during consultations. *Medical teacher*. 2006, 28(7), pp.e198-203.
229. Kurth, D.G., Bein, T. Surface reactions on thin layers of silane coupling agents. *Langmuir*. 1993, 9(11), pp.2965-2973.
230. Sugimura, H., Nakagiri, N. Nanoscopic Surface Architecture Based on Scanning Probe Electrochemistry and Molecular Self-Assembly. *Journal of the American Chemical Society*. 1997, 119(39), pp.9226-9229.
231. Baruah, J.B. Catalysts for Silane and Silanol Activation. In: *Science and Technology of Silicones and Silicone-Modified Materials*. American Chemical Society, 2007, pp.69-80.
232. Cooper, T.M., Campbell, A.L., Crane, R.L. Formation of polypeptide-dye multilayers by electrostatic self-assembly technique. *Langmuir*. 1995, 11(7), pp.2713-2718.
233. Chang, Y.-C., Frank, C.W. Vapor Deposition-Polymerization of α -Amino Acid N-Carboxy Anhydride on the Silicon(100) Native Oxide Surface. *Langmuir*. 1998, 14(2), pp.326-334.
234. Peter, W. Silane and Other Adhesion Promoters in Adhesive Technology. In: *Handbook of Adhesive Technology, Revised and Expanded*. CRC Press, 2003.
235. Decher, G., Hong, J.D. BUILDUP OF ULTRATHIN MULTILAYER FILMS BY A SELF-ASSEMBLY PROCESS .2. CONSECUTIVE ADSORPTION OF ANIONIC AND CATIONIC BIPOLAR AMPHIPHILES AND POLYELECTROLYTES ON CHARGED SURFACES. *Berichte Der Bunsen-Gesellschaft-Physical Chemistry Chemical Physics*. 1991, 95(11), pp.1430-1434.
236. Decher, G., Hong, J.D. BUILDUP OF ULTRATHIN MULTILAYER FILMS BY A SELF-ASSEMBLY PROCESS .1. CONSECUTIVE ADSORPTION OF ANIONIC AND CATIONIC BIPOLAR AMPHIPHILES ON CHARGED SURFACES. *Makromolekulare Chemie-Macromolecular Symposia*. 1991, 46, pp.321-327.
237. Decher, G., Hong, J.D., Schmitt, J. BUILDUP OF ULTRATHIN MULTILAYER FILMS BY A SELF-ASSEMBLY PROCESS .3. CONSECUTIVELY ALTERNATING ADSORPTION OF ANIONIC AND CATIONIC POLYELECTROLYTES ON CHARGED SURFACES. *Thin Solid Films*. 1992, 210(1-2), pp.831-835.
238. France, R.M., Short, R.D., Dawson, R.A., MacNeil, S. Attachment of human keratinocytes to plasma co-polymers of acrylic acid octa-1,7-diene and allylamine octa-1,7-diene. *Journal of Materials Chemistry*. 1998, 8(1), pp.37-42.
239. Tang, L.P., Wu, Y.L., Timmons, R.B. Fibrinogen adsorption and host tissue responses to plasma functionalized surfaces. *Journal of Biomedical Materials Research*. 1998, 42(1), pp.156-163.
240. Li, Z.F., Netravali, A.N. SURFACE MODIFICATION OF UHSPE FIBERS THROUGH ALLYLAMINE PLASMA DEPOSITION .2. EFFECT ON FIBER AND FIBER EPOXY INTERFACE. *Journal of Applied Polymer Science*. 1992, 44(2), pp.333-346.
241. Loh, I.H. PLASMA SURFACE MODIFICATION FOR BIOMEDICAL APPLICATIONS. *Abstracts of Papers of the American Chemical Society*. 1993, 205, pp.150-POLY.
242. Arkles, B. TAILORING SURFACES WITH SILANES. *Chemtech*. 1977, 7(12), pp.766-778.
243. Pasternack, R.M., Amy, S.R., Chabal, Y.J. Attachment of 3-(Aminopropyl)triethoxysilane on Silicon Oxide Surfaces: Dependence on Solution Temperature. *Langmuir*. 2008, 24(22), pp.12963-12971.
244. Zhang, F., Srinivasan, M.P. Self-Assembled Molecular Films of Aminosilanes and Their Immobilization Capacities. *Langmuir*. 2004, 20(6), pp.2309-2314.

245. White, L.D.,Tripp, C.P. Reaction of (3-Aminopropyl)dimethylethoxysilane with Amine Catalysts on Silica Surfaces. *Journal of Colloid and Interface Science*. 2000, 232(2), pp.400-407.
246. Zhu, M. Investigation and Preparation of Hydrolytically Stable Aminosilane-derived Layers on Silica Surfaces. thesis, Mount Holyoke College, 2011.
247. Heiney, P.A.,Gruneberg, K.,Fang, J.Y.,Dulcey, C.,Shashidhar, R. Structure and growth of chromophore-functionalized (3-aminopropyl)triethoxysilane self-assembled on silicon. *Langmuir*. 2000, 16(6), pp.2651-2657.
248. Chang, Y.C.,Frank, C.W. Vapor deposition-polymerization of alpha-amino acid N-carboxy anhydride on the silicon(100) native oxide surface. *Langmuir*. 1998, 14(2), pp.326-334.
249. Emoto, K.,Van Alstine, J.M.,Harris, J.M. Stability of poly(ethylene glycol) graft coatings. *Langmuir*. 1998, 14(10), pp.2722-2729.
250. Kohler, N.,Fryxell, G.E.,Zhang, M.Q. A bifunctional poly(ethylene glycol) silane immobilized on metallic oxide-based nanoparticles for conjugation with cell targeting agents. *Journal of the American Chemical Society*. 2004, 126(23), pp.7206-7211.
251. Emoto, K.,Harris, J.M.,VanAlstine, J.M. Grafting poly(ethylene glycol) epoxide to amino-derivatized quartz: Effect of temperature and pH on grafting density. *Analytical Chemistry*. 1996, 68(21), pp.3751-3757.
252. Malmsten, M.,Emoto, K.,Van Alstine, J.M. Effect of chain density on inhibition of protein adsorption by poly(ethylene glycol) based coatings. *Journal of Colloid and Interface Science*. 1998, 202(2), pp.507-517.
253. Miksa, D.,Irish, E.R.,Chen, D.,Composto, R.J.,Eckmann, D.M. Dextran functionalized surfaces via reductive amination: Morphology, wetting, and adhesion. *Biomacromolecules*. 2006, 7(2), pp.557-564.
254. Sugimura, H.,Hozumi, A.,Kameyama, T.,Takai, O. Organosilane self-assembled monolayers formed at the vapour/solid interface. *Surface and Interface Analysis*. 2002, 34(1), pp.550-554.
255. Fiorilli, S.,Rivolo, P.,Descrovi, E.,Ricciardi, C.,Pasquardini, L.,Lunelli, L.,Vanzetti, L.,Pederzoli, C.,Onida, B.,Garrone, E. Vapor-phase self-assembled monolayers of aminosilane on plasma-activated silicon substrates. *Journal of Colloid and Interface Science*. 2008, 321(1), pp.235-241.
256. Haller, I. COVALENTLY ATTACHED ORGANIC MONOLAYERS ON SEMICONDUCTOR SURFACES. *Journal of the American Chemical Society*. 1978, 100(26), pp.8050-8055.
257. Wieringa, R.H.,Schouten, A.J. Oriented Thin Film Formation by Surface Graft Polymerization of γ -Methyl L-Glutamate N-Carboxyanhydride in the Melt. *Macromolecules*. 1996, 29(8), pp.3032-3034.
258. Siqueira Petri, D.F.,Wenz, G.,Schunk, P.,Schimmel, T. An Improved Method for the Assembly of Amino-Terminated Monolayers on SiO₂ and the Vapor Deposition of Gold Layers. *Langmuir*. 1999, 15(13), pp.4520-4523.
259. Song, X.,Zhai, J.,Wang, Y.,Jiang, L. Self-assembly of amino-functionalized monolayers on silicon surfaces and preparation of superhydrophobic surfaces based on alkanolic acid dual layers and surface roughening. *Journal of Colloid and Interface Science*. 2006, 298(1), pp.267-273.
260. Janssen, D.,De Palma, R.,Verlaak, S.,Heremans, P.,Dehaen, W. Static solvent contact angle measurements, surface free energy and wettability determination of various self-assembled monolayers on silicon dioxide. *Thin Solid Films*. 2006, 515(4), pp.1433-1438.
261. Lee, S.H.,Ishizaki, T.,Saito, N.,Takai, O. Surface characterization on binary nano/micro-domain composed of alkyl- and amino-terminated self-assembled monolayer. *Applied Surface Science*. 2008, 254(22), pp.7453-7458.

262. Plueddemann, E.P. REMINISCING ON SILANE COUPLING AGENTS. *Journal of Adhesion Science and Technology*. 1991, 5(4), pp.261-277.
263. Pape, P.G.,Plueddemann, E.P. METHODS FOR IMPROVING THE PERFORMANCE OF SILANE COUPLING AGENTS. *Journal of Adhesion Science and Technology*. 1991, 5(10), pp.831-842.
264. Chu, C.W.,Kirby, D.P.,Murphy, P.D. Interactions of aminosilane with alumina and silica substrates deposited from nonaqueous and aqueous media. *Journal of Adhesion Science and Technology*. 1993, 7(5), pp.417-433.
265. Okabayashi, H.,Shimizu, I.,Nishio, E.,Connor, C.J.O. Diffuse reflectance infrared Fourier transform spectral study of the interaction of 3-aminopropyltriethoxysilane on silica gel. Behavior of amino groups on the surface. *Colloid and Polymer Science*. 1997, 275(8), pp.744-753.
266. Trens, P.,Denoyel, R. Adsorption of (γ -Aminopropyl)triethoxysilane and Related Molecules at the Silica/Heptane Interface. *Langmuir*. 1996, 12(11), pp.2781-2784.
267. Smith, E.A.,Chen, W. How to prevent the loss of surface functionality derived from aminosilanes. *Langmuir : the ACS journal of surfaces and colloids*. 2008, 24(21), pp.12405-9.
268. Fadeev, A.Y.,McCarthy, T.J. Self-assembly is not the only reaction possible between alkyltrichlorosilanes and surfaces: Monomolecular and oligomeric covalently attached layers of dichloro- and trichloroalkylsilanes on silicon. *Langmuir*. 2000, 16(18), pp.7268-7274.
269. Acres, R.G.,Ellis, A.V.,Alvino, J.,Lenahan, C.E.,Khodakov, D.A.,Metha, G.F.,Andersson, G.G. Molecular Structure of 3-Aminopropyltriethoxysilane Layers Formed on Silanol-Terminated Silicon Surfaces. *The Journal of Physical Chemistry C*. 2012, 116(10), pp.6289-6297.
270. McGovern, M.E.,Kallury, K.M.R.,Thompson, M. Role of Solvent on the Silanization of Glass with Octadecyltrichlorosilane. *Langmuir*. 1994, 10(10), pp.3607-3614.
271. Vandenberg, E.T.,Bertilsson, L.,Liedberg, B.,Uvdal, K.,Erlandsson, R.,Elwing, H.,Lundström, I. Structure of 3-aminopropyl triethoxy silane on silicon oxide. *Journal of Colloid and Interface Science*. 1991, 147(1), pp.103-118.
272. Simon, A.,Cohen-Bouhacina, T.,Porte, M.C.,Aime, J.P.,Baquey, C. Study of two grafting methods for obtaining a 3-aminopropyltriethoxysilane monolayer on silica surface. *Journal of Colloid and Interface Science*. 2002, 251(2), pp.278-283.
273. Moiseev, L.,Unlu, M.S.,Swan, A.K.,Goldberg, B.B.,Cantor, C.R. DNA conformation on surfaces measured by fluorescence self-interference. *Proceedings of the National Academy of Sciences of the United States of America*. 2006, 103(8), pp.2623-2628.
274. Hu, M.H.,Noda, S.,Okubo, T.,Yamaguchi, Y.,Komiya, H. Structure and morphology of self-assembled 3-mercaptopropyltrimethoxysilane layers on silicon oxide. *Applied Surface Science*. 2001, 181(3-4), pp.307-316.
275. Metwalli, E.,Haines, D.,Becker, O.,Conzone, S.,Pantano, C.G. Surface characterizations of mono-, di-, and tri-aminosilane treated glass substrates. *Journal of Colloid and Interface Science*. 2006, 298(2), pp.825-831.
276. Wang, L.K.,Feng, X.Z.,Hou, S.,Chan, Q.L.,Qin, M. Microcontact printing of multiproteins on the modified mica substrate and study of immunoassays. *Surface and Interface Analysis*. 2006, 38(1), pp.44-50.
277. Chiang, C.H.,Liu, N.I.,Koenig, J.L. MAGIC-ANGLE CROSS-POLARIZATION C-13 NMR-STUDY OF AMINOSILANE COUPLING AGENTS ON SILICA SURFACES. *Journal of Colloid and Interface Science*. 1982, 86(1), pp.26-34.
278. Shirai, K.,Yoshida, Y.,Nakayama, Y.,Fujitani, M.,Shintani, H.,Wakasa, K.,Okazaki, M.,Snauwaert, J.,Van Meerbeek, B. Assessment of

- decontamination methods as pretreatment of silanization of composite glass fillers. *Journal of Biomedical Materials Research*. 2000, 53(3), pp.204-210.
279. Cras, J.J.,Rowe-Taitt, C.A.,Nivens, D.A.,Ligler, F.S. Comparison of chemical cleaning methods of glass in preparation for silanization. *Biosensors & Bioelectronics*. 1999, 14(8-9), pp.683-688.
280. Onyiriuka, E.C.,Moore, C.B.,Fehlner, F.P.,Binkowski, N.J.,Salamida, D.,King, T.J.,Couillard, J.G. Effect of RCA cleaning on the surface chemistry of glass and polysilicon films as studied by ToF-SIMS and XPS. *Surface and Interface Analysis*. 1998, 26(4), pp.270-277.
281. Tsukruk, V.V.,Bliznyuk, V.N. Adhesive and Friction Forces between Chemically Modified Silicon and Silicon Nitride Surfaces. *Langmuir*. 1998, 14(2), pp.446-455.
282. Davies, P.R.,Keel, J.M. The reaction of carbon dioxide with amines at a Cu(211) surface. *Surface Science*. 2000, 469(2-3), pp.204-213.
283. Han, Y.,Mayer, D.,Offenhäusser, A.,Ingebrandt, S. Surface activation of thin silicon oxides by wet cleaning and silanization. *Thin Solid Films*. 2006, 510(1-2), pp.175-180.
284. Argekar, S.U.,Kirley, T.L.,Schaefer, D.W. Determination of structure-property relationships for 3-aminopropyltriethoxysilane films using x-ray reflectivity. *Journal of Materials Research*. 2013, 28(08), pp.1118-1128.
285. Puniredd, S.R.,Srinivasan, M.P. Covalent molecular assembly of oligoimide ultrathin films in supercritical and liquid solvent media. *Langmuir*. 2005, 21(17), pp.7812-7822.
286. Puniredd, S.R.,Srinivasan, M.P. Covalent Molecular Assembly in Supercritical Carbon Dioxide: A Comparative Study between Amine- and Anhydride-Derivatized Surfaces. *Langmuir*. 2006, 22(9), pp.4092-4099.
287. Zhang, F.,Srinivasan, M.P. Cross-linked polyimide-polythiophene composite films with reduced surface resistivities. *Thin Solid Films*. 2005, 479(1-2), pp.95-102.
288. Tsuru, N.,Kikuchi, M.,Kawaguchi, H.,Shiratori, S. A quartz crystal microbalance sensor coated with MIP for "bisphenol A" and its properties. *Thin Solid Films*. 2006, 499(1-2), pp.380-385.
289. Matsuura, K.,Tsuchida, A.,Okahata, Y.,Akaike, T.,Kobayashi, K. A quartz-crystal microbalance study of adsorption behaviors of artificial glycoconjugate polymers onto chemically modified gold surfaces and their interactions with lectins. *Bulletin of the Chemical Society of Japan*. 1998, 71(12), pp.2973-2977.
290. Fleming, N.,Mathisen, A.M.,Eriksen, S.H.,Moldrheim, E.,Johansen, T.R. Productivity Impairment From Kaolinite Mobilization: Laboratory and Field Experience, Oseberg Sor. *SPE Production & Operations*. 2008, 23(3), pp.318-330.
291. Fleming, N.,Ramstad, K.,Nelson, A.C.,Kidd, S. Innovative Use of Kaolinite in Downhole Scale Management: Squeeze-Life Enhancement and Water Shutoff. *SPE Production & Operations*. 2009, 24(3), pp.439-449.
292. Zhang, X.Q.,Yang, W.Y.,You, X.Z.,Wei, Y. Preparation and characterization of self-assembly organic multilayer films on silica surface. *Applied Surface Science*. 1995, 84(3), pp.267-271.
293. Ekeröth, J.,Konradsson, P.,Bjorefors, F.,Lundström, I.,Liedberg, B. Monitoring the interfacial capacitance at self-assembled phosphate monolayers on gold electrodes upon interaction with calcium and magnesium. *Analytical Chemistry*. 2002, 74(9), pp.1979-1985.
294. Karpovich, D.S.,Blanchard, G.J. Direct Measurement of the Adsorption Kinetics of Alkanethiolate Self-Assembled Monolayers on a Microcrystalline Gold Surface. *Langmuir*. 1994, 10(9), pp.3315-3322.
295. Amemiya, Y.,Hatakeyama, A.,Shimamoto, N. Aminosilane Multilayer Formed on a Single-Crystalline Diamond Surface with Controlled

- Nanoscope Hardness and Bioactivity by a Wet Process. *Langmuir*. 2008, 25(1), pp.203-209.
296. O'Sullivan, C.K.,Guilbault, G.G. Commercial quartz crystal microbalances - theory and applications. *Biosensors & Bioelectronics*. 1999, 14(8-9), pp.663-670.
297. Brown, M.E.,Gallagher, P.K. HANDBOOK OF THERMAL ANALYSIS AND CALORIMETRY VOLUME 5 RECENT ADVANCES, TECHNIQUES AND APPLICATIONS PREFACE. 2008.
298. Gallagher, P.K. HANDBOOK OF THERMAL ANALYSIS AND CALORIMETRY VOLUME 5 RECENT ADVANCES, TECHNIQUES AND APPLICATIONS FOREWORD. 2008.
299. Mavredaki, E. Barium Sulphate Formation Kinetics and Inhibition at Surfaces. PhD thesis, University of Leeds, 2009.
300. McCann, D.F.,French, L.A.,Wark, M.S.,Vetelino, J.F. Recent advances in lateral field excited and monolithic spiral coil acoustic transduction bulk acoustic wave sensor platforms. *Measurement Science & Technology*. 2009, 20(12).
301. KSV, T.N.-. WHAT IS A QUARTZ CRYSTAL MICROBALANCE – QCM. [Online]. October 2004. [Accessed 27/01]. Available from: www.terralab.biz/edoc/ksv/KSV_QCM_Article_What_is_QCM.pdf
302. Professor Robert B. Laughlin, S.L.H. Introduction to Quartz Crystal Microbalance. [Online]. 2007. [Accessed 24/07]. Available from: <http://large.stanford.edu/courses/2007/ph210/hellstrom2/>.
303. INFICON. The Technology of The Intelligent Oscillator for Quartz Crystal Measurement and Its Advantages for Thin Film Processes. [Online]. 2002. [Accessed 19/04/2010]. Available from: http://www.inficon.com/download/en/Intelligent_Oscillator.pdf.
304. Hu, J.,Yang, D.,Kang, Q.,Shen, D. Estimation the kinetics parameters for non-specific adsorption of fibrinogen on quartz surface from the response of an electrode-separated piezoelectric sensor. *Sensors and Actuators B: Chemical*. 2003, 96(1-2), pp.390-398.
305. Hempel, U.,Lucklum, R.,Hauptmann, P.R.,EerNisse, E.P.,Puccio, D.,Diaz, R.F. Quartz crystal resonator sensors under lateral field excitation - a theoretical and experimental analysis. *Measurement Science & Technology*. 2008, 19(5).
306. Anderson, H.,Jonsson, M.,Vestling, L.,Lindberg, U.,Aastrup, T. Quartz crystal microbalance sensor design I. Experimental study of sensor response and performance. *Sensors and Actuators B-Chemical*. 2007, 123(1), pp.27-34.
307. Higuchi, R.,Kanno, Y. New analysis from the strength of materials of Sauerbrey's equation concerning the quartz crystal microbalance. *Japanese Journal of Applied Physics Part 1-Regular Papers Brief Communications & Review Papers*. 2006, 45(5A), pp.4232-4233.
308. Kankare, J. Sauerbrey equation of quartz crystal microbalance in liquid medium. *Langmuir*. 2002, 18(18), pp.7092-7094.
309. Jones, J.L.,Mieure, J.P. A PIEZOELECTRIC TRANSDUCER FOR DETERMINATION OF METALS AT MICROMOLAR LEVEL. *Analytical Chemistry*. 1969, 41(3), pp.484-&.
310. Ward, M.D.,Delawski, E.J. RADIAL MASS SENSITIVITY OF THE QUARTZ CRYSTAL MICROBALANCE IN LIQUID-MEDIA. *Analytical Chemistry*. 1991, 63(9), pp.886-890.
311. Rekhviashvili, S.,Kishtikova, E. Adsorption and surface energy issues in experiments with quartz crystal microbalance. *Technical Physics*. 2008, 53(4), pp.526-528.

312. Du, X., Wang, Z., Huang, J., Tao, S., Tang, X., Jiang, Y. A new polysiloxane coating on QCM sensor for DMMP vapor detection. *Journal of Materials Science*. 2009, **44**(21), pp.5872-5876.
313. Tsuchida, A., Matsuura, K., Kobayashi, K. A Quartz-crystal microbalance study of adsorption behaviors of artificial glycoconjugate polymers with different saccharide chain lengths and with different backbone structures. *Macromolecular Chemistry and Physics*. 2000, **201**(17), pp.2245-2250.
314. Liebau, M., Bendas, G., Rothe, U., Neubert, R.H.H. Adhesive interactions of liposomes with supported planar bilayers on QCM as a new adhesion model. *Sensors and Actuators B: Chemical*. 1998, **47**(1-3), pp.239-245.
315. Mirmohseni, A., Oladegaragoze, A. Application of the quartz crystal microbalance for determination of phenol in solution. *Sensors and Actuators B: Chemical*. 2004, **98**(1), pp.28-36.
316. Yan, D., Jennings, G.K., Weinstein, R.D. Controlling the Properties of n-Alkanethiolate Self-Assembled Monolayers on Gold by Using Supercritical Carbon Dioxide/Ethanol Mixtures as Solvents. *Industrial & Engineering Chemistry Research*. 2002, **41**(18), pp.4528-4533.
317. Puniredd, S.R., Srinivasan, M.P. Covalent Molecular Assembly in Supercritical Carbon Dioxide: A Comparative Study between Amine- and Anhydride-Derivatized Surfaces. *Langmuir*. 2006, **22**(9), pp.4092-4099.
318. Sauerbrey, G. *The Use of Quartz Crystal Oscillators for Weighing Thin Layers and for Microweighing Applications*. 1959.
319. Kanazawa, K.K., Gordon, J.G. FREQUENCY OF A QUARTZ MICROBALANCE IN CONTACT WITH LIQUID. *Analytical Chemistry*. 1985, **57**(8), pp.1770-1771.
320. Glassford, A.P.M. RESPONSE OF A QUARTZ CRYSTAL MICROBALANCE TO A LIQUID DEPOSIT. *Journal of Vacuum Science & Technology*. 1978, **15**(6), pp.1836-1843.
321. Siegbahn, K., Uppsala, K.V.-s.i. *ESCA; atomic, molecular and solid state structure studied by means of electron spectroscopy*. Almqvist & Wiksells, 1967.
322. Jagst, E. *Surface Functional Group Characterization Using Chemical Derivatization X-ray Photoelectron Spectroscopy (CD-XPS)*
- thesis, der Freien Universität Berlin
- 2010.
323. Briggs, D., Seah, P. *Practical Surface Analysis: Auger and X-ray photoelectron spectroscopy*. Wiley, 1990.
324. Riviere, J.C., Myhra, S. *Handbook of Surface and Interface Analysis: Methods for Problem-Solving*. Taylor & Francis, 1998.
325. Nowicki, B. Multiparameter representation of surface roughness. *Wear*. 1985, **102**(3), pp.161-176.
326. Thomas, T.R. Characterization of surface roughness. *Precision Engineering*. 1981, **3**(2), pp.97-104.
327. Gadelmawla, E.S., Koura, M.M., Maksoud, T.M.A., Elewa, I.M., Soliman, H.H. Roughness parameters. *Journal of Materials Processing Technology*. 2002, **123**(1), pp.133-145.
328. Karpovich, D.S., Blanchard, G.J. An Undergraduate Laboratory Experiment for the Direct Measurement of Monolayer-Formation Kinetics. *Journal of Chemical Education*. 1995, **72**(5), p.466.
329. Liu, J.H., Zhan, Z.W., Yu, M., Li, S.M. Adsorption behavior of glycidoxypropyl-trimethoxy-silane on titanium alloy Ti-6.5Al-1Mo-1V-2Zr. *Applied Surface Science*. 2013, **264**, pp.507-515.

330. Chen, S.H., Frank, C.W. n-Alkanoic Acid Self-Assembled Monolayers. In: *Fourier Transform Infrared Spectroscopy in Colloid and Interface Science*. American Chemical Society, 1990, pp.160-176.
331. Laidler, K.J. *Chemical kinetics*. 3rd ed. New York ; London: Harper & Row, 1987.
332. Atkins, P.W. *Physical Chemistry*. Macmillan Higher Education, 1997.
333. McCarley, R.L., Kim, Y.T., Bard, A.J. Scanning tunneling microscopy and quartz crystal microbalance studies of gold exposed to sulfide, thiocyanate, and n-octadecanethiol. *The Journal of Physical Chemistry*. 1993, **97**(1), pp.211-215.
334. Sato, T., Serizawa, T., Okahata, Y. Recognition of Monosialoganglioside (GM3) Reconstituted in Sphingomyelin and Glucosylceramide Membranes against Wheat Germ Agglutinin: Quantitative Analyses by a Quartz Crystal Microbalance. *Biochemical and Biophysical Research Communications*. 1994, **204**(2), pp.551-556.
335. Ebara, Y., Okahata, Y. A Kinetic Study of Concanavalin A Binding to Glycolipid Monolayers by Using a Quartz-Crystal Microbalance. *Journal of the American Chemical Society*. 1994, **116**(25), pp.11209-11212.
336. Kalfayan, L. *Production enhancement with acid stimulation*. 2nd ed. Tulsa, Okla.: PennWell, 2008.
337. Doyle, J.D., Oldring, K., Churchley, J., Parsons, S.A. Struvite formation and the fouling propensity of different materials. *Water Research*. 2002, **36**(16), pp.3971-3978.
338. Liu, Y., Wang, A., Claus, R.O. Layer-by-layer electrostatic self-assembly of nanoscale Fe₃O₄ particles and polyimide precursor on silicon and silica surfaces. *Applied Physics Letters*. 1997, **71**(16), pp.2265-2267.
339. Kurth, D.G., Bein, T. Thin Films of (3-Aminopropyl)triethoxysilane on Aluminum Oxide and Gold Substrates. *Langmuir*. 1995, **11**(8), pp.3061-3067.
340. Chauhan, A.K., Aswal, D.K., Koiry, S.P., Gupta, S.K., Yakhmi, J.V., Surgers, C., Guerin, D., Lenfant, S., Vuillaume, D. Self-assembly of the 3-aminopropyltrimethoxysilane multilayers on Si and hysteretic current-voltage characteristics. *Applied Physics a-Materials Science & Processing*. 2008, **90**(3), pp.581-589.
341. Aissaoui, N., Bergaoui, L., Landoulsi, J., Lambert, J.-F., Boujday, S. Silane Layers on Silicon Surfaces: Mechanism of Interaction, Stability, and Influence on Protein Adsorption. *Langmuir*. 2011, **28**(1), pp.656-665.
342. Howarter, J.A., Youngblood, J.P. Optimization of Silica Silanization by 3-Aminopropyltriethoxysilane. *Langmuir*. 2006, **22**(26), pp.11142-11147.
343. Gunn, D.J. Effect of surface roughness on the nucleation and growth of calcium sulphate on metal surfaces. *Journal of Crystal Growth*. 1980, **50**(2), pp.533-537.
344. Martinod, A., Neville, A., Euvrad, M., Sorbie, K. Electrodeposition of a calcareous layer: Effects of green inhibitors. *Chemical Engineering Science*. 2009, **64**(10), pp.2413-2421.
345. Eroini, V., Kapur, N., Neville, A., Euvrad, M. Preventing Scale Formation Using Modified Surfaces. In: *CORROSION 2011, 01/01/2011, Houston, Texas*. NACE International, 2011.
346. Andritsos, N., Karabelas, A.J., Koutsoukos, P.G. Morphology and Structure of CaCO₃ Scale Layers Formed under Isothermal Flow Conditions. *Langmuir*. 1997, **13**(10), pp.2873-2879.
347. Han, Y.S., Hadiko, G., Fuji, M., Takahashi, M. Factors affecting the phase and morphology of CaCO₃ prepared by a bubbling method. *Journal of the European Ceramic Society*. 2006, **26**(4-5), pp.843-847.

348. Wucher, B., Yue, W., Kulak, A.N., Meldrum, F.C. Designer Crystals: Single Crystals with Complex Morphologies. *Chemistry of Materials*. 2007, **19**(5), pp.1111-1119.
349. Kallury, K.M.R., Macdonald, P.M., Thompson, M. Effect of Surface Water and Base Catalysis on the Silanization of Silica by (Aminopropyl)alkoxysilanes Studied by X-ray Photoelectron Spectroscopy and ¹³C Cross-Polarization/Magic Angle Spinning Nuclear Magnetic Resonance. *Langmuir*. 1994, **10**(2), pp.492-499.
350. Kosmulski, M. pH-dependent surface charging and points of zero charge II. Update. *Journal of Colloid and Interface Science*. 2004, **275**(1), pp.214-224.
351. Churchill, H., Teng, H., Hazen, R.M. Correlation of pH-dependent surface interaction forces to amino acid adsorption: Implications for the origin of life. *American Mineralogist*. 2004, **89**(7), pp.1048-1055.
352. Pradubmook, T., O'Haver, J.H., Malakul, P., Harwell, J.H. Effect of pH on adsolubilization of toluene and acetophenone into adsorbed surfactant on precipitated silica. *Colloids and Surfaces A: Physicochemical and Engineering Aspects*. 2003, **224**(1-3), pp.93-98.
353. Patai, S. ed. *The chemistry of the amino group*. New York ; London: Interscience, 1968.
354. Zhang, F., Srinivasan, M.P. Layer-by-layer assembled gold nanoparticle films on amine-terminated substrates. *Journal of Colloid and Interface Science*. 2008, **319**(2), pp.450-456.
355. Caravajal, G.S., Leyden, D.E., Quinting, G.R., Maciel, G.E. Structural characterization of (3-aminopropyl)triethoxysilane-modified silicas by silicon-29 and carbon-13 nuclear magnetic resonance. *Analytical Chemistry*. 1988, **60**(17), pp.1776-1786.
356. Graf, N., Yegen, E., Gross, T., Lippitz, A., Weigel, W., Krakert, S., Terfort, A., Unger, W.E.S. XPS and NEXAFS studies of aliphatic and aromatic amine species on functionalized surfaces. *Surface Science*. 2009, **603**(18), pp.2849-2860.
357. Truica-Marasescu, F., Wertheimer, M.R. Nitrogen-Rich Plasma-Polymer Films for Biomedical Applications. *Plasma Processes and Polymers*. 2008, **5**(1), pp.44-57.
358. Pippig, F., Hollaender, A. Fluram labeling of high density NH₂ surfaces. *Applied Surface Science*. 2007, **253**(16), pp.6817-6823.
359. Horner, M.R., Boerio, F.J., Clearfield, H.M. An XPS investigation of the adsorption of aminosilanes onto metal substrates. *Journal of Adhesion Science and Technology*. 1992, **6**(1), pp.1-22.
360. Moulder, J., Chastain, J., King, R. *Handbook of X-ray Photoelectron Spectroscopy: a reference book of standard spectra for identification and interpretation of XPS data*. Physical Electronics, 1995.
361. Holländer, A., Pippig, F., Dubreuil, M., Vangeneugden, D. Distinguishing Surface OH and NH_x Using TFAA Derivatization and XPS. *Plasma Processes and Polymers*. 2008, **5**(4), pp.345-349.
362. Tsai, W.H., Cave, N.G., Boerio, F.J. CHARACTERIZATION OF INTERFACES BETWEEN PYROMELLITIC DIANHYDRIDE 2,2-BIS 4-(4-AMINOPHENOXY)PHENYL HEXAFLUOROPROPANE POLYIMIDES AND SILVER AND HIGHLY ORIENTED PYROLYTIC-GRAPHITE SUBSTRATES USING X-RAY PHOTOELECTRON-SPECTROSCOPY. *Langmuir*. 1992, **8**(3), pp.927-935.
363. Harder, P., Bierbaum, K., Woell, C., Grunze, M., Heid, S., Effenberger, F. Induced Orientational Order in Long Alkyl Chain Aminosilane Molecules by Preadsorbed Octadecyltrichlorosilane on Hydroxylated Si(100)†. *Langmuir*. 1997, **13**(3), pp.445-454.
364. Kristensen, E.M.E., Nederberg, F., Rensmo, H., Bowden, T., Hilborn, J., Siegbahn, H. Photoelectron Spectroscopy Studies of the Functionalization

- of a Silicon Surface with a Phosphorylcholine-Terminated Polymer Grafted onto (3-Aminopropyl)trimethoxysilane. *Langmuir*. 2006, **22**(23), pp.9651-9657.
365. Wake, W.C. *Adhesion and the formulation of adhesives*. London: Applied Science, 1976.
366. Hollaender, A., Pippig, F., Dubreuil, M., Vangeneugden, D. Distinguishing surface OH and NH_x using TFAA derivatization and XPSa. *Plasma Processes and Polymers*. 2008, **5**(4), pp.345-349.
367. Blum, F.D., Meesiri, W., Kang, H.J., Gambogi, J.E. HYDROLYSIS, ADSORPTION, AND DYNAMICS OF SILANE COUPLING AGENTS ON SILICA SURFACES. *Journal of Adhesion Science and Technology*. 1991, **5**(6), pp.479-496.
368. Bierbaum, K., Kinzler, M., Woell, C., Grunze, M., Haehner, G., Heid, S., Effenberger, F. A Near Edge X-ray Absorption Fine Structure Spectroscopy and X-ray Photoelectron Spectroscopy Study of the Film Properties of Self-Assembled Monolayers of Organosilanes on Oxidized Si(100). *Langmuir*. 1995, **11**(2), pp.512-518.
369. Magalhães, J.L., Moreira, L.M., Rodrigues-Filho, U.P., Giz, M.J., Pereira-da-Silva, M.A., Landers, R., Vinhas, R.C.G., Nascente, P.A.P. Surface chemistry of the iron tetraazamacrocyclic on the aminopropyl-modified surface of oxidized n-Si(100) by AFM and XPS. *Surface and Interface Analysis*. 2002, **33**(4), pp.293-298.
370. Allen, G.C., Sorbello, F., Altavilla, C., Castorina, A., Ciliberto, E. Macro-, micro- and nano-investigations on 3-aminopropyltrimethoxysilane self-assembly-monolayers. *Thin Solid Films*. 2005, **483**(1-2), pp.306-311.
371. Hurst, K.M., Ansari, N., Roberts, C.B., Ashurst, W.R. Self-Assembled Monolayer-Immobilized Gold Nanoparticles as Durable, Anti-Stiction Coatings for MEMS. *Journal of Microelectromechanical Systems*. 2011, **20**(2), pp.424-435.
372. Wu, Y., Buranda, T., Metzner, R.L., Sklar, L.A., Lopez, G.P. Diazo coupling method for covalent attachment of proteins to solid substrates. *Bioconjugate Chemistry*. 2006, **17**(2), pp.359-365.
373. Waddell, T.G., Leyden, D.E., DeBello, M.T. THE NATURE OF ORGANOSILANE TO SILICA-SURFACE BONDING. *Journal of the American Chemical Society*. 1981, **103**(18), pp.5303-5307.
374. Siqueira-Petri, D.F., Wenz, G., Schunk, P., Schimmel, T., Bruns, M., Dichtl, M.A. Surface modification of thin polystyrene films. *Colloid and Polymer Science*. 1999, **277**(7), pp.673-679.
375. Simon, A., Cohen-Bouhacina, T., Porté, M.C., Aimé, J.P., Baquey, C. Study of Two Grafting Methods for Obtaining a 3-Aminopropyltriethoxysilane Monolayer on Silica Surface. *Journal of Colloid and Interface Science*. 2002, **251**(2), pp.278-283.
376. Blum, F.D., Meesiri, W., Kang, H.-J., Gambogi, J.E. Hydrolysis, adsorption, and dynamics of silane coupling agents on silica surfaces. *Journal of Adhesion Science and Technology*. 1991, **5**(6), pp.479-496.
377. Zhang, Z., Hu, R., Liu, Z. Formation of a Porphyrin Monolayer Film by Axial Ligation of Protoporphyrin IX Zinc to an Amino-Terminated Silanized Glass Surface. *Langmuir*. 1999, **16**(3), pp.1158-1162.
378. Kim, J., Seidler, P., Wan, L.S., Fill, C. Formation, structure, and reactivity of amino-terminated organic films on silicon substrates. *Journal of Colloid and Interface Science*. 2009, **329**(1), pp.114-119.
379. Shen, W., He, H., Zhu, J., Yuan, P., Ma, Y., Liang, X. Preparation and characterization of 3-aminopropyltriethoxysilane grafted montmorillonite and acid-activated montmorillonite. *Chinese Science Bulletin*. 2009, **54**(2), pp.265-271.

380. Jessem Landoulsi, Michel J. Genet, Karim El Kirat, Caroline Richard, Sylviane Pulvin, Rouxhet, P.G. *Silanization with APTES for Controlling the Interactions Between Stainless Steel and Biocomponents: Reality vs Expectation*. *Biomaterials - Physics and Chemistry*, 2011.
381. Heise, A., Menzel, H., Yim, H., Foster, M.D., Wieringa, R.H., Schouten, A.J., Erb, V., Stamm, M. Grafting of Polypeptides on Solid Substrates by Initiation of N-Carboxyanhydride Polymerization by Amino-Terminated Self-Assembled Monolayers. *Langmuir*. 1997, **13**(4), pp.723-728.
382. Demirel, G., Caglayan, M.O., Garipcan, B., Duman, M., Piskin, E. Formation and organization of amino terminated self-assembled layers on Si(001) surface. *Nanoscale Research Letters*. 2007, **2**(7), pp.350-354.
383. Cui, N.-Y., Liu, C., Yang, W. XPS and AFM characterization of the self-assembled molecular monolayers of a 3-aminopropyltrimethoxysilane on silicon surface, and effects of substrate pretreatment by UV-irradiation. *Surface and Interface Analysis*. 2011, **43**(7), pp.1082-1088.
384. Zhang, F., Srinivasan, M.P. Ultra thin films of oligoimide through molecular assembly. *Colloids and Surfaces A: Physicochemical and Engineering Aspects*. 2005, **257–258**(0), pp.295-299.
385. Kuther, J., Seshadri, R., Nelles, G., Butt, H.J., Knoll, W., Tremel, W. Rough surfaces by design: Gold colloids tethered to gold surfaces as substrates for CaCO₃ crystallization. *Advanced Materials*. 1998, **10**(5), pp.401-404.
386. Park, R.J., Meldrum, F.C. Synthesis of single crystals of calcite with complex morphologies. *Advanced Materials*. 2002, **14**(16), pp.1167-1169.
387. Park, R.J., Meldrum, F.C. Shape-constraint as a route to calcite single crystals with complex morphologies. *Journal of Materials Chemistry*. 2004, **14**(14), pp.2291-2296.
388. Gabrielli, C., Jaouhari, R., Joiret, S., Maurin, G., Rousseau, P. Study of the electrochemical deposition of CaCO₃ by in situ Raman spectroscopy - I. Influence of the substrate. *Journal of the Electrochemical Society*. 2003, **150**(7), pp.C478-C484.
389. Moritz, T., Benfer, S., Arki, P., Tomandl, G. Investigation of ceramic membrane materials by streaming potential measurements. *Colloids and Surfaces a-Physicochemical and Engineering Aspects*. 2001, **195**(1-3), pp.25-33.
390. Fleming, N., Ramstad, K., Hoeth, L.W., Kidd, S. Mechanical Alteration of Near-Wellbore Mineralogy for Improved Squeeze Performance.
391. Wu, Z., Francis, L.F., Davidson, J.H. Scale formation on polypropylene and copper tubes in mildly supersaturated tap water. *Solar Energy*. 2009, **83**(5), pp.636-645.
392. Zhang, F., Srinivasan, M.P. Ultra-thin composite films from polyimide and electroactive polymer through covalent molecular assembly. *Colloids and Surfaces A: Physicochemical and Engineering Aspects*. 2005, **257–258**(0), pp.509-514.

Appendix A

```
clc
clear all
format long
raw_data=load('12 05 11 2.txt'); %load file

%plot(raw_data(:,5));%plot the 5th colume raw data

%figure
%plot(raw_data(486:end,5));%plot the 5th colume raw data start from 486 points
raw_data_1=raw_data(268:end,5);

%filter remove the high frequency noise
[x_HP_pressure, y_HP_pressure] = butter(7, 0.01, 'low');
flitered_data = filtfilt(x_HP_pressure, y_HP_pressure,raw_data_1);

%figure
%plot(flitered_data);% plot filered data

%do gradient
d_raw_data=gradient(flitered_data);
%figure
%plot(d_raw_data);

KK=[];
nn = size (flitered_data);
n = max (nn);
A = max (flitered_data);
B = flitered_data;
for x = 1 : n;
    KKK = log(1-(B(x,1)/A))/x;
    if KKK ~= -inf
        KK = [KK, KKK];
    end
end
end
```



```
Method = 'Average Method'
K = mean (KK)
x = 1 : n;
f = A * (1-exp(K * x));
A

figure
plot(f)
title('2% organosilane on 12.05.11 ')
ylabel('ug/cm2')
xlabel('Time(s)')
hold on
plot(flitered_data,'red');% plot filered data
h = legend('Fitted data','Smooth data',4);

d1_raw_data=gradient(f);
figure
plot(d1_raw_data);
title('2% organosilane on 12.05.11')
ylabel('dm/dt')
xlabel('Time(s)')

t = raw_data(:,6) ;
m = raw_data(:,5);

% Define your exponential function
fh = @(x,p) p(1) * (1 - exp(-x.*p(2)));

% define the error function. this is the function to
% minimize: you can also use norm or whatever:
errfh = @(p,x,y) sum((y(:)-fh(x(:,p))),.^2);

% an initial guess of the exponential parameters
p0 = [A K];

% search for solution
```

```
Method = 'All data include water with fminsearch function'
```

```
P = fminsearch(errfh,p0,[],t,m);
```

```
A1 = P(1)
```

```
Kobs1 = P(2)
```

```
figure
```

```
% plot the result
```

```
plot(t,m,'b',t,fh(t,P),'-r')
```

```
title('2% organosilane on 12.05.11 ')
```

```
ylabel('ug/cm2')
```

```
xlabel('Time(s)')
```

```
h = legend('Exp. data','Fitted data',4);
```

```
t = 0 : n-1;
```

```
m = flitered_data;
```

```
% search for solution
```

```
Method = 'Organosilane data exclude water with fminsearch function'
```

```
P2 = fminsearch(errfh,p0,[],t,m);
```

```
A2 = P2(1)
```

```
Kobs2 = P2(2)
```

```
% plot the result
```

```
figure
```

```
plot(t,m,'b',t,fh(t,P2),'-r')
```

```
title('2% organosilane on 12.05.11 ')
```

```
ylabel('ug/cm2')
```

```
xlabel('Time(s)')
```

```
h = legend('Exp. data','Fitted data')
```